Transdifferentiation of cancer stem cells in brain tumours: Lessons from *Drosophila* neural stem cells

By Hannah TRUONG Thi-Hong Hanh
ORCID: 0000-0002-1364-8709

COMPREHENSIVE CANCER DOCTOR OF PHILOSOPHY

July 2020

Peter MacCallum Cancer Centre, and
Department of Anatomy and Neuroscience, The University of Melbourne

Submitted in total fulfillment of the requirements of the degree of Comprehensive Cancer Doctor of Philosophy
Printed on archival quality paper

Abstract

Background:

In human brain cancers, glioblastoma stem cells (GSCs) originate from neoplastic transformation of neural stem cells (NSCs) or dedifferentiation of other neural cells. Similar to normal NSCs, GSCs possess stem-cell properties to self-renew and differentiate into multiple neural lineages. However, GSCs are more plastic than normal NSCs, as they can transdifferentiate into other cell types. At the present, we do not fully understand the cellular step-wise conversion from GSCs into other distinct cell lineages, and the molecular mechanism responsible for this event. *Drosophila* NSCs, called neuroblasts (NBs), also asymmetrically divide to renew themselves, and generate neurons or glia that make up the adult central nervous system. Disrupting either asymmetric cell division or neuronal maintenance allows differentiated cells to dedifferentiate into ectopic NBs, which then continue to proliferate and form tumours.

Methods and aims:

We utilised several *in vivo* brain tumour models in *Drosophila* to study how GSCs function in brain cancers and how they undergo transdifferentiation. In this thesis, I induced loss-of-function of transcription factors Prospero or Nerfin-1 in NB lineages to generate dedifferentiation-driven tumours, and found a class of cells which exhibited glial cell identity. I sought to investigate the behaviours and characteristics of these ectopic glia to elucidate some aspects about GSC transdifferentiation by answering three questions: (1) What are the cell numbers and cell types within the *pros*$^{-}$ and *nerfin-1*$^{-}$ tumours. (2) Do ectopic glia arise by transdifferentiation of NBs in the tumours? (3) Which transcription factors and signal transduction pathways drive the formation of ectopic glia, and are ectopic glia required for tumour growth?

Results:

(1) I found that the expansion of ectopic glia population is correlated with overall tumour growth. Ectopic glia exhibit glial identity and their formation is not dependent on the location of tumours in the central nervous system.

(2) By performing live-cell imaging of *pros*$^{-}$ tumours and molecular marker analysis, I found a subset of NBs switch to glial cell fate.

(3) I performed genetic experiments to manipulate the transcription factors *dichaete*, *tailless* and *glial cells missing* (*gcm*) in *pros*$^{-}$ tumour and found that they are required for ectopic glial formation and tumour growth. Their target gene *reversed polarity* (*repo*) regulates the formation of ectopic glia, which in turn, promote the tumour growth. I showed that Notch promotes tumour growth independently of its effect on ectopic glial formation, as Notch regulates the tumour growth in the absence of ectopic glia. I also showed that FGF signalling pathway promotes tumour growth by regulating ectopic glia formation, as it does not affect the tumour growth in the absence of ectopic glia. Hippo pathway also plays a role in promoting the formation of ectopic glia and tumour growth.

Our study of *pros*$^{-}$ and *nerfin-1*$^{-}$ tumour models in the context of transdifferentiation may extend our understanding of the biology of NBs and may shed light on GSC behaviours upon their transdifferentiation into different cell types. We can use the underlying mechanisms of these phenotypes to gain a better understanding of the transdifferentiation events at the molecular and cellular levels. As most genes and signalling pathways examined in this study are also found in human brain cancers, this study will enhance the knowledge of how cell fate changes can influence the tumour malignancy.

Declaration

This is to certify that

i. the thesis comprises only my original work towards the PhD except where indicated in the

Preface,

ii. due acknowledgement has been made in the text to all other material used,

iii. the thesis is less than 100,000 words in length, exclusive of tables, maps, bibliographies and appendices.

Hannah TRUONG Thi-Hong Hanh

July 2020

Preface

I would like to acknowledge the assistance of the following people who contributed to the work presented in this thesis.

First, thank you to Dr. Louise Cheng, who tirelessly assisted me with both developing ideas and performing experiments for this project. Louise helped me a lot to create various *Drosophila* strains and perform dissections for the preliminary data from which my project stems. I wish to thank Louise particularly for her assistance in the dissection of brain tissues for fluorescence-activated cell sorting experiments (data not shown). I am also grateful to Dr. Francesca Froldi for showing me how to collect and analyse data.

Thank you to Dr. Sheng Le (Olympus) and Dr. Ellie Cho (The University of Melbourne) who assisted me with collecting and analysing live-cell imaging data (**Video 3.1**, **Figure 3.12**).

I am very grateful to Prof. Markus Noll (The University of Zurich) for providing me the *pox^{n}-Gal4* stock (used in **Figure 3.10**, **3.30** and **3.33**). Thanks to Professor Andrea Brand for providing me the *grh-Gal4* stock that was used in many figures in this study (including **Figure 3.8** and **3.9**).

Acknowledgements

There are many people who helped me to make this PhD possible:

First and foremost, I want to thank and express my sincere appreciation to my principle supervisor Dr. Louise Cheng and my co-supervisor Dr. Francesca Froldi who gave me the opportunity to carry out this project. I remember the first time I saw an amazing picture of neural stem cell lineages within a fly brain under Louise's profile, and I was curious how fly brains were used to model human brain cancers – the research field that I am really interested in. I was interested by these fly model techniques and their findings on stem cell fate maintenance, and how they could improve my knowledge of intratumour microenvironments. I was very lucky to receive the chance to carry out this project about 'Cell-fate conversion (transdifferentiation) of cancer stem cells in brain tumour'. Louise and Francesca were always willing to lend a hand in experiments, to discuss results and to motivate me to pursue this research throughout the course of this PhD. Louise was more than just a supervisor, as she was always happy to manage my experiments whenever I could not continue conducting them. Francesca has a very good memory and gave me useful advice about experimental methods and technical solutions for data interpretation. My PhD could never have been possible without their help and support.

I am also grateful to all members of the Cheng and Harvey laboratories for providing overwhelming care, great support, and a joyful laboratory environment. Thank you also to the fellow students of the Cheng and Harvey laboratories including Qian Dong, Kellie Veen, Kat Michell, Abdul J. Saiful and Jonathan Pojer, for sharing many good conversations about your life and research experiences. My thesis could never have been completed without their support and inspiration.

My appreciation also goes to the core facilities at the Peter MacCallum Cancer Centre. The staff at the Center for Advanced Microscopy and Histology – in particular, Sarah Ellis, Chad Johnson, Metta Jana and Cameron Skinner – gave me great training on the

microscopes, optimisation of imaging parameters, and introduced me to microscopy experts. Thanks to the expert from Olympus – in particular, Sheng Le and Chun Song who helped me to achieve my live-cell imaging data. Thank you, Dr. Shane Cheung, for helping to optimise my live-cell imaging parameters. Thank you, Metta and Cameron, for approaching me whenever I needed help at the facilities. Thanks to the staff at the Advanced Centre for Cancer Cell Isolation and Flow Cytometry – in particular, Viki Milovac, Aydogan Elle and Ralph Rossi, who helped me with cell sorting. I would like to thank Gisela Mir Arnau at the Molecular Genomics core who helped me with sequencing. Thanks also to the Media Kitchen at Peter MacCallum Cancer Centre and the Insectary at the Bio21 Institute for making the *Drosophila* food used in my experiments.

Thanks must also be given to the Biological Optical Microscopy Platform at The University of Melbourne, for providing me with the greatest possible help to obtain data. I could never forget the help I received from Ellie Cho to process my very large live-cell imaging with Imaris, when I was hopelessly trying almost every software to process the data. I really appreciate The University of Melbourne and my supervisors for funding me with a Melbourne Research Scholarship to carry out this project.

I am also grateful to the Peter MacCallum Cancer Centre and the Victorian Comprehensive Cancer Centre for funding my electronic devices, software and overseas conference travel. My PhD could never have been fulfilled without the support from student mentors Caroline Owen, Niranga Nawagamuwa, Erika Cretney, and especially my mentor, Jessica Beach, who always quickly responded to answer my questions.

Finally, the completion of this study would not have been possible without the full support of my family and friends. Thank you all for chatting with me, taking me out for coffee, and listening to me on my pathway to pursuing a science career.

Table of Contents

Abstract I
Declaration III
Preface IV
Acknowledgements V
Table of Contents VII
List of Figures, Tables and Videos X
Common Abbreviations XIII
Chapter 1 1
Introduction 1
1.1. Cancer stem cells form as cancer cell of origin 1
1.2. *In vivo* and *in vitro* models to study CSC behaviours 1
1.3. *Drosophila* life cycle 4
1.4. *Drosophila* neuroblasts as a model to study stem-cell biology 6
1.4.1. *Drosophila* CNS 6
1.4.2. Asymmetric segregation of *Drosophila* cell-fate determinants during asymmetric cell division 10
1.4.3. Notch signalling plays an important role in neurogenesis 11
1.4.4. Key cell-fate determinants 12
1.4.4.1. Numb 12
1.4.4.2. Pros 13
1.4.4.3. Brat 14
1.4.5. Disruptions in asymmetric cell division can cause tumours 15
1.4.6. Maintenance of neuronal differentiation and tumorigenesis 16
1.4.6.1. Lola and Midlife crisis 16
1.4.6.2. Nerfin-1 17
1.5. Regulation of timing of *Drosophila* neurogenesis 18
1.5.1. Embryonic neurogenesis 19
1.5.2. Temporal patterning of embryonic NBs 19
1.5.3. Quiescence period of embryonic NBs 21
1.5.4. Postembryonic (secondary) neurogenesis and termination of NB division 21
1.6. Gliogenesis 23
1.6.1. Glial subtypes of *Drosophila* CNS 24
1.6.2. Glial determinant genes 25
1.6.3. Gliogenesis 26
1.7. Summary and thesis aims 29

Chapter 2 31
Materials and Methods 31
2.1. Fly husbandry 31
2.2. *Drosophila melanogaster* strains 31
2.3. Antibodies and immunohistochemistry 33
2.4. Image acquisition and processing 34
2.5. Clone/lineage volume measurements 34
2.6. Cell number quantifications and cell size measurements 35
2.7. Statistical analysis 35
Chapter 3 42
Results 42
3.1. Ectopic glia are found in dedifferentiation-driven tumours lacking Pros or Nerfin-1 42
3.2. Ectopic glia arise by the transdifferentiation of NBs upon loss of Pros or Nerfin-1 72
3.3. Temporal patterning regulates the formation of ectopic glia 98
3.3.1. Neuroblast temporal series is involved in the formation of ectopic glia 98
3.3.2. Glial determinant genes regulate the formation of ectopic glia to promote NB lineage growth upon Pros loss-of-function. 100
3.3.3. Notch signalling pathway promotes the growth of Pros/Nerfin-1-deficient lineages independently of ectopic glia formation. 101
3.3.4. Fibroblast growth factor (FGF) signalling pathway regulates *pros*$^{-}$ lineage growth through promoting ectopic glial formation. 103
3.3.5. Hippo signalling pathway is required for ectopic glia formation and Pros-deficient lineage growth. 104
Chapter 4 131
Discussion 131
4.1. Ectopic glia are found in dedifferentiation-driven tumours lacking Pros or Nerfin-1. 132
4.2. Ectopic glia arise by transdifferentiation of NBs upon loss of Pros or Nerfin-1 135
4.3. Temporal patterning regulates the formation of ectopic glia. 137
4.4. The glial determinant genes regulate the formation of ectopic glia, which in turn promote the growth of Pros-deficient lineages. 140
4.5. Future directions on the temporal progression in Pros-deficient lineages. 142
4.6. Implication of temporal patterning and glial determinant genes in the growth of Pros-deficient lineages and questions for future studies 143
4.7. Notch signalling regulates the growth of Pros-deficient lineages independently of ectopic glia 144
4.8. FGF signalling pathway regulates the formation of ectopic glia, which in turn promote the growth of Pros-deficient lineages. 145
4.9. Hippo signalling pathway may be implicated in the formation of ectopic glia 145
4.10. Implication of ectopic glia generated by NB transdifferentiation in promoting Pros-deficient lineage growth. 146

4.11. Final conclusions 148
References 153

List of Figures, Tables and Videos

Figures for Chapter 1:

Figure 1.1. The model of CSC hierarchy for brain cancers related to current studies in human and mice. 4
Figure 1.2. *Drosophila* life cycle. 6
Figure 1.3. Developing *Drosophila* larval CNS. 7
Figure 1.4. Asymmetric cell division of type I and type II NBs. 9
Figure 1.5. Location of OL NBs in the larval CNS and their mode of division. 9
Figure 1.6. Asymmetric segregation of protein complex during NB asymmetric division. 11
Figure 1.7. *Drosophila* neurogenesis timeline. 19

Figures for Chapter 2:

Figure 2.1. Two *UAS-pros*^{RNAi} lines used in this study both target all *pros* mRNA transcripts. 41

Figures for Chapter 3:

Figure 3.1. Loss of Nerfin-1 or Pros disrupts neuronal differentiation and gives rise to ectopic NBs in type I lineages during larval development. 52
Figure 3.2. Ectopic glia cells arise in type I *pros*$^{-}$ and *nerfin-1*$^{-}$ mutant clones during adult stages. 54
Figure 3.3. Glial clones derived from glial precursors during pupal and adult stages. 56
Figure 3.4. The number of ectopic glia in *pros*$^{-}$ clones increases with developmental timing. 58
Figure 3.5. The number of ectopic glia in *nerfin-1*$^{-}$ clones increases with developmental timing. 60
Figure 3.6. Ectopic glia display variable cell sizes. 61
Figure 3.7. Ectopic glia formation is common to most locations in *Drosophila* CNS upon *pros* or *nerfin-1* loss-of-function. 63
Figure 3.8. Ectopic glia are generated by type I NB lineages of the larval VNC upon *pros* knockdown via *grh-gal4>pros*$^{RNAi\ SH}$*(II)*. 65
Figure 3.9. Ectopic glia are generated by type I NB lineages of larval VNC upon *pros* knockdown via *grh>pros*$^{RNAi\ LH}$. 67
Figure 3.10. Ectopic glia were never recovered in *pox*^{n} lineages of the VNC upon *pros* knockdown. 69
Figure 3.11. Three different models of neural dedifferentiation-derived tumours to study ectopic glia formation. 71
Figure 3.12. Upon loss of Pros, NBs of type I lineages ectopically turn on Repo and transdifferentiate into ectopic glia in *Drosophila* VNC. 77
Figure 3.13. Additional example of NB-to-glia transdifferentiation in *pros*$^{-}$ clone located in superficial VNC section. 79
Figure 3.14. Some cells within *pros*$^{-}$ clones did not turn on Repo. 83
Figure 3.15. Ectopic glia arise by transdifferentiation of NBs upon *pros* loss-of-function (A-D), and *nerfin-1* loss-of-function (E-F) in type I lineages. 85

Figure 3.16. Ectopic glia in *pros* and *nerfin-1* – deficient clones/lineages express the NB marker Dpn. 87
Figure 3.17. Ectopic glia in *pros* and *nerfin-1* – deficient clone/lineages do not express type I NB marker Ase....88
Figure 3.18. Ectopic glia never express the neuronal marker Elav upon *pros* or *nerfin-1* loss-of-function. 90
Figure 3.19. CNS lipid droplets accumulate in $pros^{-}$ mutant clones and near ectopic glia from live-cell imaging. 92
Figure 3.20. CNS lipid droplets accumulate in $pros^{-}$ mutant clones and near ectopic glia from fixed-cell imaging. 94
Figure 3.21. CNS lipid droplets accumulate in $pros^{-}$ mutant clone and especially near ectopic glia. 95
Figure 3.22. Medulla NB temporal patterning might be active in Pros-deficient NB lineages. 107
Figure 3.23. Slp is ectopically expressed in the $pros^{-}$ clones in pupal VNC. 109
Figure 3.24. D is ectopically expressed in the Pros-deficient NB lineages and is required for the formation of ectopic glia, and the lineage growth. 111
Figure 3.25. Tll is ectopically expressed in the Pros-deficient NB lineages and is required for the formation of ectopic glia, and the lineage growth....113
Figure 3.26. Gcm is required for the formation of ectopic glia and for the growth of lineages lacking Pros. 115
Figure 3.27. Repo is required for the formation of ectopic glia and for the $grh>pros^{RNAi\ LH}$ lineage growth. 117
Figure 3.28. Repo is only required for the formation of ectopic glia, which in turn, promote the $pros^{-}$ clonal growth. 119
Figure 3.29. Notch is hyperactivated in $pros^{-}$ clone but not in the *wildtype* clone. 120
Figure 3.30. Notch signalling pathway is required but not sufficient to induce the formation of ectopic glia in NB lineages lacking Pros. 122
Figure 3.31. Notch signalling functions in $pros^{-}$ NB lineages to stimulate clonal growth independent of ectopic glia. 124
Figure 3.32. Notch signalling promotes $nerfin\text{-}1^{-}$ clonal growth independently of ectopic glia formation. 126
Figure 3.33. FGF signalling pathway is required but not sufficient to induce the formation of ectopic glia in NB lineages lacking Pros. 128
Figure 3.34. Hippo signalling pathway is required for the formation of ectopic glia and $grh>pros^{RNAi\ LH}$ lineage growth. 129

Figures for Chapter 4:

Figure 4.1. Hypothetical models for the transdifferentiation of NBs into ectopic glia upon loss of Pros or Nerfin-1 151
Figure 4.2. Hypothetical mechanism by which $pros^{-}$ NBs transdifferentiate into ectopic glia to promote the tumour growth. 153

Table for Chapter 2:

Table 2.1. Detailed descriptions of antibodies, reagents, fly strains and analysis software used in this study. 37

Videos for Chapter 3:

Video 3.1. Upon loss of Pros, NBs of type I lineages ectopically turn on Repo and transdifferentiate into ectopic glia in *Drosophila* VNC. 96
Video 3.2. Additional example of NB-to-glia transdifferentiation in *pros*$^{-}$ clone located in a superficial VNC section. 96
Video 3.3. Some cells within *pros*$^{-}$ clones did not turn on Repo. 97
Video 3.4. CNS lipid droplets accumulate in *pros*$^{-}$ mutant clones and especially, near ectopic glia. 97

Common Abbreviations

AAH	After adult hatching
AEL	After egg laying
AML	Acute myeloid leukaemia
APF	After pupal formation
aPKC	Atypical protein kinase C
ASCL1	Achaete-scute complex 1
Ase	Asense
BDSC	Bloomington *Drosophila* Stock Centre
brat	*brain tumour*
Br-C	Broad Complex
Cas	Castor
CB	Central brain
Chinmo	Chronologically inappropriate morphogenesis
CNS	Central nervous system
CSC	Cancer stem cell
D	Dichaete
DL	Dorsal lateral
Dll	Distalless
DM	Dorsal medial
Dpn	Deadpan
EdU	Ethynyl deoxyuridine
Elav	Elavi
en	*engrailed*
Ey	Eyeless
FBS	Foetal Bovine serum
FGF	Fibroblast growth factor
FoxO	Forkhead box class O
GB	Glioblast
gcm	*glial cells missing*
GFAP	*glial fibrillary acidic protein*
GFP	Green fluorescent protein
Glide	Glial cell deficient
GMC	Ganglion mother cell
Grh	Grainyhead
grh-gal4	*grainyhead-gal4*
GSC	Glioblastoma stem cell
Gαi	G-iα65A
Hth	Homothorax
Htl	Heartless
Imp	IGF-II mRNA-binding protein
INP	Intermediate neural progenitor
Insc	Inscuteable
INSM-1	Human insulinoma associated-1
IOA	Inner optic anlagen
IPC	Inner proliferation center

IQR	Interquartile range
Klu	Klumpfuss
Kr	Kruppel
L'sc	Lethal of scute
L1	First instar
L2	Second instar
L3	Third instar
LOF	Loss-of-function
lola	*longitudinals lacking*
MARCM	Mosaic analysis with a repressive cell marker
Mira	Miranda
mlc	*midlife crisis*
NB	Neuroblasts
NE	Neuroepithelium
nerfin-1	*nervous finger-1*
NGB	Neuroglioblast
OL	Optic lobe
OPC	Outer proliferation center
PBS	Phosphate-buffered saline
PenStrep	Penicillin-Streptomycin solution
pH3	Phospho-Histone H3
Pins	Partner of Inscuteable
PntP2	PointedP2
pros	*prospero*
Prox1	*Prospero-related homeobox 1*
repo	*reversed polarity*
RFP	Red fluorescent protein
ROI	Region of interest
SEM	Standard error of the mean
Slp	Sloppy paired
Svp	Seven-up
SVZ	subventricular zone
TF	Transcription factor
Tll	Tailless
tOPC	Tips of the OPC
Tor	Target of rapamycin
TRIM2	Tripartite Motif Protein 2
TTF	Temporal transcription factor
TUNEL	Terminal deoxynucleotidyl transferase dUTP nick end labelling
VDRC	Vienna *Drosophila* Resource Centre
VNC	Ventral nerve cord
wts	*warts*
Yki	Yorkie

Chapter 1

Introduction

1.1. Cancer stem cells form as cancer cell of origin

Cancer stem cells (CSCs) that possess stem-cell properties similar to normal stem cells are widely used to explain tumour formation in many cancer types. The CSCs generate a replica of itself (CSC) which can migrate to distant sites and form new tumours, and a downstream progenitor cell (non-CSC) which can differentiate into various cancer cell lineages (Bradshaw et al., 2016; Lathia et al., 2011). The theory that cancer arises from highly tumorigenic CSCs is evidenced by the findings of CSCs in various tumour types; including brain (Dirks, 2010; Kong, 2012; Lasky et al., 2009; Lathia et al., 2011), breast (Bozorgi et al., 2015; McDermott and Wicha, 2010; Velasco-Velázquez et al., 2011), lung (Alamgeer et al., 2013; Codony-Servat et al., 2016; Hardavella et al., 2016; Miyata et al., 2015; Templeton et al., 2014), and colon cancers (Khalek et al., 2010; Shimokawa et al., 2017; Vaiopoulos et al., 2012). One line of evidence comes from studies of acute myeloid leukaemia (AML) in which only a rare subset of 1% or less of the total dissociated cells could induce leukaemia when transplanted into immunodeficient mice (Bonnet and Dick, 1997; Lapidot et al., 1994; Visvader and Lindeman, 2008). Moreover, this cell population was able to self-renew as well as reconstitute the full spectrum of cells seen in AML (Lapidot et al., 1994). Several studies of brain CSCs proposed that these cells constitute only 1% of a benign tumour, and only 30% of malignant tumour cells (Kobayashi and de Noronha, 2014). Thus, new cancer therapies should directly target these rare but important CSCs (Shimokawa et al., 2017; Zhang et al., 2014).

1.2. *In vivo* and *in vitro* models to study CSC behaviours

Human brain tumours, such as pediatric medulloblastoma and adult glioblastoma, are usually malignant and refractory to conventional therapies, leading to poor patient

prognosis and low survival rate of less than one year (Holland, 2000; Maher et al., 2001; Northcott et al., 2019; Zhu and Parada, 2002). Medulloblastoma is the most common malignant brain tumour in children, accompanied with the accumulation of transformed neuronal progenitor cells with unrestricted proliferative abilities (Packer and Vezina, 2008; Read, 2011). In adults, the most common and aggressive form is glioblastoma (Holland, 2000; Taylor et al., 2019; Witte et al., 2009), whereby glial cells (astrocytes and oligodendrocytes) or their progeny dedifferentiate and acquire stem cell-like properties (Bachoo et al., 2002; Lee et al., 2018; Lindberg et al., 2009; Marumoto et al., 2009; Uhrbom et al., 2002; Zong et al., 2012). Glioblastoma has been shown to be induced from neural stem and progenitor cells localised at the subventricular zone (SVZ) in mice (Bachoo et al., 2002; Gimple et al., 2019; Sanai et al., 2005; Zhu et al., 2005), and interestingly, this brain region harbours neural stem cells (NSCs) with astrocyte-like characteristics in humans (Doetsch et al., 1999; Lim et al., 2007; Quiñones-Hinojosa et al., 2006; Sanai et al., 2004) favouring the model SVZ-derived NSCs are the cell-of-origin for glioblastoma (Gimple et al., 2019; Lee et al., 2018; Singh et al., 2003).

Normal NSCs asymmetrically self-renew and generate multiple neural lineages (**Figure 1.1**) (Garnier et al., 2019; Singh et al., 2003). According to the CSC hierarchy concept (Garnier et al., 2019; Gimple et al., 2019), glioblastoma stem cells (GSCs) arise by neoplastic transformation of NSCs. Like normal NSCs, GSCs exhibit highly proliferative capacity to self-renew and differentiate into multiple lineages, including neurons, astrocytes or oligodendrocytes (**Figure 1.1**) (Garnier et al., 2019). GSCs only make up a small fraction of tumour cells but contribute disproportionately to malignant growth and therapy resistance (Galli et al., 2004; Johannessen et al., 2009; Singh et al., 2003). In addition, tumour cells within glioblastoma are plastic and can dedifferentiate to acquire GSC-like state, and therefore GSC cell plasticity poses to be an attractive target for therapy (Lee et al., 2016). Studies in mouse models show that differentiated neurons or astrocytes can revert back into stem-cell-like state to initiate malignant tumourigenesis (**Figure 1.1**) (Feliciano, 2012; Friedmann-Morvinski et al., 2012). During tumour progression, GSCs can also potentially transdifferentiate into other cell lineages distinct from the original lineages that give rise to tumour. GSCs have been

found to transdifferentiate into vascular endothelial cells to support angiogenesis (**Figure 1.1**) (Baisiwala et al., 2019; Dong et al., 2011; Ricci-Vitiani et al., 2010; Wang et al., 2010), and vessel-like tumour cells to form microvascular channels (Scully et al., 2012). These complex characteristics of GSCs complicate current treatments, as they are responsible for intratumour heterogeneity.

Cultured *in vitro* glioblastoma cell lines and *in vivo* mouse models have been employed to better understand important aspects of glioblastoma. However, these models still have some technical limitations. The culture techniques could not retain full genetic alterations and phenotypes of tumour cells, as well as the niche in tumour microenvironments (Lathia et al., 2015; Read, 2011). In mouse models, glioblastoma can be induced by transplanting human cell lines into mouse brains or using transgenic mice with brain tumours (Alcantara Llaguno et al., 2009; Read, 2011; Read et al., 2009; Ward et al., 2009). Although this reflects the interaction between tumour and brain tissue, limited host genotypes and lack of long term ability to study these tumours limits the use of mouse models (Read, 2011).

Drosophila melanogaster is one of the most common models for studying genetics, developmental biology and human diseases, such as cancers. *Drosophila* central nervous system (CNS) has been extensively used to study genetic, cellular and molecular mechanisms underlying NSC behaviours and brain tumourigenesis (Hakes and Brand, 2019; Halder and Mills, 2011; Mirzoyan et al., 2019; Rudrapatna et al., 2012). *Drosophila* NSCs renew themselves and produce differentiating daughter cells; however, defective daughter cells can revert to a stem cell-like state (dedifferentiation) and lead to tumourigenesis (Januschke and Gonzalez, 2008). Loss of function of genes regulating asymmetric cell division and differentiation; including *brain tumour* (*brat*) (Bello et al., 2006), *prospero* (*pros*) (Choksi et al., 2006; Narbonne-Reveau et al., 2016; Shaw et al., 2018), *nervous finger-1* (*nerfin-1*) (Froldi et al., 2015b; Vissers et al., 2018) in NSC lineages has allowed dedifferentiation of neurons or immature progenitor cells into ectopic NSCs, resulting in malignant tumours. As neuronal dedifferentiation into GSCs is a feature of glioblastoma (Friedmann-Morvinski et al., 2012), *Drosophila* brain

tumour models has the potential to recapitulate some genetic and phenotypic aspects of this human malignancy and improve our understanding of GSCs.

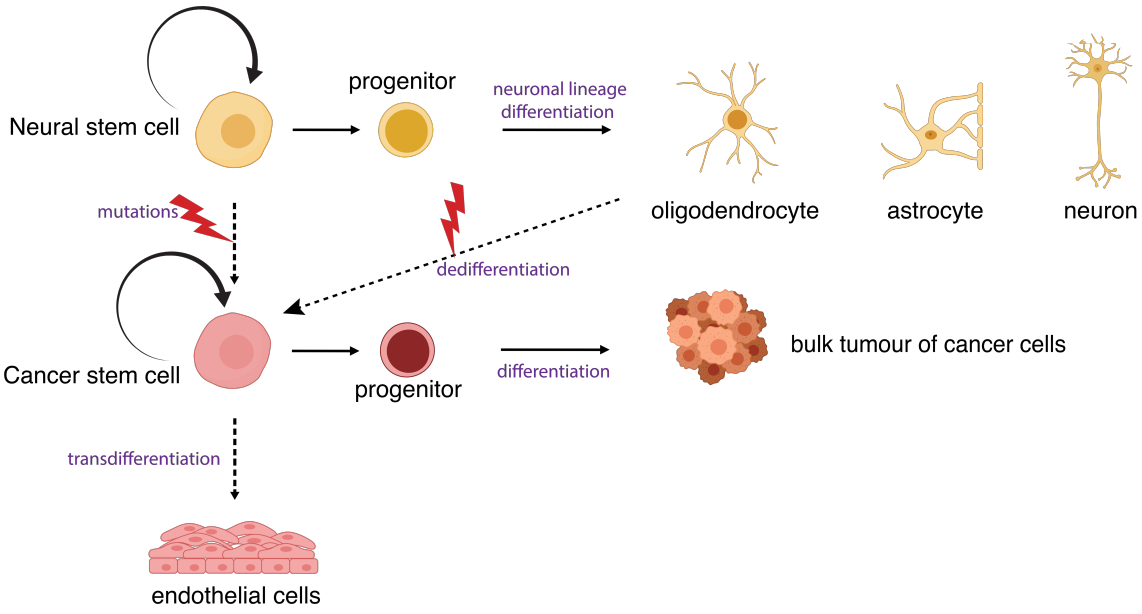

Figure 1.1. The model of CSC hierarchy for brain cancers related to current studies in human and mice. Normal NSCs asymmetrically self-renew and generate neurons, astrocytes and oligodendrocytes. GSCs (a type of CSCs) are derived from NSCs after acquisition of some mutations. Like NSCs, GSCs show stemness by renewing themselves and generating multiple neural lineages. The tumour cells are plastic and can dedifferentiate back into a stem cell-fate. During tumour progression, GSCs can also potentially transdifferentiate into other stem cell types, distinct from the original lineages, to produce other cells such as endothelial cells.

1.3. *Drosophila* life cycle

Drosophila melanogaster, also known as the fruit fly, is a model of choice in this study. They belong to a species of the genus *Drosophila* and of the family *Drosophilidae* (Hales et al., 2015). The *wildtype Drosophila* life span varies with the temperature (Deepa et al., 2009), which averages about 45 days at 25°C and 30% humidity (Oxenkrug, 2010). Their developmental time period from eggs to adults decreases as temperature increases, which lasts for 19 days at 18°C, 8.5 days at 25°C, and 7 days at 28°C.

Drosophila mate and breed at the ratio of 3 females to one male on food containing corn, dextrose, sugar and yeast extract (Deepa et al., 2009). After mating, females start to lay eggs onto their nesting food source. Each adult female can lay a lot of fertilised eggs during a life cycle. The fruit fly's life cycle (**Figure 1.2**) begins when the female lays her eggs and ends when her first offspring hatch. The life cycle is complete in approximately 10 days (25ºC), and contains four developmental stages: eggs, larvae, pupae and adults (Hales et al., 2015). The *Drosophila* egg is about 0.5 mm long (Deepa et al., 2009). Within a day after fertilisation, the egg hatches into a larva (L1) which burrows into and feeds on the nesting food (Jennings, 2011). The larval body is organised into head segments, thoracic segments and abdominal segments (Deepa et al., 2009). The first-instar larva moults within one day and then develops into second (L2) and third instar (L3) at 2 day and 3 days after hatching. They stay at third-instar larval stage for 2 days and then wander out of the food source to pupate. *Drosophila* live in the pupal case for 4 to 5 days (Hales et al., 2015) and finally hatch into adult flies. The newly hatched flies start to mate after the next 10 hours (Deepa et al., 2009), and the life cycle begins again. In association of these developmental progression is the process of neurogenesis.

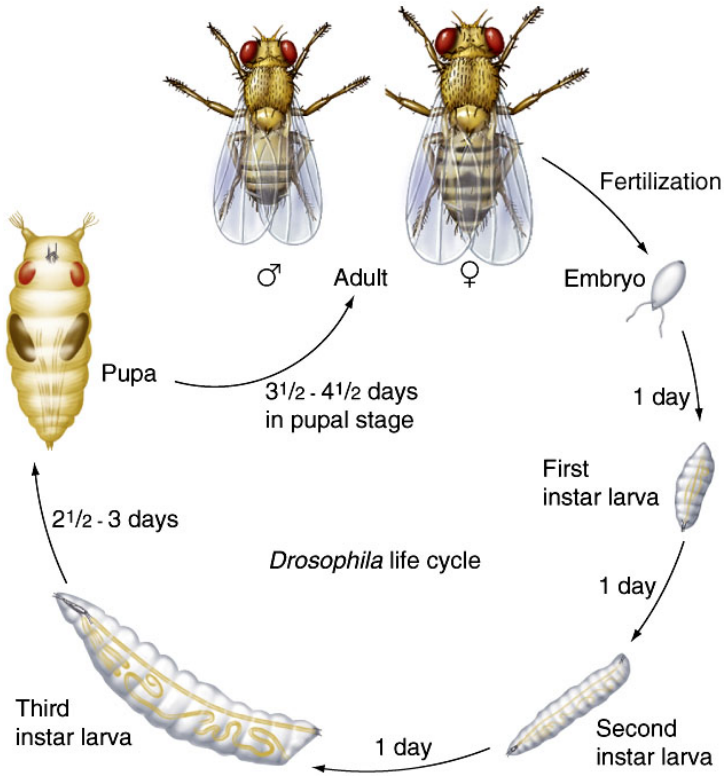

Figure 1.2. *Drosophila* life cycle. The life cycle begins when a female lays her eggs and ends when her offspring hatch. The whole life cycle consists of four developmental stages: egg (embryo), larva (first instar, second instar, and third instar larva), pupa, adult (http://skenderianscience.weebly.com/drosophila-melanogaster.html).

1.4. *Drosophila* neuroblasts as a model to study stem-cell biology

1.4.1. *Drosophila* CNS

The *Drosophila* CNS arises from neural stem and progenitor cells. The developing *Drosophila* CNS contains a large number of different neural stem cell lineages, and can serve as an excellent model system to study certain aspects of stem cell biology (Harding and White, 2018; Homem and Knoblich, 2012). The developing *Drosophila* CNS (**Figure 1.3**) can be subdivided into three areas: 1) the central brain (CB) which contains mushroom bodies responsible for olfactory learning and memory (Akalal et al., 2006), 2) optic lobes (OLs) which develop into adult visual system, and 3) the ventral nerve cord (VNC) which is subdivided into 3 thoracic and 9 abdominal neuromeres (Froldi et al., 2015a; Saini and Reichert, 2012). The *Drosophila* neural stem cells, called neuroblasts (NBs), possess the capacity to undergo multiple rounds of asymmetric cell division (Chia et al., 2008; Homem and Knoblich, 2012; Kelsom and Lu, 2012; Prehoda, 2009), and therefore, can provide us with key insights into the mechanisms which regulate asymmetric stem cell division. Mitotic NB divides asymmetrically to self-renew, and also produces a population of differentiated progeny (differentiation) that constitute the CNS (Froldi et al., 2015b). In the CB, NBs are classified into type I NBs, type II NBs and mushroom body NBs based on their location and lineage features (Homem and Knoblich, 2012) (**Figure 1.3**). Type I NBs are the most common in the CB and are also found in VNC (Froldi et al., 2015a; Saini and Reichert, 2012). In the CB, type I NBs are found in both dorsal and ventral surfaces (Homem and Knoblich, 2012); whereas, type II NBs are only found on the dorsal surface and mushroom body NBs are locate in the post anterior region of the CB (Boone and Doe, 2008; Homem and Knoblich, 2012).

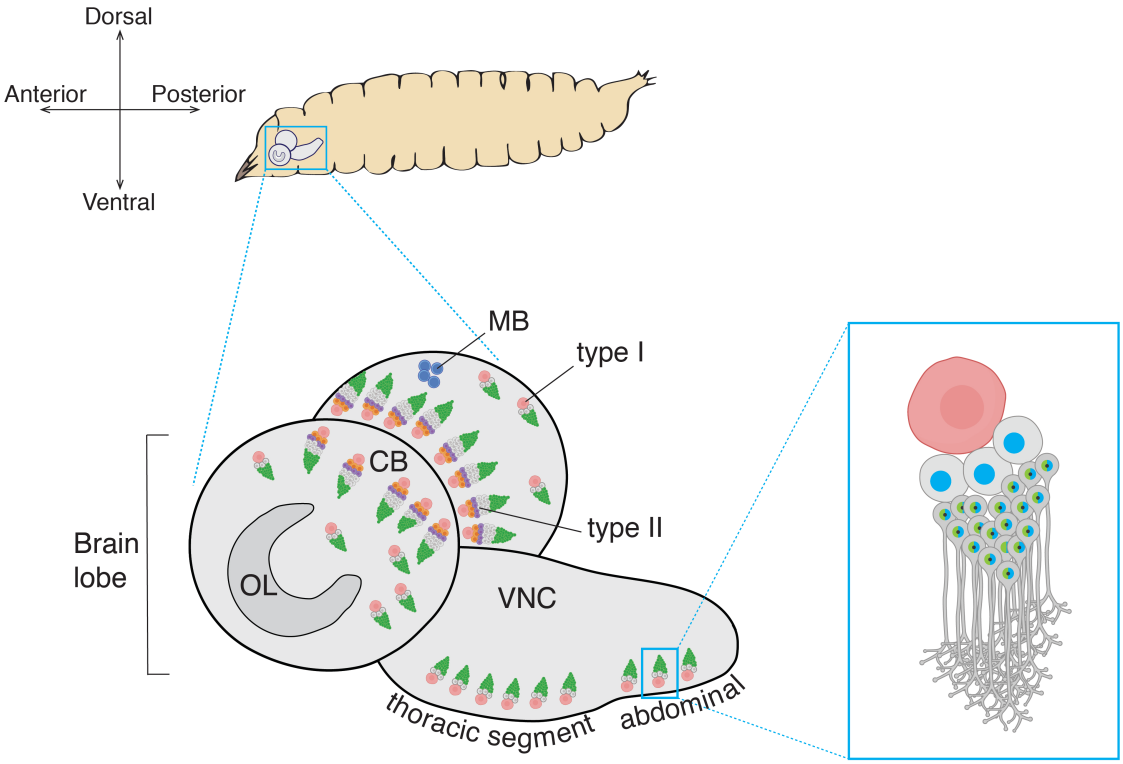

Figure 1.3. Developing *Drosophila* larval CNS. The developing larval CNS is organised into three parts: 1) the central brain (CB), 2) paired optic lobes (OLs) which are located laterally to the brain hemispheres and develop into adult visual system, and 3) the ventral nerve cord (VNC) which is subdivided into 3 thoracic and 9 abdominal neuromeres (Froldi et al., 2015a; Saini and Reichert, 2012). In the CB (posterior of the CNS), all 3 types of NBs; namely, type I, type II, and mushroom body (MB) NBs; are found. Only type I NBs are found in VNC (anterior of the CNS). Modified from Homem and Knoblich (2012).

Upon each division, a CB type I NB expressing transcription factors Deadpan (Dpn) and Asense (Ase) (Walsh and Doe, 2017) to gives rise to (1) a new NB; which retains NB characteristics and continues to self-renew; and (2) a ganglion mother cell (GMC; Dpn^{-} Ase^{+}), that, in turn, divides symmetrically once only to generate 2 terminally differentiating neurons or glial cells (Homem and Knoblich, 2012; Joy et al., 2015) (**Figure 1.4A**). Type II NBs [expressing Dpn but not Ase (Walsh and Doe, 2017)] also self-renew, but unlike type I NBs, they generate an immature self-renewing intermediate neural progenitor (INP), which must go through a maturation process, to become mature INPs (Bayraktar et al., 2010; Homem and Knoblich, 2012; Homem et al., 2015) (**Figure 1.4B**). The mature INPs [Dpn^{+} Ase^{+} (Walsh and Doe, 2017)] then

divide asymmetrically several times to self-renew, and generate a GMC that divides symmetrically once to form two neurons or glia (Bayraktar et al., 2010; Homem et al., 2015). Although there are only 8 lineages in each CB lobe (by comparison to 95 type I NB lineages) (Bayraktar et al., 2010; Carney et al., 2012; Viktorin et al., 2013), type II NBs generate much more neurons than type I NBs via amplification of neural proliferation via its intermediate progenitor cells (Bayraktar et al., 2010; Boone and Doe, 2008). In addition, neural cells produced by type II NBs contribute towards the majority of neuropils of the adult CB (Bayraktar et al., 2010; Homem and Knoblich, 2012). Therefore, different proliferative activity of various NB lineages can considerably affect the number of neurons produced. There are only four mushroom body lineages in the CB, and they all contain mushroom body interneurons called Kenyon cells (Ito and Hotta, 1992; Lee, 2017). Mushroom body NBs renew themselves and produce a GMC that give rise to two identical Kenyon cells (Lee, 2017). By contrast, in developing OLs, another type of neural progenitor cells, neuroepithelium (NE) cells, initially divide symmetrically and form two different proliferation centers in the OLs, called an outer optic anlagen, outer proliferation center [OPC]) and an inner optic anlagen (IOA, inner proliferation center [IPC]) (Hofbauer and Campos-Ortega, 1990; Morante et al., 2013; Yasugi et al., 2008) (**Figure 1.5A**). The NE cells of the IPC then give rise to a large NB pool (Hofbauer and Campos-Ortega, 1990; White and Kankel, 1978) (**Figure 1.5B**). The OL NBs (also called medulla NBs) then divide asymmetrically to re-new, and generate GMCs that further differentiate into postmitotic neuronal progeny (Brand and Livesey, 2011; Egger et al., 2007; Egger et al., 2011; Yasugi et al., 2008). In contrast the VNC consists of only type I NBs (Skeath and Thor, 2003).

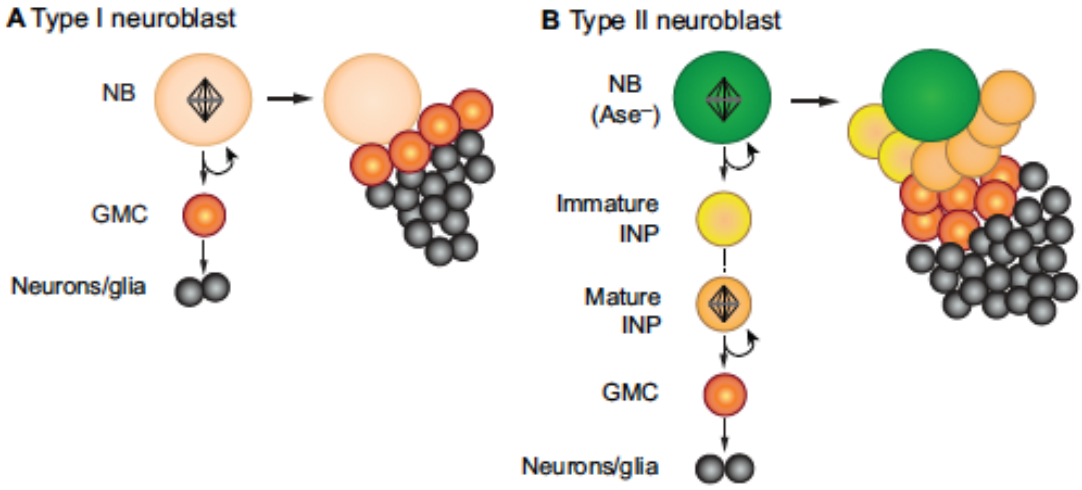

Figure 1.4. Asymmetric cell division of type I and type II NBs. (**A**) Upon a division, a type I NB renews itself and buds off a GMC (orange), that in turn, divides symmetrically once only to generate 2 terminally differentiating neurons or glial cells (black). (**B**) A type II NB generates an immature INP (yellow), which then transforms into a mature INP (light orange). The mature INP then divides asymmetrically several times to self-renew, and to generate a GMC that divides symmetrically once to form two neurons or glia. Adapted from Homem and Knoblich (2012).

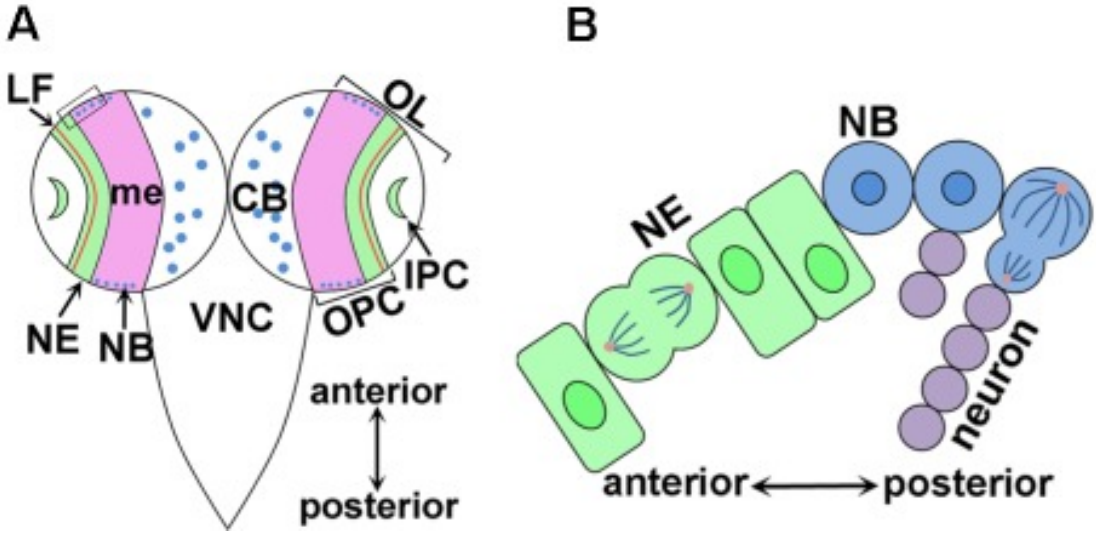

Figure 1.5. Location of OL NBs in the larval CNS and their mode of division. (**A**) OL NBs develop into adult visual system. (**B**) In developing OLs, NE initially divide symmetrically to give rise to a large NB pool. The OL NBs then divide asymmetrically

a few times to renew, and generate GMCs that further differentiate into only postmitotic neuronal progeny. Adapted from Chen et al., 2014.

1.4.2. Asymmetric segregation of *Drosophila* cell-fate determinants during asymmetric cell division

The molecular mechanism underlying asymmetric cell division involves asymmetric localisation of cell fate determinants. During mitosis, cell fate determinant proteins are asymmetrically segregated into the distinct apical and basal cortical domains of NBs (Homem and Knoblich, 2012) (**Figure 1.6**). Two protein complexes form to define cell polarity and establish the apical-basal axis for mitotic spindle orientation (Homem and Knoblich, 2012; Saini and Reichert, 2012). The two protein complexes are: 1) the apical complex, which is partitioned into the daughter NB, and 2) the basal protein complex, which is inherited by GMC (Neumüller and Knoblich, 2009; Saini and Reichert, 2012). The apical complex, also known as Par complex, maintains stem cell identity and promotes self-renewal in the daughter NB. The members of Par complex; including atypical protein kinase C (aPKC), and PDZ domain containing proteins Par3 and Par6 (Neumüller and Knoblich, 2009; Wu et al., 2008); recruit Inscuteable (Insc) which is linked to Pins (Partner of Inscuteable)/Mud/Gαi (G-iα65A) complex at the apical cell cortex (Homem and Knoblich, 2012; Kraut and Campos-Ortega, 1996; Kraut et al., 1996; Wu et al., 2008). The interactions between these protein complexes at the cell cortex mediate the proper mitotic spindle orientation, and trigger a series of phosphorylation events to direct the cell fate determinants to the basal cell cortex (Homem and Knoblich, 2012). The basal protein complex consists of cell fate determinants Numb, Miranda (Mira), and Mira cargo proteins Pros, Brat, Staufen (Doe, 2008; Homem et al., 2015); transiently accumulate into a basal cortical crescent in the NBs, and is subsequently localised into the GMC. There it inhibits self-renewal and promotes neuronal differentiation (Saini and Reichert, 2012).

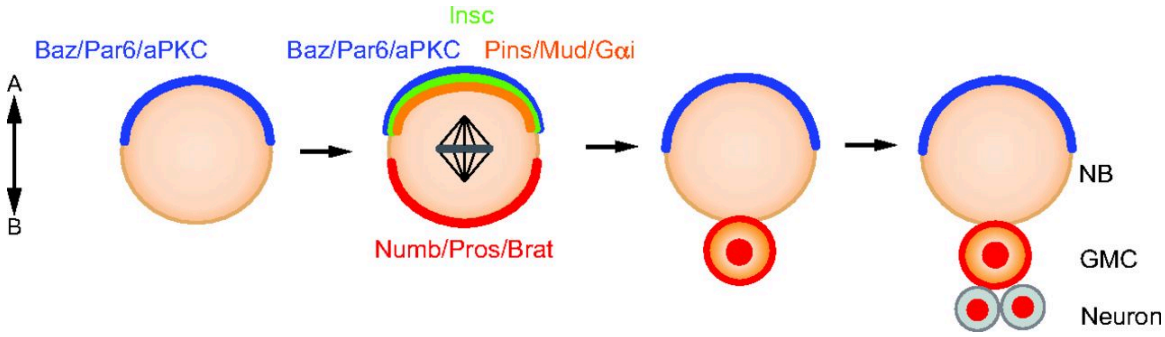

Figure 1.6. Asymmetric segregation of protein complex during NB asymmetric division. The apical complex (aPKC/Par3/Par6; blue curve) is partitioned into the large daughter NB to maintain stem cell identity and promote self-renewal. The basal complex (Numb, Mira, Pros, Brat; red curve) is inherited by small GMC to inhibit the self-renewal and promote neuronal differentiation (Homem and Knoblich, 2012).

1.4.3. Notch signalling plays an important role in neurogenesis

Notch signalling is a key regulator of a majority of developmental processes in *Drosophila*, including neurogenesis in developing nervous system. The Notch signalling pathway has been shown to modulate the balance between NB self-renewal and differentiation in NB asymmetric cell division (Gómez-López et al., 2014; Kelsom and Lu, 2012). Notch is a transmembrane receptor protein which can be activated by the ligand Delta (Parks et al., 2006). Notch target genes include the transcription factor Dpn essential for NBs self-renewal (San-Juán and Baonza, 2011). Enhancing Notch activity in NBs, by either upregulating the active Notch intracellular domain or silencing the Notch inhibitor Numb, expands the pool of CB NBs and inhibits neuronal differentiation (Lee et al., 2006a; Wang et al., 2006). By contrast, repressing Notch activity in the larval CNS reduces the number of CB type I NB, and causes a complete loss of type II NBs (Bowman et al., 2008; Homem et al., 2015), but has no effects on VNC NB number (Almeida and Bray, 2005). In the OLs, Notch signalling plays an important role in maintaining the initial NE cell population and inhibiting the wave of NE differentiation into OL NBs (Artavanis-Tsakonas et al., 1991; Doe, 2008). The level of Notch activity and the expression level of proneural genes regulate NE differentiation in the OLs (Doe, 2008; Kageyama et al., 2008). Notch also functions in vertebrate neurogenesis, and must be antagonised by Numb to promote neural differentiation of neural progenitor cells (Zilian et al., 2001).

1.4.4. Key cell-fate determinants

1.4.4.1. Numb

In *Drosophila*, the trans-membrane protein Numb is an inhibitor of Notch signalling pathway (Couturier et al., 2012; Schweisguth, 2004) and also a key target of the Par complex during NB asymmetric division (Prehoda, 2009). The basal accumulation of Numb is a result of its phosphorylation by aPKC on the apical side of the mitotic NB (Neumüller and Knoblich, 2009). In particular, during mitosis, aPKC directly phosphorylates the positively charged N terminus of Numb (Smith et al., 2007), neutralising the charges of this region (Neumüller and Knoblich, 2009) which releases Numb from the plasma membrane (Knoblich et al., 1997). Release of Numb from the apical NB cortex allows its asymmetric localisation on the opposite site of the plasma membrane (Wirtz-Peitz et al., 2008) where it then is partitioned into the daughter GMC. Numb is a main regulator of Notch-Delta signalling required for stem cell division (Frise et al., 1996).

After its localisation into the differentiating GMC, Numb induces endocytosis of the Notch receptor to repress self-renewal and stimulate cell-cycle exit (Homem and Knoblich, 2012). In NBs, loss of numb allows upregulation of Notch signalling and results in tumours that favour the generation of ectopic NBs over the formation of differentiated neurons (Lee et al., 2006a; Neumüller and Knoblich, 2009; Wang et al., 2006) and give rise to uncontrolled proliferation and tumour-like overgrowth (Kelsom and Lu, 2012). The vertebrate homologs of Numb have also been found to play a role in neurogenesis (Johnson, 2003), but their precise roles in NSC self-renewal remain to be clarified. During brain development in the vertebrate CNS, the protein product of *numb* is also asymmetrically localised at the cortical side of mitotic progenitor cells, and is also inherited by a single daughter cell that commits to a progenitor fate to promote neurogenesis (Zhong et al., 2000). Overexpression of *numb* triggers the formation of neuronal progeny; whereas, repression of Numb allows more cells to adopt a progenitor cell fate (Zhong et al., 2000). In mouse brain, Numb enhances Notch signalling by stabilising Notch1 intracellular domain, and is required for maintaining neural progenitor cell pool (Luo et al., 2019). Downregulation of Numb causes decreased

expression of endogenous cleaved Notch1 (Luo et al., 2019). The altered Numb-mediated control of Notch signalling also has implications for many human diseases, including cancer (Pece et al., 2004).

1.4.4.2. Pros

The homeodomain transcription factor Pros is one of the cell fate determinants that is inherited by the GMCs. *pros* gene is transcribed and translated in the NBs (Broadus et al., 1998; Hirata et al., 1995), and is exported out of the nucleus by the guanine-nucleotide exchange factor called Bj1 (Joy et al., 2015) during interphase. Bj1 assists the translocation of Pros RNA and proteins through the nuclear pore complex (Joy et al., 2015; Wu et al., 2019). Inactive Pros accumulates in the NB cytoplasm, then moves basally during mitosis, and is subsequently segregated into the GMC with the aid of the adapter protein Mira (Hirata et al., 1995; Ikeshima-Kataoka et al., 1997; Matsuzaki et al., 1998; Shen et al., 1997). In fact, Pros is one of the Mira cargo proteins and is asymmetrically localised through binding to Mira (Lee et al., 2006b). In addition, the *pros* mRNA is asymmetrically localised through another Mira cargo protein, called Staufen (Lee et al., 2006b; Matsuzaki et al., 1998). At the end of mitosis, Pros is accumulated exclusively in the cortex of the budding GMC, and translocates to the nucleus of the GMC (Wodarz et al., 1999) when Mira is degraded (Choksi et al., 2006; Hirata et al., 1995; Knoblich et al., 1995). There it inhibits cell-cycle genes and activates terminal differentiation genes (Saini and Reichert, 2012). However, not all NBs use the same cell division mechanism. Bowman and colleagues (2008) have discovered that type II NBs never express Pros, but asymmetrically divide and generate Pros-expressing GMCs, which then differentiate into neurons (Bowman et al., 2008).

Pros acts as a cell fate determinant in GMCs and plays important roles in inducing neuronal differentiation and promoting cell cycle exit of NBs. Pros acts as a cell fate determinant, which controls the transition from NB self-renewal to differentiation (Choksi et al., 2006). Pros directly represses NB genes; such as stem cell fate genes and cell cycle genes; and activates transcription of neuronal differentiation genes in GMCs (Choksi et al., 2006; Li and Vaessin, 2000). In the absence of Pros, GMCs fail to inhibit NB gene expression, and show increased mitotic activity and finally revert to stem cell-

like fate, instead of committing to a differentiated, neuronal fate (Choksi et al., 2006; Kelsom and Lu, 2012). Therefore, a *pros* mutant clone contains several GMCs and a lot of ectopic NBs, with uncontrolled proliferative ability. Thus, *pros* functions as tumour suppressor gene in this context. In addition to regulating the behavior of GMCs, Pros also promotes the NB cell cycle exit in the NB before these cells enter quiescence at the end of embryonic neurogenesis (Lai and Doe, 2014), and before NBs terminate proliferation at end of postembryonic neurogenesis (Yasugi and Nishimura, 2016) (see section **5.2**). In these cases, transient localisation of Pros into the NB nucleus induces its terminal differentiation.

The mammalian Pros homologue Prox1 (Prospero-related homeobox 1), acts in a similar fashion to stop division and promote differentiation of progenitor cells in many different regions of the brain (Choksi et al., 2006; Li and Vaessin, 2000). Furthermore, Prox1 regulates the transition from multipotent precursor cells to more differentiated cells (Choksi et al., 2006). Therefore, the Pros function in maintaining the balance between stem self-renewal and neuronal differentiation is conserved in veterbrates and flies.

1.4.4.3. Brat

Brat is another cell fate determinant that restrains cell growth and promotes differentiation in the GMC. The *Drosophila brat* gene encodes one of the NHL domain proteins which are involved in regulating the balance between growth and differentiation in specific regions (Arama et al., 2000). Brat co-localises with Mira to be partitioned into the GMC (Betschinger et al., 2006; Lee et al., 2006b), through the direct interaction between its NHL domain and the Mira cargo domain (Lee et al., 2006b). In the GMC, Brat also collaborates with Pros to specify GMC fate by inhibiting NB genes and inducing neuronal differentiation genes (Betschinger et al., 2006).

Brat has several identified but still poorly understood functions. Firstly, Brat regulates the translation of *hunchback* (*hb*) which is expressed during embryogenesis. Brat targets the 3' untranslated region of *hb* mRNA through the interaction of RNA-bound Pumilio/Nanos complex (Sonoda and Wharton, 2001). This interaction is mediated by

the Brat NHL domain and finally results in the translational repression of *hb* gene. The repression of *hb* blocks the production of a subset of embryonic neurons. The second known function of Brat is to downregulate *Drosophila* transcription factor Myc in the GMC to inhibit cell growth and proliferation (Betschinger et al., 2006). *Drosophila* Myc protein is a central regulator of DNA replication and protein synthesis necessary for the control of various stem cell types, including NBs. In addition, Brat limits the nuclear transport of Notch intracellular domain in NBs to attenuate Notch signalling, and hence, to regulate NB proliferation (Mukherjee et al., 2016). Furthermore, several studies suggest that Brat also regulates Pros levels (Bello et al., 2006) and directly binds to Mira (Betschinger et al., 2006). Similar to *pros*, loss of *brat* causes INPs to adopt a NB cell fate and to continue dividing, leading to the formation of larval brain tumours (Bello et al., 2006; Lee et al., 2006b; Reichardt et al., 2018).

At least three human homologues of *brat* have been identified and are considered as tumour suppressor genes in human. These human homologues are called Tripartite Motif Protein 2 (TRIM2), TRIM3, and TRIM32 which all belong to the same TRIM-NHL family of stem cell proliferation regulators (Boulay et al., 2009; Loedige et al., 2014). Among them, TRIM3 is the most characterised and is located in 11p15.4, within the loss of allelic heterozygosity region that is frequently observed in many cancer types, including brain, ovary and breast tumours (Boulay et al., 2009).

1.4.5. Disruptions in asymmetric cell division can cause tumours

Neural stem cells are involved in neurogenesis, and disruption of their differentiation program may promote tumour formation in the CNS. Upon division, stem cells have to continuously balance the stem cell self-renewal with production of progeny (Froldi et al., 2015a). If the NBs fail to maintain this balance, tumours will form. So far, from previous sections of this review, brain tumours can potentially arise from the reversion of GMCs or INPs to NBs due to dysregulated asymmetric cell division involving *numb*, *mira*, *pros*, or *brat*. After being transplanted into *wildtype* flies, the tissues mutant for each of these genes can induce neoplastic tumours and metastases, and finally kill the hosts (Caussinus and Gonzalez, 2005; Lee et al., 2006b). Therefore, *numb*, *pros* and *brat* are all classified as tumour suppressor genes (Betschinger et al., 2006; Bowman et

al., 2008; Choksi et al., 2006). In addition, postmitotic neurons, rather than intermediate progenitors, are also found to be tumour cells of origin due to defects in the maintenance of cellular differentiation.

1.4.6. Maintenance of neuronal differentiation and tumorigenesis

Neuronal maintenance following asymmetric division is crucial to lock neurons into their differentiated state and to prevent their reversion to NBs. In fact, neuronal differentiation is a plastic and reversible process at which differentiated neurons can be reprogrammed into a stem cell-like fate (dedifferentiation), or into another differentiated state (transdifferentiation) (Southall et al., 2014). Several transcription factors have been identified that maintain neuronal differentiation and prevent dedifferentiation from neurons to NBs. The identified transcription factors include *longitudinals lacking* (*lola*), *midlife crisis* (*mlc*), and *nerfin-1*. These studies in *Drosophila* can potentially shed light into dedifferentiation and neuron-derived tumorigenesis in human cancers, by using tumour models mutant for each of these transcription factors. Given that neoplastic dedifferentiation of differentiated neural cells have been found to cause glioblastoma, dedifferentiation-derived tumours in *Drosophila* CNS may elucidate some aspects about this tumour malignancy (Feliciano, 2012; Friedmann-Morvinski et al., 2012).

1.4.6.1. Lola and Midlife crisis

Lola is a BTB-zinc finger transcription factor that is a cofactor of Pros, and they act redundantly to maintain neuronal differentiation (Southall et al., 2014). Lola expression is induced by the low levels of Pros partitioned in newly-born neurons after GMCs divide (Southall et al., 2014). Lola directly binds to most of the *pros* target genes; including NB genes and differentiation genes; to inhibit self-renewal and maintain the differentiated state of postmitotic neurons (Southall et al., 2014). While *pros* mutation alone is not sufficient to cause neuronal dedifferentiation, *lola* mutants result in dedifferentiation of postmitotic neurons to NBs, leading to the formation of tumours (Southall et al., 2014). Mlc is a RNA splicing factor, which regulates *pros* expression (Froldi et al., 2015b) and represses NB gene expression in larval neurons (Froldi and Cheng, 2016). Loss of Mlc results in decreased levels and aberrant splicing of *pros*

transcripts (Carney et al., 2013; Froldi and Cheng, 2016). Neurons mutant for *mlc* express NB genes, but these ectopic NBs fail to proliferate or form tumours (Carney et al., 2013).

1.4.6.2. Nerfin-1

Nerfin-1 is another cell fate determinant that governs neuronal differentiation in *Drosophila*. The *nerfin-1* gene encodes a zinc finger transcription factor that belongs to a highly conserved subfamily of Zn-finger proteins also found in vertebrate (Goto et al., 1992; Kuzin et al., 2005; Stivers et al., 2000). The *Drosophila* Nerfin-1 and its human homolog (called human insulinoma associated-1 [INSM-1]), share the EIN domain that contains a set of tandem Zn-fingers (Kuzin et al., 2005). In the embryo, *nerfin-1* mRNA is transiently expressed in early embryonic NBs, but later only detected in a subset of these cells (Kuzin et al., 2005). The absence of the Nerfin-1 protein in these late progenitor cells is due to the repression of its translation as the mRNA contains multiple microRNA docking sites (Kuzin et al., 2005). Another possible reason is that Nerfin-1 is rapidly degraded in these progenitor cells (Kuzin et al., 2005). Nerfin-1 is inherited by nascent neurons generated by NBs of both type I and type II to maintain neuronal differentiation (Kuzin et al., 2005). Loss of *nerfin-1* does not change the number of embryonic neurons or cause embryonic lethality (Kuzin et al., 2005). By contrast, at larval stages, Nerfin-1 is expressed in postmitotic neurons to lock them into a differentiated state, and prevent their reversion back to NBs (Froldi et al., 2015b). Loss of *nerfin-1* leads to the reversion from neurons to NBs, and subsequently tumorigenesis in several neural lineages (Froldi et al., 2015b). The NB reversion has been found to be dependent on Myc- and target of rapamycin (Tor)-mediated cellular growth (Froldi et al., 2015b). In *nerfin-1* mutants, neurons dedifferentiate and grow rapidly up to a cell size threshold through Myc and Tor signalling pathway (Froldi et al., 2015b). These reverted cells then reactivate NB-specific genes, including *mira*, but still express differentiation genes, including *pros* (Froldi et al., 2015b). These cells continue to grow, and switch off Pros, and then adopt a NB cell fate to undergo asymmetric cell division. The pool of NBs is then increased at the expense of neurons (Froldi et al., 2015b). In contrast to a *wildtype* clone which contains only one NB, several GMCs, and a lot of neurons, a *nerfin-1*$^{-}$ mutant clone contains several GMCs and a large number of ectopic

NBs. Furthermore, ectopic Nerfin-1 expression forces larval NBs to decrease in size and prematurely exit the cell cycle by size-symmetric division, causing premature NB loss (Froldi et al., 2015b). The mouse homolog of *nerfin-1*, called INSM1, is also essential for differential maintenance of neuroendocrine cells located in murine endocrine glands, such as the pancreas (Froldi and Cheng, 2016; Froldi et al., 2015b). INSM1 is abundantly found in many different types of tumours, such as insulinoma and neuroblastoma (Froldi and Cheng, 2016). However, the roles of this gene in human tumours need to be further characterised.

1.5. Regulation of timing of *Drosophila* neurogenesis

Neurogenesis in *Drosophila* (**Figure 1.7**) occurs in two distinct phases, embryonic neurogenesis and postembryonic neurogenesis. During the embryonic phase, the embryonic NBs delaminate from the neuroectoderm (Altenhein, 2015; Lanet and Maurange, 2014; Prokop et al., 1998; Prokop and Technau, 1991; Saini and Reichert, 2012; Schober et al., 1999), and then undergo divisions to generate the larval CNS (Novotny et al., 2002; Sousa-Nunes et al., 2010; Wodarz et al., 2000). The embryonic NBs do not regrow after each division (Betschinger et al., 2006), and generate neurons which account for around 10% of the adult CNS (Prokop and Technau, 1991). At late embryogenesis, all postembryonic NBs in CB and VNC are reversibly arrested in G1 phase and enter quiescence (Caldwell and Datta, 1998), except for the four mushroom body NBs which produce very large neuronal lineages (Datta, 1995; Lee et al., 1999). The NBs stay quiescent for around 24 hours (Ou et al., 2014) before they are reactivated to enter the postembryonic phase at which larval NBs regrow after each cell division (Homem et al., 2015; Truman and Bate, 1988). During postembryonic neurogenesis, some NB lineages specifically produce neurons only while other lineages continue to generate both neurons and glia that make up the adult CNS (Viktorin et al., 2013). NBs exit the cell cycle and disappear during the pupal stages with different NB subtypes exiting at different times via different mechanisms. In the VNC, abdominal type I NBs undergo cell death (Bello et al., 2003) while thoracic type I NBs undergo Pros-dependent terminal differentiation (Maurange et al., 2008). In the CB, mushroom body NBs exit from the cell cycle by caspase-mediated apoptosis (Siegrist et al., 2010).

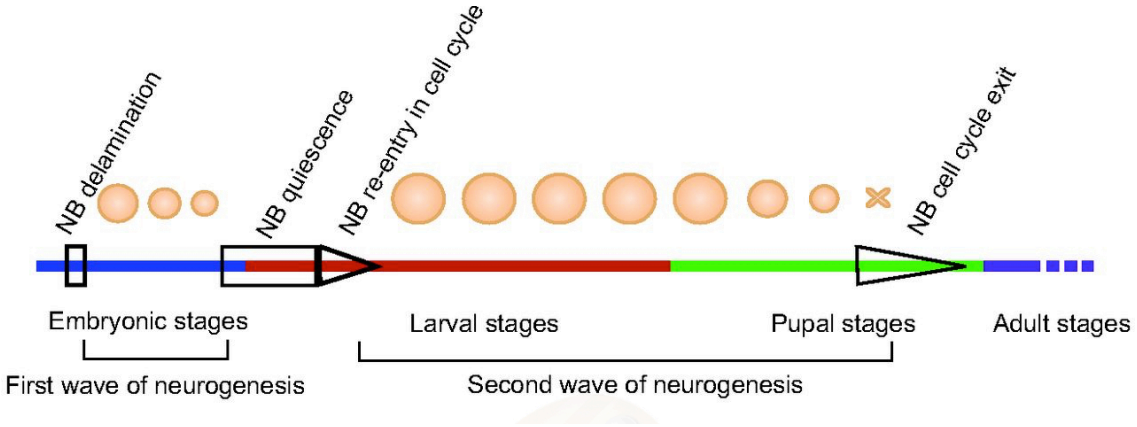

Figure 1.7. *Drosophila* neurogenesis timeline. Neurogenesis in *Drosophila* occurs in two distinct phases, embryonic and post-embryonic neurogenesis. During the embryonic phase, embryonic NBs are generated by delaminating from the neuroectoderm. They then proliferate several times but do not regrow after each division. At late embryogenesis, most NBs become quiescent for about 24h before they re-enter the postembryonic phase at larval stage. Larval NBs regrow after each division. During pupal stages, different NBs terminate proliferation by different mechanism and at different time points (Homem and Knoblich, 2012).

1.5.1. Embryonic neurogenesis

After delaminating from the neuroectoderm, embryonic NBs divide asymmetrically about 12 times (Betschinger et al., 2006; Bossing et al., 1996) to give rise to all the neurons in the larval CNS (Izergina et al., 2009; Yasugi and Nishimura, 2016) and these neurons make up around only 10% of the adult CNS (Prokop and Technau, 1991; Sousa-Nunes et al., 2010). Embryonic NB proliferation causes an increase in cell number (Betschinger et al., 2006). Embryonic NBs shrink after each embryogenic division, as they are unable to regrow (Betschinger et al., 2006). Therefore, at the end of embryogenesis, once NBs approach a certain size threshold, a number of NBs undergo cell death (Pinto-Teixeira et al., 2016), while other NBs enter a quiescence period and re-enter the cell cycle during the second wave of neurogenesis (Homem et al., 2015).

1.5.2. Temporal patterning of embryonic NBs

During embryonic neurogenesis, NBs sequentially express at least four different transcription factors (TFs) in an invariant sequence series to generate different types of

neurons and glia (Brody and Odenwald, 2000; Isshiki et al., 2001; Kambadur et al., 1998; Yasugi and Nishimura, 2016). The currently identified members of this temporal series [Hunchback→Kruppel (Kr) → Pdm → Castor (Cas) and Grainyhead (Grh)] are temporally expressed in NBs (Baumgardt et al., 2009; Maurange et al., 2008), and are then inherited by the progeny, leading to neuronal and glia diversity (Brody and Odenwald, 2000; Isshiki et al., 2001; Kambadur et al., 1998; Yasugi and Nishimura, 2016). Therefore, neurons born at different times would inherit different temporal members which specify various different neuronal identity or cell fate. These temporal factors act via feedback inhibition, whereby one TF induces the expression of the next factor and downregulates the previous one (Grosskortenhaus et al., 2005; Yasugi and Nishimura, 2016). For instance, Hb which specifies first-born neuronal fates promotes Kr expression, which, in turn, inhibits Hb expression (Yasugi and Nishimura, 2016). Kr next promotes Pdm expression, and then is downregulated by Pdm (Yasugi and Nishimura, 2016). As this temporal sequence progresses, an embryonic NB is able to produce four different types of neurons and/or glia with different temporal fates (Maurange et al., 2008). In addition, a nuclear receptor Seven-up (Svp) has been found to be involved in the Hb→Kr transition, and is believed to be the fifth member of the temporal series (Kanai et al., 2005; Mettler et al., 2006). Svp is transiently expressed in in Hb-expressing NBs to terminate Hb expression and move the NBs towards the Kr^{+} window (Kanai et al., 2005; Mettler et al., 2006).

Either inhibiting or persistently expressing any of these temporal factors can block the temporal progression (Cleary and Doe, 2006; Grosskortenhaus et al., 2006; Isshiki et al., 2001). For instance, loss of Svp function blocks the switch from Hb to Kr, resulting in the production of more Hb-expressing progeny at the expense of progeny with later temporal fates (Kanai et al., 2005; Mettler et al., 2006). Similarly, overexpression of Hb also generates additional Hb^{+} progeny (Isshiki et al., 2001). Although the Hb→Kr transition happens at cytokinesis, the Kr→Pdm→Cas transition is independent of the cell cycle (Grosskortenhaus et al., 2005; Yasugi and Nishimura, 2016). In contrast, much less is known about the temporal progression in the eight type II neuroblasts. Embryonic type II NBs are formed in the embryos and express part of this temporal transcription cascade (Pdm→Cas→Grh) to specify neuronal identities, and the

embryonic INPs are known to express the temporal TF Dichaete (D) (Walsh and Doe, 2017).

1.5.3. Quiescence period of embryonic NBs

At the end of embryogenesis, embryonic NBs stop dividing and become quiescent for about 24 hours (Chell and Brand, 2010). The mitotic quiescence marks the developmental transition from embryo to larva and also, is essential for normal CNS formation (Ebens et al., 1993). The quiescence process is regulated by several known factors. First, the cell fate determinant Pros, which is normally exported out of the NB nucleus during mitosis, is now transiently expressed in the NB nucleus to induce NB cell-cycle exit (Lai and Doe, 2014; Maurange et al., 2008). Second, the embryonic temporal factors also affect the timing at which NBs enter quiescence (Maurange et al., 2008). That is why NB quiescence is delayed and more neurons are generated in *cas* mutants, compared to *wildtype* CNSs (Lai and Doe, 2014; Tsuji et al., 2008). Furthermore, in early larval stages, a signalling protein, called Anachronism, is released by glia to keep NBs quiescent (Ebens et al., 1993).

1.5.4. Postembryonic (secondary) neurogenesis and termination of NB division

The second wave of neurogenesis, known as postembryonic neurogenesis, takes place right after NB reactivation to give rise to the adult CNS. A large number of secondary neurons are generated during this second phase while a certain subset of primary neurons still persists until adulthood. Larval NBs grow and increase in cellular volume to counteract the cytoplasmic loss after every division (Datta, 1995; Homem et al., 2013). Therefore, larval NBs are able to constantly divide for many more times to produce a larger number of neurons than embryonic NBs.

There are only six larval type I NBs in the abdominal VNC (**Figure 1.3**), and they terminate dividing by apoptosis at around 72 hours after larval hatching (Bello et al., 2003; Cenci and Gould, 2005). These abdominal lineages only generate a small neuronal subset, contributing about 12 neurons per NB lineage (Maurange et al., 2008).

The reason for the early termination of these abdominal NBs is that they upregulate the expression of the Hox protein Abdominal-A that then activates pro-apoptotic proteins to induce apoptosis in this cell type at mid-larval stages (Bello et al., 2003; Maurange et al., 2008; Peterson et al., 2002; Yasugi and Nishimura, 2016).

The timing of the thoracic NB cell-cycle exit is modulated by temporal transcription factors (TTFs). In particular, after larval hatching, most thoracic embryonic NBs progressively express Cas and Svp, to sequentially generate two types of neurons, large Chinmo (Chronological inappropriate morphogenesis)$^{+}$ neurons are produced early and small Br-C (Broad Complex)$^{+}$ neurons are produced late (Maurange et al., 2008). The temporal progression from Cas to Svp triggers the postembryonic Chinmo → Br-C neuronal switch (Maurange et al., 2008), emphasising the important role of temporal progression in controlling NB activity and defining neuronal identities during *Drosophila* neurogenesis. Loss of any temporal factor can disrupt the temporal progression during postembryonic neurogenesis, and affect formation of the correct number of neuronal progeny. For example, loss of Cas can give rise to immortal NBs which are able to proliferate in adult stage (Maurange et al., 2008).

OL NBs enter the cell cycle right after being generated from OL neuroepithelial cells during larval life stages (Saini and Reichert, 2012). This process is similar to the epithelial-mesenchymal transition in vertebrates (Mani et al., 2008). In *Drosophila*, the proneural wave mediated by the factor Lethal of scute (L'sc) regulates the timing and the direction of the transition from NE to NB (Yasugi 2015) (Yasugi et al., 2008). The OPC is organised into the main OPC and the tips of the OPC (tOPC). The main OPC NBs have been found to temporally express a sequence of at least 6 transcription factors; including Homothorax (Hth), Klumpfuss (Klu), Eyeless (Ey), Sloppy paired (Slp), D, and Tailless (Tll); to produce different types of neurons (Li et al., 2013b; Suzuki et al., 2013). Tll has been found to repress Ase to promote NSC fate in type II NB lineages (Hakes and Brand, 2020). At Tll^{+} stage, NBs are transformed into *glial cells missing (gcm)*$^{+}$ glioblasts (GBs) that can produce medulla glia (Li et al., 2013b). Ey induces the expression of downstream TTFs (Slp, D and Tll), and regulates the production of medulla neuropile glia through *gcm* (Suzuki et al., 2016). The tOPC NBs

express different temporal factors; namely Distalless (Dll), Ey, Slp, and D (Yasugi and Nishimura, 2016). Notch signalling functions differently in cells generated from different NBs by some unknown mechanisms (Yasugi and Nishimura, 2016). For example, activation of Notch initiates apoptosis in cells produced by Ey^+ NBs, while loss of Notch initiates apoptosis in cells generated by Slp^+ or D^+ NBs (Yasugi and Nishimura, 2016). Larval INPs transit through a temporal TF cascade D→Grh→Ey (Walsh and Doe, 2017). In the distal IPC, two phases of NBs that give rise to distinct populations of neurons have been identified (Yasugi and Nishimura, 2016). Early-born NBs express D and Asense (Ase), and later-born NBs express Tll, Atonal, and Dachshund (Apitz and Salecker, 2015). This temporal series is also regulated by feed-forward and feed-back inhibition, for example, D expression initiates the expression of Tll and Tll inhibits D (Yasugi and Nishimura, 2016). Little is known about the termination of OL NBs. The oldest Tll^+ NBs have been found to express nuclear Pros and glial determinant gene *gcm* to terminally differentiate into two glia (Li et al., 2013b); whereas apoptosis has also been reported in pupal NBs of OPC and IPC (Hofbauer and Campos-Ortega, 1990). Therefore, it is suggested that both OL NBs possess both Pros-dependent and apoptosis-dependent mechanism to stop cell division (Yasugi and Nishimura, 2016).

Mushroom body NBs can stay in the cell cycle and proliferate over a longer period than other types of NBs (Ito and Hotta, 1992). They terminate at 96 hour after pupal formation by apoptosis (Siegrist et al., 2010). The apoptosis is not triggered by Pros, but the transcription factor Forkhead box class O (FoxO) (Siegrist et al., 2010). They start to shrink by downregulating InR/Pi3K signalling (Siegrist et al., 2010). The reduced activity of insulin signalling results in the nuclear localisation of FoxO (Siegrist et al., 2010) which then induces caspase-dependent apoptosis (Siegrist et al., 2010). Loss of FoxO and *reaper* family proapoptotic proteins can prolong NB proliferation into adulthood (Siegrist et al., 2010).

1.6. Gliogenesis

Glia are the second most abundant cell type in *Drosophila* CNS, and are essential for reactivating NBs following quiescence. They can potentially play an important role in ectopic NB proliferation and tumour growth. Much of my project stems from the observation that ectopic glia cells are found in tumours that arise from neurons or GMCs. The review below will focus on glia cell development in the *Drosophila* CNS.

1.6.1. Glial subtypes of *Drosophila* CNS

Glia are the second most common cell types of the *Drosophila* CNS, after neurons, and play an important role in CNS development. *Drosophila* glia share various common features with vertebrate glia and therefore, are an excellent paradigm for better understanding of glial biology. One of the significant differences between *Drosophila* and vertebrate glia is the lower glia-neuron ratio in *Drosophila* (Foo et al., 2017). In vertebrates, there are three main types of glia: astrocytes, oligodendrocytes, and microglia (Omoto et al., 2015). *Drosophila* glial cells are also classified into three distinct classes based on their structural and functional characteristics similar to mammalian counterparts. These three glia classes include: (1) surface glia which function as the blood-brain barrier, (2) cortex glia which are structurally similar to mammalian astrocytes, (3) neuropil glia which are the equivalent of oligodendrocytes (Banerjee and Bhat, 2008; Omoto et al., 2015). The microglia class is absent in *Drosophila* but hemocytes involved in programmed cell death located outside the *Drosophila* CNS are considered to be equivalent to vertebrate microglia (Omoto et al., 2016).

These three glia classes are either derived from neuroglioblasts (NGBs), or GBs; and display different morphology and position of the cell bodies (Awasaki et al., 2008). The first glia class is surface glia which constitute the outer most layer surrounding the larval and adult CNS (Omoto et al., 2015). The surface glia are subdivided into (1) perineural glia, which form the outer-most layer of the CNS, and (2) subperineural glia, which form septate junctions similar to vertebrate tight junctions (Morante et al., 2013) to regulate the passage of molecules between the CNS and hemolymph (DeSalvo et al., 2011). Perineural glia have smaller cell bodies than subperineural glia (Hartenstein, 2011). In addition, surface glia also play a novel role in regulating neuronal metabolism

and brain development (Chell and Brand, 2010; Volkenhoff et al., 2015). The cell body glia, also termed cortex glia, encapsulate neuronal cell bodies as well as provide structural and trophic support to neurons (Melom and Littleton, 2013; Stork et al., 2012). Neuropil glia are located at the interface between cortex and neuropil regions (Kis et al., 2015; Lee et al., 2019; Omoto et al., 2016). Neuropil glia are divided into 2 types: (1) ensheathing glia which wrap around neuropil compartment boundaries and axon bundles, and (2) astrocyte-like glia which infiltrate into the inner neuropil region (Awasaki et al., 2008; Omoto et al., 2016).

1.6.2. Glial determinant genes

In *Drosophila*, the transcription factor Gcm/Glial cell deficient (Glide) is a master regulator that specifies glial fate (Akiyama-Oda et al., 1998; Bernardoni et al., 1998; Flici et al., 2011; Hosoya et al., 1995; Jones et al., 1995; Popkova et al., 2012; Vincent et al., 1996). Gcm is expressed in all embryonic glial precursors except for midline glia (Omoto et al., 2015). Gcm is necessary and sufficient to promote glial differentiation (Freeman and Doe, 2001; Mao et al., 2012); and also governs the formation of other cell types, such as hemocytes (Omoto et al., 2016). The molecular mechanism regulating *gcm* expression has been investigated in a number of studies. Gcm protein is cortically distributed in premitotic NGB6-4 (mother NGB) and is inherited by both daughter cells, including a daughter NGB6-4 and a GMC (Freeman and Doe, 2001). Once being localised into daughter cells, Gcm is excluded from the nucleus of this daughter NGB, yet it is imported into the GMC nucleus by an unknown mechanism (Freeman and Doe, 2001). It is also suggested that the Pros upregulates *gcm* expression in the GMC produced by NGB6-4 (Freeman and Doe, 2001). This is indicated by the fact that mislocalisation of Pros into the daughter NGB causes the ectopic expression of *gcm* and ectopic glia formation (Freeman and Doe, 2001). Activity of *gcm* and its downstream pathway effectors have not yet been elucidated, although a few direct target genes of *gcm* have been found (Egger et al., 2002). One of the identified *gcm* targets is *reversed polarity* (*repo*) whose protein product is commonly used as a glial marker (Egger et al., 2002). The *gcm* mutation leads to a switch from glial to neuronal fate in progeny of progenitor cells, and subsequently, more neurons are generated at the expense of glia, in embryos (Hosoya et al., 1995; Jones et al., 1995; Vincent et al., 1996). By contrast,

targeted *gcm* overexpression in progenitor cells cause a gain of ectopic glia, and loss of neurons (Flici et al., 2011; Freeman and Doe, 2001).

1.6.3. Gliogenesis

Drosophila gliogenesis occurs along with neurogenesis to generate glia for the CNS. Like neurogenesis, gliogenesis occurs in primary and secondary gliogenesis to give rise to larval glia (primary glia) and adult glia (secondary glia), respectively. Primary glia are generated by primary glial progenitors during embryogenesis; whereas, secondary glia arise from either persistent primary precursors, newly-born secondary precursors, or differentiated glia (Pereanu et al., 2005). The glial progenitor cells can be either (1) NGBs which commonly generate mixed neuron/glia lineages, or (2) GBs which produce exclusively glia (Viktorin et al., 2011). In the embryo, NGBs and GBs delaminate from the neuroepithelium of the ectoderm (Omoto et al., 2016). GBs express the glial determinant Gcm and Repo after delaminating from the neuroectoderm (Omoto et al., 2016); therefore, they only produce glia. Whereas, NGBs display a different proliferation pattern, and can be further divided into type 1, type 2 and type 3 NGBs (Altenhein, 2015; Omoto et al., 2016). In particular, type 1 NGBs generate a mixed lineage of neuronal and glial fate during each division (Altenhein, 2015; Omoto et al., 2016). Type 2 NGBs separate the gliogenic phase from the neurogenic phase during their proliferation period (Altenhein, 2015; Omoto et al., 2016) and type 3 NGBs include one or more GB progenitors (Altenhein, 2015; Omoto et al., 2016). Gcm is also expressed in these NGBs to repress neural differentiation and promote glial formation (Altenhein, 2015). Current studies have found that different glia types arise independently of each other but the mechanism specifying their cell fates is poorly understood.

Little is known about glial cells of the *Drosophila* VNC. In the VNC, primary surface glia are found to arise from several NGB lineages (Type 1: NB1-1, NB2-2, NB5-6; Type 2: NB1-3, NB7-4) (Altenhein, 2015; Beckervordersandforth et al., 2008; Omoto et al., 2016); however, the mechanism determining the choice between perineural and subperineural types is still unknown (Omoto et al., 2016). The primary cell body glia are generated from NGB7-4 (type 2) and NGB6-4 (type 3) (Altenhein, 2015; Omoto et

al., 2016). In the CB, the progenitor cell lineages that generate primary cell body, or surface glia, remain to be discovered. Subperineural glia of CBs are found to proliferate significantly during embyonic gliogenesis but they become polyploid and stop dividing at larval stages (Unhavaithaya and Orr-Weaver, 2012), and are retained into the adult CNS (Awasaki et al., 2008; Omoto et al., 2016). By contrast, perineural glia continue dividing during larval life to produce adult perineural glia (Awasaki et al., 2008; Omoto et al., 2016). Primary cell body glia only begin to proliferate in late larval stages to generate secondary glia for the adult CNS (Avet-Rochex et al., 2012; Omoto et al., 2016). Primary neuropil glia arise from embryonic progenitors, called basal procephalic longitudinal glia, and then migrate to the neuropil surface of VNC and CB (Hartenstein et al., 1998; Omoto et al., 2016; Omoto et al., 2015) . Primary neuropil glia grow in size to fill the enlarging neuropil structure (Omoto et al., 2016; Omoto et al., 2015). They do not divide and then die (Omoto et al., 2015), meanwhile a large number of secondary glia are produced by certain secondary NGBs to compensate for this loss (Izergina et al., 2009; Omoto et al., 2015; Pereanu et al., 2005).

Several NGB lineages that give rise to most postembryonic neuropil glia have been identified. In the postembryonic CNS, six type II NBs located to the dorsomedial regions of the larval brain have been identified to function as NGBs that produce both neurons and glia through transit amplifying INPs (Izergina et al., 2009; Viktorin et al., 2013). In particular, dorsal medial (DM) NBs produce the majority of neurons and glia for the neuropil structures of the central complex (Viktorin et al., 2013). Therefore, most neuropil glia are derived from INPs of the DM NBs. In addition, these postembryonic neuropil glia are found to proliferate locally around the central complex region to populate the developing neuropil during pupal stages (Viktorin et al., 2013). The glial determinant gene *gcm* is necessary and sufficient to promote the production of these INP-derived glia in DM NBs (Mao et al., 2012). In general, most adult glia of CB, like adult neurons, are generated during *Drosophila* postembryonic development through either asymmetrically dividing secondary NGBs or symmetrically dividing glia. All postembryonic glial precursors of CBs have been reported to undergo a terminal mitosis at early pupal stages (Omoto et al., 2015).

Very few aspects about glia of the OL have been revealed. OL glia are found to originate from another pair of type II NBs called dorsal lateral 1 (DL1) NBs, also through transit amplifying INPs (Viktorin et al., 2013; Yu et al., 2013). DL1 NBs generate both neurons for the central complex, as well as glia exclusively for the OLs (Viktorin et al., 2013). DL1-derived glia are generated in the CB from mid-larval development, and immediately migrate to the OL (Viktorin et al., 2013). These OL glia then differentiate into 3 distinct glial subtypes; including cortex glia, inner chiasm glia and outer chiasm glia (Viktorin et al., 2013). The DL1 NBs stop generating glia at late larval stages, and the DL1-derived glia do not undergo mitotic division during pupal stages (Viktorin et al., 2013). The development of the OL glia is difficult to study since they display even more morphological diversity than glia of CB and VNC (Edwards et al., 2012; Omoto et al., 2016). Current studies have been classifying OL glia into different categories in each OL region based on their glial features and their precursor centers.

Several signalling pathways have been found to regulate the genesis, proliferation and growth of glial cells in *Drosophila* CNS. Notch signalling is reported to cell-autonomously promote gliogenesis in type II NB lineages (Gaiano and Fishell, 2002; Ren et al., 2018). Inhibition of Notch ligand Delta in type II lineages can repress the expansion of type II lineages-derived glia (Ren et al., 2018). Notch activates *gcm* expression to specify a subclass of glia in embryonic CNS (Udolph et al., 2001; Umesono et al., 2002). Fibroblast growth factor (FGF) signalling has been identified to control the proliferation of perineural and cortex glia in larval CNS (Avet-Rochex et al., 2012). Inhibition of FGF pathway supresses the proliferation of perineural glia, and completely blocks the generation of cortex glia (Avet-Rochex et al., 2012). Activation of FGF receptor Heartless (Htl) is sufficient to cause overproliferation of perineural glia and cortex glia (Avet-Rochex et al., 2012). Merlin-Hippo signalling pathway is required for the glial proliferation in larval CNS (Reddy and Irvine, 2011). Merlin has been found to repress glial cell proliferation as its depletion causes glial overgrowth (Reddy and Irvine, 2011). The downstream transcriptional co-activator Yorkie (Yki) is known to induce glia proliferation by activating *bantam* which promotes the expression of oncogene Myc (Reddy and Irvine, 2011). Active Yki is required for normal glial growth

during development, and sufficient to promote glial overgrowth (Reddy and Irvine, 2011).

1.7. Summary and thesis aims

In human brain cancers, GSCs originate from neoplastic transformation of NSCs or dedifferentiation of other neural cells. Similar to normal NSCs, GSCs possess stem-cell properties to self-renew and differentiate into multiple neural lineages. However, GSCs have been found to be more plastic than normal NSCs, as they can transdifferentiate into other cell types. The cellular plasticity and heterogeneity of brain tumours are challenging to treat in the clinic, and better characterisation of how neural cells maintain their cell fate to prevent dedifferentiation and transdifferentiation is important for improving our current understanding. Many of the mechanisms underlying these characteristics were predominantly revealed by cell culture techniques and mouse models. The transdifferentiation of GSCs has not been well studied at the physiological and molecular level. At the present, we do not fully understand the cellular step-wise conversion from GSCs into other distinct cell lineages, and the molecular mechanisms responsible for this event.

Drosophila CNS have provided multiple insights into NSC behaviours and tumour formation that are highly conserved between flies and mammals. *Drosophila* NSCs, called NBs, also asymmetrically divide to renew themselves, and generate neurons or glia that make up the adult CNS. Disrupting either asymmetric cell division or neuronal maintenance allows differentiated cells to dedifferentiate into ectopic NBs, which then continue to proliferate and form tumours. In this study, we utilise several *in vivo* brain tumour models in *Drosophila* to study how GSCs function in brain cancers and how they undergo transdifferentiation. Specifically, we induced loss-of-function of Pros or Nerfin-1 in NB lineages to generate dedifferentiation-driven tumours, and surprisingly we found a class of cells which exhibited glial cell identity. In the *wildtype* context, glia surround NB lineages to define stem cell niche and control NB proliferation. This thesis explores the hypothesis that ectopic NBs in *pros*$^{-}$ or *nerfin-1*$^{-}$ tumours transdifferentiate into ectopic glia to support tumour growth, and are presented in three main results:

Result 1: I characterised in detail the number and types of ectopic glia found within the tumours which arised via *pros*$^{-}$ or *nerfin-1*$^{-}$ mutation in the larval CNS (**Chapter 3.1**).

Result 2: Ectopic glia were predicted to originate (1) as the progeny of asymmetric division of neural progenitors, or (2) by transdifferentiation of neurons or neural progenitors cells. I performed live-cell imaging of RFP-labelled *pros*$^{-}$ tumour to visualise the formation of ectopic glia using time-lapse confocal microscopy and GFP-tagged Repo. We also performed molecular marker analysis on these ectopic glia to characterise the cell of origin for these cells (**Chapter 3.2)**.

Result 3: We aimed to identify the transcription factors and related signal transduction pathways that drive the formation of ectopic glia. We interrogated the pathways to manipulate the ectopic glial population, and then assessed whether the changes in their number can affect the tumour growth (**Chapter 3.3)**.

Chapter 2

Materials and Methods

2.1. Fly husbandry

Flies were raised on standard cornmeal/agar food supplemented with dry yeast as previously described (Sousa-Nunes et al., 2011). For larval dissection, brains were dissected at wandering L3 stages [~9 days after egg laying (AEL) at 18°C, 5-6 days AEL at 25°C, and 5 days AEL at 29°C]. For pupal dissection, white pupae were selected and then allowed to age at 25°C, dissections were made at either 2 or 3 days after pupal formation (APF). For adult dissection, embryos were allowed to develop at 25°C, and adult stages were calculated chronologically relative to egg laying (at 0 h). After egg laying (0 h), adult formation starts 9 days later (including 5 days of larval development and 4 days of pupal development).

2.2. *Drosophila melanogaster* strains

Unless otherwise indicated, all fly stocks were obtained from Bloomington *Drosophila* Stock Centre (BDSC) and Vienna *Drosophila* Resource Centre (VDRC). Most genetic elements are described in Flybase (https://flybase.org).

Wildtype or loss-of-function CNS clones were generated using the mosaic analysis with a repressive cell marker (MARCM) technique (Lee and Luo, 1999, 2001). (1) To generate *pros*$^{-}$ mutant MARCM clones for lineage analysis, flies of *GFP MARCM82B* stock (*w, tub-Gal4, UAS-nlsGFP::6xmyc::NLS, hs-flp; FRT82B, tubP-Gal80 LL3/TM6B*) (Lee and Luo, 1999, 2001) were crossed to *w;; FRT82B, pros*^{17}*/TM6B* flies. (2) To generate *pros*$^{-}$ mutant MARCM clones for live-cell imaging and Bodipy staining, flies of *RFP MARCM82B* stock (*yw, hs-flp;; UAS-myrRFP, tub-Gal4, FRT82B, tub-Gal80/TM6B*) (Froldi et al., 2015b) were crossed to *w; repo-GFP/CyO*$_{yfp}$*; pros*^{17}*,*

FRT82B/TM6B flies (compound stock was made from BDSC 56153 and *FRT82B, pros*^{17}). (3) To generate *nerfin-1*$^{-}$ mutant clones, flies of *MARCM2A* stock (*w, tub-Gal4, UAS-nlsGFP::6xmyc::NLS, hs-flp; FRT2A, tubP-Gal80LL9/TM6B*) (Lee and Luo, 2001) were crossed to *w;; FRT2A, Df(3L)nerfin-1*^{159}*/TM6B* flies (Kuzin et al., 2005). (4) To generate *wildtype* control MARCM clones, flies of *MARCM82B* stocks were crossed to *w;; FRT82B/TM6B* flies; or *MARCM2A* flies were crossed to *w;; FRT2A/TM6B* flies. Progeny were raised at 25°C, and were shifted to 29°C at 48h AEL to induce higher transgene expression. Unless otherwise stated, MARCM clones were induced by heat-shock at 37°C at 48h AEL for 8 mins (*pros*$^{-}$) or 30 min (*nerfin-1*$^{-}$), and were dissected at 3 days APF. For the analysis of ectopic glial number versus clonal volume (**Figure 3.2D** and **E**, **Chapter 3.1**) and versus developmental stages (**Figure 3.4** and **3.5**, **Chapter 3.1**), MARCM clones were induced at 48 hours AEL, and were dissected 72 h later (L3 stage); or at 1, 2, 3 and 4 days APF; or at 1, 2, 3, 4 and 5 days after adult hatching (AAH).

The *UAS-pros*$^{RNAi\ SH}$ (Bloomington TRiP 42538) and *UAS-pros*$^{RNAi\ LH}$ (Bloomington 26745) (**Figure 2.1**) were induced by using *Gal4* driver lines: (1) *w; grh-gal4, UAS-mCD8RFP/CyO; w* (Chell and Brand, 2010) which is expressed in a subset of NB lineages (2) *grh-Gal4, UAS-RFP*^{nls}*/CyO*$_{yfp}$*; +/TM6B*$_{yfp}$ (this study) and (3) *w;; pox*^{n}*-gal4, UAS-mCD8GFP/TM6B* (Narbonne-Reveau et al., 2016) which is only expressed in six VNC lineages. *grh>pros*$^{RNAi\ SH}$ crosses were raised at 18°C to lower the expression level of the *RNAi*, which causes larval lethality at 25°C. *grh>pros*$^{RNAi\ LH}$ crosses were initially raised at 25°C and shifted to 29°C at 24 h AEL to increase expression levels of the *Gal4*-mediated *RNAi* knockdown. *pox*^{n}*>pros*$^{RNAi\ SH}$ crosses were raised at 25°C.

Other *UAS*-transgenes and genotypes used in this study are as follows: (1) *lacZ*^{RNAi}*; pros*$^{RNAi\ LH}$ stock was used as control for driving a *UAS*-transgene on the second chromosome simultaneously with *pros*$^{RNAi\ LH}$. (2) *pros*$^{RNAi\ SH}$*; mCherry*^{RNAi} stock was used as control for driving *pros*$^{RNAi\ SH}$ simultaneously with *UAS*-transgene on the third chromosome. (3) To knockdown *dichaete* (*D*) in *pros*^{RNAi}-expressing lineages, *grh-gal4, UAS-mCD8RFP/CyO* flies were crossed to *D*^{RNAi}*; pros*$^{RNAi\ LH}$ flies. (4) To knockdown *tll*

in *pros*^{RNAi}-expressing lineages, *grh-gal4, UAS-mCD8RFP/CyO* flies were crossed to *tll*^{RNAi}*; pros*$^{RNAi\ LH}$ flies. (5) To knockdown *gcm* in *pros*^{RNAi}-expressing lineages, *grh-Gal4, UAS-RFP*^{nls}*/CyO*$_{yfp}$ flies were crossed to *pros*$^{RNAi\ SH}$*; gcm*^{RNAi} flies. (6) To knockdown *repo* in *pros*^{RNAi}-expressing lineages, *grh-Gal4, UAS-RFP*^{nls}*/CyO*$_{yfp}$ flies were crossed to *repo*^{RNAi}*; pros*$^{RNAi\ LH}$ flies. (7) To knockdown *repo* in *pros*$^{-}$ clones, flies of *GFP MARCM82B* genotype were crossed to *UAS-repo*^{RNAi}*; pros*^{17}*, FRT82B* flies. (8) To knockdown *notch* in *grh>pros*^{RNAi}-expressing lineages, *grh-gal4, UAS-mCD8RFP/CyO* flies were crossed to *notch*^{RNAi}*; pros*$^{RNAi\ LH}$ flies. (9) To induce *notch* activation in *pox*^{n}*>pros*$^{RNAi\ SH}$ lineages, *pox*^{n}*-gal4, UAS-mCD8GFP* flies were crossed to *pros*$^{RNAi\ SH}$*; notch*^{ACT} flies. (10) To knockdown *delta* (*dl*) in *pros*$^{-}$ clones, flies of *GFP MARCM82B* genotype were crossed to *UAS-dl*^{RNAi}*; pros*^{17}*, FRT82B* flies. (11) To knockdown *dl* in *nerfin-1*$^{-}$ clones, flies of *MARCM2A* genotype were crossed to *UAS-dl*^{RNAi}*; nerfin-1*^{159}*, FRT2A* flies. (12) To inhibit *htl* function in *pros*^{RNAi}-expressing lineages, *grh-gal4, UAS-mCD8RFP/CyO* flies were crossed to *htl*^{DN}*; pros*$^{RNAi\ LH}$ flies. (13) To activate *htl* in *pox*^{n}*>pros*^{RNAi} lineages, *pox*^{n}*-gal4, UAS-mCD8GFP* flies were crossed to *pros*$^{RNAi\ SH}$*; notch*^{ACT} flies. (14) To knockdown *warts* (*wts*) in *pros*^{RNAi}-expressing lineages, *grh-gal4, UAS-mCD8RFP/CyO* flies were crossed to *wts*^{RNAi}*; pros*$^{RNAi\ LH}$ flies. Detailed genotypes are provided in **Table 2.1**.

2.3. Antibodies and immunohistochemistry

For fixed-cell immunofluorescence imaging, CNSs were dissected in phosphate-buffered saline (PBS) in a PYREX™ spot plate, fixed in 4% formaldehyde/PBS (v/v) for 20 min. The formaldehyde solution was discarded, and the samples were washed 3 times with PBT (0.5% Triton X-100 diluted in 1X PBS), and then incubated overnight at 4°C in primary antibodies. The antibody solution was discarded, and samples were then washed 3 times with PBT, and then incubated overnight or 2 h at 4°C in secondary antibodies. The samples were then rinsed 3 times with PBT and mounted in 80% glycerol in PBT (0.5% Triton X-100 diluted in 1X PBS), and were imaged using Leica SP5 confocal microscope. Details of primary and secondary antibodies used in this study are described in **Table 2.1**.

For lipidTOX and Bodipy staining following immunostaining, the brains were washed three times with PBT and 3 times with PBS after immunostaining, and were then incubated overnight at 4°C in LipidTOX in PBS (1/1000 dilution), or in Bodipy in PBS (1/500 dilution), rinsed twice with PBS and mounted in 80% glycerol/PBS (v/v).

For live-cell imaging, pupal brains (3 days APF) were dissected in Schneider's medium containing 10% Foetal Bovine serum (FBS), 2% PenStrep (v/v) in a PYREX™ spot plate. The tissues were then cultured in a µ-slide 8 well (Ibidi GmbH) containing Schneider's medium supplemented with 10% FBS, 2% PenStrep and 10% L-Glutamine (v/v) for imaging. The samples were imaged live at 25°C or room temperature, using Olympus SpinSR10 spinning disk microscope for 5-10 hours.

2.4. Image acquisition and processing

For volume and cell number quantifications, fluorescent fixed images were acquired using Leica SP5 confocal microscope equipped with a 63X glycerol objective (488 nm Argon, 561 nm diode, 633 nm HeNe lasers). Every clone/lineage was imaged as Z-stacks of 1.5 µm-spaced confocal images and visualised as three-dimensional (3D) reconstruction using Volocity software. MARCM clones are shown as single section images, and $pros^{RNAi}$ lineages are shown as maximum-intensity projection images, unless otherwise stated.

For live-cell imaging, 3D images were acquired as Z-stack series (~1.5 µm step size) and over time (every 12 min) using Olympus SpinSR10 spinning disk microscope with 60X oil immersion objective. The Z-stack was then merged into a time-lapse video with a single plane using Imaris software. Lateral drift was corrected, and NBs (identified by their large size of ≥10 µm) were tracked over the course of imaging by Imaris.

2.5. Clone/lineage volume measurements

Clone/lineage volumes were measured by selecting objects with a fluorescence intensity threshold from 3D reconstructions of Z-stacks with Volocity software. We first defined

a region of interest (ROI), and manually adjusted the fluorescence threshold to create a surface rendering on the entire ROI for volume measurements.

Only NB clones located in the VNC were analysed in this study, unless otherwise specified. Merged clones were either manually segmented or excluded from the analysis. As the whole VNC containing all *grh>pros*^{RNAi} lineages is too big to image under 63X magnification, all *pros*$^{RNAi\ LH}$-expressing lineages of the thoracic VNC (**Figure 3.24C-F**; **Figure 3.25D-G**, **Figure 3.27 A-D**, **Figure 3.30A-D**, **Figure 3.33A-D**, **Figure 3.34A-D**) and *pros*$^{RNAi\ SH}$-expressing lineages of the abdominal VNC (**Figure 3.26B-E** were defined as ROIs for quantification. The volumes of *pros*^{RNAi}-expressing lineage were measured based on the total fluorescence intensity using Volocity software.

2.6. Cell number quantifications and cell size measurements

Ectopic glia were identified as cells that are both labelled by Repo (glia marker) and are also positively labelled by GFP (clones) or RFP (lineages). Among these ectopic glia, Repo was expressed in the nucleus of some cells, and also in the whole membrane of the others. Due to the variable Repo expression in these cells, they are manually marked at the cell center, and counted as total number of glia per clone or per lineage using Volocity. Glial cell diameter was measured from single slice images using FIJI software.

2.7. Statistical analysis

All numerical measurements are presented in scatter plots or bar graphs, and statistical tests were performed using Prism and R. The replicates and statistical details of all experiments are mentioned in figures and figure legends.

Ectopic glial number versus clonal volume were plotted as XY graph with linear regression line. Pearson correlation coefficients and p values with 95% confidence interval were computed using Prism, with *p<0.0332, **p<0.0021, ***p<0.0002, ****p<0.0001 (**Figure 3.2D** and **E**, **Chapter 3.1**). All other data on glia number and

clone/lineage volume are presented in column graphs with error bars. Error bars represent standard error of the mean (SEM). To assess the difference between control and experiment with 95% confidence interval, two-tailed unpaired t-test statistical analyses were performed assuming equal variance, with *p<0.05; **p<0.01; ***p<0.001 ****$P < 0.0001$. To compare the difference in the mean ectopic glial number over developmental stages, we performed one-way ANOVA with Bartlett's test for equal variances (**Figure 3.4** and **3.5**, **Chapter 3.1**). The one-way ANOVA compares the means of different age groups, and the significant p values provide the evidence for the difference among group means.

Table 2.1. Detailed descriptions of antibodies, reagents, fly strains and analysis software used in this study.

REAGENT OR RESOURCE	SOURCE or REFERENCE	IDENTIFIER
Antibodies and chemical dyes		
Chick anti-GFP (green fluorescent protein) (1:1000)	Abcam	Ab13970
Guinea pig anti-Ase (1:5000)	(Jarman et al., 1993)	N/A
Guinea pig anti-Slp (1:200)	National Institute of Genetics	53
Guinea pig anti-Tll (1:100)	gift from Claude Desplan (Li et al., 2013b)	N/A
Mouse anti-Elavi (Elav) (1:50)	Developmental Studies Hybridoma Bank (DSHB)	Ab528217
Mouse anti-Eyeless (1:50)	DSHB	Ab2253542
Mouse anti-Notch intra (1:50)	DSHB	C17.9C6
Mouse anti-Repo (1:50)	DSHB	Ab528448
Rabbit anti-Ase (1:50)	gift of F. Matsuzaki	N/A
Rabbit anti-Dichaete (1:200)	gift from Claude Desplan (Li et al., 2013b)	N/A
Rabbit anti-Mira (1:200)	gift of Rita Sousa-Nunes	N/A
Rabbit anti-RFP (red fluorescent protein) (1:100)	Abcam	Ab62341
Rat anti-Dpn (1:200)	Abcam	Ab195172
Rat anti-Elav (1:50)	DSHB	Ab528218
Rat anti-Mira (1:100)	Abcam	Ab197788
Rat anti-pH3 (phospho-Histone H3) (1:5000)	Abcam	Ab10543
Rat anti-PntP2 (1:200)	gift from Joseph Bateman (Avet-Rochex et al., 2012)	N/A
Donkey anti-mouse 488 (1:500)	Thermo Fisher Scientific	A21202
Donkey anti-mouse 555 (1:500)	Thermo Fisher Scientific	A31570
Donkey anti-mouse 647 (1:500)	Life Technologies	A31571
Donkey anti-rabbit 555 (1:500)	Invitrogen	A31572
Donkey anti-rat 488 (1:500)	Thermo Fisher Scientific	A21208

Goat anti-chicken 488 (1:500)	Thermo Fisher Scientific	A11039
Goat anti-guinea pig 647 (1:500)	Thermo Fisher Scientific	A21235
Goat anti-rat 555 (1:500)	Invitrogen	A21434
Goat anti-rat 647 (1:500)	Thermo Fisher Scientific	A21247
C11-BODIPY 581/591 (1:500)	Invitrogen	D3861
LipidTOX red (1:1000)	Thermo Fisher Scientific	H34351
Chemicals, peptides and recombinant proteins		
Foetal Bovine serum (FBS)	Sigma-Aldrich	F4135
Formaldehyde solution	Sigma-Aldrich	252549
Glycerol	Sigma-Aldrich	G5516
L-Glutamine	Sigma-Aldrich	G7513
Normal goat serum	Jackson ImmunoResearch	005-000-121
PBS (Phosphate-buffered saline: 137mM NaCl, 8.1 mM Na2HPO4, 2.7 mM KCl, KH2PO4, pH 7.4)	N/A	N/A
Penicillin-Streptomycin solution (PenStrep)	Sigma-Aldrich	P4458
Schneider's *Drosophila* medium	Thermo Fisher Scientific	21720024
Triton X-100	Sigma-Aldrich	X100
Experimental models: Organisms/strains		
(3R) *w, tub-Gal4, UAS-nlsGFP::6xmyc::NLS, hs-flp; FRT82B, tubP-Gal80 LL3/TM6B (GFP MARCM82B)*	(Lee and Luo, 1999, 2001)	N/A
(3R) *yw, hs-flp;; UAS-myrRFP, tub-Gal4, FRT82B, tub-Gal80/TM6B (RFP MARCM82B)*	(Lee and Luo, 1999, 2001)	N/A
w;; FRT82B/TM6B	Bloomington Stock Center	N/A
w;; FRT82B, pros^{17}/TM6B	Bloomington Stock Center	N/A
w, tub-Gal4, UAS-nlsGFP::6xmyc::NLS, hs-flp; FRT2A, tubP-Gal80LL9/TM6B (MARCM2A)	Bloomington Stock Center	N/A
w;; FRT2A, Df(3L)nerfin-1^{159}/TM6B	(Kuzin et al., 2005)	N/A
w;; FRT2A/TM6B	Bloomington Stock Center	N/A
grh-Gal4/CyO; MKRS/TM6B	gift from Andrea H. Brand (Chell and Brand, 2010)	N/A
w; grh-gal4, UAS-mCD8RFP/CyO; w	gift from Andrea H. Brand	N/A

	(Chell and Brand, 2010)	
grh-Gal4, UAS-RFP^{nls}/CyO$_{yfp}$; +/TM6B$_{yfp}$	recombined from *grh-gal4/CyO* with *UAS-RFP^{nls}*	N/A
w;; pox^{n}-gal4, UAS-mCD8GFP/TM6B	gift from Cédric Maurange (Narbonne-Reveau et al., 2016)	N/A
w; UAS-pros$^{RNAi\ SH}$; w	Bloomington Stock Center	TRiP 42538
w;; UAS-mCherry^{RNAi}	Bloomington Stock Center	35785
w; UAS-pros$^{RNAi\ SH}$/CyO; UAS-mCherry^{RNAi}/TM6B	compound stock was made from Bloomington 42538 and 35785	N/A
w;; UAS-pros$^{RNAi\ LH}$/TM3	Bloomington Stock Centre	26745
w; UAS-lacZ^{RNAi}; w	VDRC	51446
w; UAS-lacZ^{RNAi}/CyO$_{yfp}$; UAS-pros$^{RNAi\ LH}$/TM6C	compound stock was made from Bloomington 26745 and VDRC 51446	N/A
w; repo-GFP/CyO; w	Bloomington Stock Centre	56153
w; repo-GFP/CyO$_{yfp}$; pros^{17}, FRT82B/TM6B	compound stock was made from from Bloomington 56153 and *FRT82B, pros^{17}*	N/A
w; UAS-D^{RNAi}; w	VDRC	KK107194
w; UAS-D^{RNAi}; UAS-pros$^{RNAi\ LH}$/TM6B$_{yfp}$	compound stock was made from VDRC 107194 and Bloomington 26745	N/A
w; UAS-tll^{RNAi}; w	VDRC	330031
w; UAS-tll^{RNAi}; UAS-pros$^{RNAi\ LH}$/TM6B$_{yfp}$	compound stock was made from VDRC 330031 and Bloomington 26745	N/A
w;; UAS-gcm^{RNAi}	Bloomington Stock Centre	31518
w; UAS-pros$^{RNAi\ SH}$/CyO; UAS-gcm^{RNAi}/TM6B	compound stock was made from Bloomington 42538 and 31518	N/A
w; UAS-repo^{RNAi}; w	VDRC	GD 10424
w; UAS-repo^{RNAi}/CyO$_{yfp}$; UAS-pros$^{RNAi\ LH}$/TM6B	compound stock was made from VDRC 10424 and Bloomington 26745	N/A
w; UAS-repo^{RNAi}/CyO$_{yfp}$; pros^{17}, FRT82B/TM6B	compound stock was made from VDRC 10424 and *FRT82B, pros^{17}*	N/A
w; UAS-notch^{RNAi}; w	VDRC	KK 100002
w; UAS-notch^{RNAi}/CyO$_{yfp}$; UAS-pros$^{RNAi\ LH}$/TM6C	compound stock was made from VDRC 100002 and	N/A

	Bloomington 26745	
w;; UAS-N^{ACT}	(Kidd et al., 1998)	N/A
w; UAS-pros$^{RNAi\ SH}$/CyO; UAS-N^{ACT}/TM6B	compound stock was made from Bloomington 42538 and *UAS-N^{ACT}*	N/A
w; UAS-dl^{RNAi}; w	Bloomington Stock Centre	36784
w; UAS-dl^{RNAi}/CyO; pros^{17}, FRT82B/TM6C	compound stock was made from Bloomington 36784 and *FRT82B, pros^{17}*	N/A
w; UAS-dl^{RNAi}/CyO; nerfin-1^{159}, FRT2A/TM6C	compound stock was made from Bloomington 36784 and *nerfin-1^{159}*	N/A
w; UAS-htl^{DN}; UAS-htl^{DN}	Bloomington Stock Centre	BL5366
w; UAS-htl^{DN}/CyO; UAS-pros$^{RNAi\ LH}$/TM6B	compound stock was made from Bloomington 5366 and 26745	N/A
w;; UAS-htl^{ACT}	Bloomington Stock Centre	5367
w; UAS-pros$^{RNAi\ SH}$/CyO; UAS-htl^{ACT}/TM6B	compound stock was made from Bloomington 42538 and 5367	N/A
w; UAS-wts^{RNAi}; w	VDRC	KK 106174
w; UAS-wts^{RNAi}/CyO$_{yfp}$; UAS-pros$^{RNAi\ LH}$/TM6C	compound stock was made from VDRC 106174 and Bloomington 26745	N/A
Dissecting & Imaging equipment		
µ-slide 8 well (live imaging chamber)	Ibidi GmbH	80826
Jewelers forceps Dumont No.5 (for dissection)	Sigma-Aldrich	F6521
Pin holder (for pupal dissection)	Fine Science Tools	26016-12
PYREX™ spot plates (dissection wells)	Thermo Fisher Scientific	13-748B
Sylgard 184 silicone elastomer (for pupal dissection)	Sigma-Aldrich	761036
Tungsten needles (for pupal dissection)	Fine Science Tools	10130-20
Software/ Software and Algorithms		
Adobe Illustrator 2019	Adobe Systems	http://www.adobe.com/Illustrator
Adobe Photoshop CC 2017	Adobe Systems	https://www.adobe.com/au/products/photoshop.html
BioRender	BioRender	https://biorender.com

FIJI (ImageJ) 1.53c	National Institute of Health	http://imagej.net/Fiji
Imaris 9.4	Bitplane	https://imaris.oxinst.com/newrelease
Prism 8	GraphPad	https://www.graphpad.com/scientific-software/prism/
R 3.6.0	R Core Team	https://www.r-project.org
Volocity 6.5	Improvision	https://quorumtechnologies.com/volocity/volocity-downloads/downloads

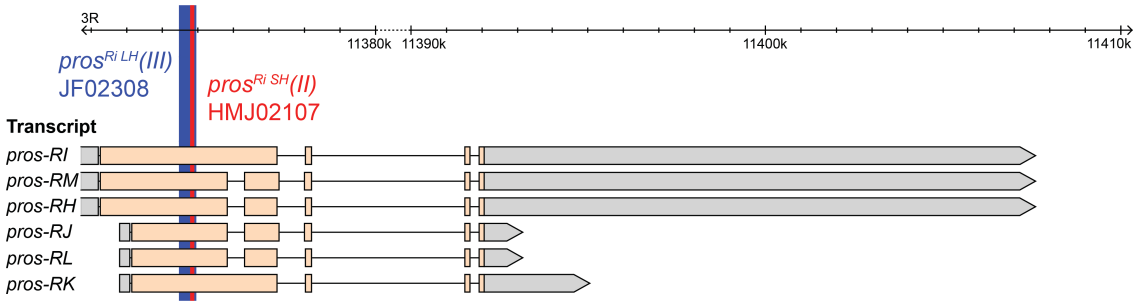

Figure 2.1. Two *UAS-pros*^{RNAi} lines used in this study both target all *pros* mRNA transcripts. The schematic represents all six annotated *pros* mRNA transcripts (*pros-RI*, *pros-RM*, *pros-RH*, *pros-RJ*, *pros-RL*, *pros-RK*) and the target regions for *pros*$^{RNAi\ SH}$*(II)* (red line) and *pros*$^{RNAi\ LH}$*(III)* (blue line). Grey boxes illustrate untranslated regions of exons. Orange boxes represent coding regions (modified from https://flybase.org/reports/FBgn0004595).

Chapter 3

Results

3.1. Ectopic glia are found in dedifferentiation-driven tumours lacking Pros or Nerfin-1.

Neural stem cells divide to expand the progenitor cell pool and subsequent neural lineages. In both mammals and flies, the ultimate lineage and brain size are regulated by the neural progenitors' ability to undergo asymmetric cell division, their cell cycle speed, and timely entry and exit from postembryonic neurogenesis (See **Chapter 1.4** and **1.5**). In addition, the ultimate function of the brain is determined by neuronal diversity, including the neuronal subtypes and their population size produced in the brain (See **Chapter 1.5** and **1.6**). In this study, we are interested in regulation of both cell type and cell number in the developing *Drosophila* brain, and furthermore, we explore how cell fate is affected during tumourigenesis. We generated GFP-positive *wildtype* control and mutant MARCM clones, and immunostained with antibodies against Repo (red) to mark the glial niche, and the mitotic marker anti-pH3 (blue) to mark mitotic cells.

We take advantage of transcription factor-mediated reprogramming (Choksi et al., 2006; Froldi et al., 2015b), to alter the cellular state of neural progenitors and their progeny. As introduced in **Chapter 1.4**, there are two main types of neural stem cell populations in the developing *Drosophila* CNS. For the purpose of this study, we concentrate on the type I NB lineages in the VNC. Type I NBs express Mira (red), and asymmetrically divide to generate a differentiating GMC (**Figure 3.1A**). In mitotic NBs, homeodomain transcription factor Pros is tethered to the basal cortex via Mira, which facilitates the selective segregation of Pros into the daughter GMC during cytokinesis (Choksi et al., 2006). Once inherited by the GMC followed by Mira degradation, Pros (blue) enters the nucleus to promote cell-cycle exit and terminal

differentiation (Choksi et al., 2006). The GMC then divides once only to produce two post-mitotic neurons, which are locked into differentiated states by the zinc finger transcription factor Nerfin-1 (green). Therefore, a *wildtype* type I clone generated by MARCM, contains only one parental NB, several GMCs, and numerous terminally differentiating neurons (**Figure 3.1A, D-D'''**). The parental NB (white arrowhead) is also positive for the mitotic marker pH3^{+} (**Figure 3.1D'''**; blue), as expected due to its asymmetrically self-renewing capabilities.

In the absence of Pros, GMCs do not differentiate but rather revert to stem cell-like fate, and express NB genes; such as Mira (**Figure 3.1B**). GMCs lacking Pros display unregulated mitotic potential and fail to differentiate in a timely fashion (Choksi et al., 2006; Froldi et al., 2015b). Larval *pros*$^{-}$ mutant lineages contain supernumerary highly-proliferative NBs (Mira^{+}) at the expense of differentiated neurons (**Figure 3.1B**), and as expected none of the cells within the clone are positive for glial marker Repo (**Figure 3.1E''**; red). These ectopic NBs which are highly proliferative (**Figure 3.1E'''**; pH3^{+}) generated a large mutant neural lineage.

Once postmitotic neurons are generated via symmetric division of the GMC, the zinc finger transcription factor Nerfin-1 is required in the neurons to maintain their differentiation (Froldi et al., 2015b). Loss of Nerfin-1 leads to dedifferentiation, whereby neurons are transformed into NSC-like cells (**Figure 3.1C**), by initially switching on NB identity while still expressing neuronal markers (such as Pros) (Froldi et al., 2015b). Over time, they switch off neuronal markers, and eventually adopt NB cell fate to become ectopic NBs (Mira^{+}; red) that can undergo asymmetric self-renewal and mitotic division (**Figure 3.1C**) (Froldi et al., 2015b). The neuron-to-NB reversion, therefore, results in the expanding pool of proliferative NBs (**Figure 3.1F'''**; pH3^{+}) at the expense of neurons. A typical *nerfin-1*$^{-}$ mutant lineage consists of ectopic NBs, interspersed with neurons and dedifferentiating cells (**Figure 3.1F'**; GFP), but no Repo^{+} glia cells (**Figure 3.1F''**; red).

We next examined *wildtype*, *pros*- and *nerfin-1*-deficient clones at adult stages to characterise the clone composition throughout development. Adult flies bearing *pros*$^{-}$ or

nerfin-1^{-} clones were able to survive more than 10 days AAH as were *wildtype* adult flies. In this study, we investigated clones in adults of up to 5 days AAH. *Wildtype* type I NBs undergo terminal differentiation at 20-30 hour after pupation (Maurange et al., 2008). Consistent with published reports, we observed no NBs or pH3^{+} cells in type I *wildtype* lineages during adult stages (n= 44 *wildtype* clones; **Figure 3.2A**). In contrast, when *pros* or *nerfin-1* were mutated, highly proliferative ectopic NBs (**Figure 3.2B'''** and **C'''**; pH3^{+}), were found in mutant clones (**Figure 3.2B**, n=50 *pros*$^{-}$ clones and **3.2C**, n=120 *nerfin-1*$^{-}$ clones).

To assess the identity of the cells that make up the *pros*$^{-}$ and *nerfin-1*$^{-}$ clones that were derived from NBs, we examined the expression of progenitor marker Mira (see **Figure 3.15**, **Chapter 3.2**), neuronal marker Elav (see **Figure 3.18**, **Chapter 3.2**) and glial marker Repo. Glia are normally found to surround NBs and neurons (**Figure 3.2A**; red), to provide structural and trophic support of neural cells (Omoto et al., 2016; Stork et al., 2008; Stork et al., 2014). Unexpectedly, these adult clones expressed both Mira (see **Figure 3.15**, **Chapter 3.2**) and Repo (**Figure 3.2B''**, n=29 *pros*$^{-}$ clones; and **3.2C''**, n=86 *nerfin-1*$^{-}$ clones). A subset of the Repo^{+} cells were also mitotic (**Figure 3.2B'''** and **C'''**; pH3^{+}). By comparison, Repo was never expressed within *wildtype* adult clones that were derived from NBs (**Figure 3.2A''**; n= 44 *wildtype* clones). The ectopic Repo expression in adult NB clones mutant for *pros* or *nerfin-1* implies the presence of an ectopic glia population, distinct from *wildtype* glia located outside the clone. However, it is important to note that MARCM system also randomly generated adult clones in glial precursors, such as GBs and NGBs (**Figure 3.3**), and they are not concerned in this study. As most adult glia are generated through postembryonic proliferation of GBs and NGBs (see **Chapter 1.6.3**, **Introduction**), the clones derived from glial precursors solely contain adult glia in both *wildtype* (**Figure 3.3A-B**; n= 17 *wildtype* glial clones) and mutant contexts (**Figure 3.3C**; n= 10 *pros*$^{-}$ glial clones; **3.3D**; n= 9 *nerfin-1*$^{-}$ glial clones).

To address whether the ectopic glial formation is linked to tumour progression, we quantified their cell number (marked by GFP and Repo) and tumour clone volume (**Figure 3.2D** and **E**). We found a positive correlation between the number of ectopic

glia and mutant clone volume [r(56) = 0.5, p<0.0001 in *pros*$^{-}$ clones; r(282) = 0.7, p<0.0001 in *nerfin-1*$^{-}$ clones]. This indicates that more ectopic glia were detected in larger mutant clones, suggesting that the expansion of ectopic glial population is correlated with overall tumour growth.

If ectopic NBs never exit the cell cycle and are able to generate ectopic glia, we next asked when this event starts and when the largest glial amplification occurs during development. To characterise the generation rate of glia from mutant NB lineages, we quantified glial cell number found in MARCM clones deficient for *pros* or *nerfin-1* at pupal and adult stages. Based on molecular marker analysis, we found ectopic glial populations are sometimes mitotic (**Figure 3.4A-A'''** and **3.5A-A'''**; yellow arrow; Repo^{+} pH3^{+}) and sometimes not dividing or non-mitotic (**Figure 3.4C-C'''**; and **3.5C-C'''**; white arrow; Repo^{+} pH3^{-}). It is unknown whether the two glial populations originated from the same progenitors or display the same characteristics; therefore, they were treated as two separate populations for these analyses. However, the possibility that they are the same glial population in different cell cycle phases should not be excluded.

In *pros*$^{-}$ clones, we observed that both mitotic and non-mitotic glia first arose at one day APF (**Figure 3.4B**: mitotic glia = 5.75 ± 1.64 cells, n = 8 clones; **Figure 3.4D**: non-mitotic glia = 1.25 ± 0.65 cells, n = 8 clones) and they persisted into adulthood (2 days AAH). There was a trend towards the increase in mitotic and overall glia cell number overtime, but the ANOVAs showed no significant differences at all time points [**Figure 3.4B**, mitotic glia: p= 0.3129 (ns); **Figure 3.4E**, overall glia: p= 0.3109 (ns); one-way ANOVA]. The number of non-mitotic glia overtime did not show any obvious trend toward change over time [**Figure 3.4D**, p= 0.2587 (ns), one-way ANOVA]. We also performed analysis of time-dependent generation of ectopic glia in *nerfin-1*$^{-}$ clones (**Figure 3.5**). Mitotic glia were detected at all time points; whereas, non-mitotic glia first appeared at the 2-day pupal stage. We saw a fairly constant average number of ectopic glia of both populations during pupal life and early adult development (1- and 2-day-old adults) (the average cell numbers were only within 2-10 cells, **Figure 3.5B**, **D-E**), with an increase at 3 days AAH (**Figure 3.5E**; n=37 clones at 3 days AAH; 40.65 ±

12.88 glia versus n= 37 clones at 2 days AAH; 9.84 ± 3.64 glia). We conducted preliminary ANOVAs on ectopic glia number between different time points (one-way ANOVA; all $p<0.001$ in **Figure 3.5B**, **D** and **E**) and observed significant differences in the overall ectopic glia number found in pupal and adult VNCs (**Figure 3.5E**). Pairwise comparisons indicated statistically a significant difference between 2 days APF and 1 day AAH, between 4 days APF and 3 days AAH, between 4 days APF and 4 days AAH and between 2 and 3 days AAH (**Figure 3.5E**; 2 days APF versus 1 day AAH: **p= 0.0021; 4 days APF versus 3 days AAH: ***p=0.0005; 4 days APF versus 4 days AAH: ****p<0.0001; 2 days AAH versus 3 days AAH: *p=0.0242). Altogether, these data suggested that ectopic glia were commonly detected in *pros*$^{-}$ or *nerfin-1*$^{-}$ mutant clones after the onset of pupal life until adulthood.

Ectopic glia display a wide range of cell sizes, prompting us to assess whether the alteration in cell size was related to cell behaviours. We measured cell diameter and quantified the number of mitotic (Repo^{+} pH3^{+}) and non-mitotic glia (Repo^{+} pH3^{-}) to build up a histogram of distribution of cell diameters (ϕ, in μm) (**Figure 3.6A** and **B**). While directly comparing the cell diameters of the two glial populations, we found that mitotic glia were generally larger and showed broader size distribution than the non-mitotic glia cells in both *pros*$^{-}$ or *nerfin-1*$^{-}$ clones. In the examined *pros*$^{-}$ pupal clones, the diameter of mitotic glia expanded from 3 to 11 μm (n=121) while all non-mitotic one were 6-10 μm large (n=111) (**Figure 3.6A**). In *pros*$^{-}$ clones, nearly half of mitotic glial population was over 6 μm large (48%, n=58); whereas, up to 75% of non-mitotic glia were only within 2.5-5-μm range (n= 83) (**Figure 3.6A**). In *nerfin-1*$^{-}$ pupal clones, the mitotic glial diameter varied from 4 up to 12 μm (n=136), while all non-mitotic glia were only between 3.5 and 8 μm (n=63) (**Figure 3.6B**). In *nerfin-1*$^{-}$ clones, the mitotic glial population contained 76% cells of over 5.5 μm (n=103); whereas, a similar percentage of non-mitotic glia was under 5 μm (77%, n=49) (**Figure 3.6B**). Altogether, these data indicate that mitotic pH3^{+} glia tended to have large size to undergo cell division, while the non-mitotic pH3^{-} ones were usually small. The different cell size measurements of ectopic glia at different phase may reflect the increased cellular growth and size of cells during mitosis.

We next determined whether regional input or lineage-specific patterning is necessary to specify ectopic glial fate (**Figure 3.7A**). As NBs display lineage-specific phenotypes due to temporal and spatial patterning (Li et al., 2013a), we assessed whether ectopic glia are generated in specific lineages. We found that *pros*$^{-}$ (n= 15 out of 24 clones) and *nerfin-1*$^{-}$ clones (n= 13 out of 25 clones examined) in the CB (**Figure 3.7B-B'''** and **C-C'''**) and VNC (**Figure 3.2B-B'''** and **3.2C-C'''**) both contained ectopic glia at pupal and adult stage. In the VNC, we manually mapped location of the clones where ectopic glia were found. In most *pros*$^{-}$ (**Figure 3.7D**) and *nerfin-1*$^{-}$ clones (**Figure 3.7E**), ectopic glia were detected everywhere throughout the entire VNC. Taken together, these results suggest that the gliogenic potential is a common feature of most, if not all, NB lineages upon loss-of-function of *pros* or *nerfin-1* (n= ~300 flies examined).

To confirm the *pros* null mutant phenotype, we next assessed if knocking down *pros* using *RNAi* is also sufficient to generate ectopic glia. Using a NB-specific driver, called *grainyhead-gal4* (*grh-gal4*) (Chell and Brand, 2010), we knocked down *pros* in a subset of type I lineages; and assessed the size of the lineage, as well as composition of cells within the lineage during larval stages (**Figure 3.8** and **3.9**). We used two *pros*^{RNAi} lines, which have been previously validated and both target all transcripts of *pros* gene (See **Figure 2.1, Chapter 2**): *pros*$^{RNAi\ SH}$*(II)* called SH line (Froldi et al., 2015b; van den Ameele and Brand, 2019), and *pros*$^{RNAi\ LH}$*(III)* termed LH line (Shaw et al., 2018). The SH line was stronger than the LH line. It induced tumour growth when overexpressed with *grh-gal4* at 18°C (where the activity of *Gal4* is low) but caused lethality at 25°C. The LH line, on the other hand, is weaker, and when overexpressed with *grh-gal4*, could allow the tumour-bearing flies to survive to adult stages even at 29°C (where the activity of *Gal4* is high). To assess the cell fate and dedifferentiation of NB lineages upon *pros* knockdown, we used RFP to mark the lineages, Mira to mark NBs, and Elav to mark postmitotic neurons.

The control *wildtype* lineages contain one large parental NB (identified by larger size and Mira expression) and a population of postmitotic neurons (indicated by Elav expression) (**Figure 3.8A-A'''**). In contrast, expression of *pros*$^{RNAi\ SH}$ in those lineages induced strong dedifferentation, resulting in the formation of tumour clusters (**Figure**

3.8B-B'''). The *pros*$^{RNAi\ SH}$-expressing lineages predominantly contained Mira^{+} ectopic NBs (**Figure 3.8B''**) and were devoid of neurons (**Figure 3.8B'''**). The ectopic NBs arose by dedifferentiation of GMCs upon *pros* knockdown in NB lineages, consistent with previous findings (Choksi et al., 2006; Shaw et al., 2018). To illustrate, Pros promotes neuronal differentiation in GMCs by inhibiting self-renewal genes and activating differentiation genes (see **Chapter 1.4.4.2**, **Introduction**). Therefore, the strong *pros* knockdown prevents the expression of differentiation genes, blocking neuronal differentiation, and reactivates cell-cycle genes (such as Mira, Dpn and Ase), allowing GMCs to revert to NBs (see **Chapter 1.4.4.2**, **Introduction**). 100% of *pros*$^{RNAi\ SH}$*(II)*-expressing lineages contained ectopic glia (n=10 brains), as revealed by their expression of Repo (**Figure 3.8D''**; red; white arrow). Interestingly, these glia cells also express the NB marker Mira (**Figure 3.8D'''**; grey; white arrow) suggesting that they could be ectopic NBs that may be reprogrammed to either further revert to ectopic glia or produce ectopic glia (these two scenarios will be further discussed in **Chapter 3.2** and **3.3**).

Using the weaker *RNAi* line (*pros*$^{RNAi\ LH}$), we found ectopic stem cells in each lineage (indicated by Mira expression; **Figure 3.9B''-B'''**; white asterisk), and some of these Mira^{+} cells were also Repo^{+} (**Figure 3.9D''-D'''**; white arrow). Ectopic Repo expression by Mira^{+} NBs was found in all *grh>pros*$^{RNAi\ LH}$ brains at L3 larval stages. In addition, we also observed a population of neurons in NB lineages after the weak knockdown of Pros, which was consistent with a prior study at which the same *RNAi* line was used (Shaw et al., 2018). Altogether, our results demonstrate that two *RNAi* lines which attenuate Pros at different levels both caused expansion of neural lineages and ultimately, ectopic glia formation. The presence of ectopic glia in *grh>pros*^{RNAi} lineages at L3 larval stage also suggests that the timing at which ectopic glia cells arise is not restricted to pupal stages as suggested by *pros*$^{-}$ mutant clones (data mentioned above), but is instead dependent on when Pros is knocked down/depleted. The *grh>pros*^{RNAi} lineages generate ectopic glia at earlier developmental stages than *pros*$^{-}$ clones because *UAS-pros*^{RNAi} was induced by *grh-gal4* in NBs in the embryo (Chell and Brand, 2010) (**Figure 3.11**) while *pros*$^{-}$ clones were heat-shock-induced at 48 hours AEL (**Figure 3.11**).

Given ectopic glia can be generated in multiple NB lineages, we next employed another driver with activity restricted to fewer NB lineages to enable lineage specific analysis. Here we utilised *pox^{n}-gal4*, expressed in two bilaterally symmetric neuronal clusters in the CB (Minocha et al., 2017; Shaw et al., 2018), and in six clusters in the VNC of developing brain (**Figure 3.10A-A''**, yellow arrows) (Narbonne-Reveau et al., 2016). Pox^{n} expression is first detected during embryogenesis and is retained in these clusters of neurons throughout development (Minocha et al., 2017). In *wildtype* brains, *pox^{n}* -expressing lineages, labeled with GFP, are small clusters that are located in the thorax of the VNC. The neurons of these lineages extend axons along and towards the neuropil of the VNC at L3 larval stages (**Figure 3.10A'**; green). Using *pox^{n}-gal4* we knocked down *pros* with *pros$^{RNAi\ SH}$*, and stained larval brains with GFP to mark *pox^{n+}* lineages and Mira to mark NBs. We found that *pox^{n+}* lineages expressing *pros$^{RNAi\ SH}$* were expanded and fused on lateral sides of the VNC (**Figure 3.10C-C''**, yellow arrows), compared to the control *betaGal^{RNAi}* (**Figure 3.10B-B''**, yellow arrows). In addition, a pronounced overlap between GFP^{+} *pox^{n+}* cells, and Mira^{+} expression was observed, showing that, upon *pros* knockdown, all cells in the lineages are supernumerary NSC-like cells (**Figure 3.10C''**). The formation of excess NSCs indicates that GMC dedifferentiation has occurred in NB lineages upon *pros* knockdown, consistent with previous findings (Choksi et al., 2006; Shaw et al., 2018). Therefore, loss-of-function of Pros could induce a striking dedifferentiation phenotype in *pox^{n}*-expressing lineages. To investigate if the *pox^{n}* -expressing lineages could give rise to ectopic glia, we labeled larval brains with GFP (lineages) and Repo (glia). We took a closer inspection of single lineages to search for ectopic glia, but never observed Repo expression within *pox^{n+}* lineages (**Figure 3.10D-E''**). We therefore conclude that unlike most lineages in the VNC, the *pox^{n}* -specific lineages never give rise to ectopic glia.

In summary, we established three different models for neural dedifferentiation-derived tumours to study ectopic glia formation (**Figure 3.11**), as follows:
(1) We generated *actin-gal4* MARCM clones mutant for *pros* or *nerfin-1*. Most of these clones generated ectopic glia from pupal stages onward [84% of *pros^{-}* clones (n=47 out of 56); 51% of *nerfin-1^{-}* clones (n= 145 out of 282)]. The ectopic glial population

increases as the clones get larger over time. We calculated the proportion of clones containing ectopic glia over the total clones found in each VNC to measure the probability of detecting ectopic glia. Remarkably, compared to no ectopic glia ever found in *wildtype* counterparts (n= 7 brains), up to 85.4 percent (n= 8 brains) of all *pros*$^{-}$ clones in each brain contain ectopic glia, while the glia could be found in half of *nerfin-1*$^{-}$ clones (n= 23 brains). This reflects that ectopic glia were frequently produced by *pros*$^{-}$ and *nerfin-1*$^{-}$ clones.

(2) We used *grh-gal4* and validated *UAS-pros*^{RNAi} transgenes to perform *pros* knockdown in all type I NB lineages. Pros knockdown also causes lineages to overgrow into tumours. Ectopic glia were reproducibly generated in *grh>pros*^{RNAi} tumours from larval stages (n=8 out of 8 brains) and persisted into adulthood (not shown). They were found throughout most, if not all, regions of the tumour.

(3) We used *pox*^{n}*-gal4* to drive *pros* knockdown in only six specific NB lineages. Lineage-specific knockdown of *pros* also causes striking lineage overgrowth and supernumerary NSCs; however, these lineages did not generate any ectopic glia cells (n= 6 out of 6 brains).

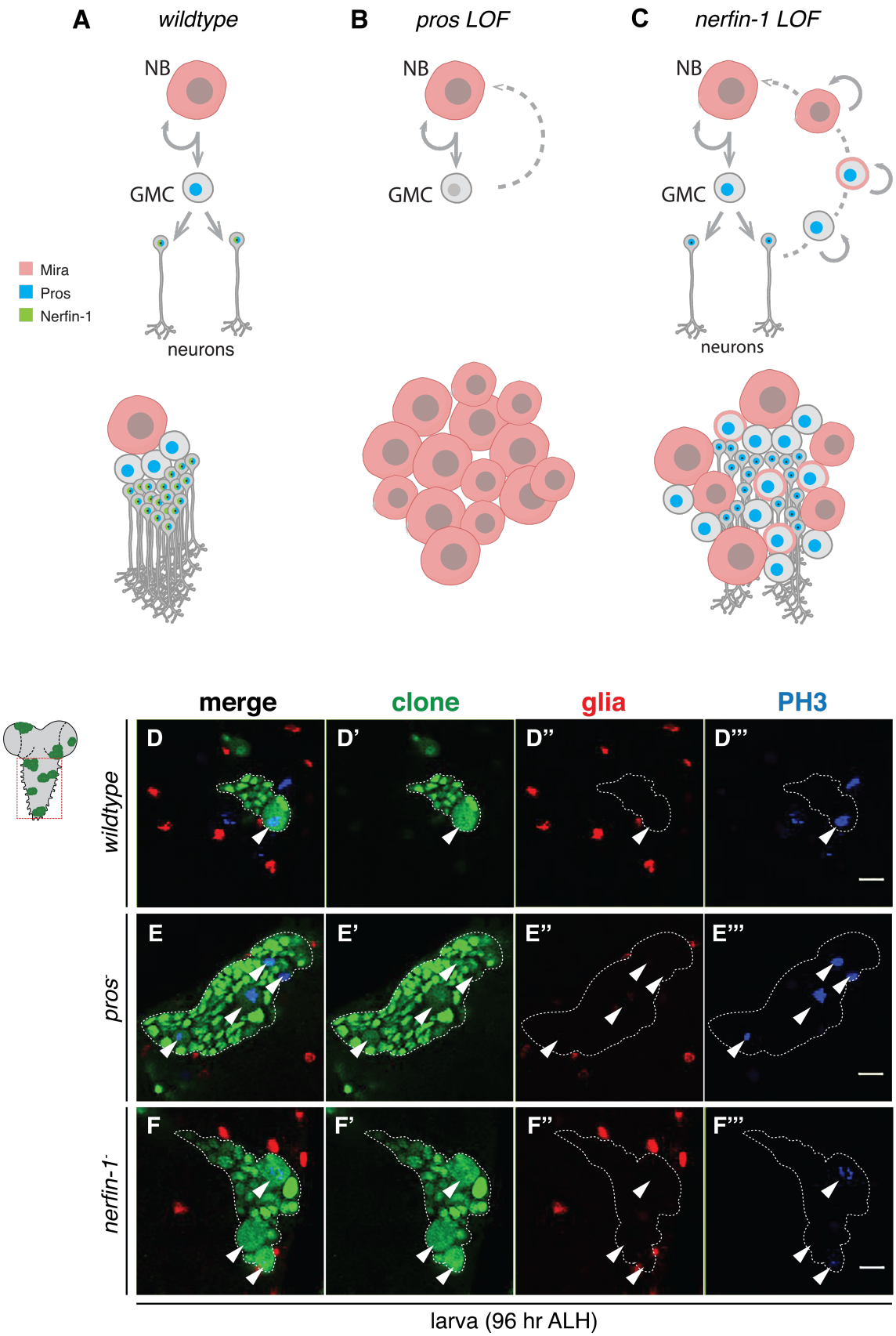
A
wildtype
B
pros LOF
C
nerfin-1 LOF
NB
GMC
neurons
Mira
Pros
Nerfin-1
merge
clone
glia
PH3
D
D'
D''
D'''
E
E'
E''
E'''
F
F'
F''
F'''
wildtype
pros-
nerfin-1-
larva (96 hr ALH)

Figure 3.1. Loss of Nerfin-1 or Pros disrupts neuronal differentiation and gives rise to ectopic NBs in type I lineages during larval development.
(A) Schematic depicting neuronal differentiation of type I lineages in the VNC. Type I NB expressing Mira (red) renews itself and gives rise to a GMC which inherits cell fate determinant Pros (blue). GMC divides once only to produce two post-mitotic neurons, which are locked into differentiated state by Nerfin-1 (green). A *wildtype* clone contains only one parental NB, several GMCs, and numerous terminally differentiating neurons.

(B) Schematic depicting the reversion from GMC to NB in type I lineages upon loss of Pros in the GMC. In the absence of Pros, GMC fails to inhibit NB gene expression, and reverts to stem-cell-like fate, instead of committing to a differentiated, neuronal fate. A *pros*$^{-}$ mutant clone contains several GMCs which are undergoing reversion, and a large population of highly-proliferative ectopic NBs.

(C) Schematic depicting the reversion from neurons to NBs in type I lineages upon loss of Nerfin-1 in neurons. The reverted cells turn on NB-specific genes, including *mira*, but still express differentiation genes, including *pros*. These cells eventually switch off Pros and adopt NB cell fate (Mira^{+}; red) that can undergo asymmetric self-renewal. The neuron-to-NB reversion, therefore, results in the expanding pool of proliferative NBs at the expense of neurons. A *nerfin-1*$^{-}$ mutant clone consists of mixture of neurons and ectopic NBs at various reversion stages.

(D-F’’’) Representative confocal images of *wildtype* control (D-D’; green), *pros*$^{-}$ (E-E’; green), and *nerfin-1*$^{-}$ clones (F-F’; green) in the larval VNC after 72 hours of clone induction. Scale bars, 10 μm. Clones are stained with anti-GFP (clone; green), anti-Repo (glial cells; red), and anti-pH3 (mitotic cells; blue) and are outlined by dashed white line. Merged and single channels are shown. Parental NBs and ectopic NBs are marked by white arrowheads. Repo^{+} glial cells (red) were only found outside of the clone region (dashed outline).

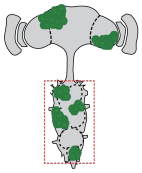

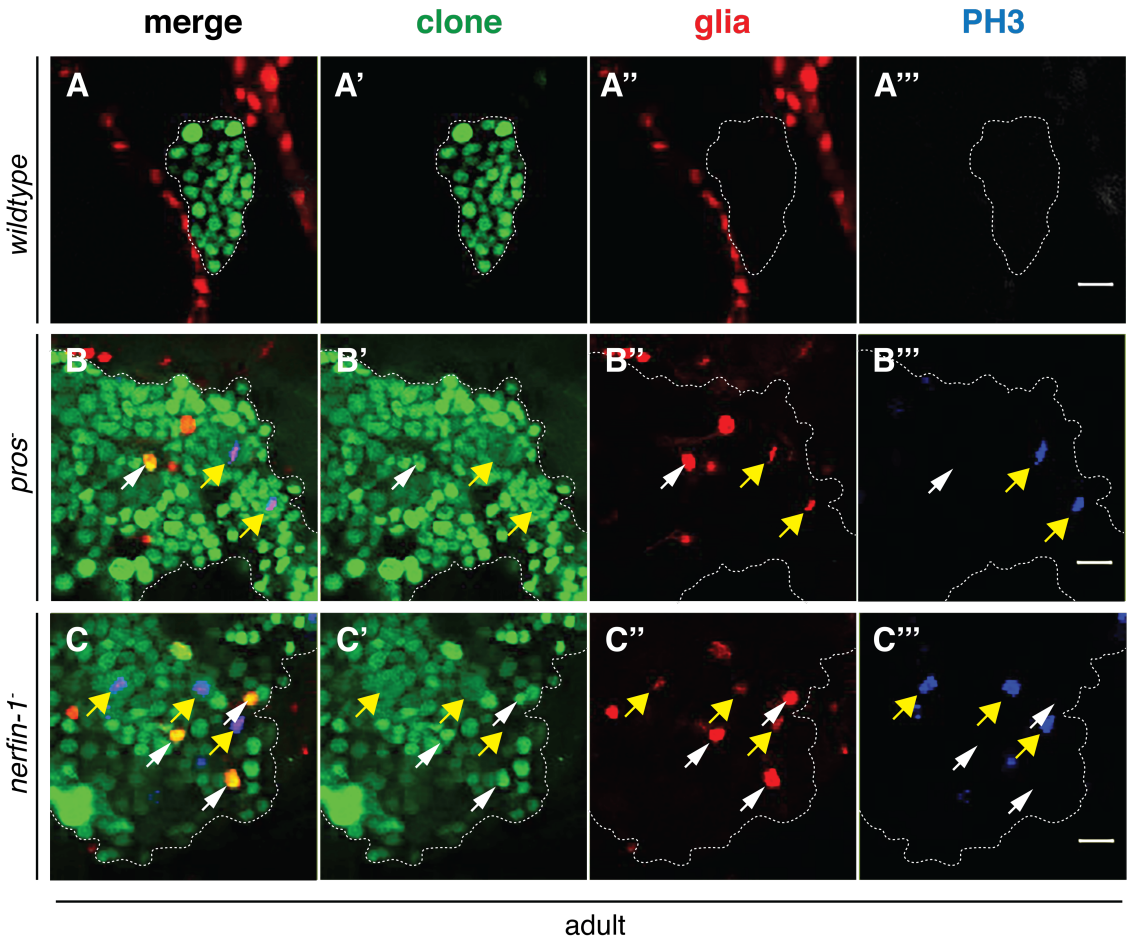
merge
clone
glia
PH3
wildtype
pros-
nerfin-1-
A
A'
A''
A'''
B
B'
B''
B'''
C
C'
C''
C'''
adult

D

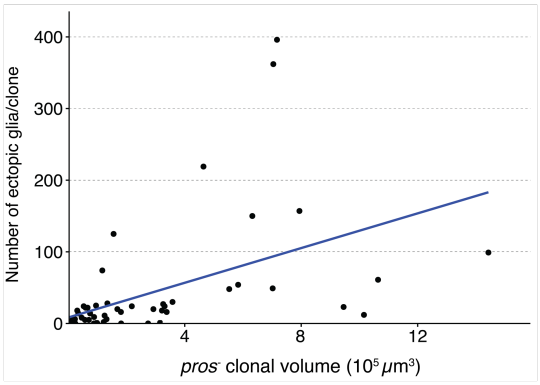
Number of ectopic glia/clone
400
300
200
100
0
4
8
12
pros- clonal volume (10⁵ μm³)

E

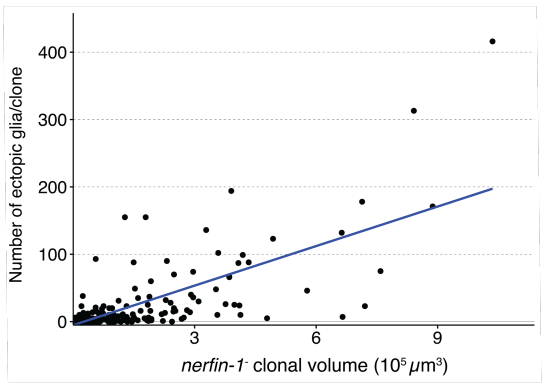
Number of ectopic glia/clone
400
300
200
100
0
3
6
9
nerfin-1- clonal volume (10⁵ μm³)

Figure 3.2. Ectopic glia cells arise in type I *pros*$^{-}$ and *nerfin-1*$^{-}$ mutant clones during adult stages.

Clones were immunostained with GFP (clone; green), Repo (glia; red) and pH3 (mitotic cells; blue). Merged and single channels are shown. Clones are outlined by dashed white line. Scale bars, 10 μm.

(A-C’’’) Representative single confocal images of *wildtype* control (A-A’), *pros*$^{-}$ (B-B’), and *nerfin-1*$^{-}$ clones (C-C’) from 2- to 3-day-old adult VNC.

(A-A’’’) An adult *wildtype* clone (A’; green; dashed outline) is fully differentiated and contains no NB. Repo^{+} glial cells are only found outside of the neuroblast clone (A’’; red; n= 44).

(B-B’’’) An adult *pros*$^{-}$ clone contains multiple proliferating NBs (B’’’; pH3^{+} yellow arrow), some of which also express Repo (B’’; red; arrows; n= 29).

(C-C’’’) An adult *nerfin-1*$^{-}$ clone contains multiple proliferating NBs (C’’’; pH3^{+} yellow arrow), some of which also express Repo (C’’; red; arrows; n= 86).

(D-E) Scatter plots depicting significant positive correlation between the number of ectopic glia and *pros*$^{-}$ tumour volume (D) [$r(56) = 0.5$, $p<0.0001$], and *nerfin-1*$^{-}$ (E) [$r(282) = 0.7$, $p<0.0001$].

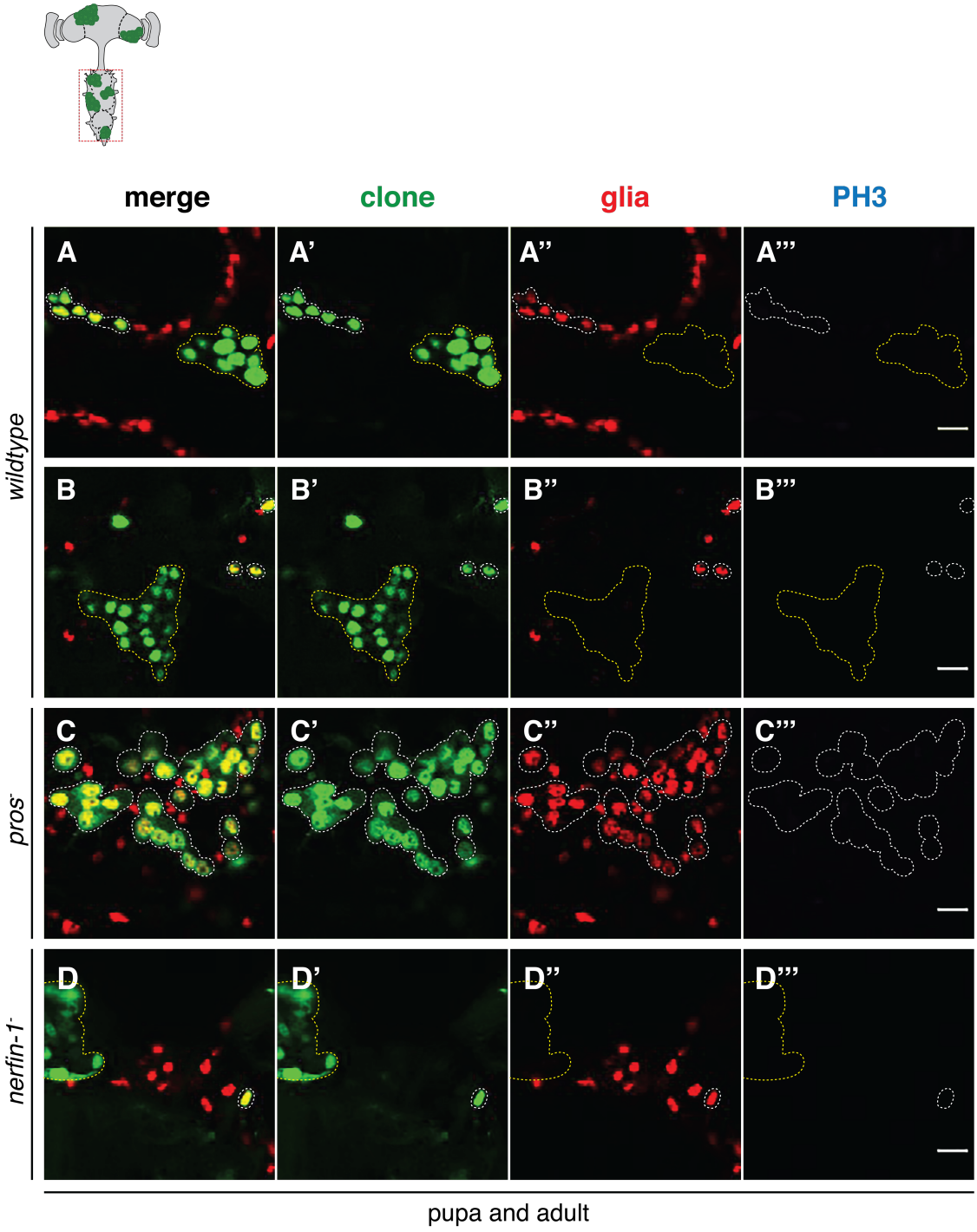
merge
clone
glia
PH3
A
A'
A''
A'''
B
B'
B''
B'''
C
C'
C''
C'''
D
D'
D''
D'''
wildtype
pros-
nerfin-1-
pupa and adult

Figure 3.3. Glial clones derived from glial precursors during pupal and adult stages.

MARCM clones were immunostained with GFP (clone; green), Repo (glia; red) and pH3 (mitotic cells; blue). Merged and single channels are shown. Glial clones are outlined by dashed white line. Neuroblast clones are outlined by dashed yellow line. Scale bars, 10 μm.

(A-D''') Representative single confocal images of *wildtype* control (A-B'), *pros*$^{-}$ (C-C'), and *nerfin-1*$^{-}$ clones (D-D') from pupal and adult VNCs.

(A-B''') Pupal and adult *wildtype* clones (A'-B'; green; white dashed outline) are generated in glial precursors and contain only Repo^{+} glial cells (A''-B''; red). The glial clones (n= 17) are separated from neuroblast clones (A'-B'; green; yellow dashed outline).

(C-C''') An adult *pros*$^{-}$ clone (C'; green; white dashed outline) is generated in glial precursors and contains only Repo^{+} glial cells (C''; red). The glial clones (n= 10) are separated from neuroblast clones (not shown).

(D-D''') An adult *nerfin-1*$^{-}$ clone (D'; green; white dashed outline) is generated in glial precursors and contains only Repo^{+} glial cells (D''; red). The glial clones (n= 9) are separated from neuroblast clones (D'; green; yellow dashed outline).

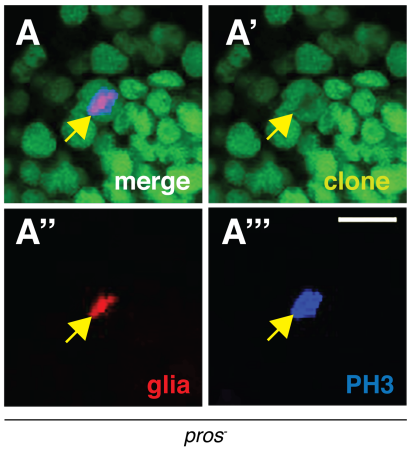
A
merge
A'
clone
A''
glia
A'''
PH3
pros-

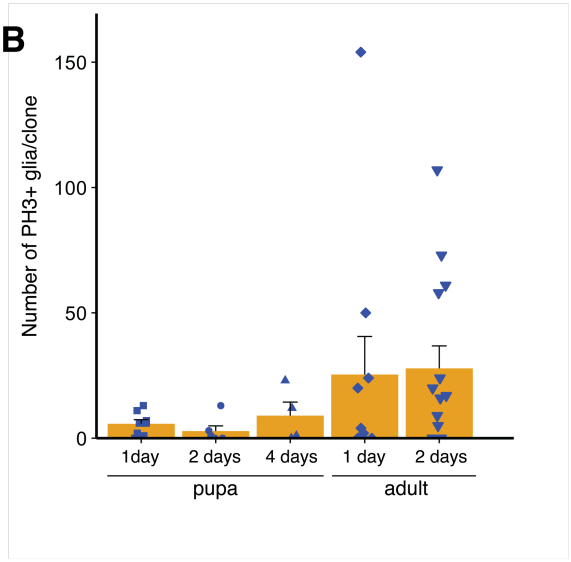
B
Number of PH3+ glia/clone
150
100
50
0
1day
2 days
4 days
1 day
2 days
pupa
adult

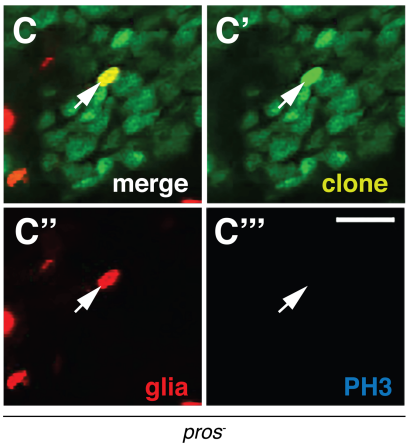
C
merge
C'
clone
C''
glia
C'''
PH3
pros-

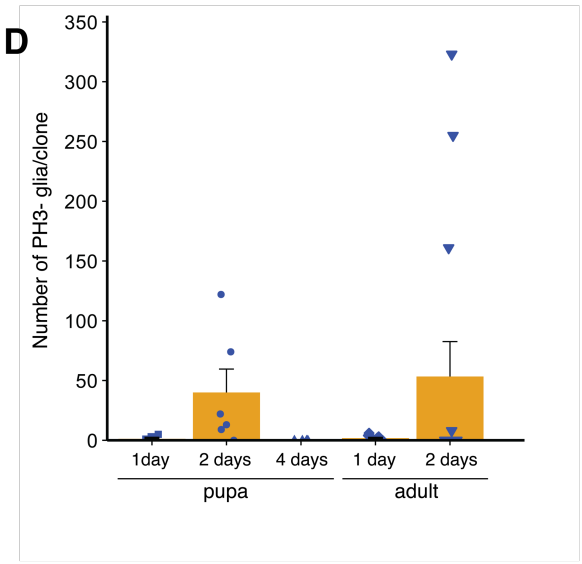
D
Number of PH3- glia/clone
350
300
250
200
150
100
50
0
1day
2 days
4 days
1 day
2 days
pupa
adult

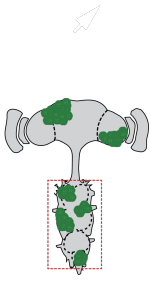

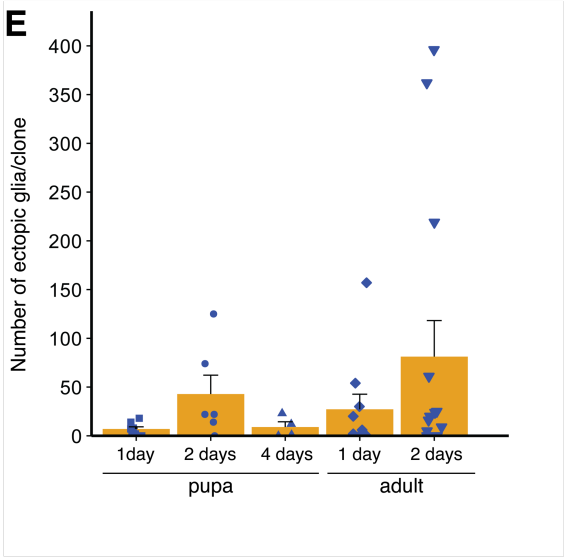
E
Number of ectopic glia/clone
400
350
300
250
200
150
100
50
0
1day
2 days
4 days
1 day
2 days
pupa
adult

Figure 3.4. The number of ectopic glia in *pros*$^{-}$ clones increases with developmental timing.

GFP-labelled MARCM clones were heat-shock-induced at 48 hours AEL. Clones from pupal and adult brains were analysed for the number of mitotic glial cells (B), non-mitotic glial cells (D) and total number of glial cells (E). Clones were immunostained with GFP (clone; nuclear green), Repo (glia; red) and pH3 (mitotic cells; blue). Clones are outlined with dashed white line. Merged and single channels are shown. Scale bars, 10 μm.

(A-B) Representative images of clones containing proliferative glia cells in *pros*$^{-}$ adult clone (A-A’’’, PH3^{+}, blue), quantified in B, (n= 8; 6; 4; 10; 14 respectively)]. There is no significant difference in the mean number of pH3^{+} glia in clones of different ages [one-way ANOVA, F= 1.235, df = 4 and 37, p=0.3129 (ns)].

(C-D) Representative images of clones containing non-mitotic glia cells (C’’’, PH3^{-}), quantified in (D) (n= 8; 6; 4; 10; 14 respectively)]. There is no significant difference in the mean number of none-pH3 glia in clones of different ages [one-way ANOVA, F= 1.383, df = 4 and 37, p= 0.2587 (ns)].

(E) Total number of ectopic glia cells found during development. n= 8; 6; 4; 10; 14 respectively. There is no significant difference in the mean number of glia in clones of different ages [one-way ANOVA, F= 1.240, df = 4 and 37, p= 0.3109 (ns)].

In all graphs, data is plotted as means ± SEM.

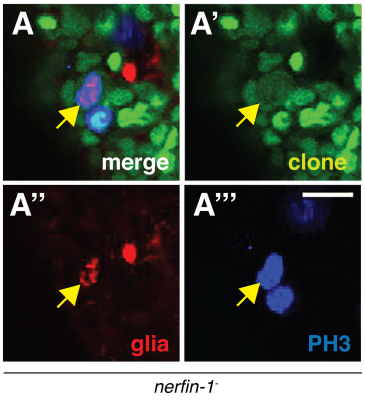
A
A'
merge
clone
A''
A'''
glia
PH3
nerfin-1-

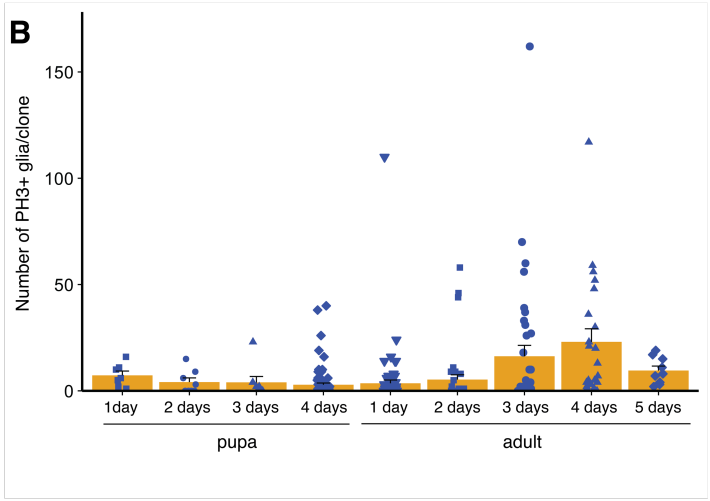
B
Number of PH3+ glia/clone
150
100
50
0
1day
2 days
3 days
4 days
1 day
2 days
3 days
4 days
5 days
pupa
adult

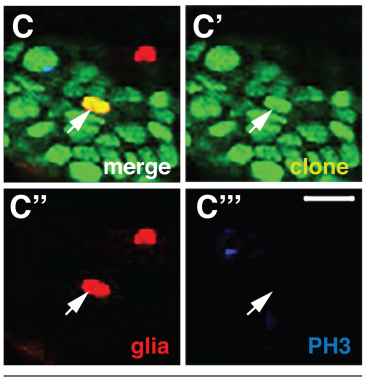
C
C'
merge
clone
C''
C'''
glia
PH3
nerfin-1-

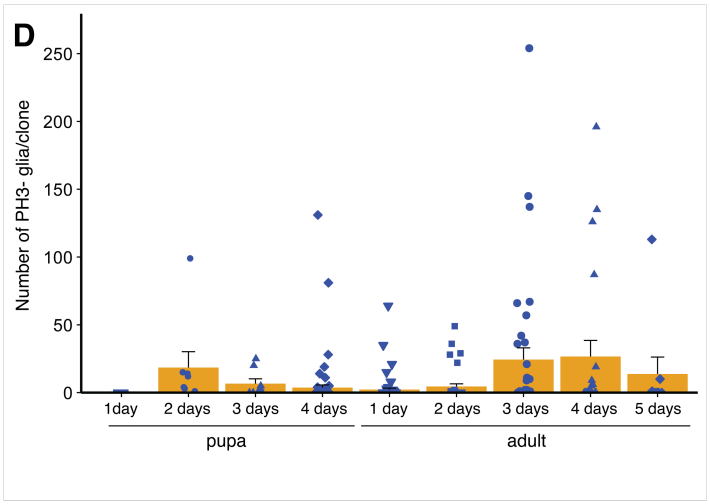
D
Number of PH3- glia/clone
250
200
150
100
50
0
1day
2 days
3 days
4 days
1 day
2 days
3 days
4 days
5 days
pupa
adult

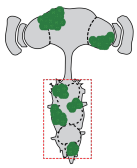

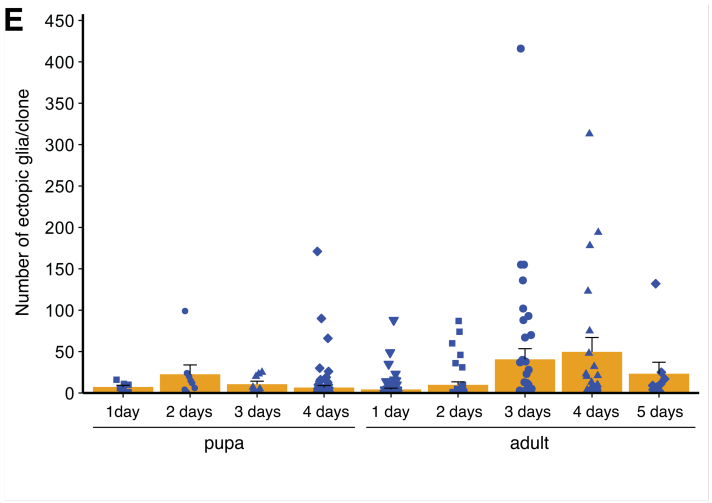
E
Number of ectopic glia/clone
450
400
350
300
250
200
150
100
50
0
1day
2 days
3 days
4 days
1 day
2 days
3 days
4 days
5 days
pupa
adult

Figure 3.5. The number of ectopic glia in *nerfin-1*$^{-}$ clones increases with developmental timing.
GFP-labelled MARCM clones were heat-shock-induced at 48 hours AEL. Clones from pupal and adult brains were analysed for the number of mitotic glial cells (B), non-mitotic glial cells (D) and total number of glial cells (E). Clones were stained with GFP (clone; nuclear green), Repo (glia; red) and pH3 (mitotic cells; blue). Clones are outlined with dashed white line. Merged and single channels are shown. Scale bars, 10 μm.

(A-B) Representative images of clones containing mitotic glia cells in *nerfin-1*$^{-}$ adult clone (A-A’’’, PH3^{+}, blue), quantified in B, (n= 7, 8, 8, 81,75, 37, 37, 22, 9 respectively)]. There are significant differences in the mean number of pH3^{+} glia in clones of different ages (one-way ANOVA, F= 5.054, df = 8 and 275, p<0.0001).

(C-D) Representative images of clones containing non-mitotic glia cells (C-C’’’, PH3^{-}), quantified in (D), (n= 7, 8, 8, 81,73, 37, 37, 22, 9 respectively)]. There are significant differences in the mean number of pH3^{-} glia in clones of different ages (one-way ANOVA, F= 3.648, df = 8 and 273, p=0.0005).

(E) Total number of ectopic glia cells found during development. n= 7, 8, 8, 81,73, 37, 37, 22, 9 respectively. There are significant differences in the mean number of glia in clones of different ages (one-way ANOVA, F= 5.091, df = 8 and 273, p<0.0001).

In all graphs, data is plotted as means ± SEM.

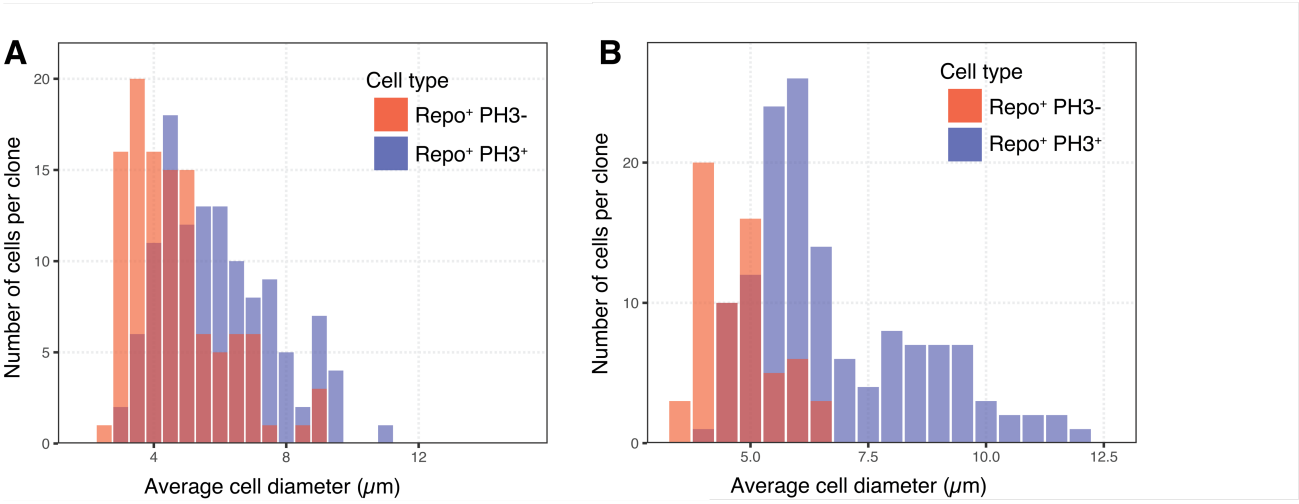

Figure 3.6. Ectopic glia display variable cell sizes.
Histograms depicting cell sizes of ectopic glia found in *pros*$^{-}$ (A) and *nerfin-1*$^{-}$ (B) clones. Cell diameters of nuclear GFP-labeled ectopic glia were measured in µm by using FIJI analysis software.

(A) In *pros*$^{-}$ pupal clones, 100% of non-mitotic glia (n=111) are between 2.5 and 9 µm in diameter; of which the majority (75%; n = 83) are within 2.5-5 µm range.
Whereas, 100% of mitotically active glia (n=121) are between 3 and 11 µm in diameter; including 48% (n=58) are between 6 and 10 µm. This indicates that PH3^{-} glia tend to have small size while PH3^{+} glia are usually larger.

(B) In *nerfin-1*$^{-}$ pupal clones, 100% of non-mitotic glia (n= 63) are between 3.5 and 8 µm in diameter; of which the majority (77%; n=49) are within 3.5-5 µm range. Whereas, 100% of mitotically active glia (n= 136) are between 4 and 12 µm in diameter; including 76% (n=103) are between 5.5 and 10 µm. This indicates that PH3^{-} glia tend to have small size while PH3^{+} glia are usually larger.

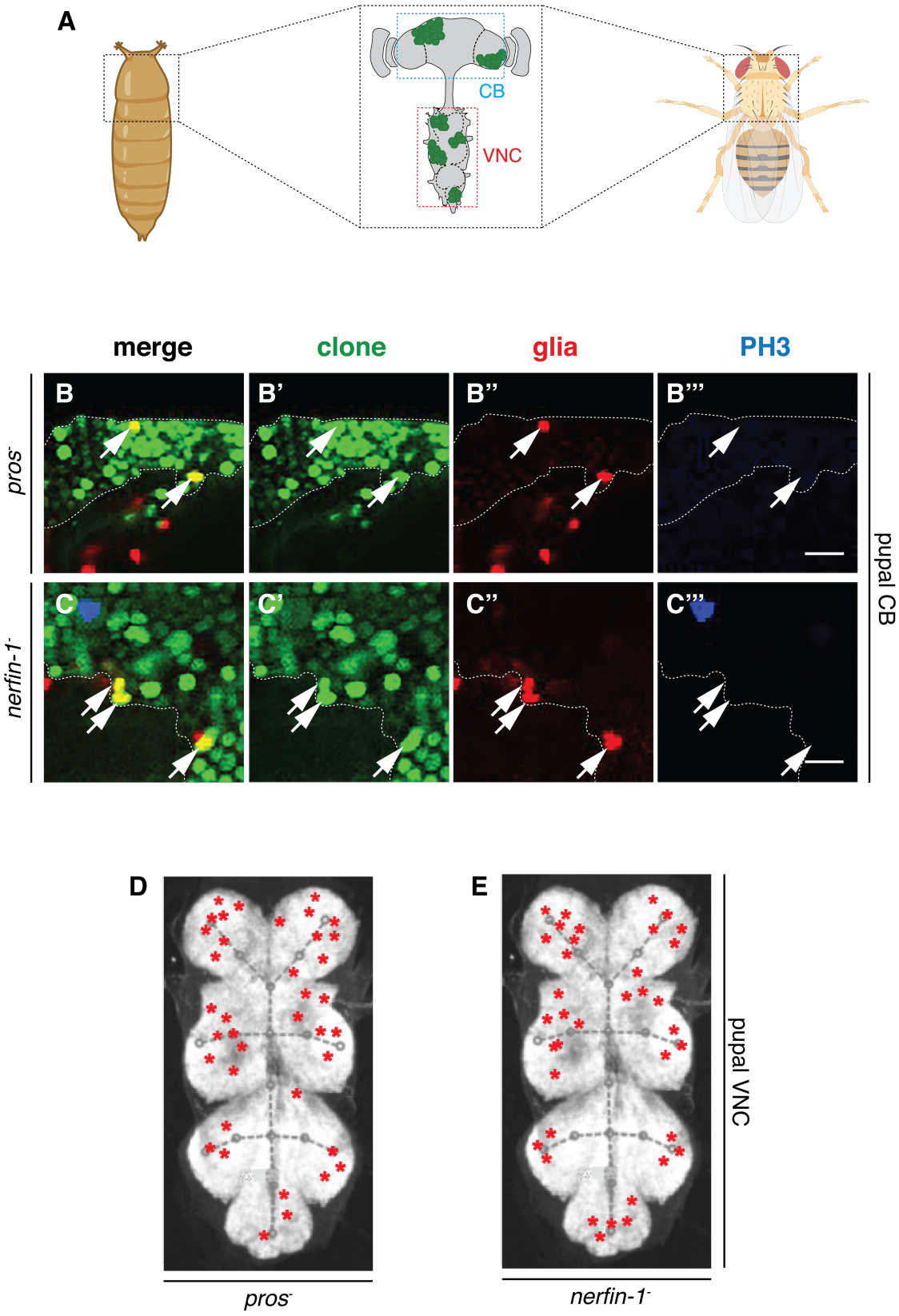
A
CB
VNC
merge
clone
glia
PH3
B
B'
B''
B'''
C
C'
C''
C'''
pros-
nerfin-1-
pupal CB
D
E
pros-
nerfin-1-
pupal VNC

Figure 3.7. Ectopic glia formation is common to most locations in *Drosophila* CNS upon *pros* or *nerfin-1* loss-of-function.
The formation of ectopic glia is not due to lineage specific effect as they were found everywhere in *Drosophila* CNS.

(A) Schematic depicting the CB and VNC regions of the pupal and adult CNS.

(B-B''') Single confocal images of representative ectopic glia (B''; red; white arrow) found in a *pros*$^{-}$ clone located in the CB. Scale bars, 10 μm.

(C-C'") Single confocal images of representative ectopic glia (C''; red; white arrow) found in a *nerfin-1*$^{-}$ clone located in CB. Scale bars, 10 μm.

(D-E) Schematics depicting the locations of ectopic glia in *pros*$^{-}$ (D) and in *nerfin-1*$^{-}$ clones (E) in the VNC. They were found everywhere, and were most abundant in the thoracic segments.

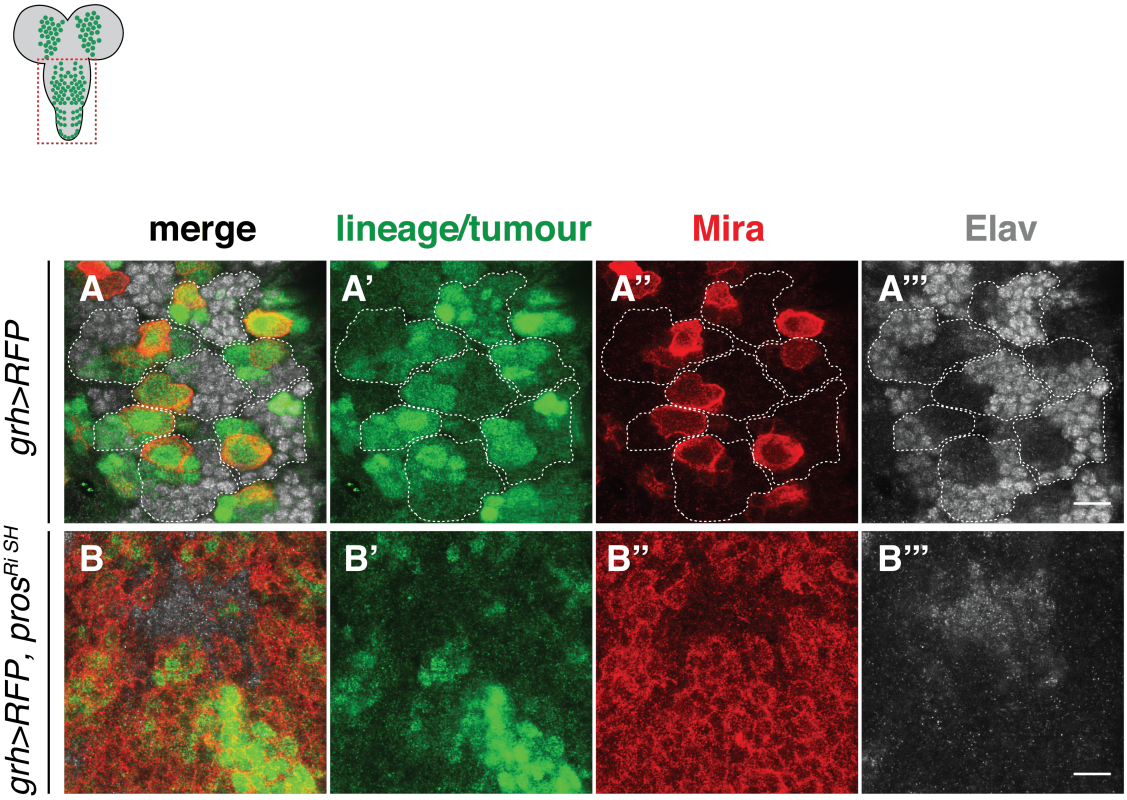
merge
lineage/tumour
Mira
Elav
grh>RFP
grh>RFP, prosRi SH
A
A'
A''
A'''
B
B'
B''
B'''

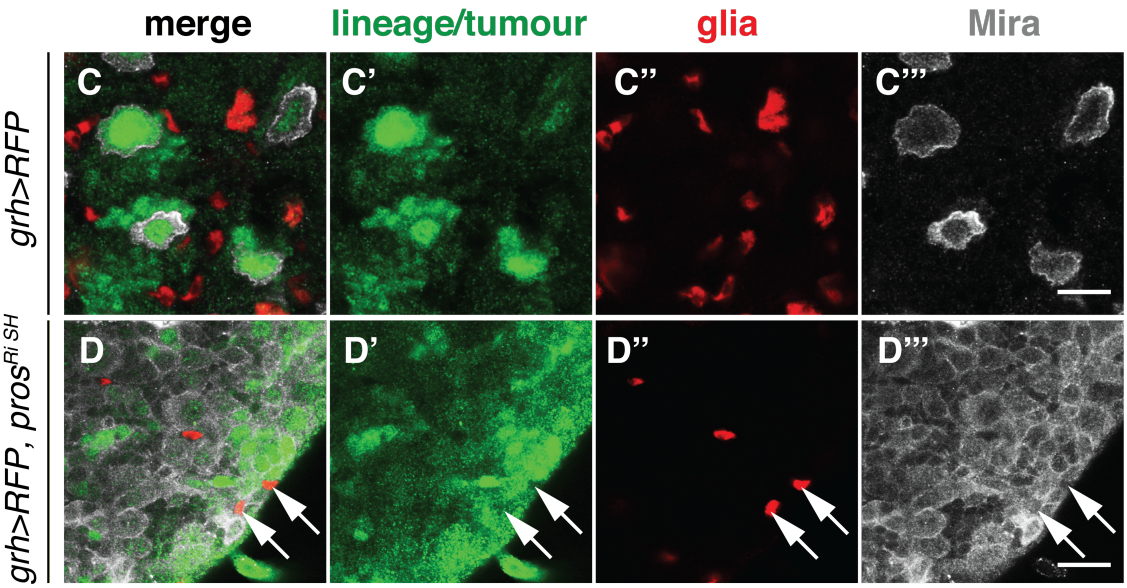
merge
lineage/tumour
glia
Mira
grh>RFP
grh>RFP, prosRi SH
C
C'
C''
C'''
D
D'
D''
D'''

Figure 3.8. Ectopic glia are generated by type I NB lineages of the larval VNC upon *pros* knockdown via *grh-gal4>pros$^{RNAi\ SH}$(II)*.
L3 larval brains (120 hours AEL) of the indicated genotypes were immunostained with different antibody combinations. In (A-B'''): RFP (lineages; false coloured as green), Mira (NB; red) and Elav (neuron; grey). In (C-D'''): RFP (lineages; false coloured as green), Repo (glia; red) and Mira (NB; grey). Merged and single channels are shown. Scale bars,10 μm.

(A-B''') Representative confocal images of several NB lineages expressing RFP only (*grh>RFP*; A-A''') or RFP and *pros$^{RNAi\ SH}$* (*grh>pros$^{RNAi\ SH}$*; B-B'; green). The *pros$^{RNAi\ SH}$*-expressing lineages contain supernumerary ectopic NBs (B'') and were devoid of neurons (B'''). The *wildtype* NB lineages are outlined with dashed white lines.

(C-D''') The *pros$^{RNAi\ SH}$*-expressing lineages give rise to ectopic glia (D''; red; white arrow) which are also Mira^{+} (D'''; grey). No Repo expression was found in *grh^{+}* lineages in control VNC.

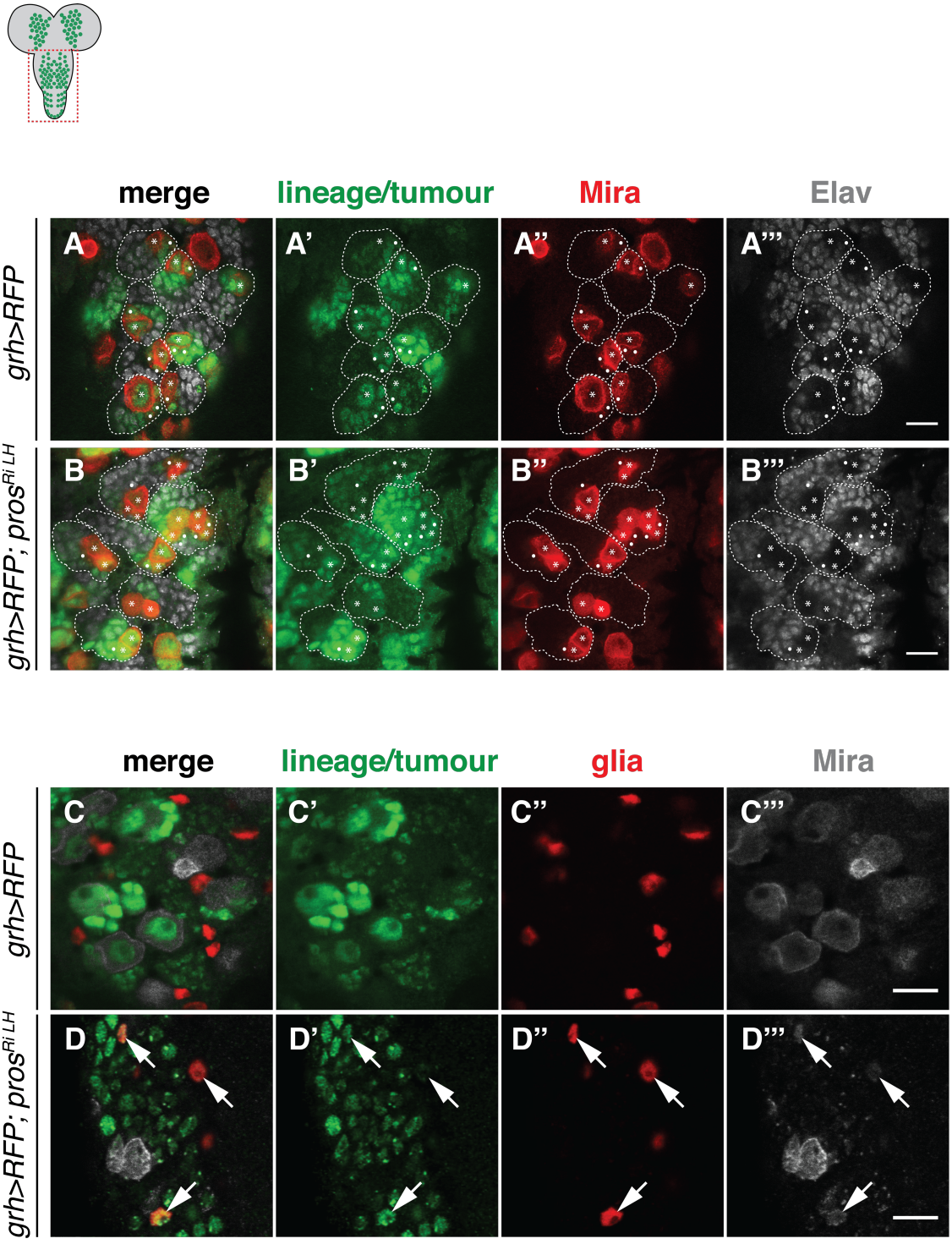
merge
lineage/tumour
Mira
Elav
grh>RFP
grh>RFP; pros^RiLH
A
A'
A''
A'''
B
B'
B''
B'''
merge
lineage/tumour
glia
Mira
grh>RFP
grh>RFP; pros^RiLH
C
C'
C''
C'''
D
D'
D''
D'''

Figure 3.9. Ectopic glia are generated by type I NB lineages of larval VNC upon *pros* knockdown via *grh>pros$^{RNAi\ LH}$*.

L3 larval brains (120 hours AEL) were immunostained with different antibody combinations. In (A-B’’’): RFP (lineages; false coloured as green), Mira (NB; red) and Elav (neuron; grey). In (C-D’’’): RFP (lineages; false coloured as green), Repo (glia; red) and Mira (NB; grey). Merged and single channels are shown. Scale bars,10 μm.

(A-B’’’) Representative confocal images of several NB lineages expressing RFP (*grh>RFP*; A-A’’’) or RFP and *pros$^{RNAi\ LH}$* (*grh>pros$^{RNAi\ LH}$*; B-B’’’). Every *wildtype* NB lineage contains one parental NB (Mira^{+}; A’’; red; white asterisk), several GMCs (Mira^{+}; A’’; red; white dot), and differentiated neurons (A’’’; grey). *pros$^{RNAi\ LH}$* -expressing lineages contain two or more Mira^{+} NBs (B’’; red; white asterisk), several GMCs (Mira^{+}; B’’; red; white dot) and mostly differentiated neurons (B’’’; grey). The NB lineages are outlined with dashed white lines.

(C-D’’’) The *pros$^{RNAi\ LH}$*-expressing lineages contain ectopic glia (D’’; red; white arrow) which are Mira^{+} (D’’’; grey). No Mira^{+}/Repo^{+} cells were found in *grh>RFP* control VNCs.

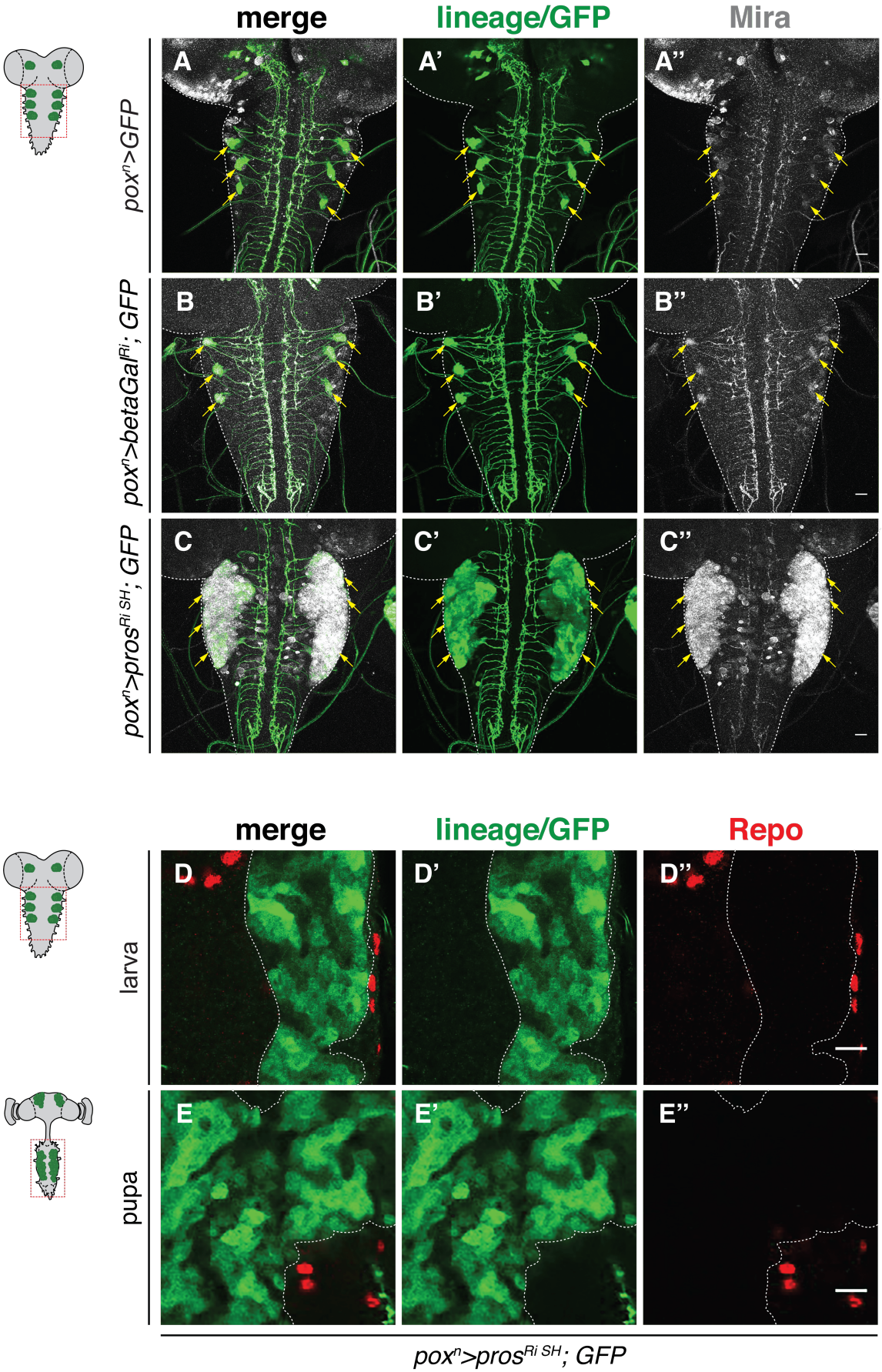
merge
lineage/GFP
Mira
A
A'
A''
pox^n>GFP
B
B'
B''
pox^n>betaGal^Ri; GFP
C
C'
C''
pox^n>pros^Ri SH; GFP
merge
lineage/GFP
Repo
D
D'
D''
larva
E
E'
E''
pupa
pox^n>pros^Ri SH; GFP

Figure 3.10. Ectopic glia were never recovered in *pox^n* lineages of the VNC upon *pros* knockdown.

pox^n-gal4 driver was used to induce the expression of GFP and *pros$^{RNAi\ SH}$(II)* in six *pox^n* lineages of larval VNC. L3 larval brains (120 house AEL) of the indicated genotypes were immunostained with GFP (lineages; green), Repo (glia; red) and Mira (NB; grey). Merged and single channels are shown. Scale bars, 20 μm in (A-C’’’) and 10 μm elsewhere.

(A-A’’) Representative confocal images of *wildtype pox^n* lineages (A-A’’; green) labelled by *gal4*-driven GFP expression in larval VNC (120 hours AEL). The six *pox^n* NB lineage clusters expressing GFP in the thorax are marked by yellow arrows. The VNC regions are outlined with dashed lines, and are shown as maximum-projection images.

(B-C’’) Representative confocal images of *pox^n* lineages expressing *betaGal^{RNAi}* (control; B-B’’; green) or *pros$^{RNAi\ SH}$* (*pox^n >pros$^{Ri\ SH}$*; C-C’’; green) induced by *pox^n-Gal4* driver. The *pros* knockdown causes tumour formation in the six lineages, and the majority of tumour cells are ectopic NBs (C’’; Mira$^+$, grey).

(D-E’’) Representative high-magnification confocal images of larval (D-D’’; green) and adult *pox^n>pros$^{RNAi\ SH}$* tumours (E-E’’; green). Ectopic glia were never observed in these tumours (D’’ and E’’; red). Tumours are outlined by dashed white lines.

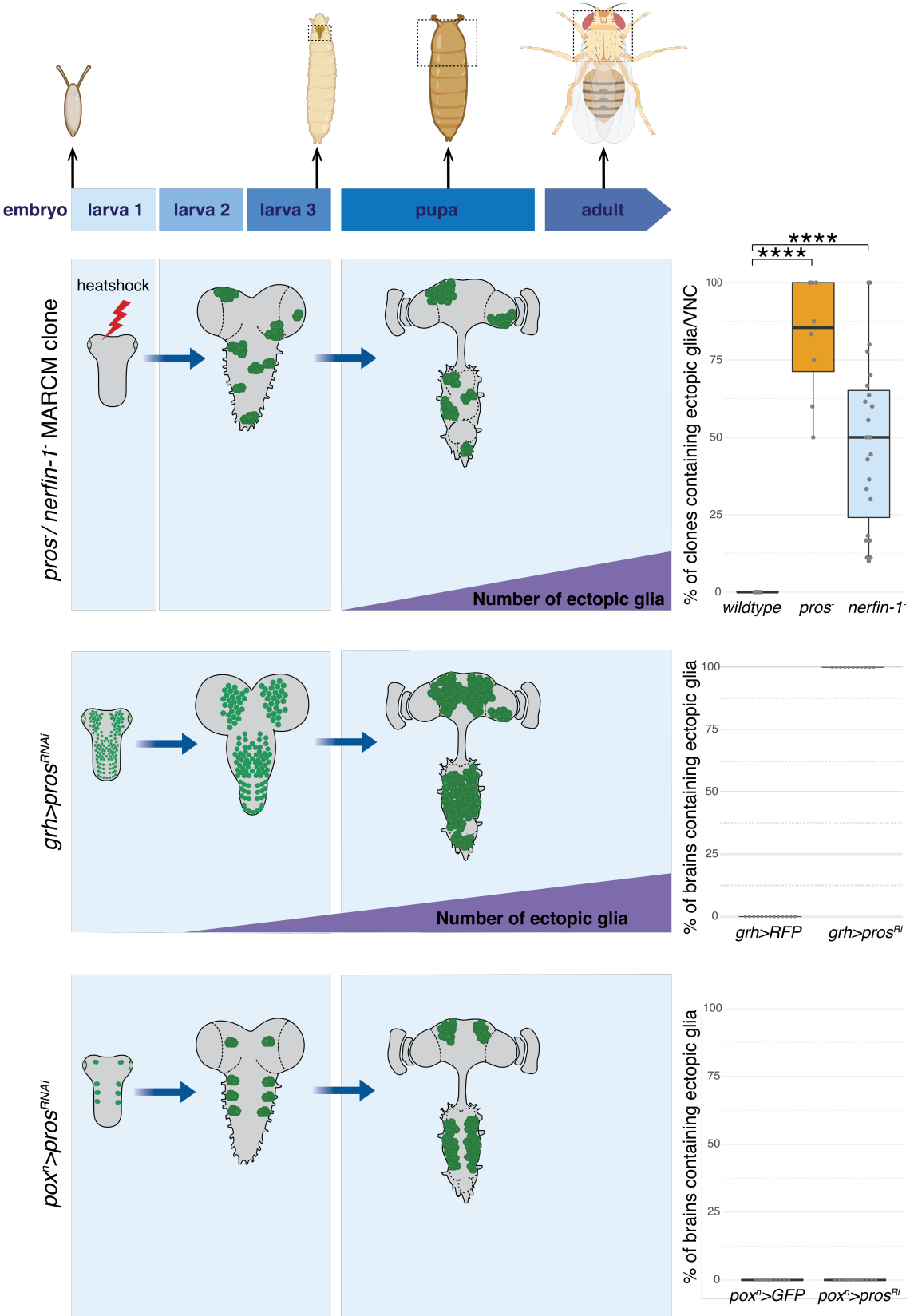
embryo
larva 1
larva 2
larva 3
pupa
adult
pros⁻ / nerfin-1⁻ MARCM clone
heatshock
Number of ectopic glia
% of clones containing ectopic glia/VNC
****
****
100
75
50
25
0
wildtype
pros⁻
nerfin-1⁻
grh>pros^RNAi
Number of ectopic glia
% of brains containing ectopic glia
100
75
50
25
0
grh>RFP
grh>pros^Ri
pox^n>pros^RNAi
% of brains containing ectopic glia
100
75
50
25
0
pox^n>GFP
pox^n>pros^Ri

Figure 3.11. Three different models of neural dedifferentiation-derived tumours to study ectopic glia formation. Schematic representing three different tumour models and their associated quantifications of ectopic glia frequencies.

(Top) *pros*$^{-}$ or *nerfin-1*$^{-}$ MARCM clones which are heat-shock induced at 48 hours AEL, and randomly distributed throughout the VNC. Ectopic glia are generated from pupal stages, onward. The ectopic glial population expands, as the clones get larger over time. Box plot illustrates the percentage of clones containing ectopic glia observed in each brain upon Pros or Nerfin-1 loss-of-function. Band= median (0% for *wildtype*, 85.4% for *pros*$^{-}$ and 50% for *nerfin-1*$^{-}$). Each box represents the middle 50% of data [Interquartile range (IQR)]. Whiskers extend toward the lowest and highest values within 1.5 IQR. There are significant differences in the percentages of *pros*$^{-}$ and *nerfin-1*$^{-}$ clones having ectopic glia compared to *wildtype* counterpart. n = 7, 8 and 23, respectively; control versus *pros*$^{-}$, ****p<0.0001; control versus *nerfin-1*$^{-}$, ****p<0.0001.

(2) *grh>pros*^{RNAi} tumours whereby *pros* is knocked down in type I NB lineages, by using *grh-gal4* and *UAS-pros*^{RNAi} transgene. Ectopic glia were detected from these lineages at larval stages and persisted into adulthood. All *grh>pros*^{RNAi} brains contain big tumours that are able to give rise to ectopic glia. n = 7 and 8, respectively.

(3) *pox*^{n}*>pros*^{RNAi} tumours whereby *pros* is knocked down in only six *pox*^{n} NB lineages of the VNC by using *pox*^{n}*-gal4* and *UAS-pros*^{RNAi} line. No *pox*^{n}*>pros*^{RNAi} tumours give rise to ectopic glia. n = 7 and 6, respectively.

3.2. Ectopic glia arise by the transdifferentiation of NBs upon loss of Pros or Nerfin-1

Neural stem cells maintain homeostasis within *Drosophila* CNS by renewing themselves and generating more differentiated neural lineages. We report for the first time that type I lineages mutant for *pros* could generate glial cells. However, it is unknown whether ectopic glia are generated (1) as the progeny of asymmetric division of neural progenitors, or (2) by transdifferentiation of neurons or neural progenitor cells. To directly test these possibilities, we performed live imaging of cultured *ex vivo* *Drosophila* brain using time-lapse confocal microscopy. The time-lapse live imaging could allow us to analyse changes in cell fate of *pros*$^{-}$ lineages in great detail, and thereby visualise the formation of ectopic glia. We generated RFP-labelled *pros*$^{-}$ MARCM clones (red) and utilised a GFP-tagged Repo (tagged at the endogeneous locus) (Mukherjee et al., 2016) to track the formation of glia cells in *pros*$^{-}$ clones. CNSs with *repo-GFP; pros*$^{-}$ clones were dissected at mid-pupal stages (2-3 days APF) as ectopic glia were previously characterised to arise during this developmental time window (**Chapter 3.1**, **Figure 3.4**).

Clones located in the pupal VNC were cultured and imaged live for at least 5 hours (**Figure 3.12A**). NBs are identified by their large cell size of around 10 µm. Some of the NBs underwent rounds of division [in 74% of examined cells (n=40/54); **Video 3.3**; **Figure 3.14**]; but in some cases, we saw that NBs gradually switched on Repo-GFP over a period of 10.5 hours (**Figure 3.12B-I**, **Video 3.1**; white arrowhead) or 9.5 hours (**Figure 3.13**, **Video 3.2**; white arrowhead). Taken together, the live-cell imaging data suggest that ectopic Repo expression was detected in 26% (n=14 of 54 cells) of examined NB cells lacking Pros.

Our live-imaging data have shown that a small population of ectopic NBs in *pros*$^{-}$ clones turned on Repo. Consistent with this, all the Repo^{+} cells in the *pros*$^{-}$ clones were Mira^{+} (100% of the cells examined, n= 50 cells in 7 clones; **Figure 3.15A-B**, white arrow, quantified in **Figure 3.18F**). In *grh>pros*^{RNAi} lineages under strong *pros* attenuation with *pros*$^{RNAi\ SH}$, 100% of the Repo^{+} cells were Mira^{+} (n= 35 cells in 4 brains; **Figure 3.15C**, white arrow); the same result was seen by weak attenuation via

pros$^{RNAi\ LH}$ (n=30 cells in 5 brains; **Figure 3.15D**, white arrow). Similarly, 100% of Repo^{+} cells were positive for the immature neural stem cell marker, Dpn (n= 10 cells in 3 *pros*$^{-}$ clones, **Figure 3.16A**; n= 74 cells in 6 *grh>pros*$^{RNAi\ SH}$ brains, **Figure 3.16B**; n= 24 cells in 3 *grh>pros*$^{RNAi\ LH}$ brains, **Figure 3.16C**). Therefore, both Mira and Dpn were expressed in ectopic glia in *pros*-deficient clones as well as *pros*^{RNAi}-expressing lineages, indicating that the ectopic glia retained NB status upon loss or depletion of Pros. Surprisingly, the Repo^{+} cells never expressed type I NB specific-marker Asense (n= 57 cells in 8 *grh>pros*$^{RNAi\ SH}$ brains, **Figure 3.17A-C**; white arrow), suggesting that the NBs which transdifferentiate into Repo^{+} glial cells may be exhibiting type II-like NB characteristics (Ase^{-} Dpn^{+} Mira^{+}), and they never expressed neuronal marker Elav (n= 67 in 5 *pros*$^{-}$ clones, **Figure 3.18A-B**, quantified in **Figure 3.18F**; and n= 30 in 3 *grh>pros*$^{RNAi\ SH}$ brains, **Figure 3.18C-D**).

We observed similar results in *nerfin-1*$^{-}$ clones: Repo^{+} cells within the clone were found to express Dpn (n= 51 Repo^{+} cells in 7 clones; **Figure 3.16D**, white arrow), but not Ase (n= 14 Repo^{+} cells in 3 clones; **Figure 3.17D**, white arrow), and none of these cells expressed neuronal marker Elav (n= 76 Repo^{+} cells in 5 clones, **Figure 3.18E**, white arrow; quantified in **Figure 3.18F**). However, only 7% of ectopic glia in *nerfin-1*$^{-}$ clone expressed Mira (approximately n= 4 out of 57 ectopic glia in one clone examined, **Figure 3.15E**, white arrow; Mira^{-} cells are labelled with yellow arrowhead in **Figure 3.15E-F**). This suggests that in *nerfin-1*$^{-}$ clones, while the ectopic glia cells exhibit type II-like NB characteristics (Ase^{-} Dpn^{+}), most of them are not mature NBs (Mira^{-}).

In summary, our live imaging and molecular marker analysis revealed that upon loss of Pros or Nerfin-1, ectopic NBs that express markers typical of type II-like NBs (Mira and Dpn), could potentially adopt glial characteristics. A subpopulation of *pros*$^{-}$ NBs originated from reverted GMCs gradually switch on Repo, while maintaining NB markers Mira and Dpn. However, *nerfin-1*$^{-}$ NBs which arise via dedifferentiation of neurons, never fully dedifferentiate to become mature NBs, or switch off mature NB markers upon expression of Repo. Further live imaging experiments in *nerfin-1*$^{-}$ clones would enable us to better understand how ectopic NBs behave to become ectopic glia in this context.

Given that NBs frequently transdifferentiate into ectopic glia during tumorigenesis, we asked if these cells play a similar function to the *wildtype* niche glia. In *Drosophila*, lipid droplets containing a core of neutral lipids, mostly localise to the glial niche to protect glia and NSCs from hypoxia and oxidative stress (Bailey et al., 2015). We, therefore, investigated if *pros*$^{-}$ NB lineages also used the ectopic glia to localise more lipid droplets. From both live (**Figure 3.19**, **Video 3.4**; n= 4 clones) and fixed-cell imaging of *pros*$^{-}$ mutant clones (**Figure 3.20B-C**, n= 6 *pros*$^{-}$ clones; and **E-F**, n= 4 *pros*$^{-}$ clones), we consistently observed high lipid droplet accumulation in the mutant clones, especially where the ectopic glia reside (schematised in **Figure 3.21**), in comparison with *wildtype* clones (**Figure 3.20A**, n= 4 clones; and **D**, n= 5 clones). From the confocal images of fixed samples stained with Bodipy and LipidTOX, we found CNS lipid droplets are around 1-2 μm in diameter, consistent with the previous statement (Bailey et al., 2015). In addition, lipid droplets that formed in niche glia (**Figure 3.19B-D**; **Figure 3.20B-C** and **E**, indicated by dashed yellow line and yellow asterisks) are primarily found in or near the ectopic glia (**Figure 3.19B'-D'**, white arrowhead; **Figure 3.20B''-C''** and **E''**; Repo; white arrowhead) within *pros*$^{-}$ mutant clones (n= 14 out of 14 clones examined; including 4 live clones in **Figure 3.19**, and 10 fixed clones in **Figure 3.20B-C, E**). This was consistent with the previous finding that cortex glia that encapsulate NB lineages contain the highest amount of lipid droplets in the larval brain (Kis et al., 2015). This raises the possibility that NB lineages generate ectopic glia to induce the accumulation of CNS lipid droplets for non-cell autonomous protection.

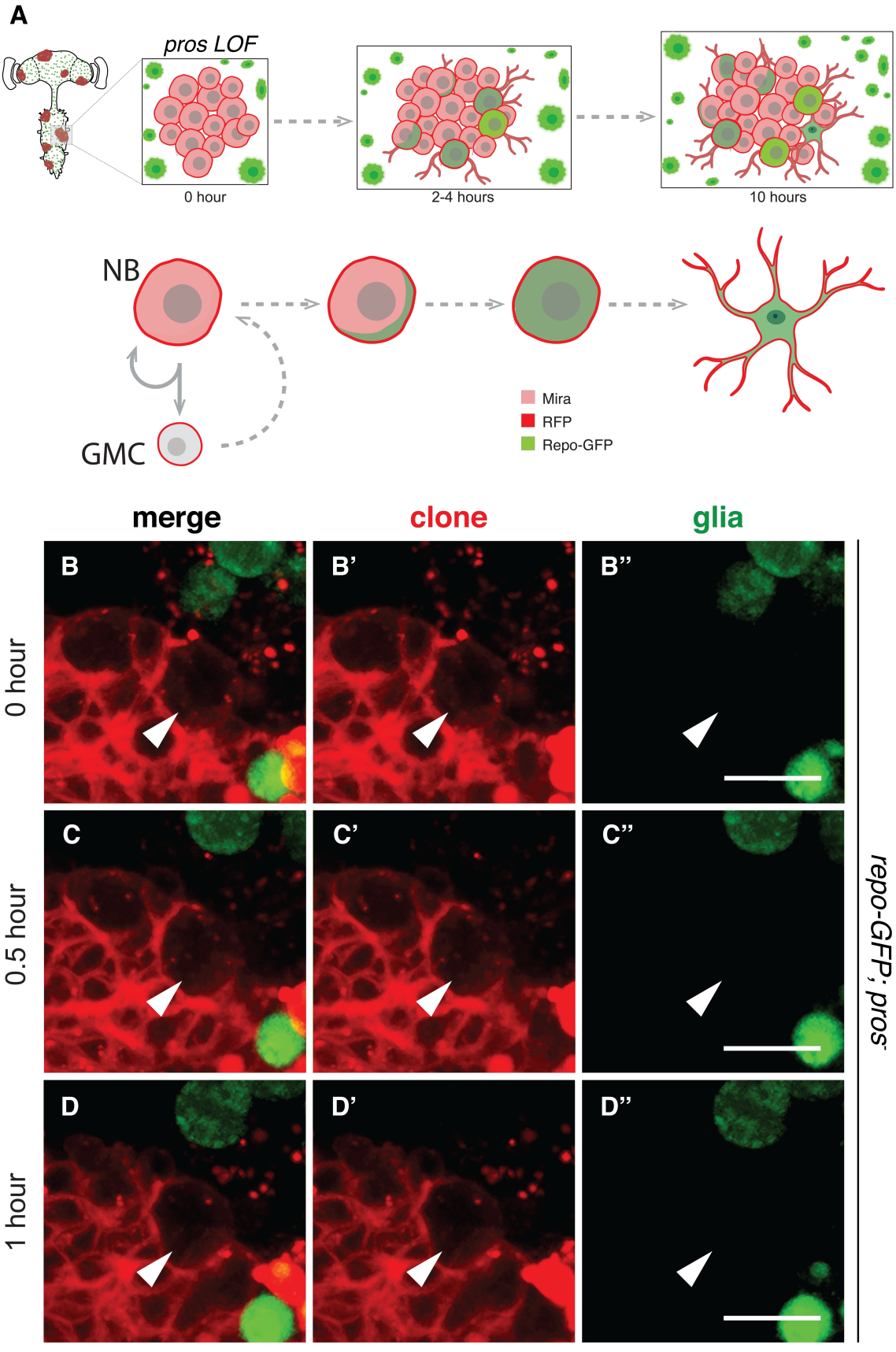
A
pros LOF
0 hour
2-4 hours
10 hours
NB
GMC
Mira
RFP
Repo-GFP
merge
clone
glia
B
B'
B''
C
C'
C''
D
D'
D''
0 hour
0.5 hour
1 hour
repo-GFP; pros-

4 hours
4.5 hours
5.5 hours
9.5 hours
10.5 hours
E
E'
E''
F
F'
F''
G
G'
G''
H
H'
H''
I
I'
I''
repo-GFP; pros-

Figure 3.12. Upon loss of Pros, NBs of type I lineages ectopically turn on Repo and transdifferentiate into ectopic glia in *Drosophila* VNC.
MARCM clones expressing membrane RFP (red) and Repo-GFP were induced at 48 hours AEL. Live *ex vivo* VNCs were imaged every 12 mins during 10-hour period at room temperature (Related to **Video 3.1**).

(A) Schematic diagram depicting the process of NB transdifferentiation into ectopic glia within *pros*$^{-}$ clone in pupal VNC. Some ectopic *pros*$^{-}$ NBs (RFP^{+} Mira^{+}) gradually turn on the glial cell fate determinant protein Repo and display typical glia features (protrusions). These reverted cells showed high Repo expression over the course of imaging.

(B-I'') Still frames from live images of *pros*$^{-}$ clones expressing Repo-GFP showing the step-wise NB-to-glia reversion in *pros*$^{-}$ clone (refer to **Video 3.1**). Scale bars, 10 μm. Times are shown as hours. The time-lapse confocal microscopy images are shown in merged, RFP (clone; red) only, and GFP (glia; green) only channels. Transmitted light channel is not shown. One representative NB (white arrowhead), identified by its large size of around 10 μm, was traced.

(B-B'') At the start of imaging (0 hour), GFP expression (B''; green) was restricted to the *wildtype* glia outside the clone, and was not found in NB (B-B'; red; arrowhead).

(C-E'') The NB at 4 hours has turned on Repo-GFP.

(E-I'') Repo–GFP expression increased in intensity over time in the marked NB, and was also observed in the nearby NB. At the end of imaging (I; 10.5 hours), the neighbour NB formed membrane protrusions (marked by yellow arrowhead) into neighbour regions.

See also Supplemental **Video 3.1**.

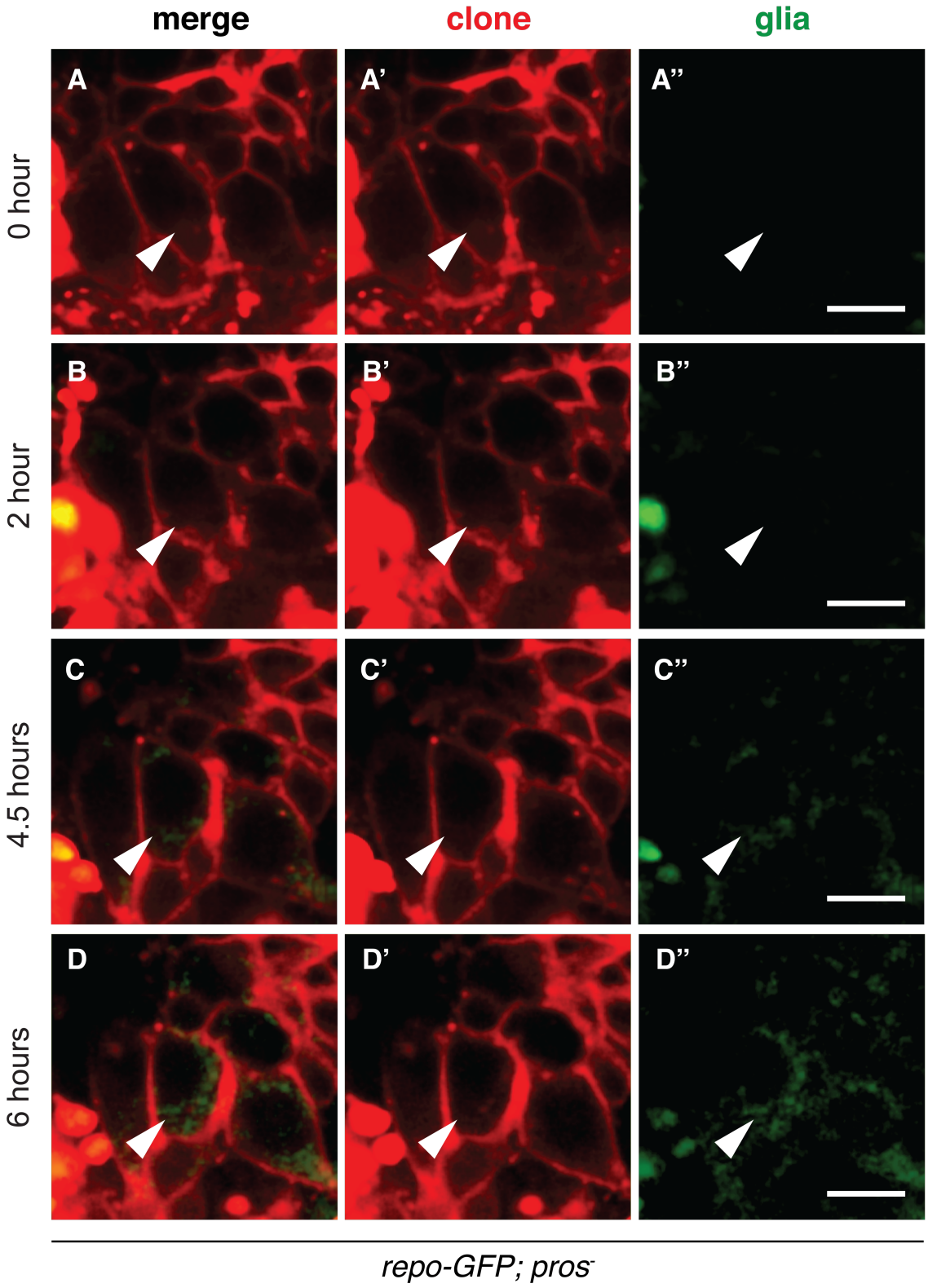
merge
clone
glia
A
A'
A''
B
B'
B''
C
C'
C''
D
D'
D''
0 hour
2 hour
4.5 hours
6 hours
repo-GFP; pros-

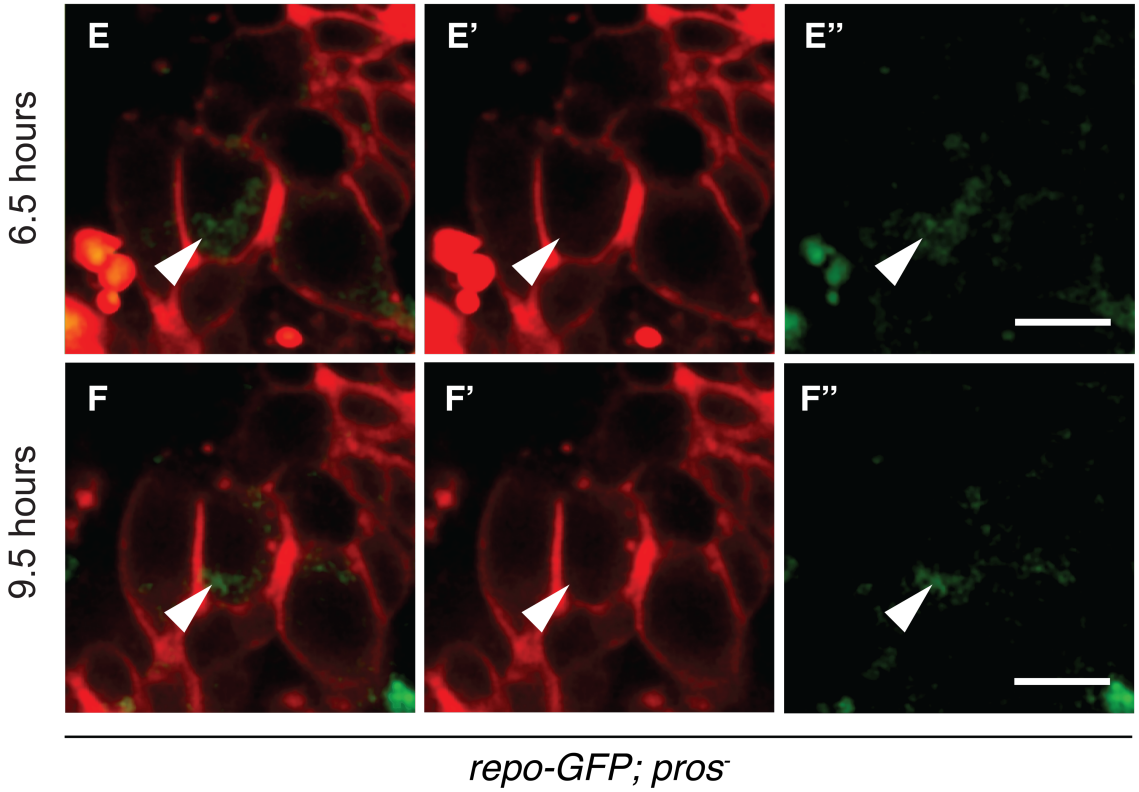

Figure 3.13. Additional example of NB-to-glia transdifferentiation in *pros*$^{-}$ clone located in superficial VNC section.
These live images were achieved from the same raw file of the ones on **Figure 3.12** but the cells of interest were located at different part of the clone (Related to Supplemental **Video 3.2**).

(A-F'') Still frames from live images of *pros*$^{-}$ clones expressing *repo-GFP* showing the step-wise NB-to-glia reversion in *pros*$^{-}$ clone (refer to **Video 3.2**). Scale bars, 10 μm. Times are shown as hours. The time-lapse confocal microscopy images are shown in merged, RFP (clone; red) only, and GFP (glia; green) only channels. Transmitted light channel is not shown. One representative NB (white arrowhead), identified by its large size of around 10 μm, was traced.

(A-A'') At the start of imaging (0 hour), GFP expression (A''; green) was restricted to the *wildtype* glia outside the clone, and was not found in NB (A-A'; red; arrowhead).

(B-C'') The NB still did not express glial marker Repo in (B) and has turned on Repo at 4.5 hour time point in (C).

(D-F'') Repo –GFP expression increased in intensity over time in the marked NB, and was also observed in the nearby NB. At the end of imaging (F; 9.5 hours), this NB

(marked by white arrowhead) and its neighbour NB still maintained RFP and Repo-GFP expression.

See also Supplemental **Video 3.2**.

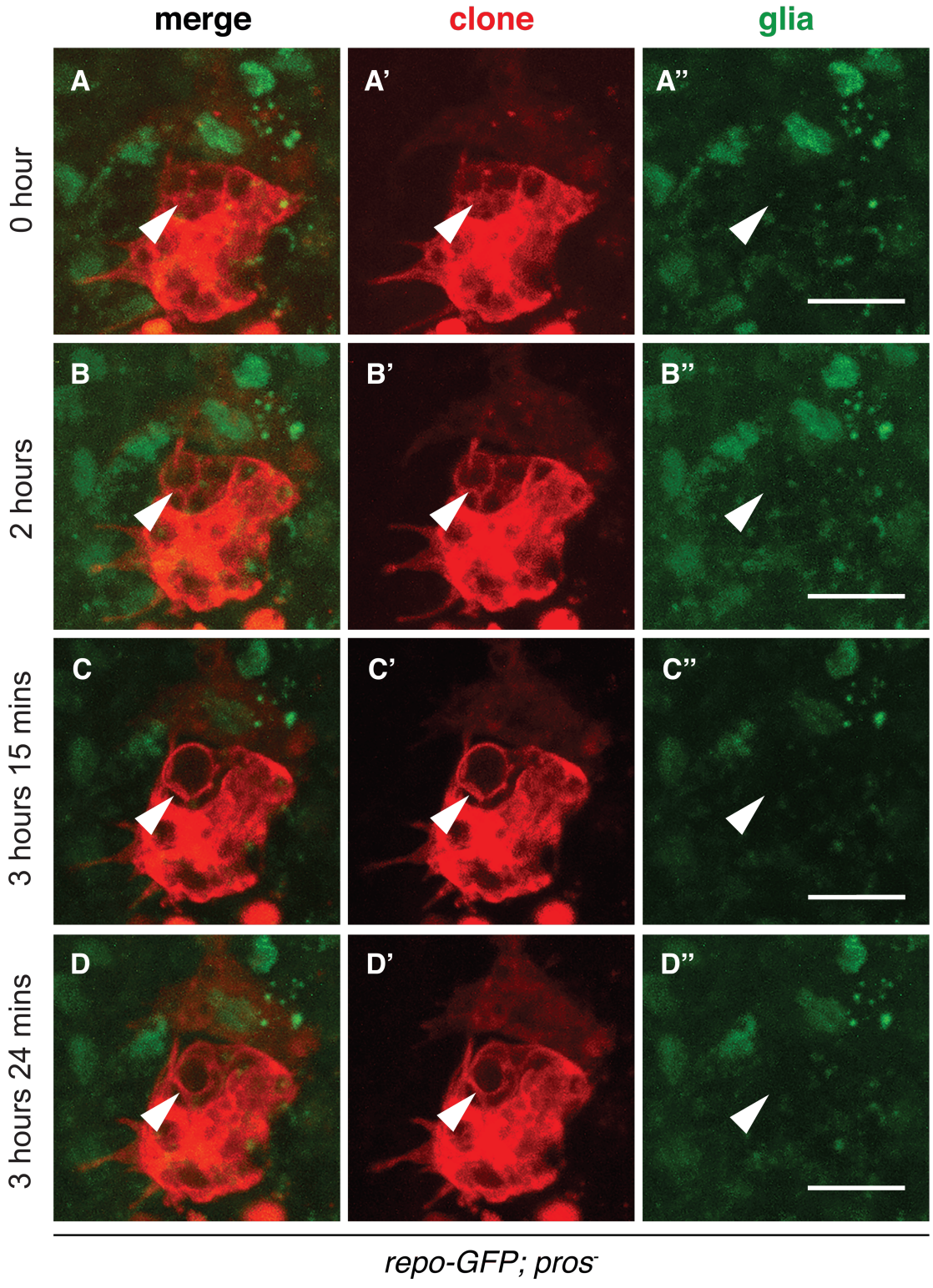
merge
clone
glia
A
A'
A"
B
B'
B"
C
C'
C"
D
D'
D"
0 hour
2 hours
3 hours 15 mins
3 hours 24 mins
repo-GFP; pros-

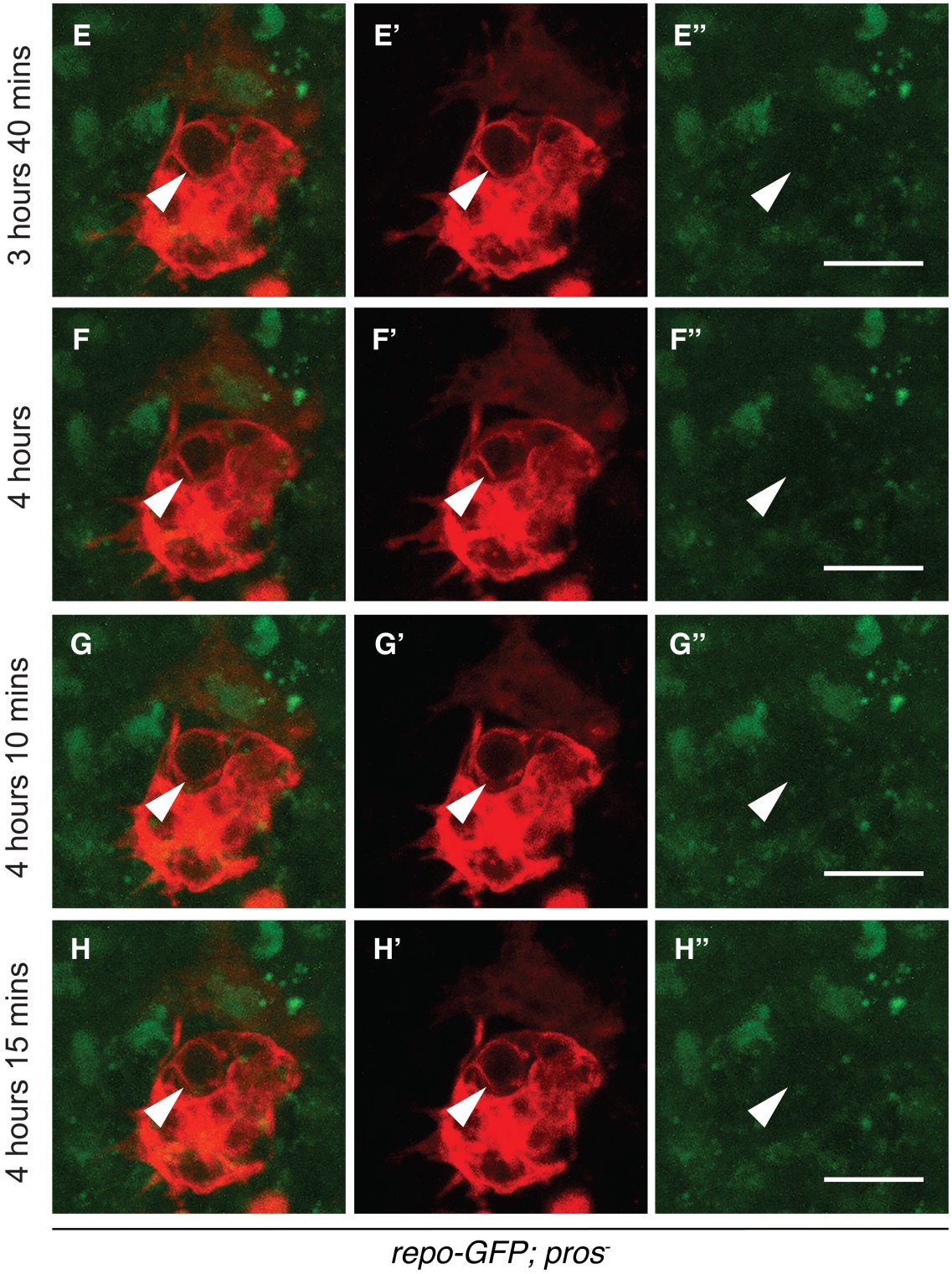
3 hours 40 mins
4 hours
4 hours 10 mins
4 hours 15 mins
E
E'
E''
F
F'
F''
G
G'
G''
H
H'
H''
repo-GFP; pros-

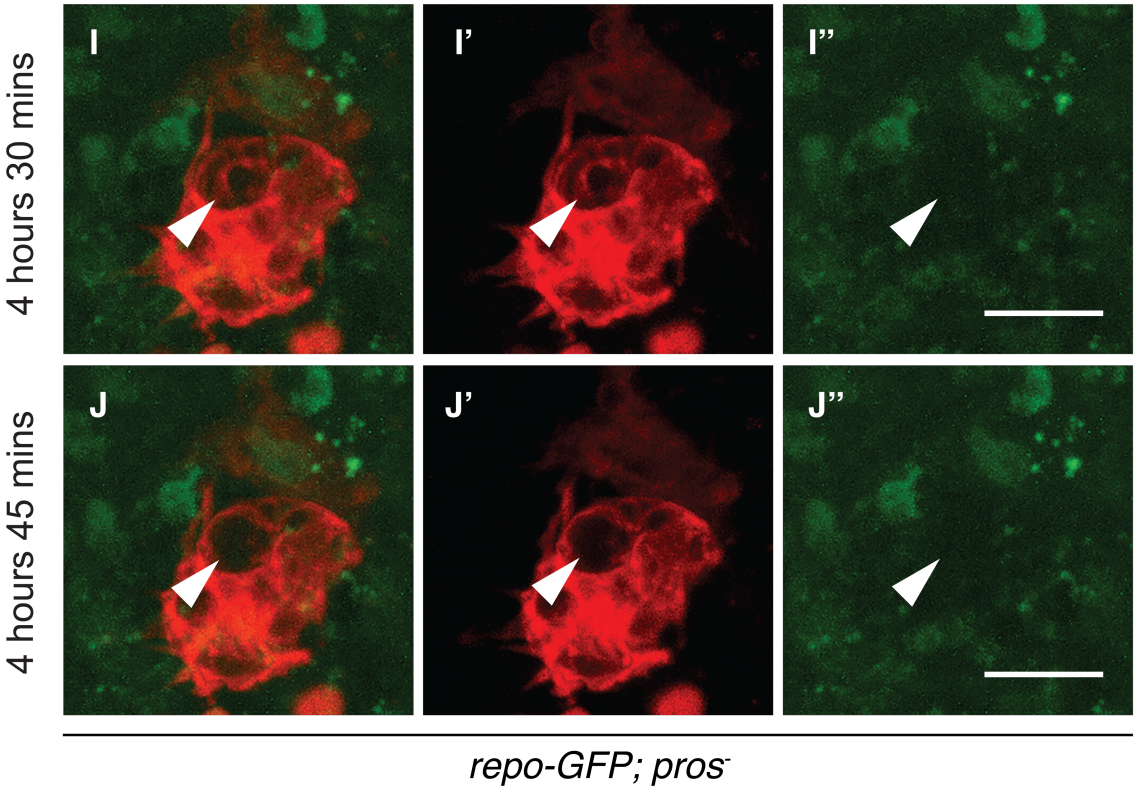

Figure 3.14. Some cells within *pros*$^{-}$ clones did not turn on Repo.
Live *ex vivo* VNCs were imaged for every 12 mins during 7-hour period at room temperature (related to Supplemental **Video 3.3**).

(A-J'') Still frames from live images of *pros*$^{-}$ clones expressing *repo-GFP* showing NBs that were proliferating and did not turn on Repo-GFP (refer to **Video 3.3**). Scale bars, 10 µm. Times are shown as hours. The time-lapse confocal microscopy images are shown in merged, RFP (clone; red) only, and GFP (glia; green) only channels. Transmitted light channel is not shown. One representative NB (white arrowhead) that was identified by its large size of around 10 µm was traced. This NB underwent several rounds of divisions during the 5-hour imaging window, but did not switch on Repo.

(A-A'') At the start of imaging (0 hour), GFP expression (A''; green) was restricted to the *wildtype* glia outside the clone, and was not found in NB (A-A'; red; white arrowhead).

(B-J'') The NB (white arrowhead) did not express glial marker Repo in (B; 2 hours) and over the course of imaging. At the end of imaging (J; 4 hours 45 mins), this NB had carried out few rounds of cell division but never expressed Repo-GFP.

See also Supplemental **Video 3.3**.

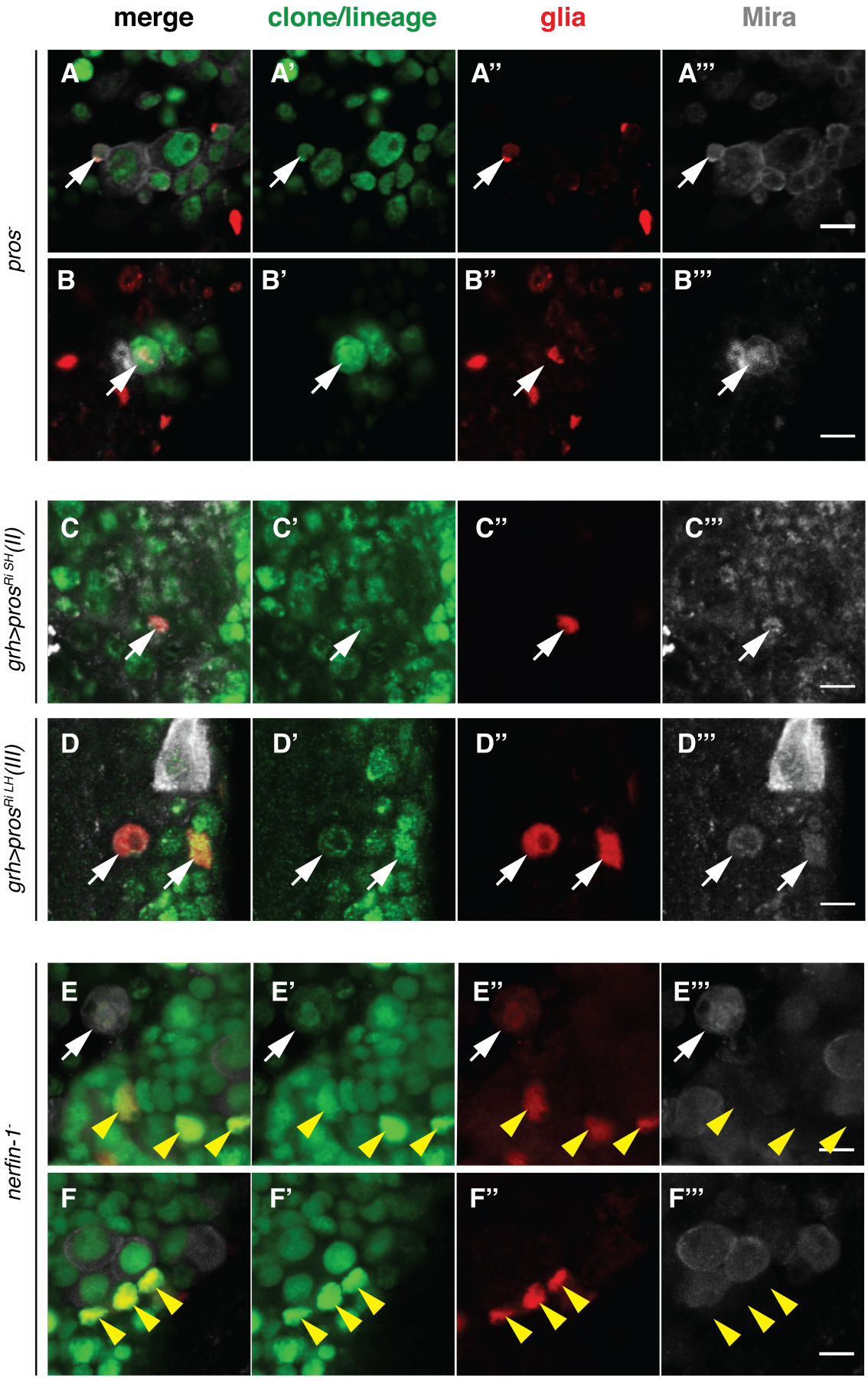
merge
clone/lineage
glia
Mira
pros-
A
A'
A''
A'''
B
B'
B''
B'''
grh>prosRi SH (II)
C
C'
C''
C'''
grh>prosRi LH (III)
D
D'
D''
D'''
nerfin-1-
E
E'
E''
E'''
F
F'
F''
F'''

Figure 3.15. Ectopic glia arise by transdifferentiation of NBs upon *pros* loss-of-function (A-D), and *nerfin-1* loss-of-function (E-F) in type I lineages.
(A-B, E-F) Adult clones were immunostained with anti-GFP (A- B' and E-F'; clone; nuclear green), glial marker Repo (A''-B'' and E''-F''; nuclear red) and NB marker Mira (A'''-B''' and E'''-F'''; Mira; cortical grey). (C-D) L3 larval brains of *grh>pros*$^{RNAi\ SH}$ or *grh>pros*$^{RNAi\ LH}$ were immunostained with RFP (tumour; false coloured green), Repo (glia; red) and Mira (neuroblast; grey). Ectopic glia are identified by coexpressing GFP and Repo. Merged and single channels are shown. Scale bars, 10 μm.

(A-B''') Single confocal image of representative ectopic glia in *pros*$^{-}$ clone (A'' and B''; red; white arrow) expressing Mira (Mira^{+}; A''' and B'''; grey). This indicates that ectopic glia originated from NB transdifferentiation and still maintain NB identity.

(C-D''') Single confocal image of representative ectopic glia found in *pros*$^{RNAi\ SH}$- (C''; red; white arrow) and *pros*$^{RNAi\ LH}$-expressing tumours (D''; red; white arrow) all expressing Mira (C''' and D'''; grey), indicating that they arise by the transdifferentiation of ectopic NBs.

(E-F''') Single confocal image of representative ectopic glia in *nerfin-1*$^{-}$ clones (E'' and F''; red) expressing Mira (Mira^{+}; E'''; grey; white arrow) and not expressing Mira (Mira^{-}; E''' and F'''; grey; yellow arrowhead), indicating that only a subset of ectopic glia still maintain NB identity.

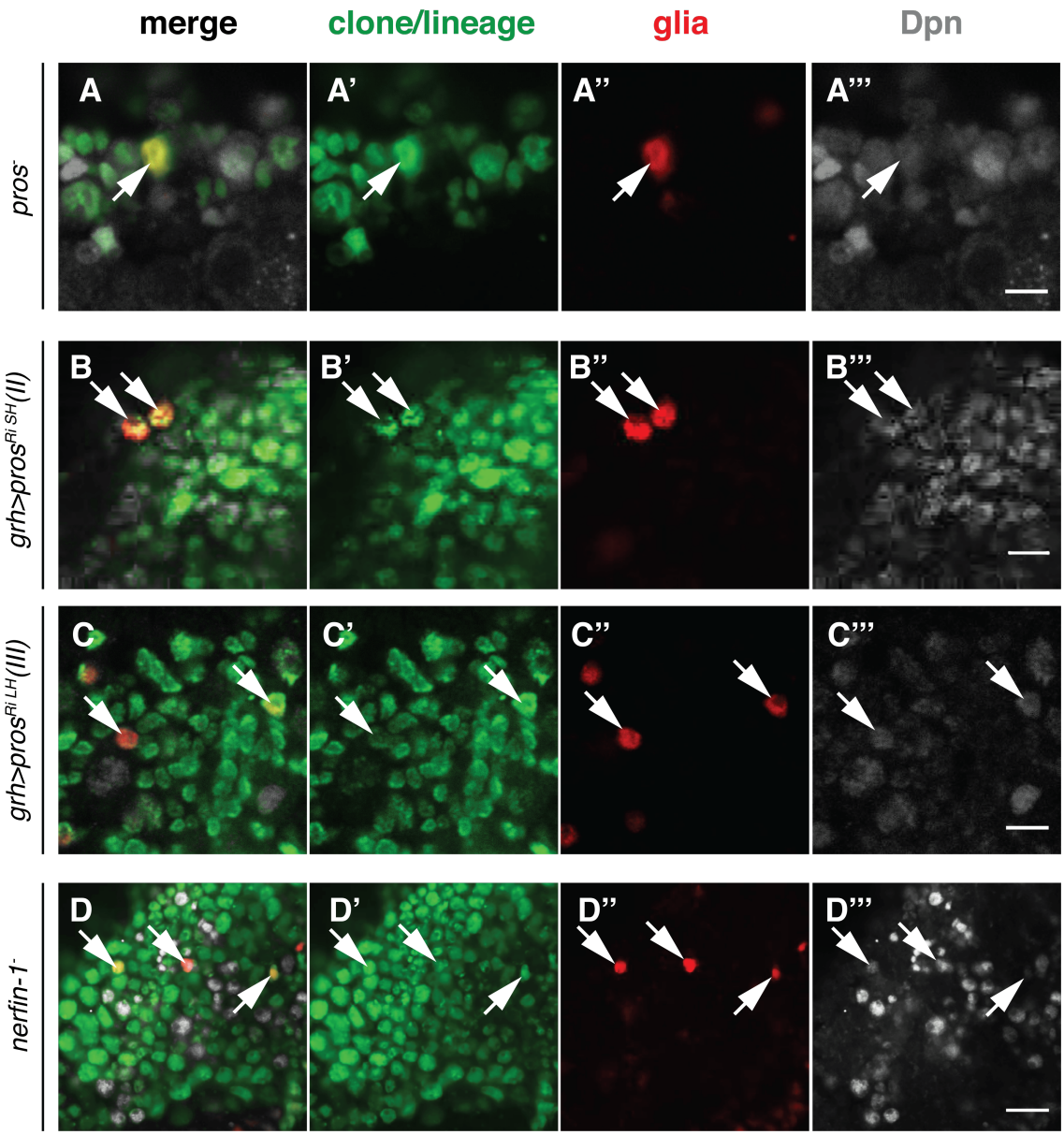
merge
clone/lineage
glia
Dpn
pros-
grh>prosRi SH (II)
grh>prosRi LH (III)
nerfin-1-
A
A'
A''
A'''
B
B'
B''
B'''
C
C'
C''
C'''
D
D'
D''
D'''

Figure 3.16. Ectopic glia in *pros* and *nerfin-1* – deficient clones/lineages express the NB marker Dpn.
(A and D) Pupal clones were immunostained with anti-GFP (A-A' and D-D'; clone; nuclear green), glial marker Repo (A'' and D''; nuclear red) and NB marker Dpn (A'''and D'''; Dpn; nuclear grey). (B-C) L3 larval brains of *grh>pros*$^{RNAi\ SH}$ or *grh>pros*$^{RNAi\ LH}$ were immunostained with RFP (tumour; false coloured green), Repo (glia; red) and Mira (neuroblast; grey). Ectopic glia are identified by coexpressing GFP and Repo. Merged and single channels are shown. Scale bars, 10 μm.

(A-A''') Single confocal image of representative ectopic glia (A''; red; white arrow) expressing NB marker Dpn in a *pros*$^{-}$ clone (Dpn^{+}; A'''; grey). This indicates that ectopic glia are originated from NB transdifferentiation and still maintain NB identity.

(B-C''') Single confocal image of representative ectopic glia found in *pros*$^{RNAi\ SH}$- (B''; red; white arrow) and *pros*$^{RNAi\ LH}$-expressing tumours (C''; red; white arrow) all expressing Dpn (B''' and C'''; grey), indicating that they arise by the transdifferentiation of ectopic NBs.

(D-D''') Single confocal image of representative ectopic glia in *nerfin-1*$^{-}$ clone (D''; red; white arrow) expressing Dpn in *nerfin-1*$^{-}$ clone (Dpn^{+}; D'''; grey), indicating that ectopic glia are originated from NB transdifferentiation and still maintain NB identity.

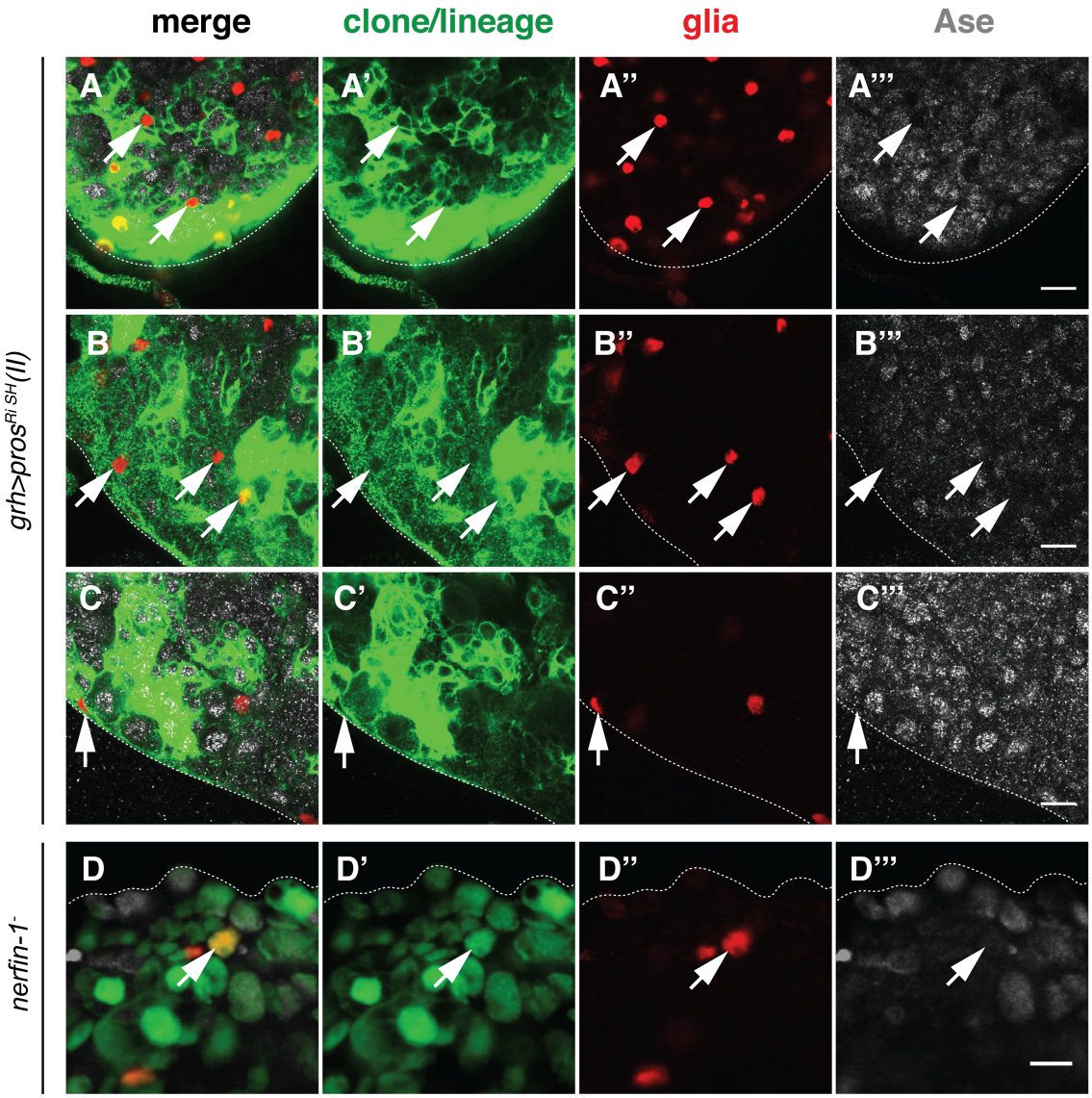

Figure 3.17. Ectopic glia in *pros* and *nerfin-1* – deficient clone/lineages do not express type I NB marker Ase.
(A-C) L3 larval brains of *grh>pros*$^{RNAi\ SH}$ genotype were immunostained with RFP (tumour; false coloured as green), Repo (glia; red) and Ase (type I NB; grey). (D) Adult *nerfin-1*$^{-}$ clones were immunostained with anti-GFP (clone; nuclear green), glial marker Repo (glia; nuclear red) and Ase (type I NB; grey). Ectopic glia are identified by coexpressing GFP and Repo. Merged and single channels are shown. Scale bars, 10 µm.

(A-C''') Single confocal image of representative ectopic glia found in *pros*$^{RNAi\ SH}$-expressing lineages (A''-C''; red; white arrow) that do not express Ase (A'''-C'''; grey).

(D-D''') Single confocal image of representative ectopic glia cell (D''; red; white arrow) in *nerfin-1*$^{-}$ clone that does not express Ase (D'''; grey).

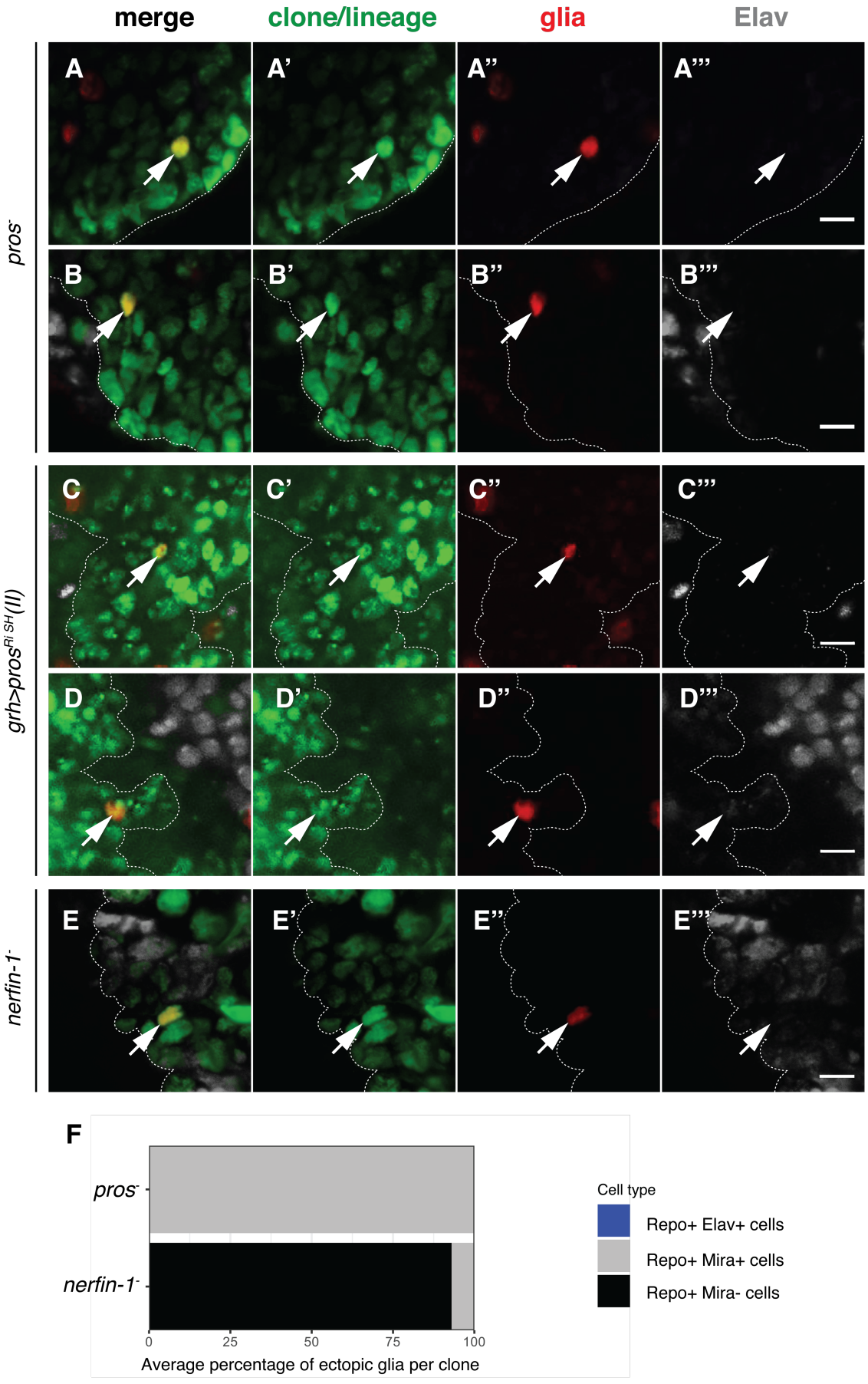
merge
clone/lineage
glia
Elav
pros-
grh>prosRi SH(II)
nerfin-1-
A
A'
A''
A'''
B
B'
B''
B'''
C
C'
C''
C'''
D
D'
D''
D'''
E
E'
E''
E'''
F
pros-
nerfin-1-
0
25
50
75
100
Average percentage of ectopic glia per clone
Cell type
Repo+ Elav+ cells
Repo+ Mira+ cells
Repo+ Mira- cells

Figure 3.18. Ectopic glia never express the neuronal marker Elav upon *pros* or *nerfin-1* loss-of-function.

(A-B and E) *Drosophila* brains carrying MARCM clones were immunostained with anti-GFP (A-B', and E-E'; clone; nuclear green), glial marker Repo (A''-B'' and E''; nuclear red) and neuronal marker Elav (A'''-B''' and E'''; Elav; nuclear grey).

(C-D) L3 larval brains of *grh>pros*$^{RNAi\ SH}$ were immunostained with RFP (tumour; false coloured green), Repo (glia; red) and Elav (neuron; grey). Ectopic glia are identified by coexpressing GFP and Repo. Merged and single channels are shown. Scale bars, 10 μm.

(A-B''') Single confocal image of representative ectopic glia (A'' and B''; red; white arrow) found in *pros*$^{-}$ clone, that do not express Elav (A'''-B'''; grey). This is consistent with the fact that neurons are absent in *pros*$^{-}$ clones (dashed line region) as indicated by the absence of Elav expression and quantified in (F)

(C-D''') Single confocal image of representative ectopic glia found in *pros*$^{RNAi\ SH}$-expressing tumours (C''-D''; red; white arrow) never expressing Elav (C''' and D'''; grey). This is consistent with the fact that neurons are absent in *grh>pros*$^{RNAi\ SH}$ tumour as indicated by the absence of Elav expression.

(E-E''') Single confocal image of representative ectopic glia found in *nerfin-1*$^{-}$ clone (E''; red; white arrow), that do not express Elav (E'''; grey) as quantified in (F). Multiple Elav^{+} cells are identified in both superficial and deep sections of *nerfin-1*$^{-}$ clone, but there was no colocalisation between Elav and Repo. This suggests that neurons do not revert to glia in *nerfin-1*$^{-}$ type I lineages.

(F) The bar graph showing the proportion of ectopic glia expressing Mira in a representative *pros*$^{-}$ or *nerfin-1*$^{-}$ clone. 100% of ectopic glia found in *pros*$^{-}$ clone are Mira^{+} (n= 50 out of 50 examined cells) while only 7% of Repo^{+} cells in *nerfin-1*$^{-}$ clone are Mira^{+} (n= 4 out of 57 examined cells). Ectopic glia were never found to express Elav in either *pros*$^{-}$ or *nerfin-1*$^{-}$ clones (n=67/67 and 76/76 examined cells, respectively).

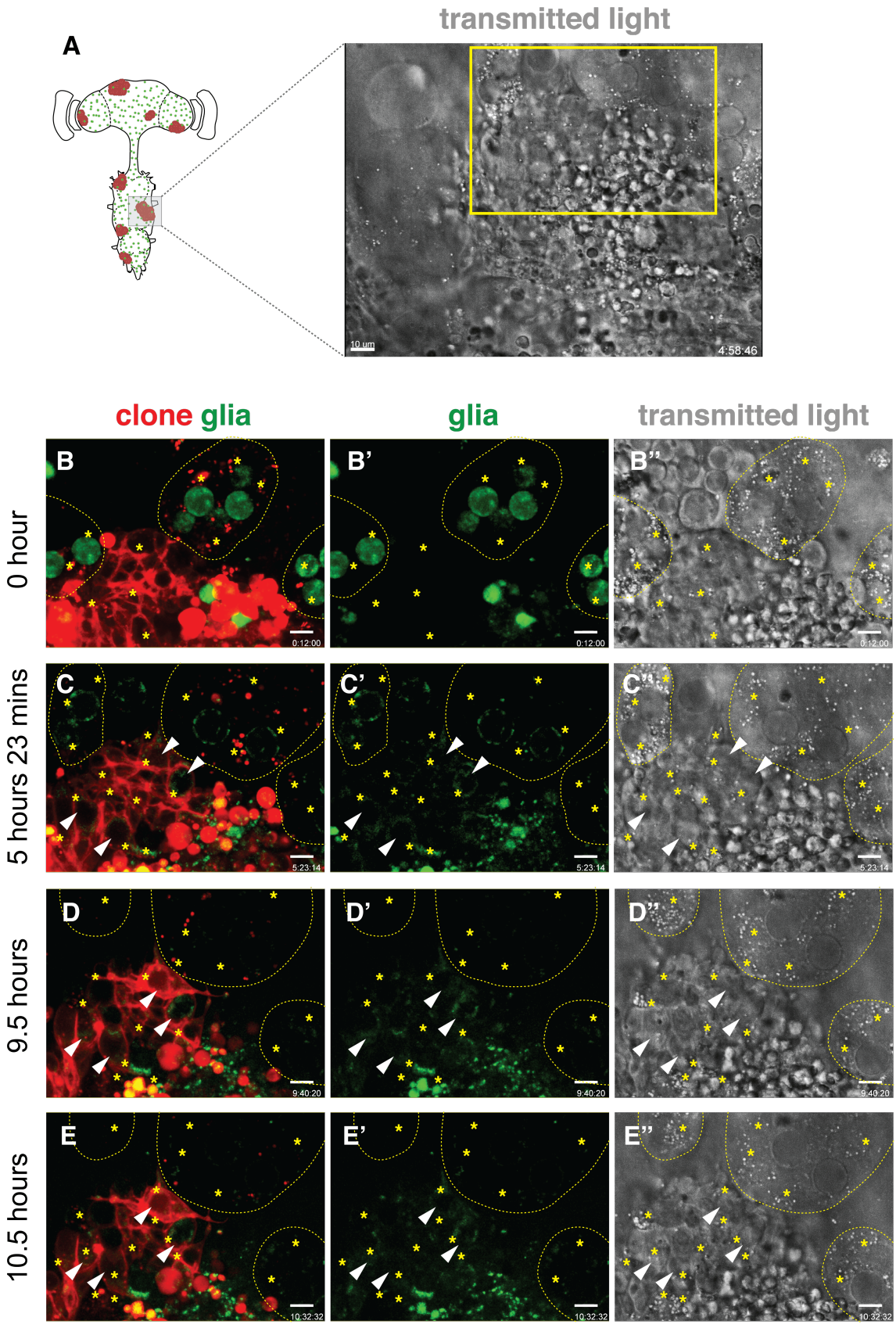
transmitted light
A
10 µm
4:58:46
clone glia
glia
transmitted light
0 hour
5 hours 23 mins
9.5 hours
10.5 hours
B
B'
B''
C
C'
C''
D
D'
D''
E
E'
E''
0:12:00
5:23:14
9:40:20
10:32:32

Figure 3.19. CNS lipid droplets accumulate in *pros*$^{-}$ mutant clones and near ectopic glia from live-cell imaging.
These live images were achieved from the same raw file of the ones on **Figure 3.1** but are shown in lower magnification maximum-intensity projection images (Related to Supplemental **Video 3.4**). The time-lapse confocal microscopy images are shown in RFP (clone; red), GFP (glia; green) and transmitted light channels. Times are shown as hours:mins. Scale bars, 10 μm.

(A) *pros*$^{-}$ clone in pupal VNC was also imaged live in transmitted light. A representative section of *pros*$^{-}$ clones and lipid droplets (grey; yellow boxed region) is magnified in (B-E)

(B-E'') Still frames from live images of *pros*$^{-}$ clones expressing *repo-GFP* showing that lipid droplets (transmitted light; grey; yellow asterisks) accumulate within the *pros*$^{-}$ clone region (B-E; red; n= 4 *pros*$^{-}$ clones).

(B-B'') At the start of imaging (0 hour), ectopic glia was not found in the clone. Lipid droplets (B''; grey; yellow asterisks) predominantly localised to *wildtype* glia (B-B'; green; yellow dashed outlined region).

(C-E'') At these time points, ectopic glia (white arrowhead) have been generated, formed membrane protrusions into neighbour regions, and accumulated more lipid droplets. Lipid droplets (C''-E''; grey; yellow asterisks) localised to *wildtype* glia (C-E'; green; yellow dashed outlined region) and nearby ectopic glia (C-E'; green; white arrowhead) over the rest of imaging time.

See also Supplemental **Video 3.4**.

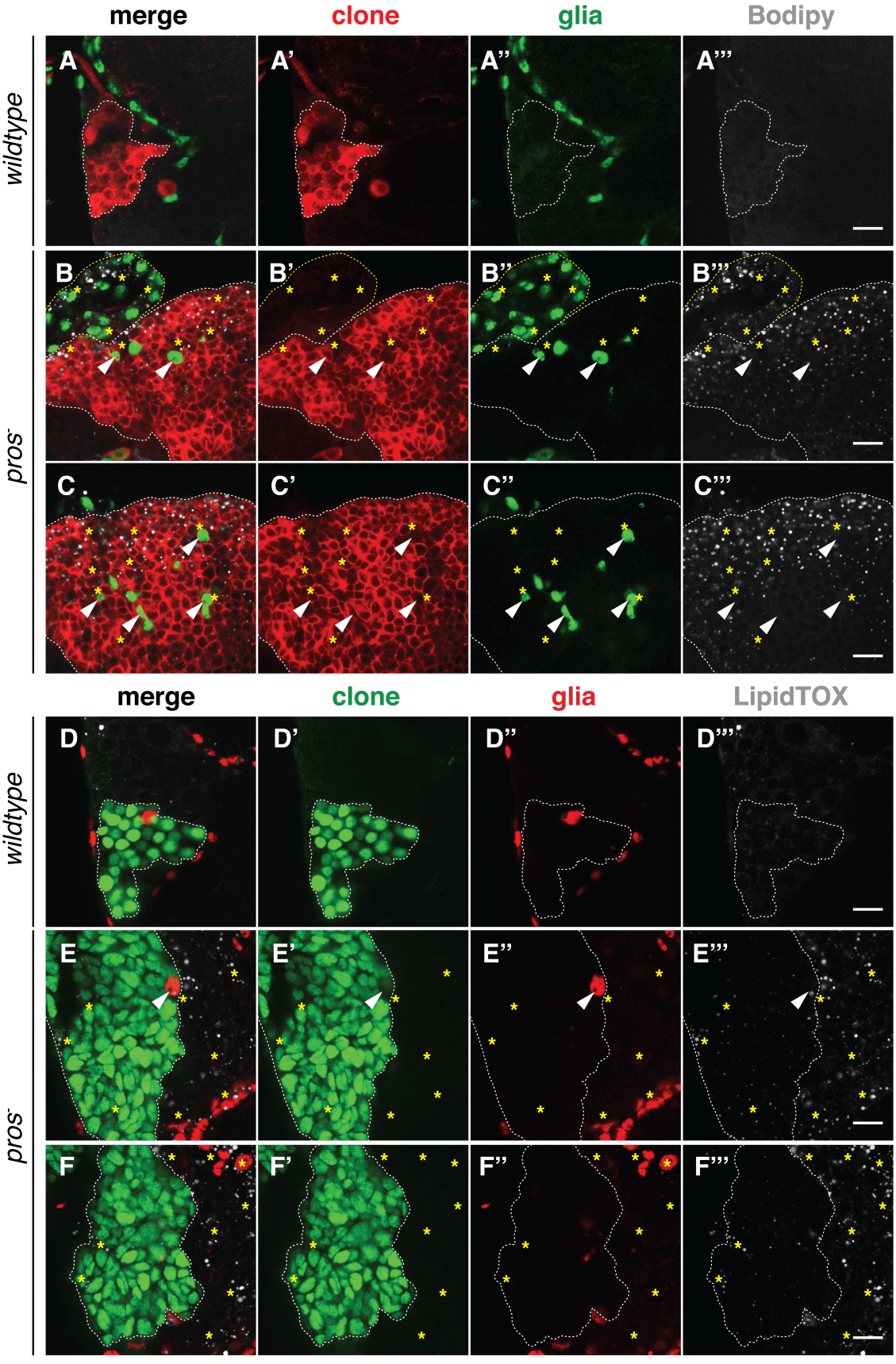
merge
clone
glia
Bodipy
wildtype
pros-
A
A'
A''
A'''
B
B'
B''
B'''
C
C'
C''
C'''
merge
clone
glia
LipidTOX
wildtype
pros-
D
D'
D''
D'''
E
E'
E''
E'''
F
F'
F''
F'''

Figure 3.20. CNS lipid droplets accumulate in *pros*$^{-}$ mutant clones and near ectopic glia from fixed-cell imaging.

In (A-C) RFP-labeled clones were immunostained with RFP (clones; membraneous red), Repo (glia; green) and Bodipy (lipid droplets; false coloured as grey). In (D-F) GFP-labeled clones were immunostained with GFP (clones; nuclear green), Repo (glia; red) and LipidTOX (lipid droplets; false coloured as grey). Clones are outlined with dashed white line. Merged and single channels are shown. Scale bars, 10 μm.

(A-C’’’) Representative single confocal images of RFP-expressing *wildtype* control (A-A’), and *pros*$^{-}$ clones (B-C’) from 2- to 3-day-old pupal VNC. Lipid droplets (Bodipy staining; false grey) accumulate within the *pros*$^{-}$ clone region (B’’’-C’’’; n= 6 *pros*$^{-}$ clone), but not in the *wildtype* clone (A’’’; n= 4 *wildtype* clone). Lipid droplets (yellow asterisk) localised to *wildtype* glia (B’’; green; yellow dashed outline) and nearby ectopic glia (B’’-C’’; green; white arrowhead).

(D-F’’’) Representative single confocal images of GFP-expressing *wildtype* control (D-D’), and *pros*$^{-}$ clones (E-F’) from 2- to 3-day-old pupal VNC. Lipid droplets (LipidTOX staining; false grey) accumulate within the *pros*$^{-}$ clone region (E’’’-F’’’, n= 4 *pros*$^{-}$ clone), but not in the *wildtype* clone (D’’’; n= 5 *wildtype* clone). Lipid droplets (yellow asterisk) localised to *wildtype* glia (E’’-F’’; red) and nearby ectopic glia (E’’; red; white arrowhead).

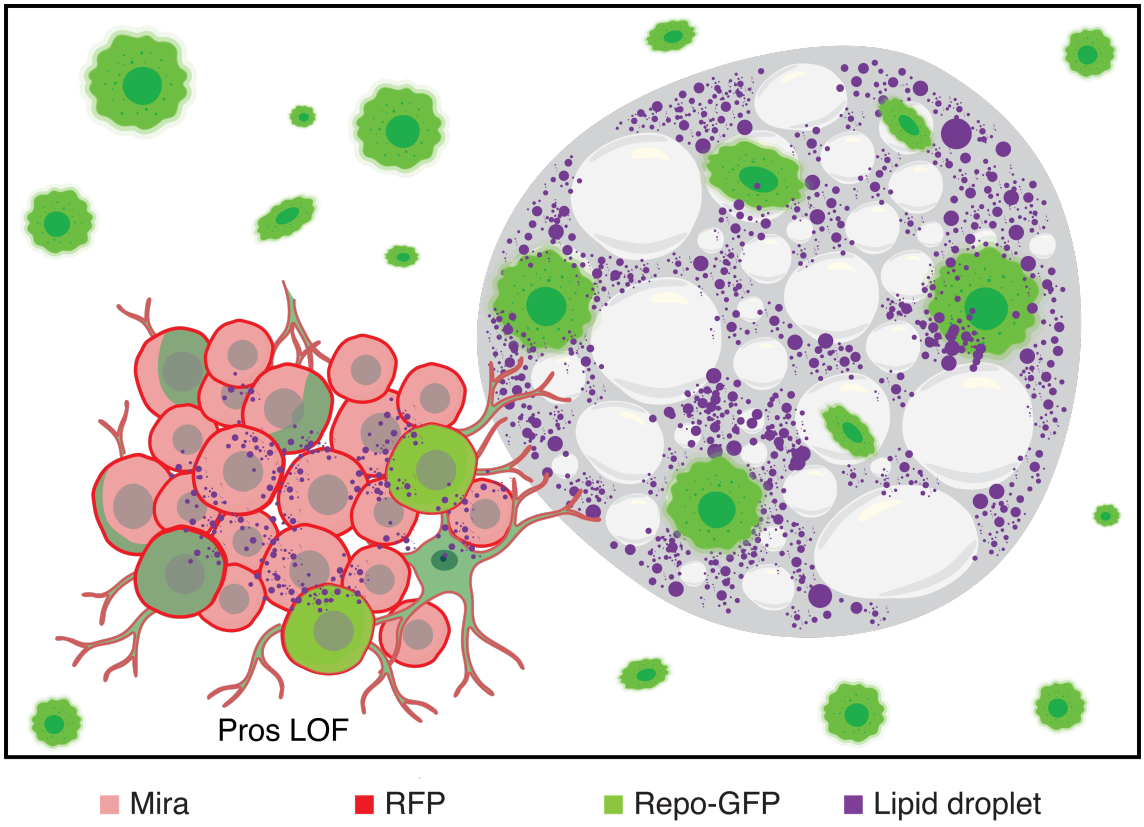

Figure 3.21. CNS lipid droplets accumulate in *pros*$^{-}$ mutant clone and especially near ectopic glia.

Schematic represents the localisation of lipid droplets (purple) to *wildtype* glia (indicated by Repo-GFP; green) and ectopic glia (RFP^{+} Mira^{+} Repo^{+}) within *pros*$^{-}$ NB lineages (RFP^{+} Mira^{+}; red).

Video 3.1. Upon loss of Pros, NBs of type I lineages ectopically turn on Repo and transdifferentiate into ectopic glia in *Drosophila* VNC.
MARCM clones expressing membrane RFP (red) and Repo-GFP were induced at 48 hours AEL. Live *ex vivo* VNCs were imaged for every 12 mins during 10-hour period at room temperature. Time-lapsed video is shown in merged RFP (clone; red) and GFP (glia; green) channels without transmitted light channel. Times are shown as hours: mins. Scale bars, 10 μm.

Time-lapse video of live *ex vivo pros*$^{-}$ clone expressing Repo-GFP showing the step-wise NB-to-glia reversion upon loss of Pros (related to **Figure 3.12**). All the cells in the *pros*$^{-}$ clones permanently express RFP in membrane, and stay confined within the clone. Video shows successive cell divisions of NBs and few transdifferentiation events. One representative NB (white arrowhead), identified by its large size of around 10 μm, was traced.

At the start of imaging (0 hour), GFP expression (green) was restricted to the *wildtype* glia outside the clone, and was not found in NB (red; arrowhead). *Wildtype* glia were observed to move around clone region to support the clonal growth. At 4 hours, the NB has turned on Repo-GFP. Repo –GFP expression increased in intensity in the marked NB, and was also observed in the nearby NBs. At the end of imaging (10.5 hours), this NB (marked by white arrowhead) and its neighbour NB formed membrane protrusions into neighbour regions.

Video 3.2. Additional example of NB-to-glia transdifferentiation in *pros*$^{-}$ clone located in a superficial VNC section. This live time-lapse video was achieved from the same raw file of **Video 3.1** but the cells of interest were located at different part of the clone. Time-lapsed video is shown in merged RFP (clone; red) and GFP (glia; green) channels without transmitted light channel. Times are shown as hours: mins. Scale bars, 10 μm.

Time-lapse video of live *ex vivo pros*$^{-}$ clone expressing Repo-GFP showing the step-wise NB-to-glia reversion in *pros*$^{-}$ clone (related to **Figure 3.13**). All the cells in the *pros*$^{-}$ clones permanently expressed bright RFP in membrane, and stayed confined within the clone. Video shows successive cell divisions of NBs and few transdifferentiation events. One representative NB (white arrowhead), identified by its large size of around 10 μm, was traced.

At the start of imaging (0 hour), GFP expression (green) was restricted to the *wildtype* glia outside the clone, and was not found in NB (red; arrowhead). *Wildtype* glia were observed to move around clone region to support the clonal growth. The NB has turned on Repo at 1.5 hour time point. Repo–GFP expression increased in intensity over time

in the marked NB, and was also observed in the nearby NBs. At the end of imaging (9.5 hours), this NB (marked by white arrowhead) and its neighbour NB still maintained RFP and repo-GFP expression.

Video 3.3. Some cells within *pros*$^{-}$ clones did not turn on Repo.
Live *ex vivo* VNCs were imaged for every 12 mins during 7-hour period at room temperature. Time-lapsed video is shown in merged RFP (clone; red) and GFP (glia; green) channels without transmitted light channel. Times are shown as hours: mins. Scale bars, 5 µm.

Time-lapse video of live *ex vivo pros*$^{-}$ clone expressing Repo-GFP showing NBs that were proliferating and did not turn on Repo-GFP (Related to **Figure 3.14**). All the cells in the *pros*$^{-}$ clones permanently express bright RFP in membrane, and stay confined within the clone. One representative NB (white arrowhead) that was identified by its large size of around 10 µm was traced. This NB underwent several rounds of divisions during the 5-hour imaging window, but did not switch on Repo.

At the start of imaging (0 hour), GFP expression (green) was restricted to the *wildtype* glia outside the clone, and was not found in NB (red; white arrowhead). The NB (white arrowhead) did not express glial marker Repo at 2 hour time point and over the course of imaging. At the end of imaging (4 hours 45 mins), this NB had carried out few rounds of cell division but never expressed Repo-GFP.

Video 3.4. CNS lipid droplets accumulate in *pros*$^{-}$ mutant clones and especially, near ectopic glia.
This live time-lapse video was achieved from the same raw file of **Video 3.1** but was shown at lower magnification. Time-lapse video is shown in merged RFP (clone; red) and GFP (glia; green) and transmitted light channels. Times are shown as hours: mins. Scale bars, 10 µm.

Time-lapse video of live *ex vivo pros*$^{-}$ clone expressing repo-GFP showing the step-wise NB-to-glia reversion and lipid droplet accumulation (transmitted light; grey) within the *pros*$^{-}$ clone region over the course of imaging (Related to **Figure 4.19**). The video shows successive cell divisions of NBs and few transdifferentiation events. A few NBs switched on Repo-GFP, and formed membrane protrusions into neighbour regions during the course of imaging. Lipid droplets were distributed within *pros*$^{-}$ NB lineages and localised to the *wildtype* glia near the clone.

Link to the folder of 4 Supplemented videos:
https://drive.google.com/drive/folders/1d7hbzk7pXcU5wzt6JtVLbBC_Hq15X_q7?usp=sharing

3.3. Temporal patterning regulates the formation of ectopic glia

We have showed that a subset of NSCs within *pros*$^{-}$/*nerfin-1*$^{-}$ type I lineages display type II-like lineage identity and ectopically switch to differentiated glial stage. To elucidate the mechanisms by which *pros*$^{-}$/*nerfin-1*$^{-}$ type I NSCs obtain their gliogenic potential, we next identified the transcriptional factors and related signal transduction pathways, which drive such mechanisms and subsequently trigger the formation of ectopic glia. In line with this, we then (1) interrogated the pathways to manipulate the ectopic glial population, and (2) assessed whether the changes in the number of ectopic glia can affect the growth of NB lineages deficient for Pros/Nerfin-1.

3.3.1. Neuroblast temporal series is involved in the formation of ectopic glia.

The Hth→Klu→Ey→Slp →D→Tll temporal cascade is sequentially expressed in the medulla NBs (**Figure 3.22A**) to specify neuronal identities, and to eventually transform Tll^{+} NBs into *gcm*$^{+}$ glioblasts that can produce glia (Li et al., 2013a). This prompted us to speculate whether these TTFs are required for the switch from NB to glial fate in the Pros-deficient type I NB lineages, similar to what they do in medulla NBs. As Hth and Klu are inherited from the neuroepithelium and do not control the transitions to the remaining factors (Li et al., 2013a), we only analysed the expression of TTFs Ey→Tll in *wildtype* and *pros*$^{-}$ clones.

Ey was reported to be expressed in several neural lineages in VNC from embryonic to larval development (Adachi et al., 2003; Birkholz et al., 2013; Kammermeier et al., 2001; Lacin and Truman, 2016). As expected, Ey expression was still maintained in *wildtype* NB (**Figure 3.22B**, white arrowhead; n= 9 clones) and a subset of its progeny (yellow arrowhead) in pupal VNCs. Similarly, Ey was also variably expressed in the majority of *pros*$^{-}$ lineages (**Figure 3.22C-D**; white arrowhead; ~70% of cells examined; n= 4 clones examined), and the Ey^{-} cells are presumably made during other NB temporal windows (**Figure 3.22C-D**; blue arrowhead).

In contrast, Slp was ectopically expressed in *pros*$^{-}$ NB lineages (**Figure 3.23B-D**; blue arrowhead; n= 7 out of 7 clones examined), and not in *wildtype* lineages (**Figure 3.23A**; n=9 out of 9 clones examined). We never detected Slp expression in

ectopic glia in *pros*$^{-}$ lineages (**Figure 3.23B** and **D**; white arrowhead; n=6/6 ectopic glia examined), indicating that ectopic glia are not derived from Slp^{+} NBs.

Late temporal TF D was ectopically expressed at varying levels by most cells within *pros*$^{-}$ NB lineages (**Figure 3.24B'''**; n= 6 out of 6 clones examined), but was absent in *wildtype* lineages (**Figure 3.24A'''**; n= 7 out of 7 clones examined). We observed some ectopic glial weakly expressed D in the *pros*$^{-}$ lineages (**Figure 3.24B'''**; white arrowhead; n= 7 out of 7 glial cells examined), suggesting that they could be born from D^{+} NBs. To assess the contribution of D to the generation of ectopic glia, we inhibited *D* using *UAS-D*^{RNAi} (Apitz and Salecker, 2015; Bayraktar and Doe, 2013) in *grh>pros*$^{RNAi\ LH}$ lineages (**Figure 3.24E-F**). We found that *D* knockdown significantly reduced the number of ectopic glia in *pros*$^{RNAi\ LH}$-expressing lineages by ~70% (**Figure 3.24C-D** and **G**; *pros*$^{RNAi\ LH}$ control: 72.73 ± 10.59 glia, n= 15 brains; *D*^{RNAi} plus *pros*$^{RNAi\ LH}$: 21.81 ± 4.52 glia; n= 16 brains), and halved the lineage volume (**Figure 3.24E-F** and **H**; *pros*$^{RNAi\ LH}$ control: 519781.19 ± 56768.5 μm^3, n= 15 brains; *D*^{RNAi} plus *pros*$^{RNAi\ LH}$: 230879.45 ± 22895.44 μm^3, n= 16 brains). Therefore, in the context of Pros loss-of-function, NBs ectopically progress through D^{+} temporal phase, and D is required for the formation of ectopic glia and for the NB lineage growth.

We then looked at the last member of the temporal series, Tll. Tll was not expressed in *wildtype* lineages (**Figure 3.25A'''**; n= 7/7 clones examined) but was detected in ectopic glia within *pros*$^{-}$ clones (**Figure 3.25B'''-C'''**; white arrowhead; n= 6/7 glia examined), suggesting that ectopic glia could be derived from Tll^{+} NBs within *pros*$^{-}$ lineages. After *tll* was knocked down with *RNAi* (Hakes and Brand, 2020) in *grh>pros*$^{RNAi\ LH}$ lineages, we observed over 50% reduction in the number of ectopic glia (**Figure 3.25D-E** and **H**; *pros*$^{RNAi\ LH}$ control: 72.73 ± 10.59 glia; n= 15 brains; *tll*^{RNAi} plus *pros*$^{RNAi\ LH}$: 30.6 ± 4.81 glia; n= 16 brains), and 40% reduction in the lineage growth (**Figure 3.25F-G** and **I**; *pros*$^{RNAi\ LH}$ control: 519781.19 ± 56768.5 μm^3, n= 15 brains; *tll*^{RNAi} plus *pros*$^{RNAi\ LH}$: 304717.70 ± 30493.57 μm^3 , n= 16 brains). This suggests that Tll is potentially a regulator in the formation of ectopic glia, and in the growth of Pros-deficient lineages. From the overall expression pattern of the above TTFs, we suggest that a population of Pros-deficient VNC type I NBs transit through at least part of the TTF cascade (D and Tll) normally expressed only in medulla NBs. Secondly,

temporal patterning is likely to direct the cell-fate switch of Pros-deficient NBs to ectopic glia, similar to the medulla NB-to-glioblast switch described by Li et al., (2013a).

3.3.2. Glial determinant genes regulate the formation of ectopic glia to promote NB lineage growth upon Pros loss-of-function.

Downstream of the TTFs, glial production in Tll^+ NBs is modulated by glia fate determinants *gcm* and *repo* (Li et al., 2013a). *gcm* is expressed in Tll^+ NBs, and is inherited by their progeny (Li et al., 2013a). The progeny then loses Tll and turns on Repo, to eventually adopt a differentiated glial fate (Li et al., 2013a). In addition to acting with temporal genes in medulla NBs, *gcm* is also known to direct gliogenesis in most, if not all, NB lineages of the *Drosophila* CNS (Cattenoz and Giangrande, 2013; Jones, 2005; Yuasa et al., 2003), while *repo* is required for promoting glial differentiation (Yuasa et al., 2003) (**Figure 3.26A**). Because we detected multiple $Repo^+$ ectopic glial cells within NB lineages lacking Pros, we next asked if *gcm* and *repo* regulate the formation of ectopic glia.

Downregulation of *gcm* with gcm^{RNAi} (Bayraktar and Doe, 2013) in $grh>pros^{RNAi\ SH}$ lineages resulted in three-fold reduction of ectopic glial number, compared to $grh>pros^{RNAi\ SH}; mcherry^{RNAi}$ control (**Figure 3.26B''-C''** and **F**, control: 188.43 ± 12.18 glia, *n*= 7 brains; $pros^{RNAi\ SH}$ plus gcm^{RNAi}: 50.67 ± 6.88 glia, *n*= 9 brains). Inhibition of *gcm* also reduced the growth of $pros^{RNAi\ LH}$-expressing lineages by 50% compared to $pros^{RNAi\ SH}; mcherry^{RNAi}$ lineages (**Figure 3.26D-E** and **G**; control: 388405.43 ± 30464.73 μm^3, n= 11 brains; $pros^{RNAi\ SH}$ plus gcm^{RNAi}: 112729.01 ± 18833.82 μm^3, n= 15 brains). These results demonstrate that the master glial regulator *gcm* is required to induce the ectopic glial formation in NB lineages lacking Pros, and to promote the growth of these lineages.

We further examined if the glial fate marker Repo is required for the formation of ectopic glia, which could result in increased Pros-deficient lineage growth. We knocked down *repo* in $grh>pros^{RNAi\ LH}$ by using $repo^{RNAi}$ line which was validated previously (Kerr et al., 2014; Mazaud et al., 2019) (**Figure 3.27B**). *repo* knockdown significantly

reduced the number of ectopic glia found in *pros*$^{RNAi\ LH}$-expressing lineages (**Figure 3.27C''-D''** and **E**; control: 190 ± 19.95 glia, n= 10 brains; *repo*^{RNAi} plus *pros*$^{RNAi\ LH}$: 68 ± 20 glia, n= 9 brains), and the lineage volume by almost 60%, compared with control lineages expressing *lacZ*^{RNAi} and *pros*$^{RNAi\ LH}$ (**Figure 3.27A-B** and **F**; control: 886714.49 ± 51598.96 µm^3, n= 10 brains; *repo*^{RNAi} plus *pros*$^{RNAi\ LH}$: 362961.77 ± 31232.01 µm^3, n= 9 brains). This suggests that Repo is required in lineages lacking Pros to regulate ectopic glial formation, and to promote lineage growth. In addition, *RNAi*-induced attenuation of *repo* only caused a reduction, but not a complete loss in ectopic glial population because of the strength of the *repo*^{RNAi} line (Mazaud et al., 2019).

To test whether ectopic glia promote NB lineage growth, we inhibited *repo* in *pros*$^-$ clones and assessed the clonal growth before and after ectopic glia arise. As characterised in **Chapter 3.1** (**Figure 3.4**), ectopic glia cells emerge at around 2-3 days APF. Inhibition of *repo* in the absence of ectopic glia (at L3 stages; **Figure 3.28A-B**) did not alter the *pros*$^-$ clonal growth (**Figure 3.28C**; *pros*$^-$ control: 134018.74 ± 35061.86 µm^3, n = 23 clones; *repo*^{RNAi}-expressing *pros*$^-$: 173610.88 ± 73759.68 µm^3, n= 10 clones). In contrast, at 3 days APF when ectopic glia cells are present (**Figure 3.28D'''-E'''**, white arrowhead), *repo* knockdown led to a ~70% reduction in ectopic glial cell number (**Figure 3.28F**; *pros*$^-$ control: 31.08 ± 10.76 glia, n=12 clones; *repo*^{RNAi}-expressing *pros*$^-$ clone: 9.32 ± 3.34 glia, n= 26 clones). *RNAi*-induced attenuation of *repo* only caused a reduction, but not a complete loss in ectopic glial population (Mazaud et al., 2019). This manipulation in turn caused a decrease of ~70% in *pros*$^-$ clonal growth (**Figure 3.28G**; *pros*$^-$ control: 274556.83 ± 61513.74 µm^3, n= 14 clones; *repo*^{RNAi}-expressing *pros*$^-$: 85252.78 ± 22032.03 µm^3, n= 28 clones). This suggests that Repo is required for the generation of ectopic glia, which in turn, promotes *pros*$^-$ lineage growth.

3.3.3. Notch signalling pathway promotes the growth of Pros/Nerfin-1-deficient lineages independently of ectopic glia formation.

The highly conserved Notch signalling has been found to govern stem cell homeostasis during development (Capaccione and Pine, 2013; Piazzi et al., 2012; Vinson et al., 2016), and is frequently dysregulated in cancers such as glioblastoma (Bazzoni and

Bentivegna, 2019; Hovinga et al., 2010). In *Drosophila*, Notch signalling regulates asymmetric division of NBs (see **Chapter 1.4**), and promotes gliogenesis in type II lineages (Ren et al., 2018) (see **Chapter 1.6.3**). To explore whether Notch is active in Pros/Nerfin-1-deficient type I lineages, we examined the expression pattern of Notch intracellular domain (NICD), which translocates to the nucleus and regulates transcription after Notch is activated by its ligand Delta (Fortini, 2009). We detected that NICD was ectopically upregulated in *pros*$^{-}$ clones (**Figure 3.29B**), indicating that Notch signalling is upregulated in *pros*$^{-}$ clones, that contain supernumerary NBs (*wildtype* clone: n= 0 /115 cells; *pros*$^{-}$ clone: n= ~240 out of 300 cells examined).

To assess if Notch is required for ectopic glial formation and the growth of Pros-deficient NB lineages, we first manipulated Notch activity in *pros*$^{RNAi\ LH}$-expressing lineages. We observed a ~50% reduction in lineage volume upon *notch*^{RNAi} expression, compared to *lacZ*^{RNAi} control (**Figure 3.30C-D** and **F**; *lacZ*^{RNAi} plus *pros*$^{RNAi\ LH}$ control: 825561.39 ± 122316.42 μm^3, n= 7 brains; *notch*^{RNAi} plus *pros*$^{RNAi\ LH}$: 462064.33 ± 79194.17 μm^3, n= 6 brains). Notch inhibition approximately halved the ectopic glia per *pros*$^{RNAi\ LH}$-expressing brain (**Figure 3.30A-B** and **E**; 74 ±13.75 glia; n= 6 brains) compared to that of control (162.14 ± 8.50 glia; n=7 brains). This data suggests that (1) Notch activity may be required for ectopic glia formation which in turn affects Pros-deficient lineage growth; or alternatively, (2) Notch activity may affect Pros-deficient lineage growth, which then results in a decrease in the formation of the ectopic glia cells. To distinguish between these two possibilities, we conducted some experiments at two different time points in *pros* loss-of-function clones. Here, we repressed Notch activity by inducing *RNAi* against Notch ligand *delta* (Vissers et al., 2018) in *pros*$^{-}$ clones.

We examined the effects of these manipulations at either (1) L3, before ectopic glia form or (2) at 3 days APF, after ectopic glia form. We predict that if Notch is specifically required for the formation of ectopic glia, which in turn affect overall clonal growth, then, we would observe an effect on clone volume at 3 days APF and not at the L3 stage. However, we found inhibition of Notch signalling significantly reduced *pros*$^{-}$ clonal volume at both L3 stage (~50% reduction; **Figure 3.31A-C**; *pros*$^{-}$ control:

77749.33 ± 8775.89 µm^3, n= 28 clones; *dl*^{RNAi}-expressing *pros*$^-$: 38484.87 ± 6096.32 µm^3, n= 23 clones), and at 3 days APF (~70% reduction; **Figure 3.31D-E** and **G**; *pros*$^-$ control: 274556.83 ± 61513.74 µm^3, n= 14 clones; *dl*^{RNAi}-expressing *pros*$^-$: 81207.46 ± 22170.72 µm^3, n= 20 clones). At 3 days APF, this in turn resulted in a reduction in overall ectopic glia cell number (**Figure 3.31F**; *pros*$^-$ control: 31.08 ± 10.76 glia, n=12 clones; *dl*^{RNAi}-expressing *pros*$^-$: 6.53±1.57 glia, n= 19 clones). In this context, Notch is also involved in the formation of ectopic glia, however, Notch regulates growth of Pros-deficient NB lineages independently of its effect on glia formation.

Similarly, downregulation of Notch signalling by *dl*^{RNAi} (Vissers et al., 2018) in *nerfin-1*$^-$ clones, strongly reduced *nerfin-1*$^-$ clonal growth to ~25% at both L3 (**Figure 3.32A-B** and **E**; *nerfin-1*$^-$ control: 6427.31 ± 1284.17 µm^3, n= 18 clones; *dl*^{RNAi}-expressing *nerfin-1*$^-$: 1654.99 ± 225.90 µm^3, n=12 clones) and at pupal stages (**Figure 3.32C-D** and **G**; *nerfin-1*$^-$: 57039.13 ± 22521.09 µm^3, n= 12 clones; *dl*^{RNAi}-expressing *nerfin-1*$^-$: 10097.55 ± 2269.19 µm^3, n= 21 clones). This overall reduction in clone size resulted also in a reduction of the glia population (94% reduction; **Figure 3.32F**; *nerfin-1*$^-$ control: 12 ± 3.73 glia, n=12 clones; *dl*^{Ri}-expressing *nerfin-1*$^-$: 0.76 ± 0.36 glia, n=21 clones). This again indicates that Notch pathway is required for the growth of *nerfin-1*$^-$ lineages, but it is not specifically required for the formation of ectopic glia.

Next, we tested if activating Notch is sufficient to induce glia cell fate. We test this in the *pox*^{n}> *pros*$^{RNAi\ SH}$ lineages that never produce ectopic glia (**Figure 3.30H**; see also **Chapter 3.1**). We found that increased Notch activity was not sufficient to induce the formation of ectopic glia (**Figure 3.30H**), but increased lineage volume by ~57% (**Figure 3.30I**; *pros*$^{RNAi\ SH}$ plus *mCherry*^{RNAi} control: 242576.04 ± 28866.49 µm^3, n= 18 brains; *pros*$^{RNAi\ SH}$ plus *notch*^{ACT}: 381514.37 ± 37825.41 µm^3, n= 14 brains). These results confirm that Notch is required for the growth of Pros-deficient lineages. Moreover, they suggest that Notch signalling alone is necessary but not sufficient to drive the formation of ectopic glia within NB lineages lacking Pros.

3.3.4. Fibroblast growth factor (FGF) signalling pathway regulates *pros*$^-$ lineage growth through promoting ectopic glial formation.

Given that FGF signalling controls the generation of multiple glial types (Avet-Rochex et al., 2012), we wondered if FGF signalling also drives the formation of ectopic glia. We first inhibited the FGF pathway by expressing a dominant-negative form of the FGF receptor Htl (htl^{DN}) (Rothenbusch-Fender et al., 2017) in $grh>pros^{RNAi\ LH}$ brains (**Figure 3.33D**). Inhibition of FGF pathway caused a significant decrease in the number of ectopic glia found in $grh>pros^{RNAi\ LH}$ lineages, compared with $lacZ^{RNAi}$ control (~40% reduction; **Figure 3.33A-B and E**; control: 162.14 ± 8.50 glia, n=7 brains; htl^{DN} plus $pros^{RNAi\ LH}$: 91.57±8.38 glia, n=7 brains). The NB lineages expressing $pros^{RNAi\ LH}$ and htl^{DN} were, on average, 1.75-fold smaller than the control lineages expressing $pros^{RNAi\ LH}$ and $lacZ^{RNAi}$ (**Figure 3.33C-D** and **F**; control: 825561.39 ± 122316.42 µm^3, n= 7 brains; htl^{DN} plus $pros^{RNAi\ LH}$: 471918.18 ± 38382.40 µm^3, n= 8 brains). These data indicate that (1) FGF signalling is required for the formation of ectopic glia, which in turn promote the growth of NB lineages lacking Pros; or (2) FGF signalling may affect Pros-deficient lineage growth, which then results in a decrease in the formation of the ectopic glia cells.

Next, we tested if activating FGF signalling is sufficient to induce glial cell fate. We tested this in the $pox^{n}>pros^{RNAi\ SH}$ lineages that never produce ectopic glia. We overexpressed an activated form of Htl [htl^{ACT}; (Irizarry and Stathopoulos, 2015)] in $pox^{n}>pros^{RNAi\ SH}$ lineages, and found no ectopic glia formation (**Figure 3.33G''-H''**) and no change in overall lineage size (**Figure 3.33I**; p = 0.9290 ns; control: 242576.04 ± 28866.49 µm^3, n= 18 brains; $pros^{RNAi\ SH}$ plus htl^{ACT}: 246311.35 ± 29740.45 µm^3, n= 20 brains). This suggests that FGF pathway alone is not sufficient to induce ectopic gliogenesis in NB lineages deficient for Pros. Together, this data indicates that the FGF pathway affects lineage size through ectopic glia formation, and confirms the role of ectopic glia in supporting Pros-deficient lineage growth.

3.3.5. Hippo signalling pathway is required for ectopic glia formation and Pros-deficient lineage growth.

We also briefly investigated if the Hippo pathway, which regulates NB proliferation and brain size (Poon et al., 2016), also contributes to the formation of ectopic glia in NB lineages lacking Pros. We inhibited Hippo pathway activity by expressing *RNAi* against

the core kinase Wts, *UAS-wts*^{RNAi} (Poon et al., 2016) in *grh>pros*$^{RNAi\ LH}$ lineages. The lineages expressing both *pros*$^{RNAi\ LH}$ and *wts*^{RNAi} were 70% smaller (**Figure 3.34D** and **F**; 250021.76 ± 40821.75 μm^3, n= 9 brains), and contained 5.23-fold less ectopic glia (**Figure 3.34B** and **E**; 31 ± 8.53 glia, n= 8 brains), compared to control *grh>lacZ*^{RNAi}*;pros*$^{RNAi\ LH}$ lineages (**Figure 3.34A** and **C**; 825561.39 ± 122316.42 μm^3; 162.14 ± 8.50 glia, n= 7 brains). These results show that Hippo pathway regulates the formation of ectopic glia and the growth of type I NB lineages lacking Pros. However, this finding is contradictory to prior study (Poon et al., 2016), in which Hippo pathway was found to restrict the growth of *wildtype* type I NB lineages.

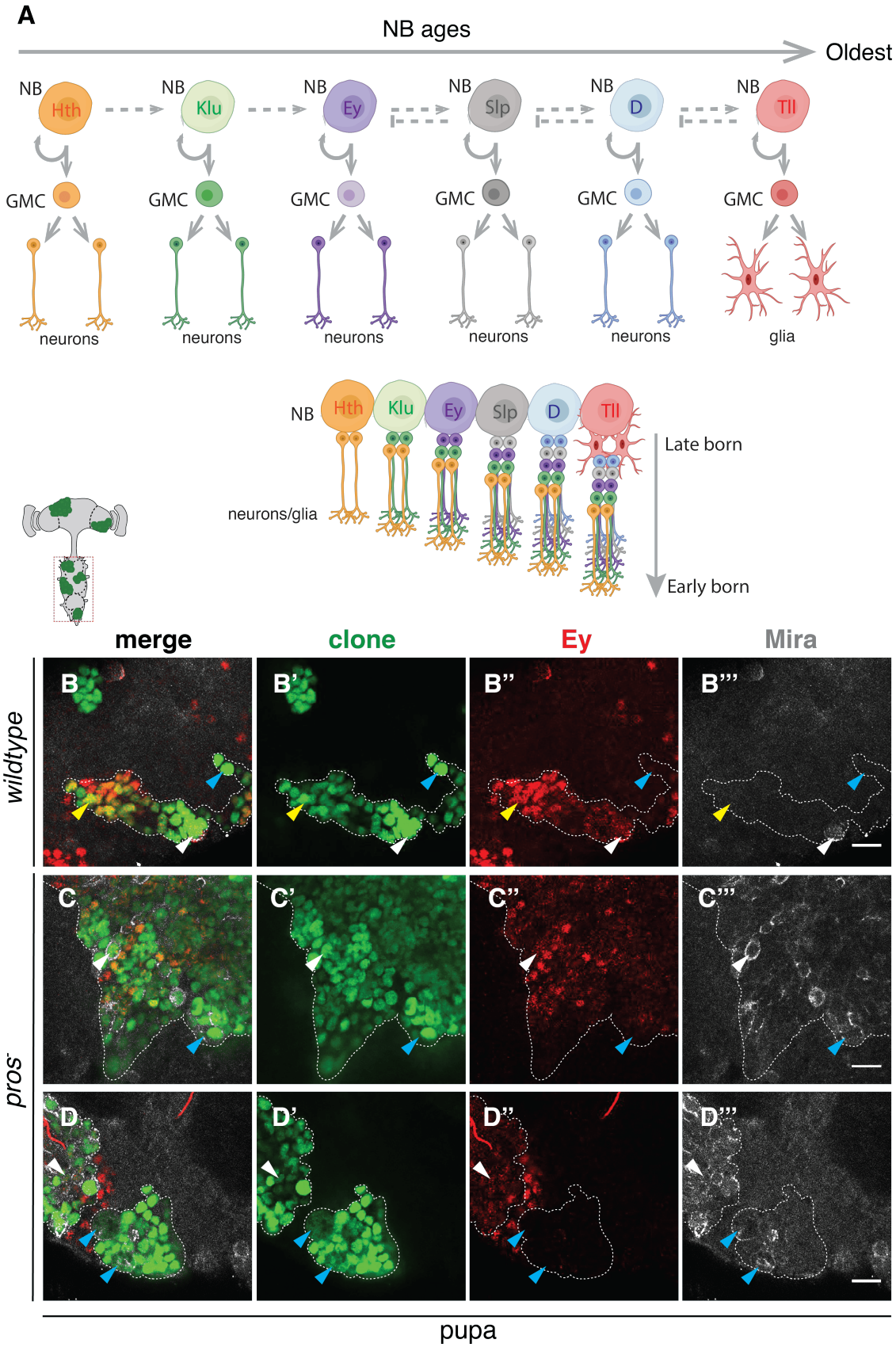
A
NB ages
Oldest
NB
Hth
Klu
Ey
Slp
D
Tll
GMC
neurons
glia
neurons/glia
Late born
Early born
merge
clone
Ey
Mira
wildtype
pros
B
B'
B''
B'''
C
C'
C''
C'''
D
D'
D''
D'''
pupa

Figure 3.22. Medulla NB temporal patterning might be active in Pros-deficient NB lineages.

A. Schematic models summarising the progression of temporal TFs that are sequentially expressed by medulla NBs and their progeny. In the main OPC, medulla NBs sequentially express a series of six temporal TFs (Hth → Klu → Ey → Slp → D → Tll) as they age (Li et al., 2013a). These TFs are inherited by GMCs and neurons to specify neuronal classes in the medulla through NB asymmetric cell divisions. Only one NB is shown for each temporal stage in cartoon (A) but in fact, NBs undergo multiple rounds of cell divisions at each stage. The progeny of each NB constitutes multiple layers of different neuronal identities linked to their birth order. Early born (oldest) neurons expressing Hth occupy the deepest layer while the late born (newest) neurons expressing the latest TFs are at the most superficial layer. This temporal series is regulated by feed-forward and feed-back fashion, meaning that one TF gradually replaces its preceding TF and activates next TF as NB ages. Slp expression represses *ey* and initiates *D* expression. D represses *slp* and initiates *tll* expression. Tll is sufficient to repress *D* expression and marks the final temporal stage of medulla NBs. The oldest Tll^+ NBs switch to glioblasts to generate medulla neuropil glia before they finally exit the cell cycle. *gcm* is expressed in Tll^+ NBs, and is inherited by their progeny. The progeny then lose Tll and turn on Repo, to eventually adopt glial fate.

(B-D’’’) Ey expression in pupal VNCs containing control *wildtype* (B-B’; outlined; green), or $pros^-$ MARCM clones (C-D’; outlined; green). Pupal clones were immunostained with GFP (B-D’; clone; nuclear green), Ey (B’’-D’’; nuclear red) and NB marker Mira (B’’’-D’’’; membraneous grey). Merged and single channels are shown. Scale bars, 10 μm.

(B-B’’’) Cross-section of a representative *wildtype* clone showing the expression of Ey in *wildtype* NB and its progeny. Ey was expressed in the parental NB (B’’-B’’’; white arrowhead) and the majority of its progeny cells (B’’; yellow arrowhead). However, a subset of *wildtype* progeny does not express Ey (B’’; red; blue arrowhead).

(C-D’’’) Cross-sections of representative $pros^-$ mutant clones showing the Ey expression in ectopic NBs and their progeny. Ey was expressed in a subset of $Mira^+$ ectopic NBs in clone (C’’-D’’’; white arrowhead). No Ey expression was detectable in a population of $Mira^+$ ectopic NBs (C’’-D’’; red; blue arrowhead), meaning that they were generated at other temporal windows.

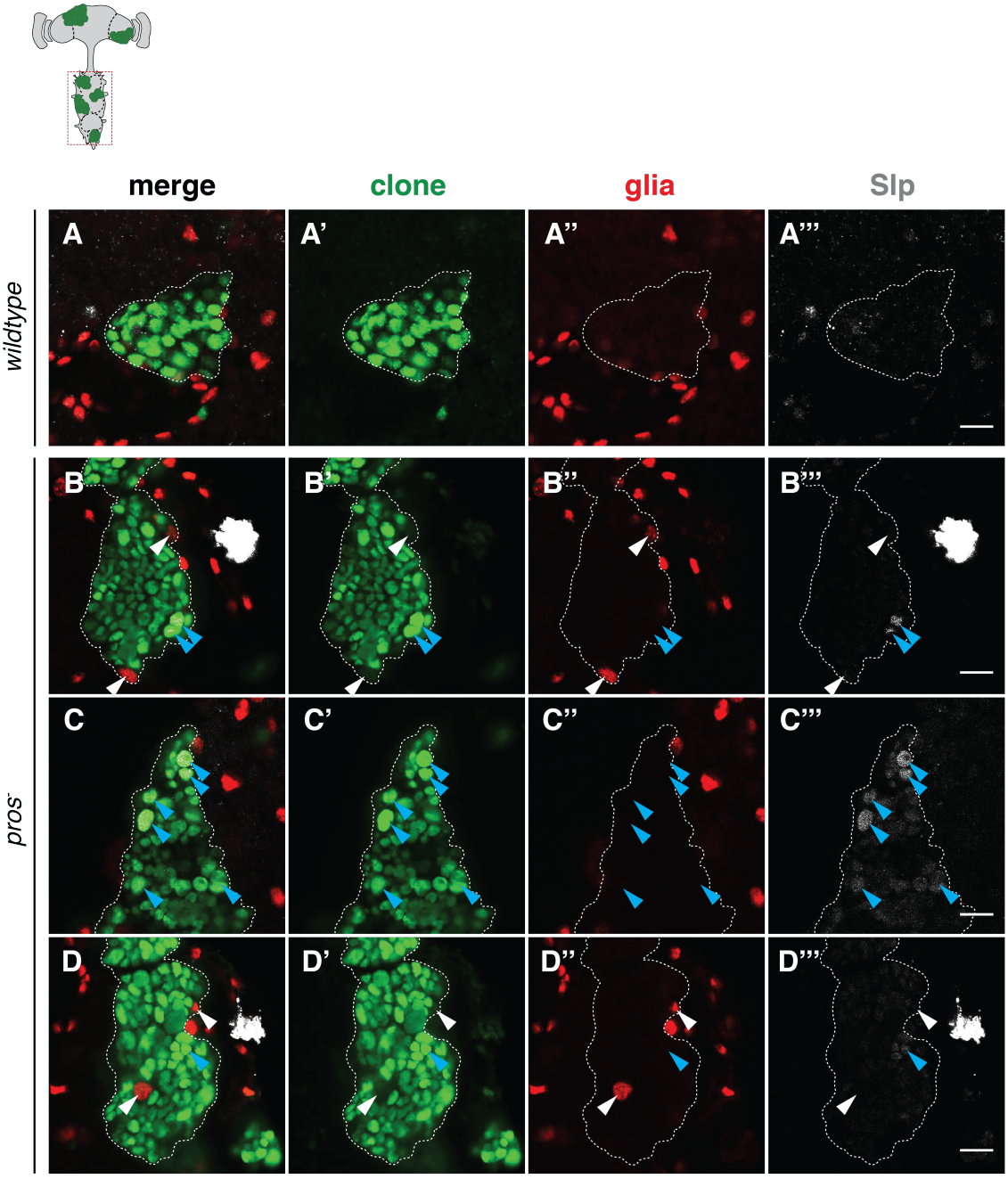
merge
clone
glia
Slp
wildtype
pros-
A
A'
A''
A'''
B
B'
B''
B'''
C
C'
C''
C'''
D
D'
D''
D'''

Figure 3.23. Slp is ectopically expressed in the *pros*$^{-}$ clones in pupal VNC.
GFP-labeled MARCM clones were generated at 48 hours AEL and visualised in the pupal VNC (2 days APF). The clones were immunostained with GFP (A-D'; clone; nuclear green), Repo (A''-D''; glia; nuclear red) and Slp (A'''-D'''; nuclear grey). Merged and single channels are shown. Scale bars, 10 μm.

(A-A''') Cross-section of a representative *wildtype* clone showing that Slp is not expressed in *wildtype* clone.

(B-D''') Cross-sections of representative *pros*$^{-}$ clone showing that Slp is expressed in *pros*$^{-}$ NB lineages (B'''-D'''; blue arrowhead), but not in ectopic glia (B'-B'' and D'-D''; white arrowhead).

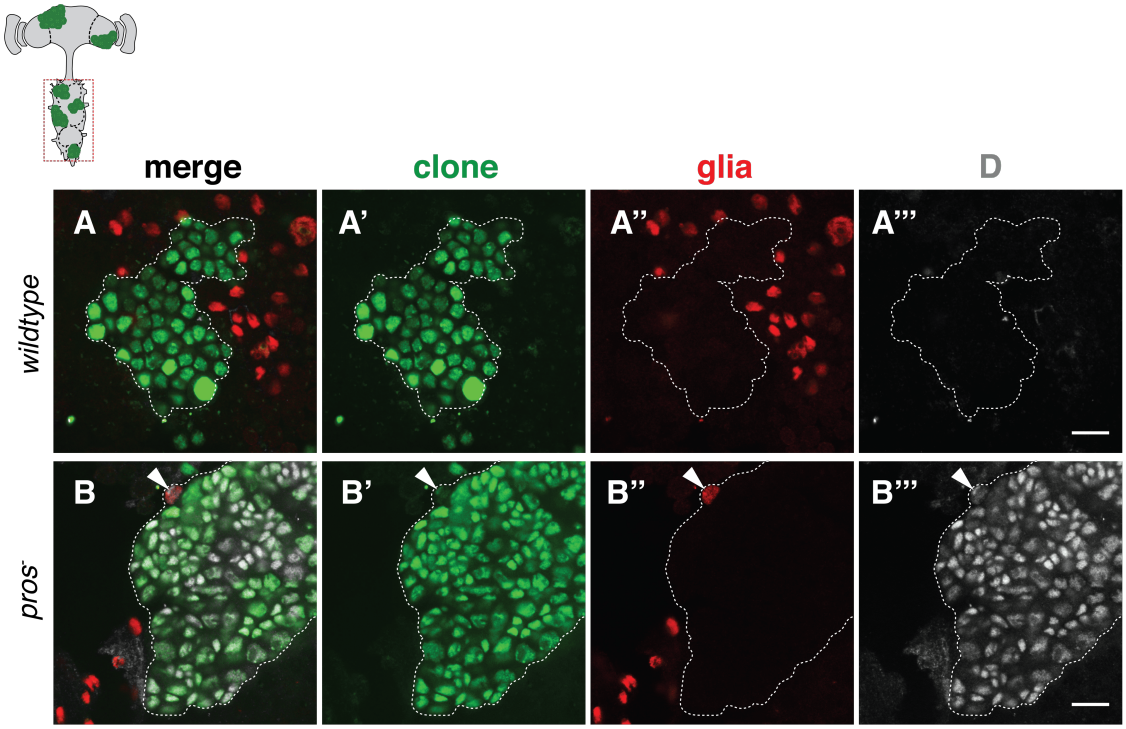



grh>pros$^{Ri\ LH}$

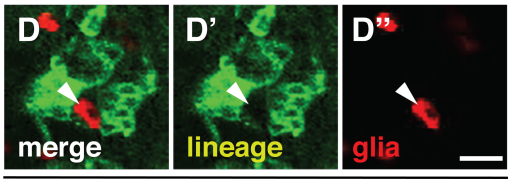

grh>D^{Ri}; pros$^{Ri\ LH}$

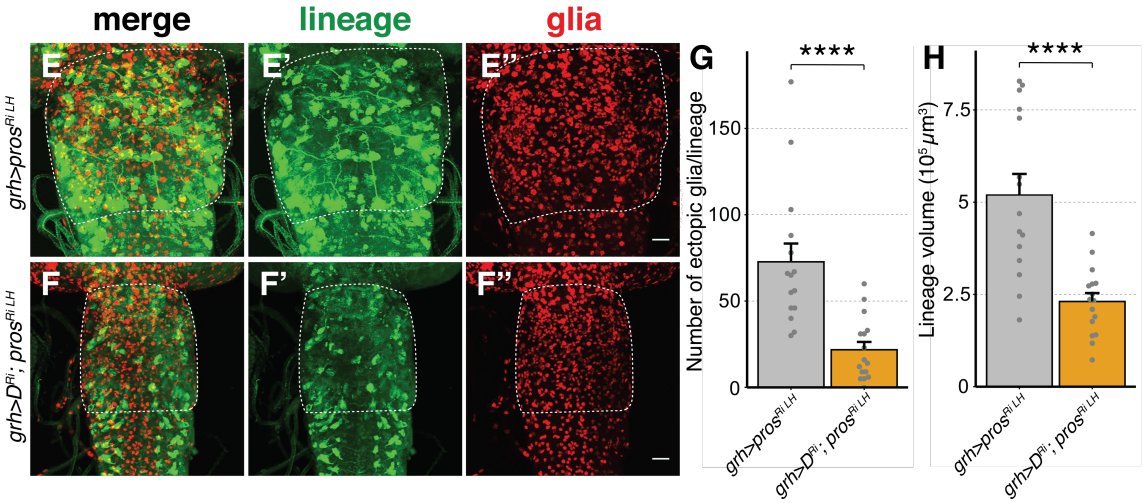

Figure 3.24. D is ectopically expressed in the Pros-deficient NB lineages and is required for the formation of ectopic glia, and the lineage growth.
(A-B’’’) Cross-section views of representative pupal *wildtype* (A-A’’’) and *pros*$^{-}$ clones (B-B’’’) showing that D was ectopically expressed in *pros*$^{-}$ clones, but not in *wildtype* clones. D was expressed in ectopic glia (B’’-B’’’; white arrowhead). GFP-labeled MARCM clones were generated 48 hours AEL and dissected at pupal stages (2 days APF). The clones were immunostained with GFP (A-B’; clone; nuclear green), Repo (A’’-B’’; glia; nuclear red) and D (A’’’-B’’’; nuclear grey). Merged and single channels are shown. Scale bars, 10 μm.

(C-D) Ectopic glia (white arrowhead) have been generated at early larval stages in lineages expressing *pros*$^{RNAi\ LH}$ (control; C-C’) and lineages expressing *D*^{RNAi} versus *pros*$^{RNAi\ LH}$ (D-D’). *Grh-Gal4* driver was used to induce the expression of membrane *RFP*, *pros*$^{RNAi\ LH}$ (control; C-C’) or *RFP*, *D*^{RNAi} versus *pros*$^{RNAi\ LH}$ (D-D’) in the NB lineages of larval CNS. L3 brains of the indicated genotypes were immunostained with RFP (lineage; false coloured as green) and Repo (glia; red). Merged and single channels are shown. Scale bar, 10 μm.

(E-F’’) Representative confocal images showing that *grh>pros*$^{RNAi\ LH}$ lineage volume is decreased upon *D* loss-of-function. The *pros*$^{RNAi\ LH}$-expressing lineages in thoracic segments of larval VNC are outlined with dashed lines, and are shown in high-magnification maximum-projection images (E-F’). Ectopic glia were observed in all regions of the lineages. Merged and single channels are shown. Scale bars, 20 μm.

(G) Total number of ectopic glia in lineages of the genotypes displayed in (C)-(D); n = 15 and 16, respectively; control versus *D*^{RNAi} plus *pros*$^{RNAi\ LH}$, ****p <0.0001.

(H) Quantification of the RFP^{+} lineage volume (measured by RFP intensity) located at the thoracic segments of brains from (E)-(F); n = 15 and 16, respectively; control versus *D*^{RNAi} plus *pros*$^{RNAi\ LH}$, ****p < 0.0001.

Data are presented as means ± SEM. p values were achieved by unpaired t test.

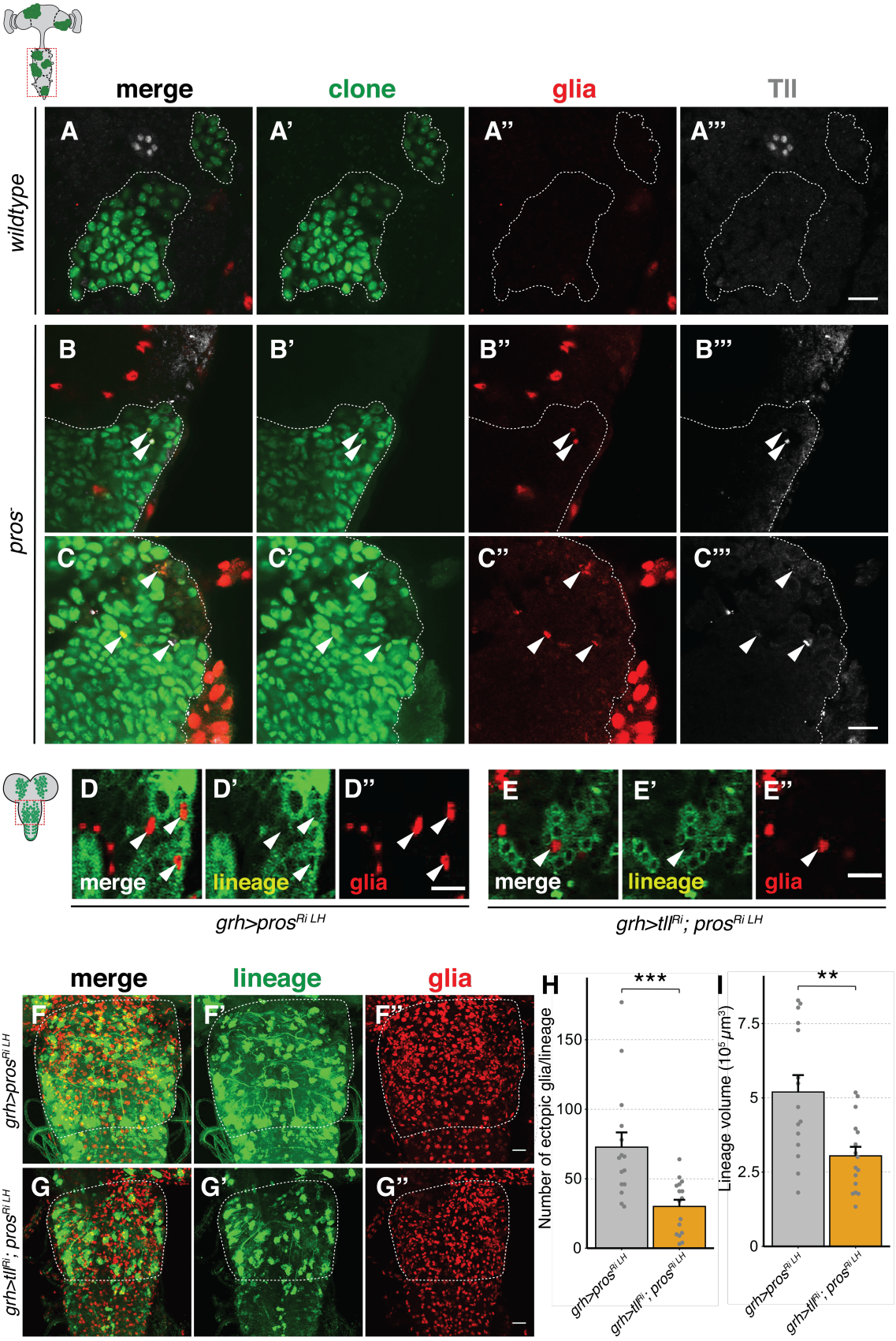
merge
clone
glia
TII
wildtype
pros-
A
A'
A''
A'''
B
B'
B''
B'''
C
C'
C''
C'''
D
D'
D''
merge
lineage
glia
E
E'
E''
merge
lineage
glia
grh>pros^Ri LH
grh>tll^Ri; pros^Ri LH
merge
lineage
glia
F
F'
F''
G
G'
G''
grh>pros^Ri LH
grh>tll^Ri; pros^Ri LH
H
Number of ectopic glia/lineage
***
150
100
50
0
grh>pros^Ri LH
grh>tll^Ri; pros^Ri LH
I
Lineage volume (10^5 µm^3)
**
7.5
5
2.5
0
grh>pros^Ri LH
grh>tll^Ri; pros^Ri LH

Figure 3.25. Tll is ectopically expressed in the Pros-deficient NB lineages and is required for the formation of ectopic glia, and the lineage growth.

(A-C’’’) Cross-section views of representative pupal *wildtype* (A-A’’’) and *pros*$^{-}$ clones (B-C’’’) showing that Tll is ectopically expressed in *pros*$^{-}$ clones, but not in *wildtype* clones. Tll expression was found in ectopic glia (B’’-B’’’ and C’’-C’’’; white arrowhead). GFP-labeled MARCM clones were generated 48 hours AEL and visualised in the pupal VNCs (2 days APF). The clones were immunostained with GFP (A-C’; clone; green), Repo (A’’-C’’; glia; red) and Tll (A’’’-C’’’; grey). Merged and single channels are shown. Scale bars, 10 μm.

(D-E’’) Ectopic glia (white arrowhead) have been generated at early larval stages in lineages expressing *pros*$^{RNAi\ LH}$ (control; D-D’) and lineages expressing *tll*^{RNAi} versus *pros*$^{RNAi\ LH}$ (E-E’). *Grh-Gal4* driver was used to induce the expression of membrane *RFP*, *pros*$^{RNAi\ LH}$ (control; D-D’) or *RFP*, *tll*^{RNAi} versus *pros*$^{RNAi\ LH}$ (E-E’) in the NB lineages of larval CNS. L3 brains of the indicated genotypes were immunostained with RFP (lineage; false coloured as green) and Repo (glia; red). Merged and single channels are shown. Scale bar, 10 μm.

(F-G’’) Representative confocal images showing that *grh>pros*$^{RNAi\ LH}$ lineage volume is decreased upon *tll* loss-of-function. The *pros*$^{RNAi\ LH}$-expressing lineages in thoracic segments of larval VNC are outlined with dashed lines, and are shown in high-magnification maximum-projection images (F-G’). Ectopic glia were observed in all regions of the lineages. Merged and single channels are shown. Scale bars, 20 μm.

(H) Total number of ectopic glia in lineages of the genotypes displayed in (D)-(E); n = 15 and 16, respectively; control versus *tll*^{RNAi} plus *pros*$^{RNAi\ LH}$, ***p =0.0008.

(I) Quantification of the RFP^{+} lineage volume (measured by RFP intensity) located at the thoracic segments of brains from (F)-(G); n = 15 and 16, respectively; control versus *tll*^{RNAi} plus *pros*$^{RNAi\ LH}$, **p = 0.002.

Data are presented as means ± SEM. p values were achieved by unpaired t test.

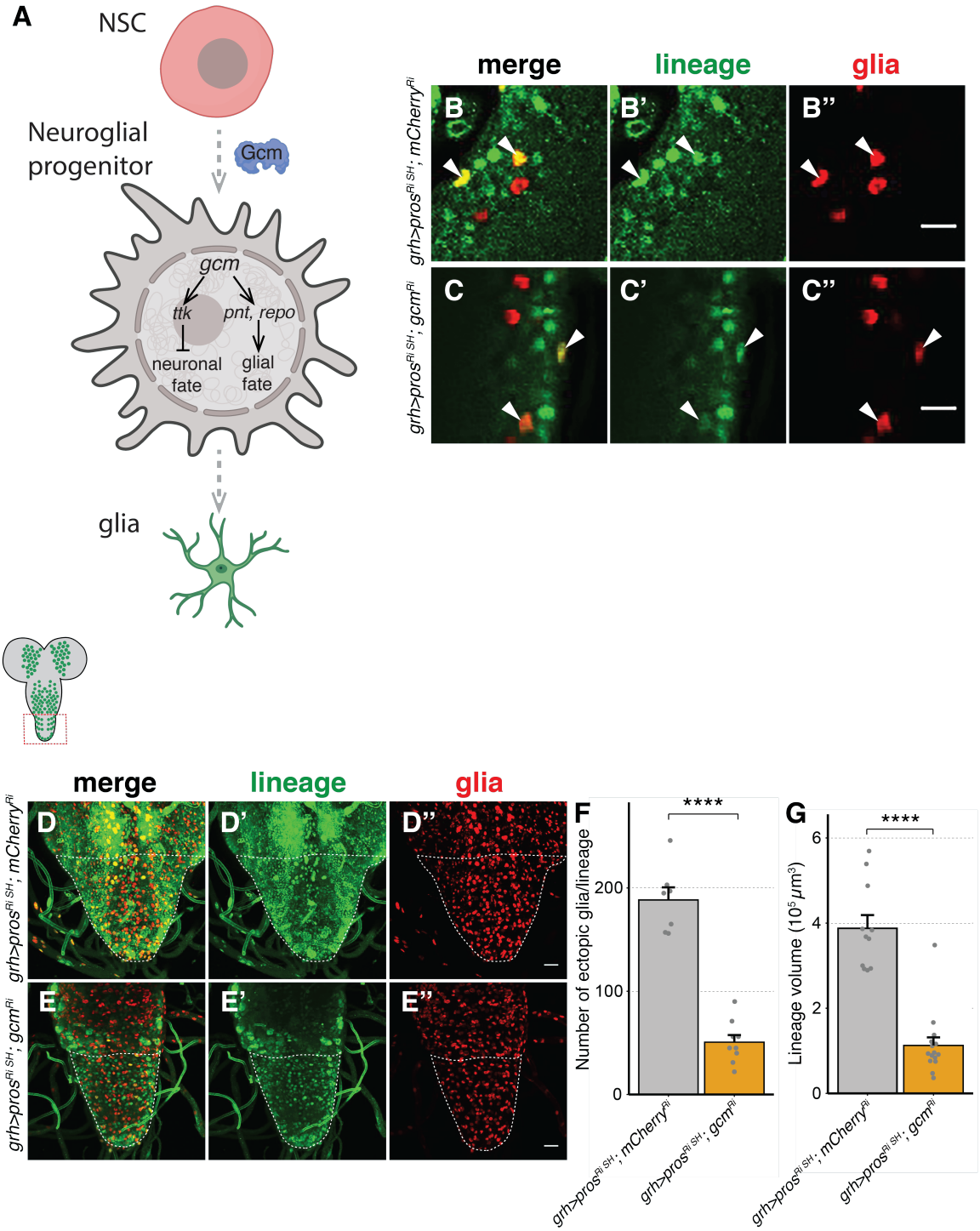
A
NSC
Neuroglial progenitor
Gcm
gcm
ttk
pnt, repo
neuronal fate
glial fate
glia
merge
lineage
glia
B
B'
B''
C
C'
C''
grh>pros^RiSH; mCherry^Ri
grh>pros^RiSH; gcm^Ri
D
D'
D''
E
E'
E''
F
Number of ectopic glia/lineage
****
200
100
0
G
Lineage volume (10^5 µm^3)
6
4
2
0
grh>pros^RiSH; mCherry^Ri
grh>pros^RiSH; gcm^Ri

Figure 3.26. Gcm is required for the formation of ectopic glia and for the growth of lineages lacking Pros.

(A) Schematic represents *gcm* pathway, which controls gliogenesis in *Drosophila*. Gcm directs NSC to enter differentiation by mediating epigenetic pathways in NSC. Young NSCs at early development are more plastic, and therefore, are more likely to be induced into glial differentiation. NSCs are first transformed into an intermediate precursor cell called neuroglial progenitor, which expresses both NSC (Mira, Dpn) and glial markers (Repo), before being fully converted into differentiated glia. In intermediate precursor cell, Gcm acts as a binary genetic switch for neuronal and glial cell fates by regulating the expression of downstream glial-specific genes. The *gcm* downstream target genes include (1) *tramtrack* (*ttk*) for inhibiting neuronal differentiation; and (2) *pointed* (*pnt*) and *repo* for promoting glial differentiation. Therefore, the expression of master glial regulator *gcm* and the glial differentiation genes; such as *repo*; is important to activate glial fate in NSC.

(B-C) Ectopic glia (white arrowhead) have been generated at larval stages in lineages expressing $pros^{RNAi\ SH}$ versus $mCherry^{RNAi}$ (control; B-B') and lineages expressing $pros^{RNAi\ SH}$ versus gcm^{RNAi} (C-C'). *Grh-Gal4* driver was used to induce the expression of RFP^{nls}, $pros^{RNAi\ SH}$ versus $mCherry^{RNAi}$ (control; B-B') or RFP^{nls}, $pros^{RNAi\ SH}$ versus gcm^{RNAi} (C-C') in the NB lineages of larval CNS. L3 brains of the indicated genotypes were immunostained with RFP (lineage; false coloured as green) and Repo (glia; red). Merged and single channels are shown. Scale bar, 10 μm.

(D-E) Representative confocal images showing that $pros^{RNAi\ SH}$-expressing lineage volume is decreased upon knockdown of *gcm*. The interested abdominal segments of larval VNC are outlined with dashed white lines, and are shown in high-magnification maximum-projection images. Merged and single channels are shown. Scale bars: 20 μm.

(F) Total number of ectopic glia (co-expressing RFP and Repo) in the lineages of genotypes displayed in (D) and (E); n = 7 and 9, respectively, ****p <0.0001.

(G) Quantification of the RFP^+ lineage volume (measured by RFP intensity) located at thoracic segments of brains from (D) and (E); n = 11 and 15, respectively, ****p <0.0001.

Data are presented as means ± SEM. p values were achieved by unpaired t test.

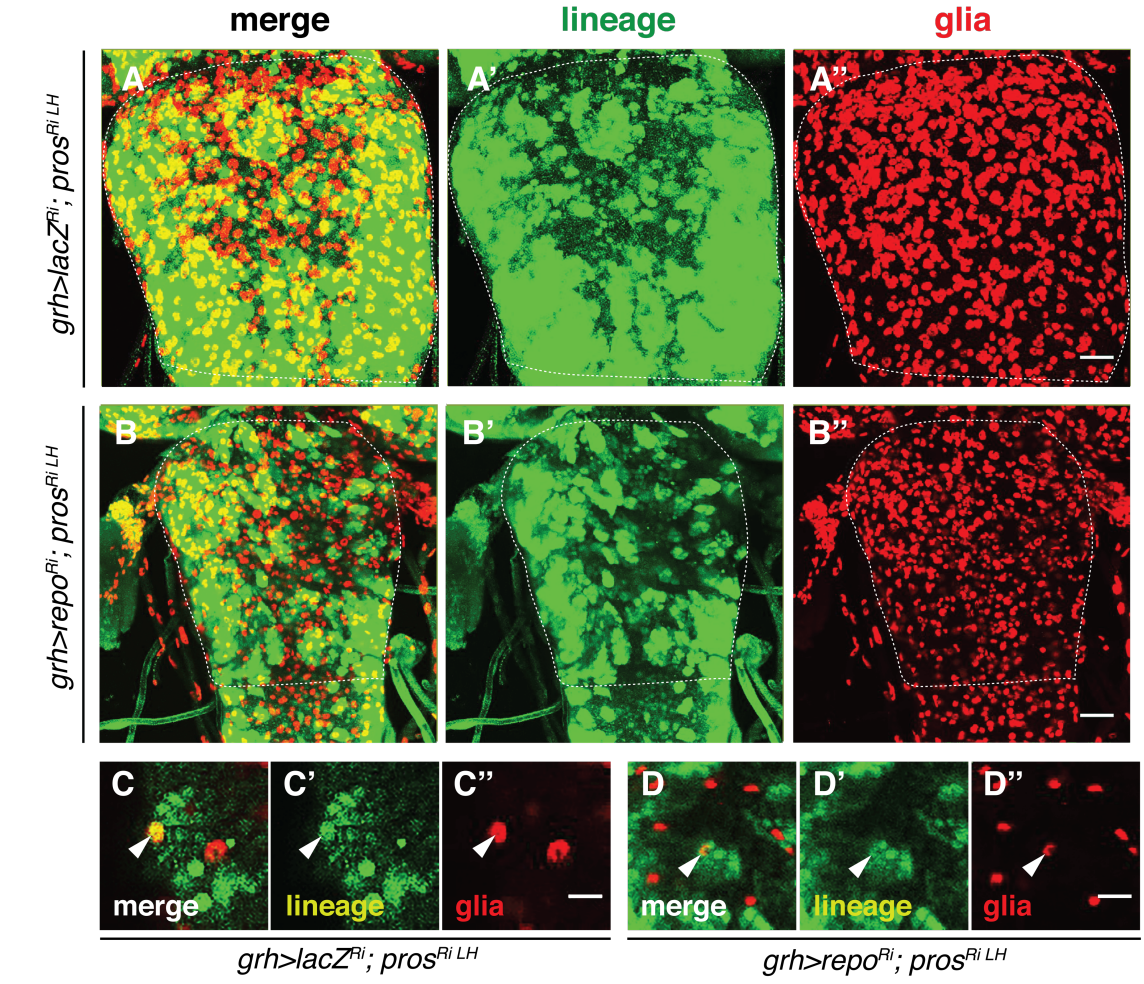
merge
lineage
glia
A
A'
A''
B
B'
B''
grh>lacZRi; prosRi LH
grh>repoRi; prosRi LH
C
C'
C''
D
D'
D''
merge
lineage
glia
grh>lacZRi; prosRi LH
grh>repoRi; prosRi LH

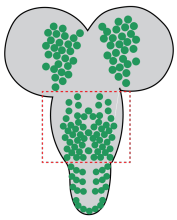

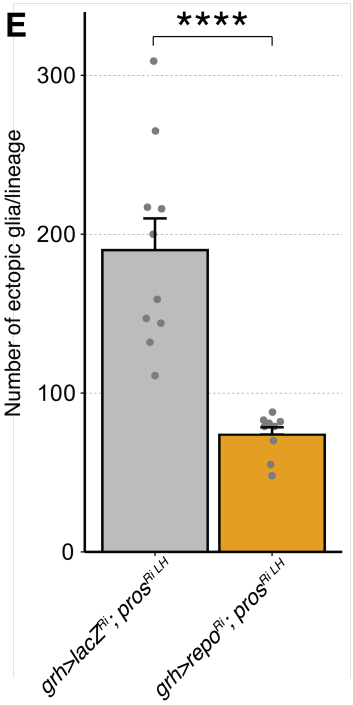
E
****
Number of ectopic glia/lineage
300
200
100
0
grh>lacZRi; prosRi LH
grh>repoRi; prosRi LH

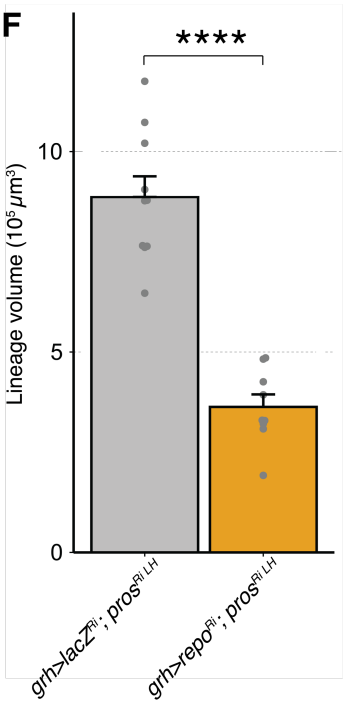
F
****
Lineage volume (10⁵ μm³)
10
5
0
grh>lacZRi; prosRi LH
grh>repoRi; prosRi LH

Figure 3.27. Repo is required for the formation of ectopic glia and for the *grh>pros$^{RNAi\ LH}$* lineage growth.

(A-B) Representative confocal images showing that *pros$^{RNAi\ LH}$*-expressing lineage volume is decreased upon knockdown of *repo*. *Grh-Gal4* driver was used to induce the expression of *RFP^{nls}*, *lacZ^{RNAi}* versus *pros$^{RNAi\ LH}$* (control; A-A'; green) or *RFP^{nls}*, *repo^{RNAi}* versus *pros$^{RNAi\ LH}$* (B-B'; green) in the NB lineages of larval CNS. L3 brains of the indicated genotypes were immunostained with RFP (lineage; false coloured as green) and Repo (glia; red). The thoracic segments of larval VNC are outlined with dashed white lines, and are shown in high-magnification maximum-projection images. Ectopic glia were observed dispersed throughout the lineages of the indicated genotypes (C and D; white arrowhead). Merged and single channels are shown. Scale bars: 20 μm in (A-B''), and 10 μm elsewhere.

(E) Total number of ectopic glia (co-expressing RFP and Repo) in lineages of the genotypes displayed in (A) and (B); n = 10 and 9, respectively, ****p <0.0001.

(F) Quantification of the RFP^{+} lineage volume (measured by RFP intensity) located at thoracic segments of brains from (A) and (B); n = 10 and 9, respectively, ****p <0.0001.

Data are presented as means ± SEM. p values were achieved by unpaired t test.

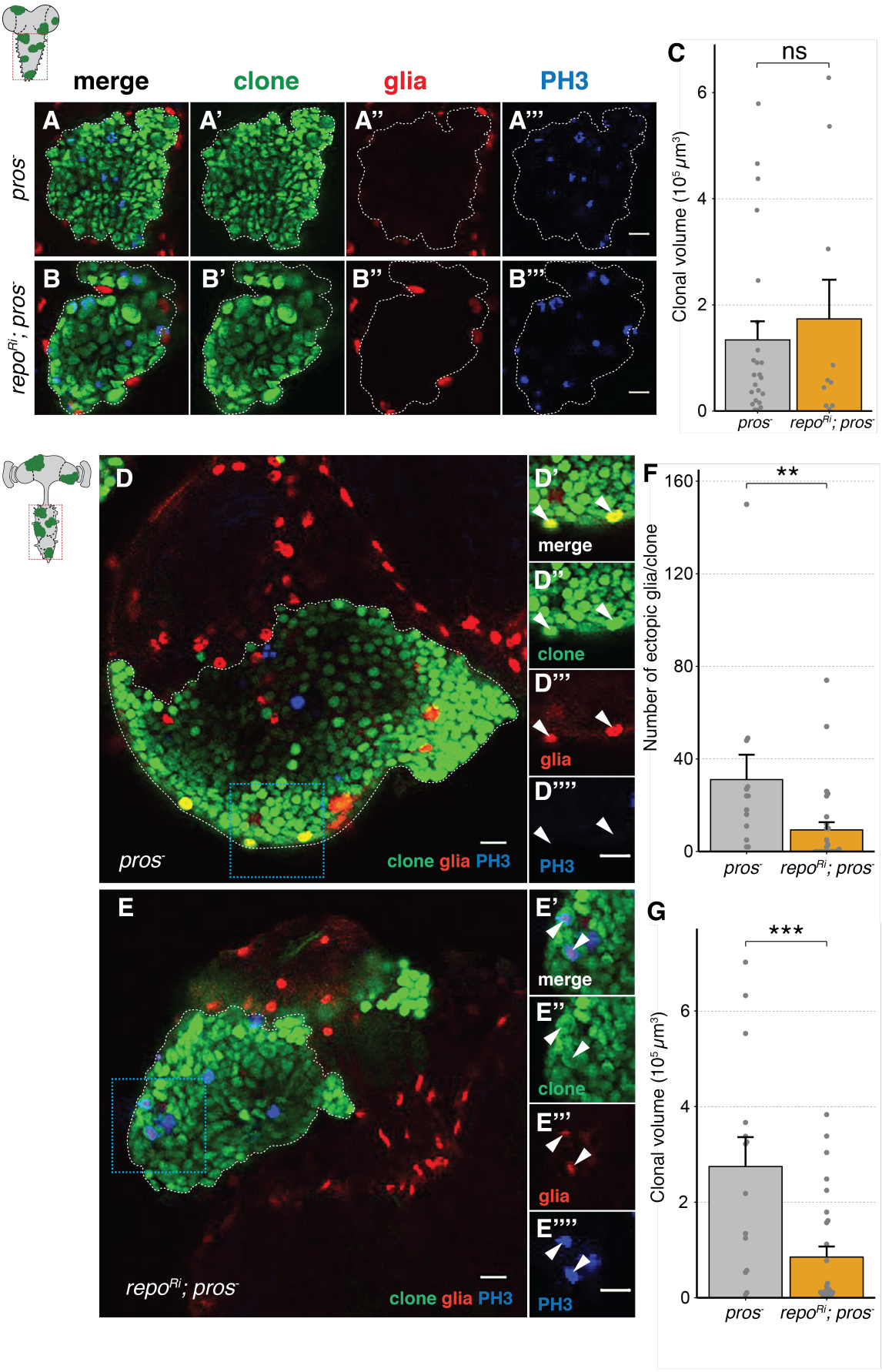
merge
clone
glia
PH3
A
A'
A''
A'''
B
B'
B''
B'''
pros-
repoRi; pros-
C
ns
Clonal volume (10^5 µm^3)
0
2
4
6
pros-
repoRi; pros-
D
D'
merge
D''
clone
D'''
glia
D''''
PH3
pros-
clone glia PH3
E
E'
merge
E''
clone
E'''
glia
E''''
PH3
repoRi; pros-
clone glia PH3
F
**
Number of ectopic glia/clone
0
40
80
120
160
pros-
repoRi; pros-
G
***
Clonal volume (10^5 µm^3)
0
2
4
6
pros-
repoRi; pros-

Figure 3.28. Repo is only required for the formation of ectopic glia, which in turn, promote the *pros*$^{-}$ clonal growth.
MARCM clones were stained for GFP (clone; green; outlined by dashed white line), Repo (glia; red), and pH3 (mitotic cells; blue). Merged and single channels are shown. Scale bars, 10 μm.

(A, B and C) Loss of Repo does not significantly alter *pros*$^{-}$ clones in larval VNC (120 hours after larval hatching). Representative *pros*$^{-}$ MARCM clones (control; A-A'), or *repo*^{RNAi}-expressing *pros*$^{-}$ MARCM clones [(*repo*^{RNAi}*; pros*$^{-}$*)*; B-B'], in the larval VNC. No ectopic glia were found in control nor *repo*^{RNAi}*; pros*$^{-}$ clones in larval VNC.
(C) Quantification of the GFP^{+} clonal volume (measured by GFP intensity) of clones from (A) and (B); n=23 and 10, respectively. p= 0.5849 (not significant, ns).

(D, E and F, G) Loss of Repo significantly supresses *pros*$^{-}$ clonal volume in the VNC of late pupal brains (3 days APF).

(D-E) Representative *pros*$^{-}$ (control; D-D'), or *repo*^{RNAi}*; pros*$^{-}$ MARCM clones (E-E'), in the pupal VNC. Ectopic glia have been formed in most VNC clones at this late pupal stage.

(D) Deep section of a representative control *pros*$^{-}$ clone (green; dashed outline); whereby the boxed region is magnified in (D'-D''''). Non-mitotic ectopic glia (Repo^{+} pH3^{-}; white arrowhead) were found in this clone.

(E) Deep section of a representative *repo*^{RNAi}*; pros*$^{-}$ clone (green; dashed outline); whereby the boxed region is magnified in (E'-E''''). Mitotic ectopic glia (Repo^{+} pH3^{+}; white arrowhead) were found in this clone.

(F) Total number of ectopic glia (co-expressing GFP and Repo) in clones of the genotypes displayed in (D) and (E); n = 12 and 26, respectively. **p = 0.0021.

(G) Quantification of the GFP^{+} clonal volume (measured by GFP intensity) of genotypes from (D) and (E); n= 14 and 28 respectively. ***p = 0.0002.

Data are presented as means ± SEM. p values were achieved by unpaired t test.

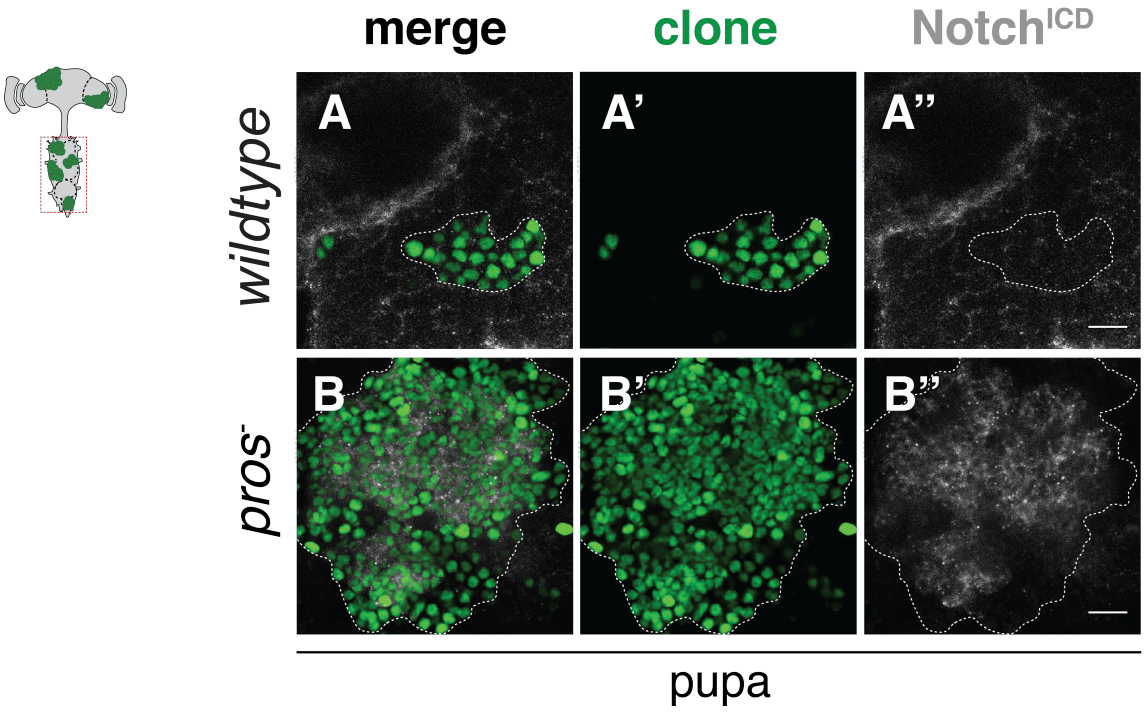

Figure 3.29. Notch is hyperactivated in *pros*$^{-}$ clone but not in the *wildtype* clone.
Wildtype (A-A') and *pros*$^{-}$ clone (B-B') marked by GFP (clone; green; outlined by dashed white line) were stained for Notch^{ICD} to mark intracellular domain of Notch expressed in the nucleus of NBs. Merged and single channels are shown. Scale bars, 10 µm. Notch expression (grayscale, detected with a Notch^{ICD} antibody) was increased and dispersed throughout *pros*$^{-}$ MARCM clones (green) located in the pupal VNC; whereas, Notch was not expressed in *wildtype* clones.

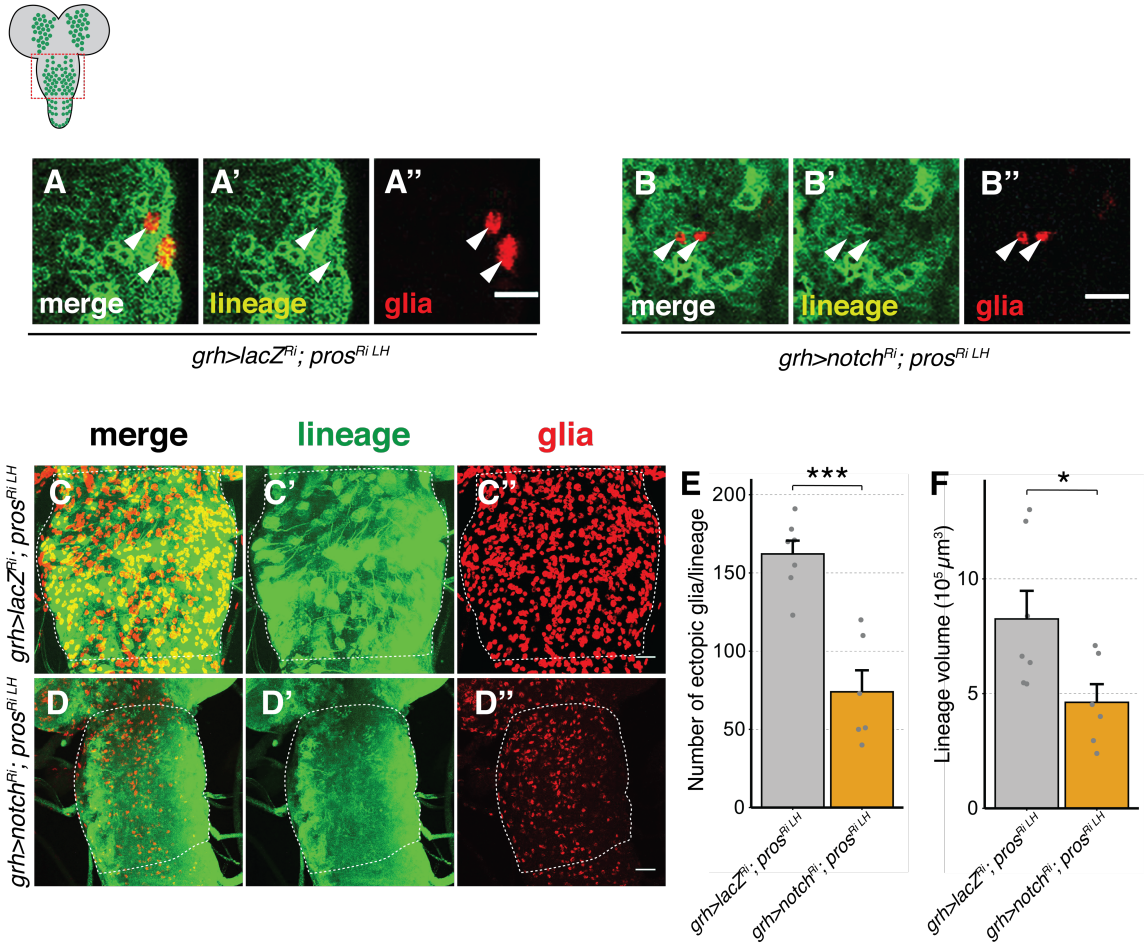
A
A'
A''
merge
lineage
glia
B
B'
B''
merge
lineage
glia
grh>lacZ^Ri; pros^Ri LH
grh>notch^Ri; pros^Ri LH
merge
lineage
glia
C
C'
C''
D
D'
D''
grh>lacZ^Ri; pros^Ri LH
grh>notch^Ri; pros^Ri LH
E
***
Number of ectopic glia/lineage
200
150
100
50
0
grh>lacZ^Ri; pros^Ri LH
grh>notch^Ri; pros^Ri LH
F
*
Lineage volume (10^5 µm^3)
10
5
0
grh>lacZ^Ri; pros^Ri LH
grh>notch^Ri; pros^Ri LH
merge
lineage
glia
PH3
G
G'
G''
G'''
H
H'
H''
H'''
pox^n>pros^Ri SH; mCherry^Ri
pox^n>pros^Ri SH; notch^ACT
I
**
Lineage volume (10^5 µm^3)
6
4
2
0
pox^n>pros^Ri SH; mCherry^Ri
pox^n>pros^Ri SH; notch^ACT

Figure 3.30. Notch signalling pathway is required but not sufficient to induce the formation of ectopic glia in NB lineages lacking Pros.
L3 larval brains (120 hours AEL) of the indicated genotypes were immunostained with different antibody combinations. In (A-D"): RFP (lineages; false coloured as green) and Repo (glia; red). In (G-H'''): GFP (lineage; green), Repo (glia; red) and pH3 (mitotic cells; grey). Merged and single channels are shown. Scale bars, 20 μm in (C-D'') and 10 μm elsewhere.

(A-B'') Ectopic glia (white arrowhead) have been generated at early larval stages in lineages expressing *lacZ*^{RNAi} plus *pros*$^{RNAi\ LH}$ (control; A-A') and lineages expressing *notch*^{RNAi} plus *pros*$^{RNAi\ LH}$ (B-B'). *Grh-Gal4* driver was used to induce the expression of membrane *RFP*, *lacZ*^{RNAi} plus *pros*$^{RNAi\ LH}$ (control; A-A') or *RFP*, *notch*^{RNAi} plus *pros*$^{RNAi\ LH}$ (B-B') in the NB lineages of larval CNS.

(C-D'') Representative confocal images showing that *grh>pros*$^{RNAi\ LH}$ lineage volume is decreased upon *notch* loss-of-function. The *pros*$^{RNAi\ LH}$-expressing lineages in thoracic segments of larval VNC are outlined with dashed lines, and are shown in high-magnification maximum-projection images (C-D''). Ectopic glia were observed in all regions of the lineages.

(E) Total number of ectopic glial cells (coexpessing RFP and Repo) in *grh>pros*$^{RNAi\ LH}$ lineages of the genotypes displayed in (A)-(B): control versus *notch*^{RNAi} plus *pros*$^{RNAi\ LH}$, ***p = 0.0002. n = 7 and 6, respectively.

(F) Quantification of the RFP$^+$ lineage volume (measured by RFP intensity) located at the thoracic segments of brains from (C)-(D): control versus *notch*^{RNAi} plus *pros*$^{RNAi\ LH}$, *p = 0.0354. n = 7 and 6, respectively.

(G-H''') Representative images showing that *notch* activation is not sufficient to induce the formation of ectopic glia in *pox*^{n} *>pros*$^{RNAi\ SH}$ lineages. *pox*^{n} *-Gal4* driver was used to induce the expression of *GFP*, *pros*$^{RNAi\ SH}$ plus *mCherry*^{RNAi} (control; G-G') or *GFP*, *pros*$^{RNAi\ SH}$ plus *notch*^{ACT} (H-H'), in 6 NB lineages of larval VNC. Lineages are outlined by dashed white lines, and are shown in higher magnification. No ectopic glia (GFP$^+$ Repo$^+$) cells were found in control or *pox*^{n}*>pros*$^{RNAi\ SH}$*; notch*^{ACT} lineages.

(I) *notch* overexpression significantly increases the *pox*^{n}*>pros*$^{RNAi\ SH}$ lineage volume. Quantification of GFP$^+$ lineage volume of brains from (G)-(H): control versus *pros*$^{RNAi\ SH}$ plus *notch*^{ACT}; n = 18 and 14, respectively; **p = 0.0057.

Data are presented as means ± SEM. p values were achieved by unpaired t test.

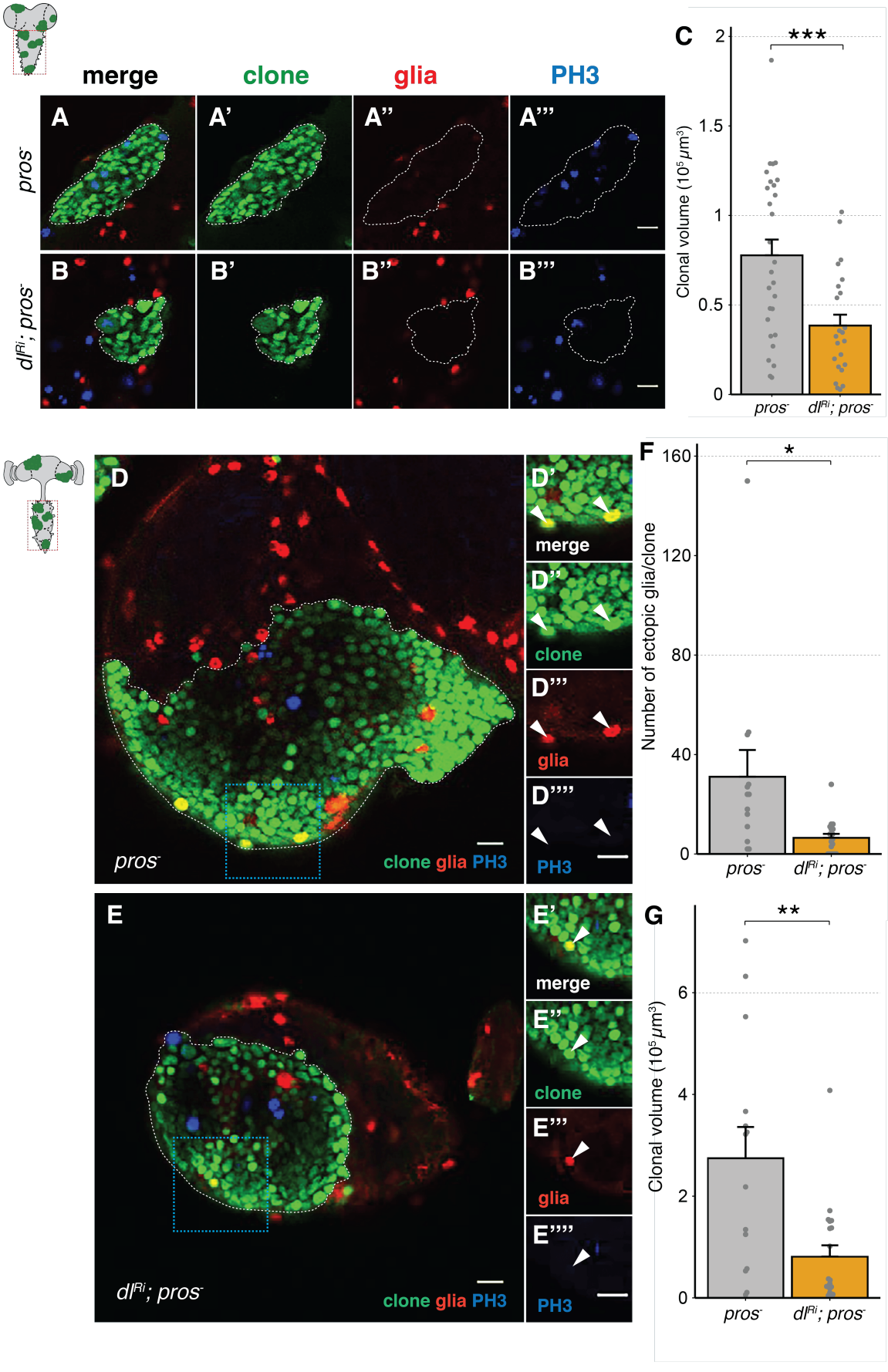
merge
clone
glia
PH3
A
A'
A''
A'''
B
B'
B''
B'''
pros-
dlRi; pros-
C
***
Clonal volume (10^5 µm^3)
2
1.5
1
0.5
0
pros-
dlRi; pros-
D
D'
merge
D''
clone
D'''
glia
D''''
PH3
pros-
clone glia PH3
E
E'
merge
E''
clone
E'''
glia
E''''
PH3
dlRi; pros-
clone glia PH3
F
*
Number of ectopic glia/clone
160
120
80
40
0
pros-
dlRi; pros-
G
**
Clonal volume (10^5 µm^3)
6
4
2
0
pros-
dlRi; pros-

Figure 3.31. Notch signalling functions in *pros*$^{-}$ NB lineages to stimulate clonal growth independent of ectopic glia.
MARCM clones were stained for GFP (clone; green; outlined by dashed white line), Repo (glia; red), and pH3 (mitotic cells; blue). Merged and single channels are shown. Scale bars, 10 μm.

(A, B and C) Loss of Notch ligand Dl suppresses *pros*$^{-}$ clonal volume in larval VNC (120 hours AEL). Representative *pros*$^{-}$ MARCM clones (control; A-A'), or *dl*^{RNAi}-expressing *pros*$^{-}$ MARCM clones [(*dl*^{RNAi}*; pros*$^{-}$*)*; B-B'], in the larval VNC. No ectopic glia were found in control nor *dl*^{RNAi}*; pros*$^{-}$ clones in larval VNC.
(C) Quantification of the GFP^{+} clonal volume (measured by GFP intensity) of clones from (A) and (B); n= 28 and 23, respectively. ***p = 0.002.

(D, E and F, G) Loss of Dl significantly suppresses *pros*$^{-}$ clone volume in the VNC of late pupal brains (3 days APF).
(D-E) Representative *pros*$^{-}$ (control; D-D'), or *dl*^{RNAi}*; pros*$^{-}$ MARCM clones (E-E'), in the pupal VNC. Ectopic glia have been formed in most VNC clones at this late pupal stage, and reside everywhere from the superficial to deeper clone sections.

(D) Deep sections of a representative control *pros*$^{-}$ clone (green; dashed outline); whereby the boxed region is magnified in (D'-D'''). Non-mitotic ectopic glia (Repo^{+} pH3^{-}; white arrowhead) were found in this clone.
(E) Deep sections of a representative *dl*^{RNAi}*; pros*$^{-}$ clone (green; dashed outline); whereby the boxed region is magnified in (E'-E'''). Non-mitotic ectopic glia (Repo^{+} pH3^{-}; white arrowhead) were found in this clone.

(F) Total number of ectopic glia (co-expressing GFP and Repo) in clones of the genotypes displayed in (D) and (E); n = 12 and 19, respectively. *p = 0.0108.

(G) Quantification of the GFP^{+} clonal volume (measured by GFP intensity) of genotypes from (D) and (E); n= 14 and 20 respectively. **p = 0.0021.

Data are presented as means ± SEM. p values were achieved by unpaired t test.

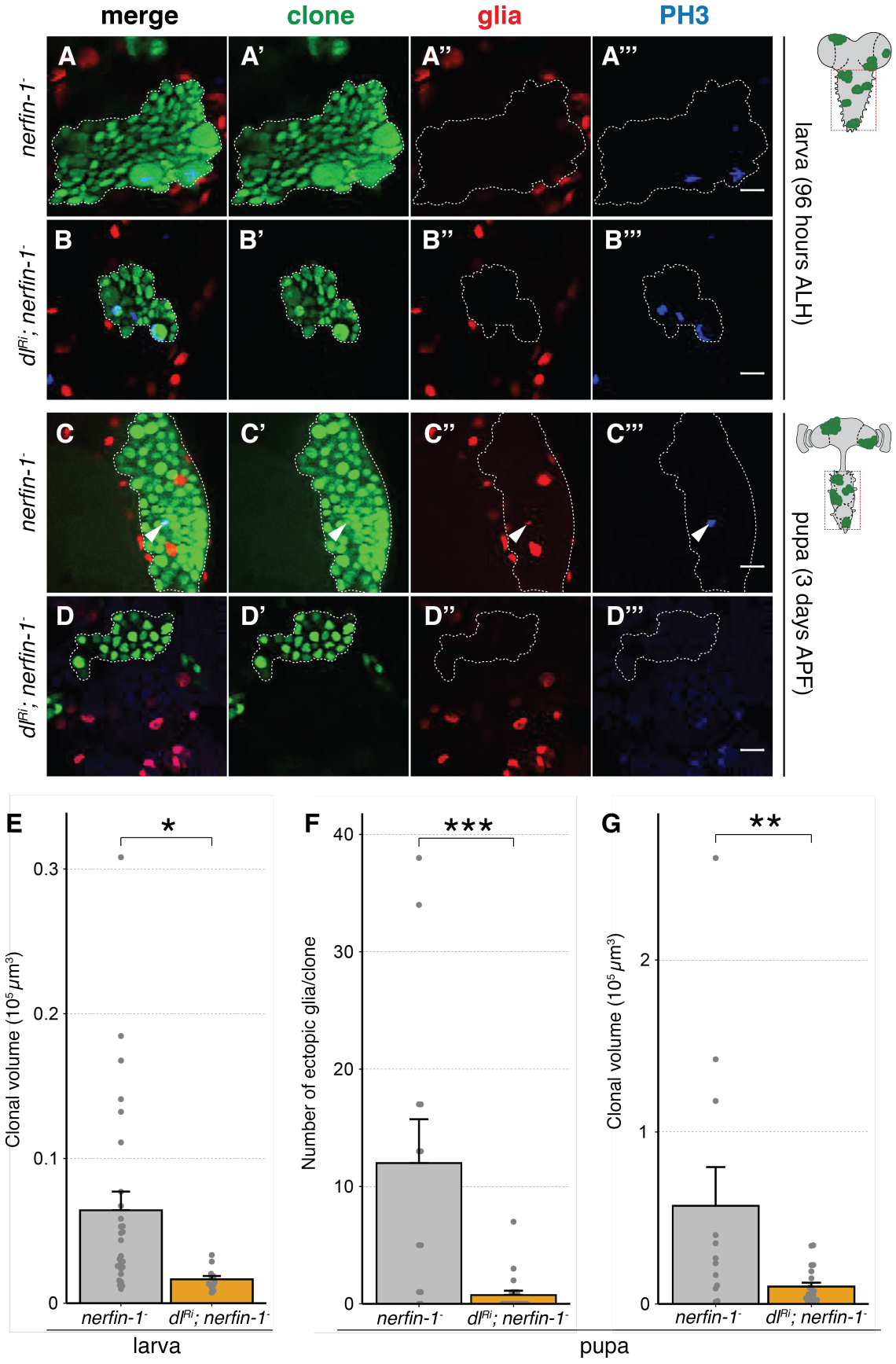
merge
clone
glia
PH3
A
A'
A''
A'''
B
B'
B''
B'''
C
C'
C''
C'''
D
D'
D''
D'''
nerfin-1-
dlRi; nerfin-1-
larva (96 hours ALH)
pupa (3 days APF)
E
F
G
*
***
**
Clonal volume (10^5 µm^3)
Number of ectopic glia/clone
0
0.1
0.2
0.3
10
20
30
40
1
2
nerfin-1-
dlRi; nerfin-1-
larva
pupa

Figure 3.32. Notch signalling promotes *nerfin-1*$^{-}$ clonal growth independently of ectopic glia formation.
MARCM clones were stained for GFP (clone; green; outlined by dashed white line), Repo (glia; red) and pH3 (mitotic cells; blue). Merged and single channels are shown. Clones are outlined by dashed white lines. Scale bars, 10 μm.

(A, B and E) Loss of Notch ligand Dl suppresses *nerfin-1*$^{-}$ MARCM clonal growth in larval VNC (120 hours AEL). Representative *nerfin-1*$^{-}$ MARCM clones (control; A-A') or dl^{RNAi}-expressing *nerfin-1*$^{-}$ MARCM clones [(dl^{RNAi}; *nerfin-1*$^{-}$); B-B'], in larval VNC. No ectopic glia were found in control nor dl^{RNAi}; *nerfin-1*$^{-}$ clones in larval VNC.

(C-D, F-G) Loss of Dl significantly suppresses *nerfin-1*$^{-}$ clonal volume in late pupal VNC (3 days APF).
(C-D) Representative *nerfin-1*$^{-}$ (control, C-C') or dl^{RNAi}; *nerfin-1*$^{-}$ MARCM clones (D-D'), in the pupal VNC. Ectopic glia have been formed in various VNC clones at this late pupal stages (C''; red; white arrowhead; 1 shown).

(E) Quantification of the GFP^{+} larval clonal volume (measured by GFP intensity) of clones from (A) and (B); n=28 and 12, respectively. *p = 0.021.

(F) Total number of ectopic glia (co-expressing GFP and Repo) in clones of the genotypes displayed in (C) and (D); n = 12 and 21, respectively. ***p = 0.0004.

(G) Quantification of the GFP^{+} pupal clonal volume of clones from (C) and (D); n= 12 and 21, respectively. **p = 0.0099.

Data are presented as means ± SEM. p values were achieved by unpaired t test.

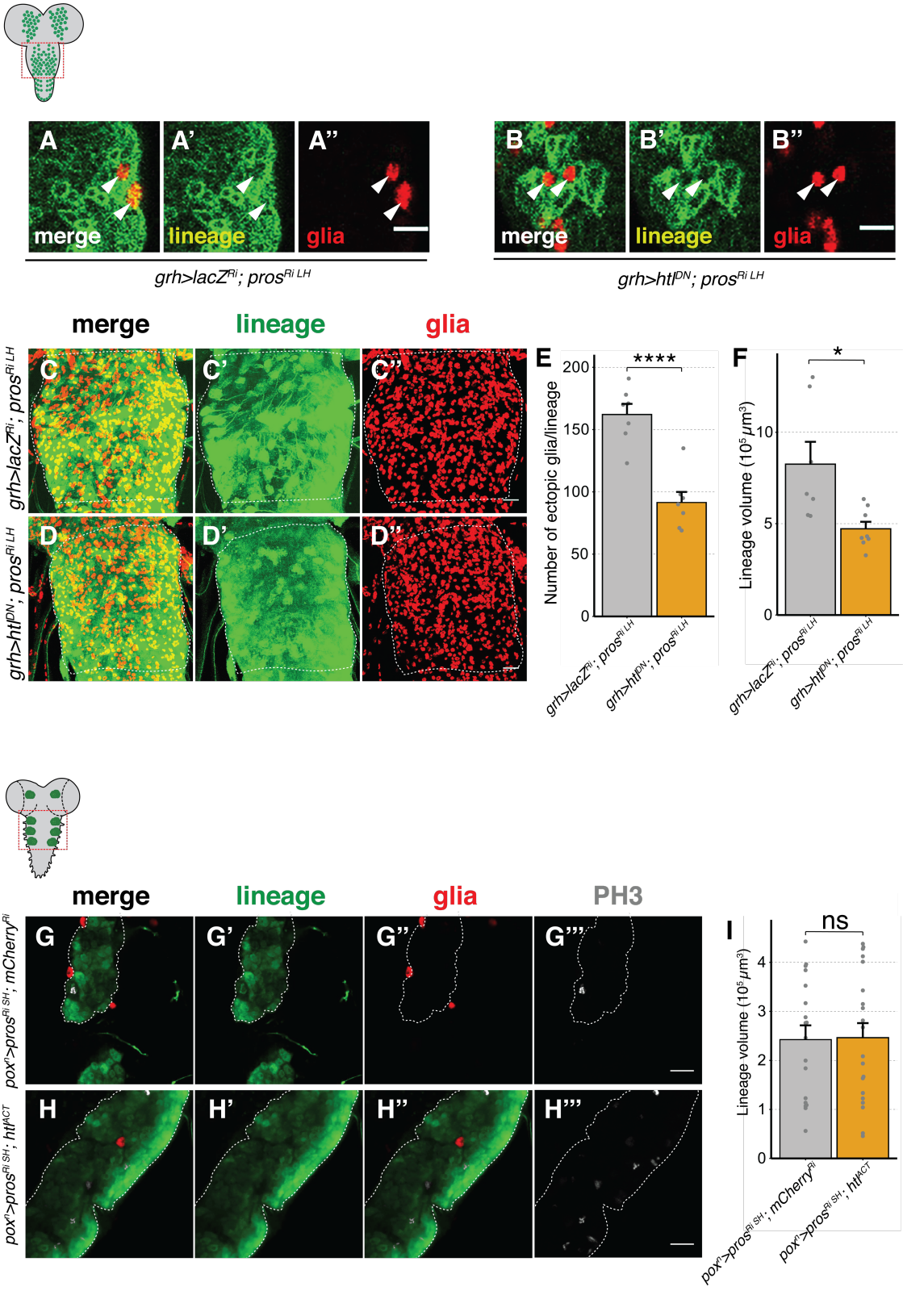
A
A'
A''
merge
lineage
glia
grh>lacZ^Ri; pros^Ri LH
B
B'
B''
merge
lineage
glia
grh>htl^DN; pros^Ri LH
merge
lineage
glia
C
C'
C''
D
D'
D''
grh>lacZ^Ri; pros^Ri LH
grh>htl^DN; pros^Ri LH
E
Number of ectopic glia/lineage
200
150
100
50
0
****
grh>lacZ^Ri; pros^Ri LH
grh>htl^DN; pros^Ri LH
F
Lineage volume (10^5 µm^3)
10
5
0
*
grh>lacZ^Ri; pros^Ri LH
grh>htl^DN; pros^Ri LH
merge
lineage
glia
PH3
G
G'
G''
G'''
H
H'
H''
H'''
pox^n>pros^Ri SH; mCherry^Ri
pox^n>pros^Ri SH; htl^ACT
I
Lineage volume (10^5 µm^3)
4
3
2
1
0
ns
pox^n>pros^Ri SH; mCherry^Ri
pox^n>pros^Ri SH; htl^ACT

Figure 3.33. FGF signalling pathway is required but not sufficient to induce the formation of ectopic glia in NB lineages lacking Pros.
L3 larval brains (120 hours AEL) of the indicated genotypes were immunostained with different antibody combinations. In (A-D''): RFP (lineages; false coloured as green) and Repo (glia; red). In (G-H'''): GFP (lineage; green), Repo (glia; red) and pH3 (mitotic cells; grey). Merged and single channels are shown. Scale bars, 20 μm in (C-D'') and 10 μm elsewhere.

(A-B'') Ectopic glia (white arrowhead) have been generated at early larval stages in lineages expressing $lacZ^{RNAi}$ plus $pros^{RNAi\ LH}$ (control; A-A') and lineages expressing htl^{DN} plus $pros^{RNAi\ LH}$ (B-B'). *Grh-Gal4* driver was used to induce the expression of membrane *RFP*, $lacZ^{RNAi}$ plus $pros^{RNAi\ LH}$ (control; A-A') or *RFP*, htl^{DN} plus $pros^{RNAi\ LH}$ (B-B') in the NB lineages of larval CNS.

(C-D'') Representative confocal images showing that $grh{>}pros^{RNAi\ LH}$ lineage volume is decreased upon dominant negative FGF receptor *htl* activity. The $pros^{RNAi\ LH}$-expressing lineages in thoracic segments of larval VNC are outlined with dashed lines, and are shown in high-magnification maximum-projection images (C-D''). Ectopic glia were observed in all regions of the lineages.

(E) Total number of ectopic glia (co-expessing RFP and Repo) in $grh{>}pros^{RNAi\ LH}$ lineages of the genotypes displayed in (A)-(B): control versus htl^{DN} plus $pros^{RNAi\ LH}$, ****p <0.0001. n = 7 and 7, respectively.

(F) Quantification of the RFP^+ lineage volume (measured by RFP intensity) located at the thoracic segments of brains from (C)-(D): control versus htl^{DN} plus $pros^{RNAi\ LH}$; n = 7 and 8, respectively. *p = 0.0119.

(G-H''') Representative confocal images showing that *htl* activation is not sufficient to induce the formation of ectopic glia in $pox^n > pros^{RNAi\ SH}$ lineages. pox^n *-Gal4* driver was used to induce the expression of *GFP*, $pros^{RNAi\ SH}$ plus $mCherry^{RNAi}$ (control; G-G') or *GFP*, $pros^{RNAi\ SH}$ plus htl^{ACT} (H-H'), in 6 NB lineages of larval VNC. Lineages are outlined by dashed white lines, and are shown in higher magnification. No ectopic glia (GFP^+ $Repo^+$) cells were found in control or $pox^n{>}pros^{RNAi\ SH}$*;* htl^{ACT} lineages.

(I) *htl* overexpression does not significantly alter the $pox^n{>}pros^{RNAi\ SH}$ lineage volume. Quantification of GFP^+ lineage volume (measured based on the total GFP intensity of tumour formed by 3 lineage clusters) of brains from (G)-(H): control versus $pros^{RNAi\ SH}$ plus htl^{ACT}, n = 18 and 20, respectively, p = 0.9290 (not significant; ns).

Data are presented as means ± SEM. p values were achieved by unpaired t test.

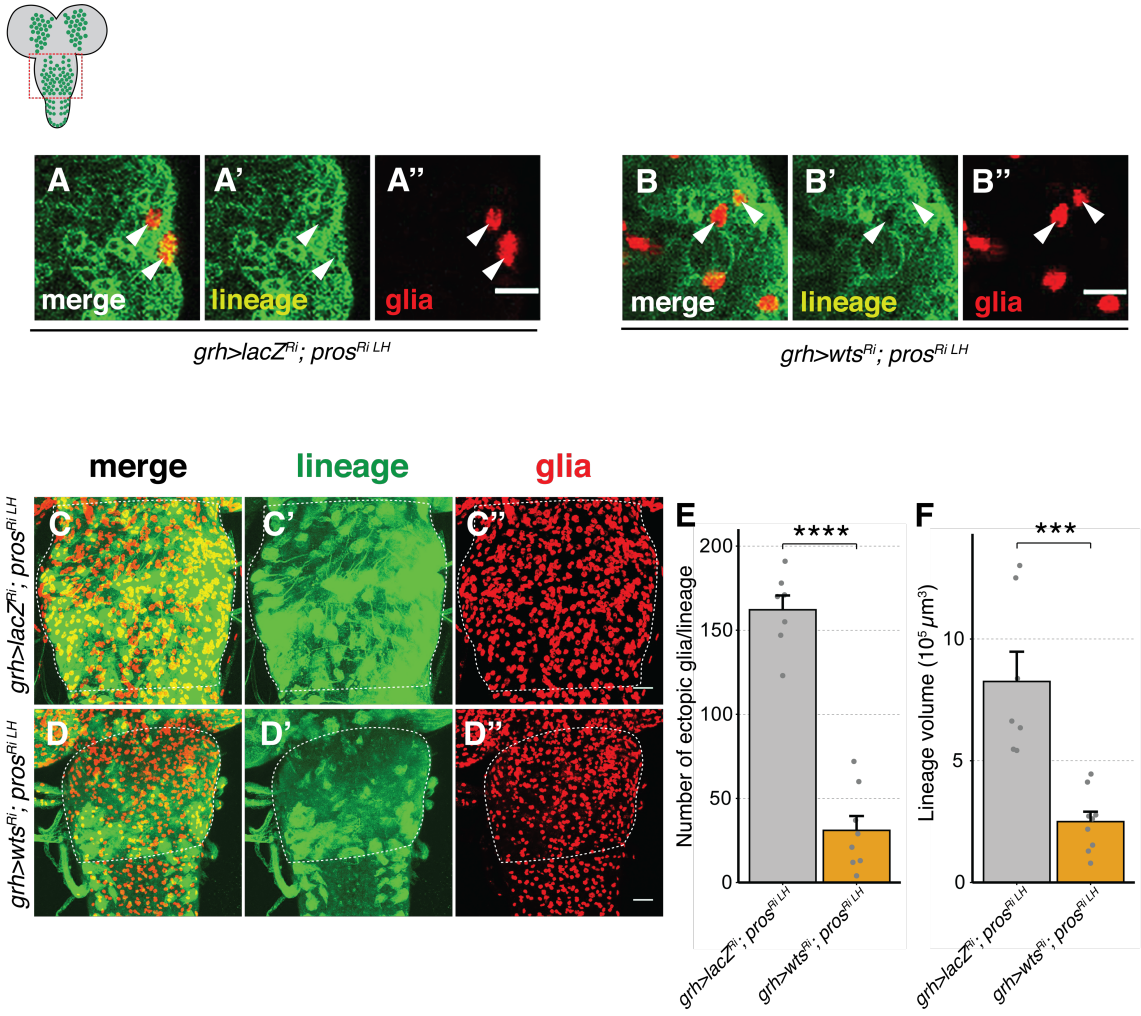

Figure 3.34. Hippo signalling pathway is required for the formation of ectopic glia and *grh>pros$^{RNAi\ LH}$* lineage growth.

L3 brains (120 hours AEL) of the indicated genotypes were immunostained with RFP (lineage; false coloured as green) and Repo (glia; red). Merged and single channels are shown. Scale bars, 10 μm in (A-B'') and 20 μm in (C-D'').

(A-B'') Ectopic glia (white arrowhead) have been generated at early larval stages in lineages expressing *lacZ^{RNAi}* plus *pros$^{RNAi\ LH}$* (control; A-A') and lineages expressing *wts^{RNAi}* plus *pros$^{RNAi\ LH}$* (B-B'). *Grh-Gal4* driver was used to induce the expression of membrane *RFP*, *lacZ^{RNAi}* plus *pros$^{RNAi\ LH}$* (control; A-A') or *RFP*, *wts^{RNAi}* plus *pros$^{RNAi\ LH}$* (B-B') in the NB lineages of larval CNS.

(C-D'') Representative confocal images showing that *grh>pros$^{RNAi\ LH}$* lineage volume is decreased upon *wts* kinase loss-of-function. The *pros$^{RNAi\ LH}$*-expressing lineages in thoracic segments of larval VNC are outlined with dashed lines, and are shown in high-magnification maximum-projection images (C-D''). Ectopic glia were observed in all regions of the lineages.

(E) Total number of ectopic glia (coexpessing RFP and Repo) in lineages expressing *lacZ*^{RNAi} plus *pros*$^{RNAi\ LH}$ (Control; A-A') and lineages expressing *wts*^{RNAi} plus *pros*$^{RNAi\ LH}$ (B-B'): n = 7 and 8, respectively; control versus *wts*^{RNAi} plus *pros*$^{RNAi\ LH}$, ****p <0.0001.

(F) Quantification of the RFP^{+} volume (measured by RFP intensity) of the lineages expressing *lacZ*^{RNAi} plus *pros*$^{RNAi\ LH}$ (Control; C-C') and lineages expressing *wts*^{RNAi} plus *pros*$^{RNAi\ LH}$ (D-D') located at the thoracic segments: n = 7 and 9, respectively; control versus *wts*^{RNAi} plus *pros*^{RNAi}, ***p = 0.0002.

Data are presented as means ± SEM. p values were achieved by unpaired t test.

Chapter 4

Discussion

In this study, we utilised *Drosophila* CNS tumour models to better understand CSC behaviours and transdifferentiation events that occur in human brain tumours, such as glioblastoma. While the cell-of-origin for glioblastoma is still controversial, recently some studies showed that glioblastoma can arise from neoplastic transformation of neurons, astrocyte glia or astrocyte-like NSCs (see **Chapter 1.2**). Various transdifferentiation events of GSCs have been reported in both glioblastoma cell lines and mouse models, and they all have implications in tumour malignant progression (see **Chapter 1.2**). However, the mechanisms underlying these events and their downstream functions are not well understood. In addition, transdifferentiation has never been studied in fly tumour models which offer simplicity and powerful genetic tools for dissecting multigene interaction and new gene functions. Here we investigated a new transdifferentiation phenotype in *Drosophila* CNS; whereby, Pros or Nerfin-1-deficient NBs convert into glial cells. In this work, we found that Pros or Nerfin-1-deficient NBs, in addition to displaying a high proliferative capacity, display type II-like NB characteristics and switch on glial cell fate.

We showed that temporal TF cascade, glial determinant genes, and FGF signalling pathway regulate the neuroblast-to-glia conversion, and subsequent ectopic glial formation within Pros-deficient lineages. We also demonstrated that the ectopic glial population is necessary to support the growth of lineages lacking Pros. By contrast, the Notch signalling pathway promotes Pros/Nerfin-1-deficient lineage growth independently of ectopic glia formation. We further showed that the ectopic glia might enhance the accumulation of lipid droplets in the niche surrounding *pros*$^{-}$ lineages; however, the significance of this observation and its link to the lineage growth of *pros*$^{-}$ tumours remain to be proved. Together, these findings identify a novel

transdifferentiation mechanism that might share some regulatory and cellular features with the GSC transdifferentiation in human glioblastoma multiforme.

4.1. Ectopic glia are found in dedifferentiation-driven tumours lacking Pros or Nerfin-1.

We discovered ectopic glia in type I *pros* and *nerfin-1*-null mutant clones and $pros^{RNAi}$-expressing lineages. In the adult VNC, type I NB lineages of these indicated genotypes were previously reported to contain proliferating ectopic adult NSCs (labelled by Dpn or Mira), and neurons (labelled by Chinmo or Elav) (Froldi et al., 2015b; Narbonne-Reveau et al., 2016; Shaw et al., 2018; Vissers et al., 2018). However, by using glial markers Repo, our study has identified a population of NSCs exhibit glial cell fate in those NB lineages lacking Pros or Nerfin-1 (see **Chapter 3.1**). In other words, in addition to the *wildtype* glial niche around the type I NB lineages, additional glia cells arise within the lineages upon loss of Pros or Nerfin-1.

By using the mitotic marker pH3, we found that a proportion of the ectopic glia cells are dividing. We quantified both the dividing and the non-dividing glia cells in our analysis in **Figure 3.4** and **3.5** (**Chapter 3.1**); however, it is likely that these are simply glia cells in different phases of the cell cycle. In the future, we should confirm this by assessing whether these cells are also cycling through S phase (DNA replication phase) of the cell cycle, by performing ethynyl deoxyuridine (EdU) incorporation (Hétié et al., 2014). If we also see a high level of EdU incorporation in the nuclei of ectopic glia, we can confidently conclude that the ectopic glia progress through the cell cycle. As $Repo^{+}$ glial precursors, which generate glia in *Drosophila* CNS, have been found to undergo apoptosis during development (Ren et al., 2018), we should also examine if the ectopic glia also undergo apoptosis by using TUNEL (terminal deoxynucleotidyl transferase dUTP nick end labelling)-staining (van den Ameele and Brand, 2019).

The emergence of ectopic glia was also detected in $pros^{RNAi}$-expressing lineages induced by NB-specific driver *grh-gal4* (see **Chapter 3.1**). Grh is expressed in all larval NBs and GMCs (Almeida and Bray, 2005; Cenci and Gould, 2005) to regulate NB

proliferation and to prevent NBs from premature cell-cycle exit (Cenci and Gould, 2005; Maurange et al., 2008). In accordance with the Grh-reporter expression pattern (Chell and Brand, 2010), we observed persistent *grh>RFP^{nls}* expression in type I NSC lineages throughout larval stages (see **Chapter 3.1**). Therefore, *grh-gal4* driver can induce NSC-specific *pros* knockdown for targeted dedifferentiation phenotype and amplification of progenitor cells.

We have demonstrated that *pros* knockdown in type I NB lineages using independent *pros^{RNAi}* lines induced ectopic glia (see **Chapter 3.1**). The *pros$^{RNAi\ SH}$* line, which causes tumour growth at 18°C and lethality at 25°C, is stronger than the *pros$^{RNAi\ LH}$* line, which allows the tumour-bearing flies to survive to adult stages even at 29°C. *pros* knockdown by *pros$^{RNAi\ SH}$* line caused dedifferentiation and supernumerary NBs, resulting tumour formation. The weaker line *pros$^{RNAi\ LH}$* induces moderate *pros* knockdown, as it both induces ectopic NB formation and allows neuronal differentiation (Shaw et al., 2018). From the study conducted by Shaw et al. (2018), weak pros attenuation allows neuronal differentiation while stronger pros depletion results in GMC dedifferentiation into NSC-like cells. They saw more NSCs in *engrailed* (*en*) lineages expressing *pros$^{RNAi\ LH}$* than the control *en>GFP* at larval and pupal stages (Shaw et al., 2018). We similarly observed ectopic NSCs (labelled by Mira) in every larval *grh>pros$^{RNAi\ LH}$*-expressing lineage, compared to control *grh>RFP^{nls}* lineages. In addition, they also stated that the weak *pros* attenuation results in the expanded lineages and also the production of supernumerary neurons, consistent with our observations in **Chapter 3.1**. Therefore, the two *RNAi* lines against *pros* used in this study both cause the generation of ectopic NSCs and lineage expansion, that enable us to establish Pros loss-of-function tumours.

The novel and interesting finding of this study is that, in clones/lineages with different levels of Pros knockout/knockdown, from complete *pros* deletion (in *pros^{-}* clones) to strong and weak *pros* attenuation (by *pros^{RNAi}*), ectopic glia were always observed in type I lineages. It will be interesting to determine the threshold effect, defined by Pros levels, which allows the NSC to express Repo to become ectopic glia. The mammalian mouse Prox1 also controls the balance between NSC asymmetric division and neuronal differentiation (Kaltezioti et al., 2010). PROX1 mRNA levels have been found to be

downregulated in glioblastoma patient samples, and this was found to be associated with tumour evolution and intratumoural heterogeneity (Goudarzi et al., 2018). However, the emergence of glia cells upon PROX loss-of-function have not been reported elsewhere. Therefore, manipulating this balance could potentially lead to lineage expansion with amplified progenitors or neurons, and possibly the emergence of ectopic glia in the mammalian nervous system. If this similar rationale is found in vertebrates, we could use both *Drosophila* and mouse models to recapitulate human glioblastoma and to better elucidate transdifferentiation in this brain malignancy.

The ectopic glia phenotype was found in both clonal and *RNAi* mediated lineage specific *pros* knockdown models. In these two models, ectopic glia cells arose at earlier developmental stages in $pros^{RNAi}$-expressing lineages than in $pros^{-}$ clones (see **Chapter 3.1**). The *grh*>$pros^{RNAi}$ lineages, which were induced in the embryonic NBs [less than 24 hours AEL (Chell and Brand, 2010)], generate ectopic glia at larval stages (**Figure 3.11**). Whereas, $pros^{-}$ clones, which were heat-shock-induced at early larval stages (48 hours AEL), give rise to ectopic glia from early pupal stages (**Figure 3.11**). It is possible that, after being induced, tumours have to develop for a period of time to be able to generate ectopic glia. This is consistent with our finding that the expansion of ectopic glia population is correlated with overall tumour growth (see **Chapter 3.1**). A study conducted by Narbonne-Reveau et al. (2016) found that the time at which tumours are generated affects the tumour malignancy, as only the NBs born at early temporal window sustain the rapid tumour growth (Narbonne-Reveau et al., 2016). The time of clone induction has also been found to influence the tumourigenity of *pros* mutation in type I neural lineages (Shaw et al., 2018). Previous comparison between $pros^{-}$ clones and $pros^{RNAi}$-expressing lineages showed that only early clone induction (early L2 stage) causes ectopic proliferation (indicated by ectopic EdU^{+} and Dpn^{+} cells) in the adult VNC, similar to the effects of *en*>$pros^{RNAi}$ (Shaw et al., 2018). Whereas, $pros^{-}$ clones induced late in larval development (mid L3 stage) are fully differentiated and non-tumourigenic at adult stages. Regarding our study, apart from neural progenitor expansion and malignant susceptibility, the formation of ectopic glia also depends on the time of tumour induction. Future experiments could test this hypothesis by inducing

pros^{-} clones at different times, and then examining the timepoint at which ectopic glia arise.

4.2. Ectopic glia arise by transdifferentiation of NBs upon loss of Pros or Nerfin-1.

Complete loss of Pros has been shown to cause GMC dedifferentiation into ectopic NBs (Bayraktar et al., 2010; Bello et al., 2006; Choksi et al., 2006), but when attenuated, low levels of Pros allows neuronal differentiation to occur (Narbonne-Reveau et al., 2016; Shaw et al., 2018). Nevertheless, in addition to these cell fate conversions, our live-cell imaging of *pros*$^{-}$ neural lineages has revealed the transdifferentiation from ectopic NBs into ectopic glia (see **Chapter 3.2**). From the live-cell imaging of RFP-labelled clones, we found cells with NB size (greater than 10 μm) turned on glial cell marker Repo-GFP (GFP-inserted into the endogenous locus of Repo). The NB cell-of-origin for ectopic glia was confirmed by molecular marker analysis, in which we found *pros*$^{-}$ clones predominantly contain supernumerary NBs, and ectopic glia express NB markers (Mira and Dpn), but not neuronal markers (Elav). Therefore, our data suggest that ectopic NBs either (1) self-renew and produce a GMC, or (2) switch on glial cell fate. After NB converts into a glial cell, it can divide (see **Chapter 3.1**), or function as a glia niche to influence tumour growth, (see **Chapter 3.2**, **3.3** and next part of this **Chapter 4**). The formation of the ectopic glia might be important for the expansion of neural lineages during tumourigenesis, which is mentioned in the next part of this Discussion.

Our clonal live-cell imaging has demonstrated the transdifferentiation from NB to ectopic glia, however, whether these glia resume proliferation post-generation could not be studied in these live imaging experiments. Our recording period (5-10 hours) was only enough to capture the formation of ectopic glia, and provided no information about the mitotic ectopic glia found in fixed clonal analyses (see **Chapter 3.1**). It could be possible that ectopic glia are capable of self-renewal like NBs, which would account for the mitotic glial population. However, newly born ectopic glia are likely to regrow and undergo a maturation period before their first division, a similar process to that of INP maturation of over 6 hours after birth (Bowman et al., 2008; Homem et al., 2013; Walsh

and Doe, 2017). If this is true, then imaging the whole process from transdifferentiation to division in cultured live tissues would be difficult, as the culture period is limited.

The transdifferentiation of *pros*$^{-}$ NBs into ectopic glia in type I lineages, involved the switch of type I to type II NB fate (see **Chapter 3.2**), and presumably happens in three phases (1) GMC reverts into ectopic type I NB (dedifferentiation), (2) type I NB then adopts type II NB characteristics, and (3) the type II-like NB transdifferentiates into ectopic glia. Our analysis of cell lineage markers showed the presence of Ase^{-} NBs in *pros*-deficient type I lineages, which resemble NBs (Ase^{-} Pros^{-}) in type II lineages (Bayraktar et al., 2010; Bowman et al., 2008; Hakes and Brand, 2020). Since type II NBs can produce glial progeny (Bayraktar and Doe, 2013; Ren et al., 2018; Ren et al., 2017; Viktorin et al., 2011), it may be possible that these type II-like NBs can adopt gliogenic potential to switch to a glia cell fate.

The absence of Ase in the type II-like NBs, which become ectopic glia, could be due to Tll expression in these cells (see **Chapter 3.3**). Although we have not shown that the Tll^{+} cells are Ase^{-}, we have shown that Tll is ectopically expressed in ectopic glia, and the ectopic glia are Ase^{-}. Furthermore, Tll knockdown was sufficient to reduce ectopic glia number and tumour volume. Tll has recently been shown to repress *ase* which in turn promotes NSC fate in type II NB lineages (Hakes and Brand, 2020). We favour this idea over the other two mechanisms known to repress *ase* transcription. The first is repression via Pros (Choksi et al., 2006); however, this cannot be the case, because Pros is lost in these clones. The second mechanism is via Notch mediated repression (Bowman et al., 2008); however, we found Notch is active in most cells of *pros*$^{-}$ clones, and not specific to the type II-like NBs (or ectopic glia) (see **Figure 3.29**, **Chapter 3.3**). As Ase is not expressed in ectopic glia, its repression may be required to promote the cell fate conversion from NB to ectopic glia. By contrast, it is possible that Ase overexpression prevents type I NBs (Ase^{+}) from converting to a fate similar to type II NBs (Ase^{-}); or causes no differences in this conversion. To distinguish between these possibilities, we should manipulate the Ase expression in Pros-deficient NB lineages and assess its influences on ectopic glial formation.

Our analysis of cell identity in *nerfin-1*-deficient lineages also reveals that ectopic glia originate from NBs, however, this cell-fate transition needs to be verified by live-cell imaging. Unlike in *pros*$^{-}$ clones, Mira is only expressed in a subset of ectopic glia found in *nerfin-1*$^{-}$ clones, and this leads to four possible non-mutually exclusive scenarios (**Figure 4.1**): (1) *nerfin-1*$^{-}$ NBs (Mira^{+}) directly transdifferentiate into Mira^{+} ectopic glia, similar to the mechanism found in *pros*$^{-}$ NBs. (2) *nerfin-1*$^{-}$ NBs may not commit to the NB fate and switch off mature NB markers (such as Mira) upon expression of Repo. (3) Reverted cells, which arise via dedifferentiation of neurons, skip the mature NB state (Mira^{+}) to become an ectopic glia. (4) The *nerfin-1*$^{-}$ NBs may produce ectopic glia. A live-cell imaging of cultured NB lineages expressing *UAS-nerfin-1*^{RNAi} (to cause dedifferentiation) (Froldi et al., 2015b), Mira-mCherry (to identify NBs) (Ramat et al., 2017), and Repo-GFP (to mark Repo expression) would allow us to verify these scenarios.

We also found that ectopic glia do not originate from neurons as they are never Elav^{+} and Repo^{+} (see **Figure 3.18**, **Chapter 3.2**). However, the absence of Elav could also imply that neurons might have to completely lose Elav expression before switching on glial cell fate. Live-cell imaging of *nerfin-1*$^{-}$ clones [RFP-expressing *nerfin-1*$^{-}$ clones and GFP-tagged Repo (*repo-GFP; nerfin-1*$^{-}$)] would also shed a light on change in cell fate of neurons (identified by small size), and NBs (large size). Using this approach, we could precisely observe if neurons, or just NBs, turn on Repo, or *nerfin-1*$^{-}$ NBs produce ectopic glia in real time, and thereby, identify the cell-of-origin of ectopic glia in Nerfin-1 loss-of-function context. In addition, a live-cell imaging of control *wildtype* NB lineages is useful to visualise the asymmetric cell division and to confirm no ectopic glia are generated by the *wildtype* NBs.

4.3. Temporal patterning regulates the formation of ectopic glia.

We next explored the genetic and regulatory control mechanism by which NBs transform into ectopic glia while maintaining their stem cell-like properties, and its consequence for tumour growth. A set of TTFs, (Ey, Slp, D, Tll) are ectopically expressed in *pros*$^{-}$ NBs and may direct the NBs to switch to glial cell fate. These TTFs

are part of the temporal series expressed sequentially in *Drosophila* medulla NBs (Hth→Klu→Ey→Slp→D→Tll) (Li et al., 2013b; Suzuki et al., 2013).

Several components of the medulla temporal patterning might be recruited in Pros-deficient lineages of the VNC; and in turn, regulate the formation of ectopic glia. As cross-regulation is only found in temporal progression of the Ey-Slp-D-Tll sequence (Li et al., 2013b), we only focused on that part of the temporal series. We found that *pros*$^{-}$ NBs express these four TFs, and produced neural clusters of different sub-temporal identities (see **Chapter 3.3**).

While Ey expression is weaker as the NB ages, we detected both strong and weak Ey in *pros*$^{-}$ and in *wildtype* lineages of the VNC. This is consistent with the previous finding that *ey* is initially weakly expressed in the neuroepithelium and then upregulated by an unknown factor (Li et al., 2013b; Suzuki et al., 2016). Ey may be a potential player for the generation of ectopic glia in Pros loss-of-function context, because: (1) Ey and its mammalian homolog Pax6 are expressed in NBs/NSCs to autonomously regulate the production of glial cells (Sakurai and Osumi, 2008; Suzuki et al., 2016). (2) Ey/Pax6 induces the expression of *tll* and *gcm* to initiate gliogenesis in medulla NBs (Suzuki et al., 2016). A possible scenario is that Ey could cell-autonomously activate *tll* and *gcm* expression, which in turn produce glia cells in the *pros* loss-of-function context. Since weak Ey expression was previously found in old Tll^{+} NBs and occasionally in *gcm*$^{+}$ NBs (Suzuki et al., 2016), in the future we should analyse the expression patterns of these TTFs in greater detail. We should also manipulate *ey* expression to investigate if it specifically affects the expression of downstream TTFs (*D*, *tll* and *gcm*), and in turn, the number of ectopic glia.

We found ectopic Slp expression in *pros*$^{-}$ NBs lineages, but not in *wildtype* lineages. Although Slp was reportedly not involved in glial production and in Ey-induced *D* expression (Suzuki et al., 2016), we cannot exclude that Slp plays a role in the formation of ectopic glia in Pros-deficient lineages. A modulation of *slp* activity in *pros*$^{-}$ clones would allow us to study the functional significance of *slp* in the regulation of ectopic glial formation.

D and Tll are required for the formation of ectopic glia (evidence from *grh>pros*^{RNAi} lineages), and are expressed in ectopic glia (evidence from *pros*$^{-}$ clones) (see **Chapter 3.3**). This could explain why *pros*$^{-}$ NBs that become ectopic glia do not express Ase, as Tll may repress *ase* and promote type II NSC fate in these cells (Hakes and Brand, 2020). It is possible that D and Tll are sufficient to induce ectopic glial formation and therefore, it would be important to test if their overexpression in *pros*$^{-}$ clones would be sufficient to increase ectopic glia cells. While temporal inputs were previously known to govern the neuronal diversity, lineage cell number and timely termination of neurogenesis (Li et al., 2013a), we now show their requirements for Pros-deficient NBs to transdifferentiate into glia.

It is possible that Tll may induce the transformation of *pros*$^{-}$ NBs from type I to type II fate. Previous studies have found that temporal identity of progenitor cells controls the gliogenic potential of type II NBs lineages (Bayraktar and Doe, 2013; Ren et al., 2018; Ren et al., 2017; Syed et al., 2017). Recently, it was shown that loss of Tll derepresses Ase in type II NBs, and allows type II NB lineages to transform into type I lineages (Hakes and Brand, 2020). If this is the case, we would expect that *tll* knockdown in *pros*$^{-}$ type I lineages would maintain type I fate (Ase^{+}) in all NBs, and prevent type I NBs from adopting glial cell fate. By contrast, overexpression of Tll would downregulate *ase* and promote the transformation from type I to type II NBs (Hakes and Brand, 2020), thereby would result in more ectopic glia in *pros*$^{-}$ lineages. Consistent with this hypothesis, we found that inhibitions of *D*, *tll* and its target genes *gcm* all significantly reduce the number of ectopic glia and the growth of Pros-deficient lineages (see **Chapter 3.3**). However, our data could be interpreted in two ways: (1) these TTFs regulate lineage growth by mediating ectopic glial formation, or (2) these genes regulate ectopic glial formation and lineage growth by two independent mechanisms.

To distinguish between these possibilities, we should alter D or Tll expression at two different time points in *pros* loss-of-function clones. We would predict that (1) if the manipulation only affects the lineage growth after ectopic glia are formed (3 days APF), and causes no growth input in their absence (L3 stage), then the first possibility should

be the case. (2) Otherwise, D Tll and Gcm are required for both ectopic glial formation and tumour growth. Furthermore, if the second scenario holds true, we should assess if these factors are also required for temporal progression and if the progression of temporal series eventually leads to the formation of ectopic glia. This will be discussed in section **4.4**.

The mammalian homolog TLX has been found to exhibit highly conserved tumourigenic potential with Tll (Hakes and Brand, 2020), and are highly expressed in human glioblastoma (Park et al., 2010; Zou et al., 2012). Interestingly, the Ase homolog ASCL1 (Achaete-scute homolog 1) is reportedly downregulated in glioblastoma, as TLX and ASCL1 expressions are mutually exclusive (Hakes and Brand, 2020). Upregulation of TLX promotes the early formation of glioblastoma-like lesions in the mouse subventricular zone where the glioblastoma originate and high expression of TLX is originally found (Liu et al., 2010).

4.4. The glial determinant genes regulate the formation of ectopic glia, which in turn promote the growth of Pros-deficient lineages.

We found that glial determinant *gcm*, also a known downstream target of the TTFs (Li et al., 2013b), positively regulates the formation of ectopic glia, and the growth of Pros-deficient lineages. To prove that *gcm* controls lineage growth by forming ectopic glia, we should further show that *gcm* has no effects on the lineage growth when ectopic glia are absent (in larval *pros*$^{-}$ clones). In addition, we also have yet to find out if *gcm* is ectopically expressed in Pros-deficient lineages. This can be achieved by *gcm-RFP* (available from Bloomington stock center 38647) or Gcm antibody (if available). If our proposed mechanism is true, *gcm* will be likely expressed in Tll^{+} NBs which are also Repo^{+}, as *gcm* expression is initiated in Tll^{+} NBs and inherited by their Repo^{+} progeny (Li et al., 2013b; Suzuki et al., 2016). Two mammalian *gcm* homologs, called *gcm1* and *gcm2*, have been identified that share the conserved DNA-binding motif with the *Drosophila gcm* (Akiyama et al., 1996; Iwasaki, 2003; Schreiber et al., 1998). Mouse Gcm1 is expressed in a subset of developing brain cells to induce astrocyte glial cell fate and suppress neuronal cell fate, giving rise to a minor subpopulation of glial cells

(Iwasaki, 2003). Forced expression of Gcm1 induces astrocyte lineage cell formation at the expense of neuronal lineages (Iwasaki, 2003; Kim et al., 1998; Reifegerste et al., 1999), reminiscent of the *gcm*-mediated binary switch between neurons and glia (Akiyama et al., 1996; Cattenoz and Giangrande, 2013; Jones, 2005; Yuasa et al., 2003). The upregulation of Gcm1 in GSCs (Balbous et al., 2014) led us to speculate that Gcm1 would potentially promote the transdifferentiation of GSCs into ectopic glial precursors.

An important finding here is that pan glia transcription factor Repo controls the growth of Pros-deficient lineage through the activity of ectopic glia. In the absence of ectopic glia, Repo inhibition does not affect lineage growth (evidence from larval $pros^{-}$ clones). After ectopic glia cells arise, Repo then becomes required for $pros^{-}$ lineage growth (evidenced from pupal $pros^{-}$ clones and $grh>pros^{RNAi}$ lineages). Therefore, on one hand, Repo may ensure the formation of ectopic glia, and on the other hand it indirectly promotes the lineage growth through ectopic glia formation. Little is currently known about *repo* mammalian homologs and their activities. Another mammalian glia-specific gene, called *GFAP* (*glial fibrillary acidic protein*) that regulates astrocyte differentiation, is upregulated in GSCs, as compared to normal NSCs (Balbous et al., 2014). In addition, GSCs have showed multipotent potential to not only differentiate into neural cells like normal NSCs do, but also transdifferentiate into other unanticipated cell types, including endothelial cells and vascular mural-like cells (Deshors et al., 2019; Scully et al., 2012). We speculate that this GFAP upregulation and multipotent potential may be related to an uncharacterised transdifferentiation of GSCs into glial lineage cells in human glioblastoma.

Although we have shown the requirements of *gcm* and *repo* for the formation of ectopic glia, more functional studies are needed to confirm that ectopic glia actively promotes lineage growth. (1) The lineage growth response to *repo* downregulation led us to predict that overexpression of Repo would generate more ectopic glia to promote the growth of Pros-deficient lineages. (2) These findings also led to the question if overexpression of *gcm* or *repo* is sufficient to induce the formation of ectopic glia in $pox^{n}>pros^{RNAi}$ lineages that normally are incapable of generating ectopic glia.

4.5. Future directions on the temporal progression in Pros-deficient lineages.

We detected four TTFs in Pros-deficient lineages within the VNC that may contribute to the generation of ectopic glia, however, this general mechanism requires further investigation. (1) It remains to be experimentally determined whether these TTFs are part of medulla TTF cascade (Hth→Klu→Ey→Slp→D→Tll) or involved in a novel TTF cascade that is not yet characterised. (2) The regulatory mechanism upstream of Ey, and whether Ey performs different functions in the *wildtype* lineages and Pros-deficient lineages, remains to be demonstrated. (3) Is the temporal progression regulated by NB-intrinsic timer (like the embryonic VNC NB cascade that uses cell cycle progression) (Grosskortenhaus et al., 2005), or extrinsic cues (like the larval type II NBs that requires hormonal regulation) (Syed et al., 2017)?

As sequential expression and cross-regulation among these TTFs (Ey→Slp→D→Tll) have been previously reported in *wildtype* medulla NBs (Li et al., 2013b), we should address if this holds true in *pros*$^{-}$ NBs. It will be informative to (1) examine their expression patterns in *pros*$^{-}$ clones. We would predict that if Ey, Slp, D and Tll are sequentially expressed in Pros-deficient lineages, then we should observe these four consecutive NB layers of increasing ages, from Ey to Tll layers (Li et al., 2013b). In addition, (2) we can examined their expression in a single *pros*$^{-}$ clones in which NBs are at certain temporal window, the clones would contain NBs/GMCs of previous competence windows (Li et al., 2013b). This suggests that the NBs have transited from early to late identity during tumourigenesis. Lastly, (3) we can ablate their expressions specifically in Pros-deficient lineages, and determine the effects on the expression of preceding and following TFs within the cascade. We would predict that downregulation of each TF induced by targeted *RNAi* would block the temporal progression, and result in the absence of the next TFs, and expanded expression of preceding TFs (Li et al., 2013b). We should also test if misexpression of each TF in *pros*$^{-}$ clones is sufficient to activate the next TF and repress the previous one. If the progression of these TTFs exists in Pros loss-of-function context, it remains to be demonstrated whether these TTFs ultimately switch on *tll*, *gcm* and *repo*, as similarly described in *wildtype* medulla.

4.6. Implication of temporal patterning and glial determinant genes in the growth of Pros-deficient lineages and questions for future studies.

We propose a general mechanism that temporal TFs and glial determinant genes expressed in Pros-deficient lineages regulate the formation of ectopic glia (**Figure 6.2**). The TTF sequence in this context presumably ensures the conversion from type I to type II-like NBs and later to glial cells. In this manner, the late TTF Tll, ectopically expressed in a subset of *pros*$^{-}$ NBs, may repress Ase (to allow the switch from type I to type II-like NBs) and induce *gcm* expression (to initiate NB-to-glia transdifferentiation). The Tll^{+} Gcm^{+} cells then turn on Repo to become ectopic glia, which then promote the growth of Pros-deficient lineages. NB temporal progression has also been reported to regulate the growth of *pros*$^{-}$ tumours in the study conducted by Narbonne-Reveau et al. (2016). The early temporal TFs Chinmo, Imp (IGF-II mRNA-binding protein), and Lin-28 are co-expressed in early NBs to promote unlimited proliferative capacity of the NBs (Narbonne-Reveau et al., 2016). In addition, our Pros-deficient lineages (*pros*$^{-}$ clones and *pros*^{RNAi}-expressing lineages) may contain these unlimitedly proliferative NBs (Chinmo^{+} Imp^{+} and Lin-28^{+}) as they are induced before Chinmo, Imp and Lin-28 are silenced in early L3 (Narbonne-Reveau et al., 2016). There might be a relationship between these NBs and the NBs that become ectopic glia. It will be worthwhile to explore the integration between tumour malignant progression (regulated by Chinmo, Imp, Lin-28) and ectopic glial formation (regulated by D, Tll, Gcm, Repo).

The next intriguing question for future studies is why only a subset of *pros*$^{-}$ NBs transdifferentiate into ectopic glia while the others do not. This could be an interesting parallel to the intratumoural heterogeneity found in human brain cancers. In the *Drosophila* medulla, the temporal patterning regulates the timely cell-cycle exit of the NBs at the end of their life (Li et al., 2013b). The oldest Tll^{+} NBs switch to Gcm^{+} glioblasts, and upon Pros localisation to the nucleus, triggers a terminal differentiation event which generates two glial cells (*gcm*$^{+}$ Repo^{+}) (Li et al., 2013b). However, in the *pros* loss-of-function context, Tll^{+} NBs after becoming glioblasts do not exit the cell cycle while still expressing *gcm*. We would predict that the Gcm expressed in these precursor cells would induce the expression of its native target gene *repo* (Akiyama et

al., 1996), to promote the switch to glial cell fate. Single-cell RNA sequencing of *pros*$^{-}$ clones would provide insight into the gene expression profile of the NBs that switch to ectopic glial cells. We have successfully isolated ectopic glia, *wildtype* glia, and tumour cells in *pros*$^{-}$ clones by using clonal marker RFP, glial marker Repo-GFP, and fluorescence-activated cell sorting (FACS) technique in a trial experiment, and will try to embark on this approach at a later date.

4.7. Notch signalling regulates the growth of Pros-deficient lineages independently of ectopic glia.

We have shown that ectopic glial cells are generated via transdifferentiation, and function in Pros-deficient NB lineages to promote lineage growth. In addition, we have identified three signalling pathways that may contribute to the formation of ectopic glia: Notch, FGF and Hippo. Here we discuss the roles of these pathways play on ectopic glial formation, and address whether they use this mechanism to promote lineage growth.

Notch signalling has been shown to promote stem cell growth, cell fate (Song and Lu, 2011) and NB self-renewal (San-Juán and Baonza, 2011) in *wildtype* lineages. Notch is also known to regulate the glial production in type II lineages (Gaiano and Fishell, 2002; Ren et al., 2018), and to activate *gcm* expression to specify a subclass of glia in embryonic CNS (Udolph et al., 2001; Umesono et al., 2002). In the vertebrate CNS, Notch promotes the differentiation of most glial subtypes other than oligodendrocytes (Bazzoni and Bentivegna, 2019; Hojo et al., 2000; Morrison et al., 2000; Pierfelice et al., 2011; Satow et al., 2001). In disease context, Notch signalling is activated in primary glioblastoma where the ASCL1/Ase is downregulated (Bazzoni and Bentivegna, 2019; Somasundaram et al., 2005), to supress differentiation and maintain stem cell self-renewal (Bazzoni and Bentivegna, 2019). Our data shows that Notch is both necessary and sufficient for dedifferentiation from GMC to NBs (lineage growth), which in turn causes a higher conversion rate of NBs to ectopic glia (data from larval *pros*$^{-}$ clones, *nerfin-1*$^{-}$ clones, and *pox*^{n}>*pros*^{RNAi} lineages, **Chapter 3.3**). This is consistent with our finding that Notch is required for lineage size control but is not

sufficient to induce the formation of ectopic glia (data from *grh>pros*^{RNAi} lineages and *pox*^{n}*>pros*^{RNAi} lineages, respectively). The similar upregulation of Notch signalling (also indicated by increased levels of NICD), and its role in governing NSC self-renewal was previously reported in *brat*^{RNAi}-expressing brain tumours (Mukherjee et al., 2016).

4.8. FGF signalling pathway regulates the formation of ectopic glia, which in turn promote the growth of Pros-deficient lineages.

FGF signalling has been identified to govern the differentiation and proliferation of surface and cortex glia in *Drosophila* (Avet-Rochex et al., 2012). This pathway was found to promote the growth of glioblastoma and, therefore, is a novel therapeutic target for cancer treatment (Auguste et al., 2001; Cuevas et al., 2011; Feng et al., 2011; Loilome et al., 2009). The ligand FGF-2, which can activate all the receptors FGFR1-4, stimulates the proliferation of glioblastoma cells (Loilome et al., 2009), and support endothelial cells to strengthen the blood brain barrier for angiogenesis (Toyoda et al., 2013). It is possible that the FGF pathway also modulates the growth of glioblastoma by stimulating a transdifferentiation mechanism similar to NB-to-glia conversion. Our results demonstrate that inhibition of FGF signalling could simultaneously reduce the ectopic glial number and the growth of lineages lacking Pros. However, there are two possible interpretations: FGF signalling could promote the growth of Pros-deficient lineages (1) by regulating the formation of ectopic glia, or (2) by controlling NSC proliferation and therefore only indirectly inducing an increase in ectopic glial number. By using *pox*^{n}*>pros*$^{RNAi\ SH}$ lineages that do not produce ectopic glia, we concluded that activation of FGF signalling alone is not sufficient to induce the formation of ectopic glia; however, we cannot exclude the possibility that *pox*^{n} lineages might not be competent to generate ectopic glia. Further comprehensive studies are needed to obtain a better understanding of the mechanism by which FGF signalling regulate Pros-deficient NB lineage growth in *Drosophila*, and in human glioblastoma.

4.9. Hippo signalling pathway may be implicated in the formation of ectopic glia.

We found that Hippo pathway is required for both ectopic glial formation and the growth of Pros-deficient lineages. However, again, we cannot distinguish whether the pathway promotes lineage growth by (1) regulating ectopic glial formation directly, or (2) by controlling NSC proliferation only. The Hippo pathway has been reported to control glial proliferation in L3 CB (Reddy and Irvine, 2011), and restrict the NSC proliferation in larval type I lineages (Poon et al., 2016). We observed a reduction in the volume of *grh>pros*^{RNAi} type I lineages when Hippo pathway activity was deregulated by *UAS-wts*^{RNAi}. However, this result contradicts previous findings (Poon et al., 2016), in which deregulation of Hippo signalling; by downregulation of *wts*, or gain-of-function of Yki (a key effector of growth control); increased type I NB lineage growth. Therefore, this phenotype induced by depleting *wts* should be confirmed by assessing the effect of Yki gain-of-function expression [*yki*^{S168A} (Poon et al., 2016)] in *pros*^{RNAi}-expressing lineages. In fact, the Hippo pathway activity in these lineages can be quickly surveyed by using endogenously tagged *hippo* allele or Yki antibody (Poon et al., 2016). It would be expected that these key component proteins are expressed in the Pros-deficient lineages and also present in ectopic glia. The Hippo/YAP signalling is known to be dysregulated and inactivated in human glioma development (Ji et al., 2020), as the mRNA and protein levels of YAP1/TAZ are amplified in glioma (Zhang et al., 2016). Our study may suggest that ectopic glia may also be involved in the Hippo-dependent tumour progression.

4.10. Implication of ectopic glia generated by NB transdifferentiation in promoting Pros-deficient lineage growth.

We found the role of ectopic glia in promoting the growth of Pros-deficient lineages, a model for brain tumours. Since the mammalian orthologues of the genes involved in the formation of ectopic glia are overexpressed (such as tll/ TLX, Gcm1, Notch, FGF-2) or deregulated (such as ase/ASCL1) in glioblastoma, the transdifferentiation of GSCs into glial lineages to support tumour malignancy may be a conserved feature of glioblastoma formation. In human glioblastoma, GSCs are commonly known to transdifferentiate into tumour cells that display genetic features of both neural lineages and another distinct lineages (Deshors et al., 2019; Scully et al., 2012). Most of these transdifferentiation

events are necessary to promote tumour development. GSCs transdifferentiate into endothelial cells to support angiogenesis (Dong et al., 2011; Ricci-Vitiani et al., 2010; Wang et al., 2010), or into mural like and smooth muscle-like cells to mediate vasculature formation (Scully et al., 2012). Transdifferentiation involving neural progenitor to glia cell fate change has not previously been reported in *Drosophila*. A cellular conversion from stromal hub cells into ectopic stem cell niches has been previously reported in *Drosophila* testis, upon forced expression of Cyclin D in the hub (Hétié et al., 2014).

In our study, we further noticed the accumulation of lipid droplets in the *pros*$^{-}$ mutant clones, and especially near the ectopic glia. These observations led us to speculate that these lipid droplets are accumulated by ectopic glia to promote mutant lineage growth. This model is supported by the previous finding that the glia niche accumulate lipid droplets to sustain NB proliferation during oxidative stress (Bailey et al., 2015) and nutrient restriction (Cheng et al., 2011). The high demand for energy and biomass forces tumour cells to rely on oxidative phosphorylation, which also triggers oxidative stress to cellular processes (Birsoy et al., 2015; Chandel, 2014; van den Ameele and Brand, 2019). As a result, antioxidant organelles called lipid droplets are formed in niche glia to protect NBs from cellular damage due to peroxidation chain reactions (Bailey et al., 2015). It would be possible that ectopic glia function in a similar way to allow *pros*$^{-}$ NBs overcome oxidative stress and continue dividing during tumourigenesis.

However, more quantitative evidence and functional analyses are needed to support this model. Although lipid droplets are only found in *pros*$^{-}$ clones, and not in *wildtype* clones, their amount in *pros*$^{-}$ clones, and near the ectopic glia should be quantified. To test if ectopic glia is required for the lipid droplet accumulation, we should modulate the ectopic glial number in *pros*$^{-}$ clones (by manipulating *repo* expression levels). Next, we can investigate if the key proteins that are required for the biosynthesis of lipid droplets, such as Lsd2 (Bailey et al., 2015), are specifically upregulated in ectopic glia. To distinguish the specific requirements of lipid droplets formed in ectopic glia for the clonal growth, we should ablate their production (by manipulating the Lsd2 expression)

and assess clonal growth. In addition, more studies are needed to investigate the sensitivities and responses of ectopic glial lipid droplets to the levels of oxidative stress. In human, lipid droplets highly accumulate in glioblastoma tissues and are undetectable in normal brain tissues (Geng et al., 2016; Taïb et al., 2019). They are found to be involved in various hallmarks of cancer, including energy supply and tumour metabolism (Cruz et al., 2020); however, the complex relationship between these organelles and tumour development remains to be further uncovered. Our finding led us to speculate that tumour cells could transdifferentiate to ectopic glia to accumulate lipid droplets to overcome their oxidative stress. Since lipid droplets are becoming potential targets for glioblastoma treatment (Geng and Guo, 2017); the ectopic glia model presented in this study could represent a useful system to further investigate the origin and functions of these organelles.

4.11. Final conclusions

In summary, we used several established *Drosophila* brain tumour models to study how CSCs undergo transdifferentaition. To generate tumours for this study, we induced dedifferentiation in NB lineages by attenuating differentiation-promoting transcription factors *pros* or *nerfin-1*. We have examined the cell-type composition of these tumours and discovered a population of NBs that transdifferentiate into glia. Previous studies in of these *Drosophila* cancer models have only revealed that dedifferentiation of neurons or GMCs can give rise to NSCs, upon the loss of Pros or Nerfin-1. Our findings suggest a previously uncharacterised cell fate choice of NSCs in $pros^-$ and $nerfin\text{-}1^-$ tumours. We show that $pros^-$ or $nerfin\text{-}1^-$ NBs can both self-renew to generate more tumour cells or transdifferentiate into ectopic glia during tumour progression.

We found that the ectopic glia that arise in type I neural tumours exhibit type II-like NB characteristics, suggesting that NBs in type I lineages that give rise to ectopic glia may do so by switching to a type II-like NB cell fate. Our data present evidence that ectopic NBs from $pros^-$ tumours have the capacity to express temporal TFs. Similar to the medulla NBs that generate glia in the Tll^+ window, we found some $pros^-$ tumour cells express both Tll and glial marker Repo. Furthermore, we found that the TFs *D* and *tll*,

and their target gene *gcm* and *repo* are all required for the formation of ectopic glia, as depletion of each gene by *RNAi* reduces ectopic glial number and tumour size, although further experiments are required to uncouple whether these temporal factors are needed for tumour growth in general or specifically required for ectopic glia formation. Therefore, ectopic NBs within *pros*$^{-}$ tumours seem to have acquired a temporal input that allows them to convert into glia during tumour progression. Our evidence suggests that the ectopic glia in turn promote the tumour growth after being generated. We made the interesting observation that ectopic glia might accumulate lipid droplets to sustain tumour growth; however, more work needs to be carried out to better characterise this.

In our study, we also assessed whether Notch, FGF and Hippo signalling pathways regulate the formation of ectopic glia and coordinate this phenotype with the tumour growth. We have shown that Notch promotes tumour growth independently of its effect on ectopic glial formation, as Notch regulates the tumour growth in the absence of ectopic glia. Notch signalling presumably promotes stem cell growth and NB self-renewal involved in tumour lineage growth. By contrast, FGF signalling pathway promotes tumour growth by regulating ectopic glial formation, as it does not affect the tumour growth in the absence of ectopic glia. Hippo pathway that controls cell proliferation and stem cell self-renewal across may tissues and in cancers, also play a role in promoting the formation of ectopic glia and tumour growth. It is possible that these pathways contribute to the formation of ectopic glia in a non-redundant fashion, but whether they require ectopic glia to promote the tumour growth remains to be elucidated. More work needs to be done to validate our findings on the mechanisms responsible for this NB-to-glia transdifferentiation.

Our study of *pros*$^{-}$ and *nerfin-1*$^{-}$ tumour models extend our understanding of the biology of NBs and may shed light on GSC behaviours upon their transdifferentiation into different cell types. We can use the underlying mechanism of these phenotypes to explain the transdifferentiation events at the molecular and cellular levels. As most genes and signalling pathways examined in this study are also found in human brain cancers, this study will enhance the knowledge of how cell fate changes can influence the tumour malignancy.

A.

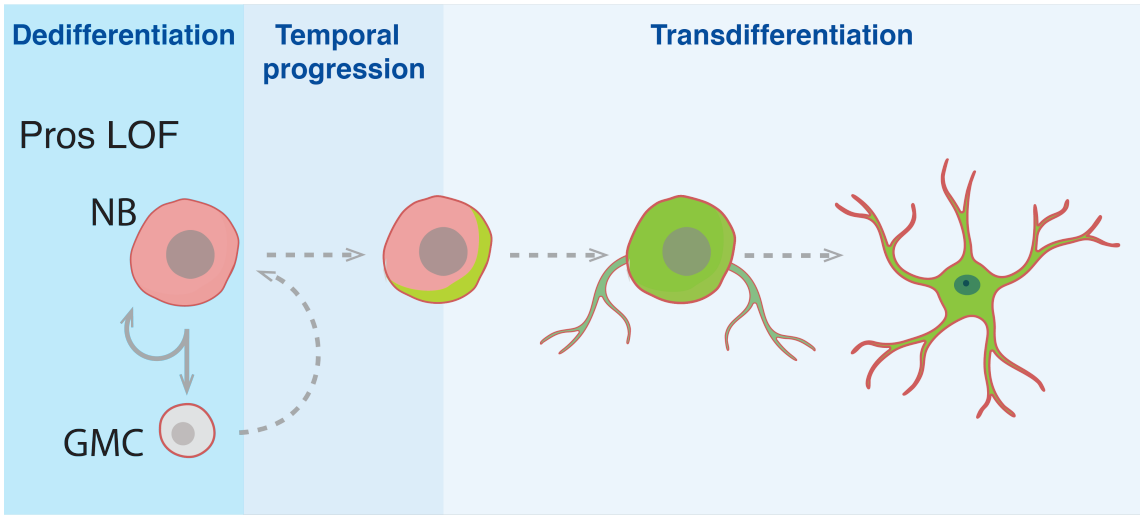
Dedifferentiation
Temporal progression
Transdifferentiation
Pros LOF
NB
GMC

B.

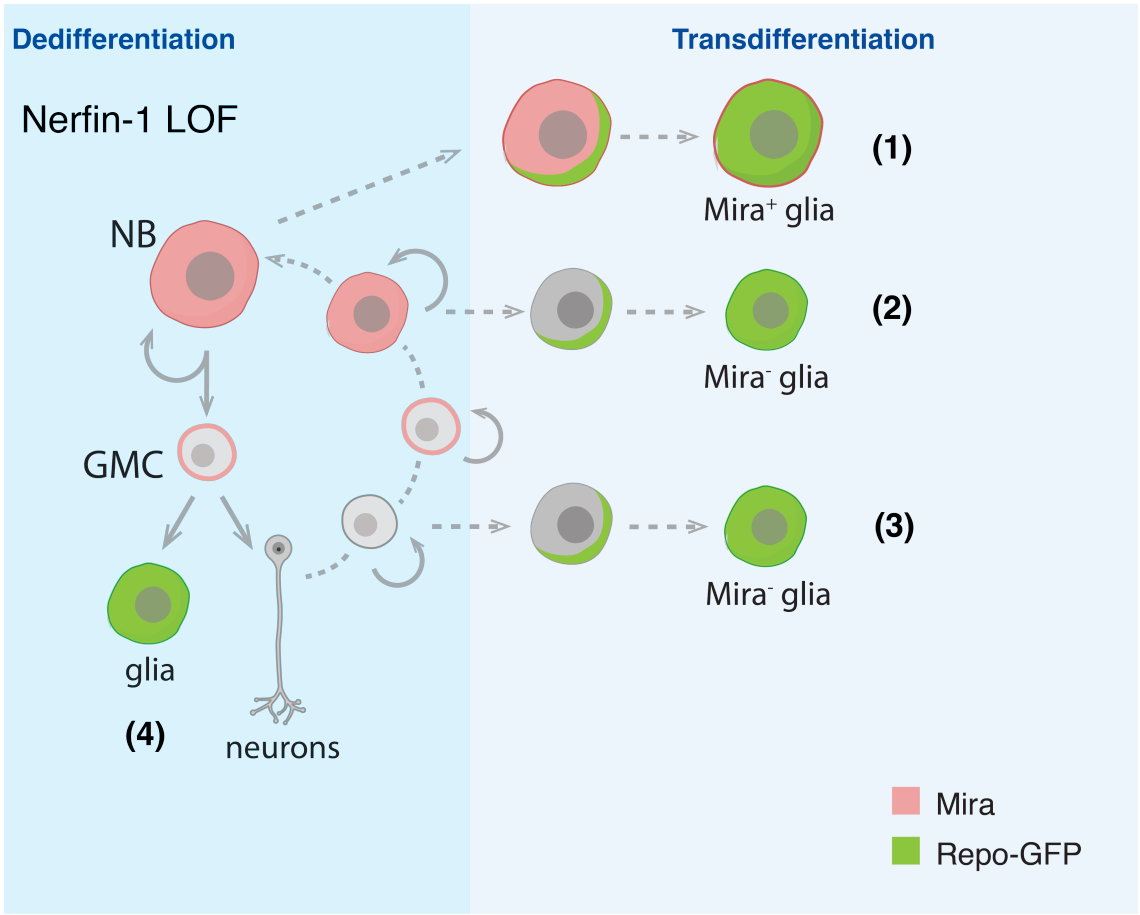
Dedifferentiation
Transdifferentiation
Nerfin-1 LOF
NB
GMC
glia
(4)
neurons
Mira+ glia
(1)
Mira- glia
(2)
Mira- glia
(3)
Mira
Repo-GFP

Figure 4.1. Hypothetical models for the transdifferentiation of NBs into ectopic glia upon loss of Pros or Nerfin-1.

(A) Upon Pros loss-of-function, NBs transdifferentiate into ectopic glia that coexpress Mira and Repo.

(B) Upon Nerfin-1 loss-of-function, NBs give rise to ectopic glia through four hypothetical routes: (1) *nerfin-1*$^{-}$ NBs (Mira^{+}) directly transdifferentiate into Mira^{+} ectopic glia; (2) *nerfin-1*$^{-}$ NBs may not committed to its fate and switch off mature NB marker Mira upon expression of Repo; (3) reverted cells, which arise via dedifferentiation of neurons, skip the mature NB state (Mira^{+}) to become an ectopic glia; *nerfin-1*$^{-}$ NBs may produce ectopic glia that are not positive for Mira.

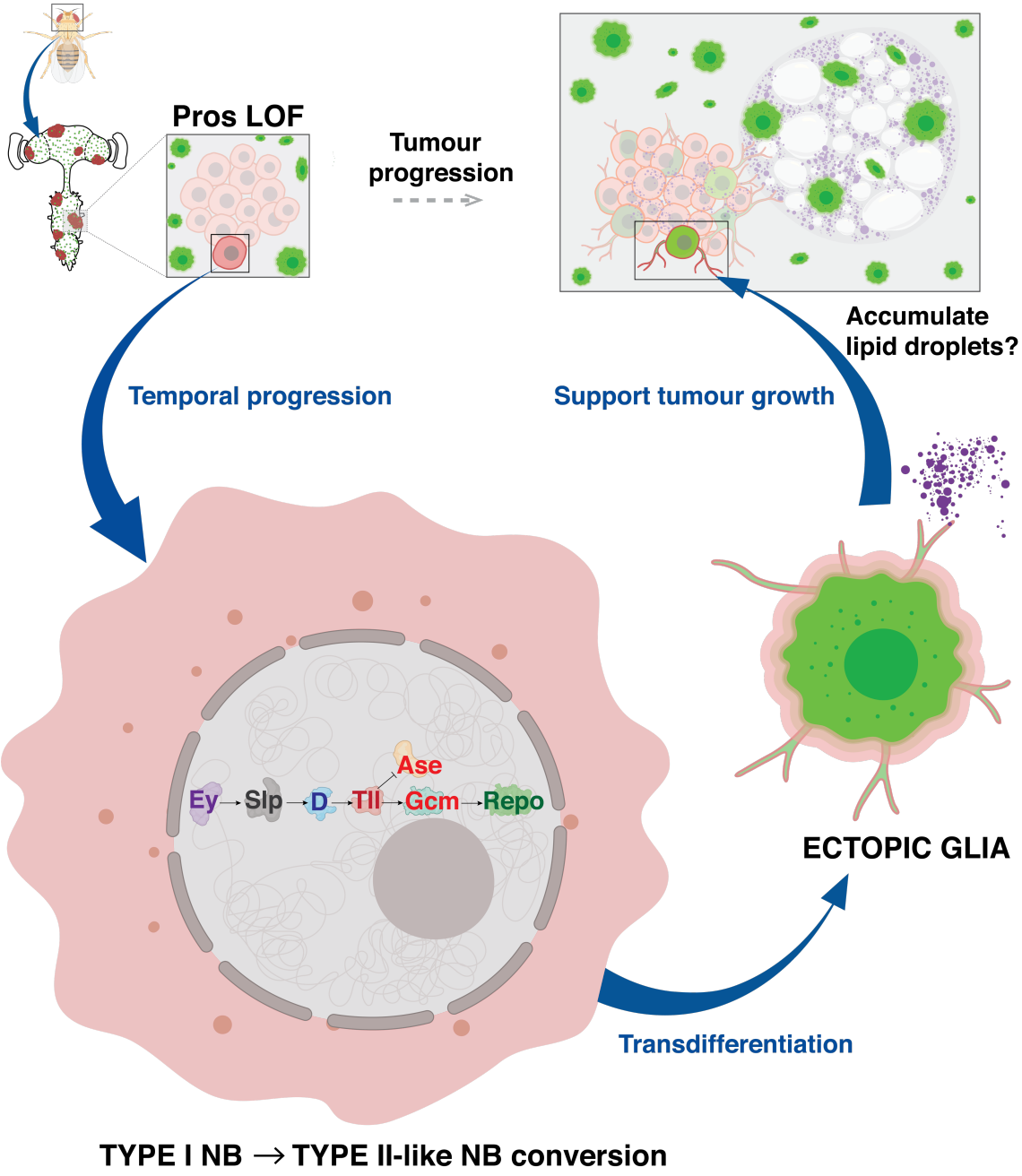
Pros LOF
Tumour progression
Accumulate lipid droplets?
Temporal progression
Support tumour growth
Ey
Slp
D
Tll
Ase
Gcm
Repo
ECTOPIC GLIA
Transdifferentiation
TYPE I NB → TYPE II-like NB conversion

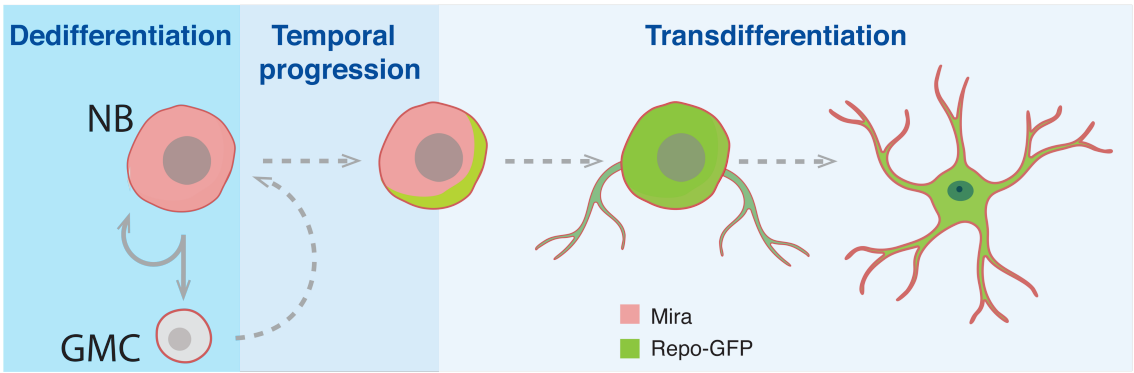
Dedifferentiation
Temporal progression
Transdifferentiation
NB
GMC
Mira
Repo-GFP

Figure 4.2. Hypothetical mechanism by which *pros*$^{-}$ NBs transdifferentiate into ectopic glia to promote the tumour growth.
The TTFs (Ey, Slp, D and Tll) expressed in *pros*$^{-}$ NB repress Ase to allow the transition from type I to type II-like NB fate. Tll then induces the expression of *gcm* to activate Repo, and subsequently initiate NB-to-glia conversion. Upon Repo expression, the ectopic glial cells form, and thereby promote the *pros*$^{-}$ tumour growth. Lipid droplets are highly enriched in *pros*$^{-}$ tumours and near the ectopic glia, but are absent in the *wildtype* NB lineage. Based on this observation, we predict that ectopic glia may accumulate lipid droplets to promote the tumour growth.

References

Adachi, Y., Hauck, B., Clements, J., Kawauchi, H., Kurusu, M., Totani, Y., Kang, Y.Y., Eggert, T., Walldorf, U., Furukubo-Tokunaga, K.*, et al.* (2003). Conserved cis-regulatory modules mediate complex neural expression patterns of the eyeless gene in the *Drosophila* brain. Mechanisms of Development *120*, 1113-1126.

Akalal, D.-B.G., Wilson, C.F., Zong, L., Tanaka, N.K., Ito, K., and Davis, R.L. (2006). Roles for *Drosophila* mushroom body neurons in olfactory learning and memory. Learn Mem *13*, 659-668.

Akiyama, Y., Hosoya, T., Poole, A.M., and Hotta, Y. (1996). The gcm-motif: a novel DNA-binding motif conserved in *Drosophila* and mammals. Proceedings of the National Academy of Sciences of the United States of America *93*, 14912-14916.

Akiyama-Oda, Y., Hosoya, T., and Hotta, Y. (1998). Alteration of cell fate by ectopic expression of *Drosophila* glial cells missing in non-neural cells. Dev Genes Evol *208*, 578-585.

Alamgeer, M., Peacock, C.D., Matsui, W., Ganju, V., and Watkins, D.N. (2013). Cancer stem cells in lung cancer: Evidence and controversies. Respirology *18*, 757-764.

Alcantara Llaguno, S., Chen, J., Kwon, C.-H., Jackson, E.L., Li, Y., Burns, D.K., Alvarez-Buylla, A., and Parada, L.F. (2009). Malignant astrocytomas originate from neural stem/progenitor cells in a somatic tumor suppressor mouse model. Cancer Cell *15*, 45-56.

Almeida, M.S., and Bray, S.J. (2005). Regulation of post-embryonic neuroblasts by Drosophila Grainyhead. Mechanisms of Development *122*, 1282-1293.

Altenhein, B. (2015). Glial cell progenitors in the *Drosophila* embryo. Glia *63*, 1291-1302.

Apitz, H., and Salecker, I. (2015). A region-specific neurogenesis mode requires migratory progenitors in the *Drosophila* visual system. Nature Neuroscience *18*, 46-55.

Arama, E., Dickman, D., Kimchie, Z., Shearn, A., and Lev, Z. (2000). Mutations in the beta-propeller domain of the *Drosophila* brain tumor (brat) protein induce neoplasm in the larval brain. Oncogene *19*, 3706-3716.

Artavanis-Tsakonas, S., Delidakis, C., and Fehon, R.G. (1991). The Notch locus and the cell biology of neuroblast segregation. Annual Review Cell Biology *7*, 427-452.

Auguste, P., Gursel, D.B., Lemiere, S., Reimers, D., Cuevas, P., Carceller, F., Di Santo, J.P., and Bikfalvi, A. (2001). Inhibition of Fibroblast growth factor/Fibroblast growth factor receptor activity in Glioma cells impedes tumor growth by both angiogenesis-dependent and -independent mechanisms (United States: Waverly Press INC), pp. 1717.

Avet-Rochex, A., Kaul, A.K., Gatt, A.P., McNeill, H., and Bateman, J.M. (2012). Concerted control of gliogenesis by InR/TOR and FGF signalling in the *Drosophila* post-embryonic brain. Development *139*, 2763-2772.

Awasaki, T., Lai, S.L., Ito, K., and Lee, T. (2008). Organization and postembryonic development of glial cells in the adult central brain of *Drosophila*. Journal of Neuroscience *28*, 13742-12753.

Bachoo, R.M., Maher, E.A., Ligon, K.L., Sharpless, N.E., Chan, S.S., You, M.J., Tang, Y., DeFrances, J., Stover, E., Weissleder, R.*, et al.* (2002). Epidermal growth factor receptor and *Ink4a/Arf* Convergent mechanisms governing terminal differentiation and transformation along the neural stem cell to astrocyte axis. Cancer Cell *1*, 269-277.

Bailey, A.P., Koster, G., Guillermier, C., Hirst, E.M.A., MacRae, J.I., Lechene, C.P., Postle, A.D., and Gould, A.P. (2015). Antioxidant role for lipid droplets in a stem cell niche of *Drosophila*. Cell *163*, 340-353.

Baisiwala, S., Auffinger, B., Caragher, S.P., Shireman, J.M., Ahsan, R., Lee, G., Hasan, T., Park, C., Saathoff, M.R., Christensen, A.C.*, et al.* (2019). Chemotherapeutic stress induces transdifferentiation of Glioblastoma cells to endothelial cells and promotes vascular mimicry. Stem Cells International *2019*, 6107456.

Balbous, A., Cortes, U., Guilloteau, K., Villalva, C., Flamant, S., Gaillard, A., Milin, S., Wager, M., Sorel, N., Guilhot, J.*, et al.* (2014). A mesenchymal glioma stem cell profile is related to clinical outcome. Oncogenesis *3*, e91-e91.

Banerjee, S., and Bhat, M.A. (2008). Glial ensheathment of peripheral axons in *Drosophila*. J Neurosci Res *86*, 1189-1198.

Baumgardt, M., Karlsson, D., Terriente, J., Díaz-Benjumea, F.J., and Thor, S. (2009). Neuronal subtype specification within a lineage by opposing temporal feed-forward loops. Cell *139*, 969-982.

Bayraktar, O.A., Boone, J.Q., Drummond, M.L., and Doe, C.Q. (2010). *Drosophila* type II neuroblast lineages keep Prospero levels low to generate large clones that contribute to the adult brain central complex. Neural Development *5*, 26.

Bayraktar, O.A., and Doe, C.Q. (2013). Combinatorial temporal patterning in progenitors expands neural diversity. Nature *498*, 449-455.

Bazzoni, R., and Bentivegna, A. (2019). Role of Notch signaling pathway in Glioblastoma pathogenesis. Cancers *11*, 292.

Beckervordersandforth, R.M., Rickert, C., Altenhein, B., and Technau, G.M. (2008). Subtypes of glial cells in the *Drosophila* embryonic ventral nerve cord as related to lineage and gene expression. Mechanisms of Development *125*, 542-557.

Bello, B., Reichert, H., and Hirth, F. (2006). The brain tumor gene negatively regulates neural progenitor cell proliferation in the larval central brain of *Drosophila*. Development *133*, 2639-2648.

Bello, B.C., Hirth, F., and Gould, A.P. (2003). A pulse of the *Drosophila* Hox protein Abdominal-A schedules the end of neural proliferation via neuroblast apoptosis. Neuron *37*, 209-219.

Bernardoni, R., Miller, A.A., and Giangrande, A. (1998). Glial differentiation does not require a neural ground state. Development *125*, 3189-3200.

Betschinger, J., Mechtler, K., and Knoblich, J.A. (2006). Asymmetric segregation of the tumor suppressor brat regulates self-renewal in *Drosophila* neural stem cells. Cell *124*, 1241-1253.

Birkholz, O., Rickert, C., Berger, C., Urbach, R., and Technau, G.M. (2013). Neuroblast pattern and identity in the *Drosophila* tail region and role of *doublesex* in the survival of sex-specific precursors. Development *140*, 1830.

Birsoy, K., Wang, T., Chen, W.W., Freinkman, E., Abu-Remaileh, M., and Sabatini, D.M. (2015). An essential role of the mitochondrial electron transport chain in cell proliferation is to enable Aspartate synthesis. Cell *162*, 540-551.

Bonnet, D., and Dick, J.E. (1997). Human acute myeloid leukemia is organized as a hierarchy that originates from a primitive hematopoietic cell. Nat Med *3*, 730-737.

Boone, J.Q., and Doe, C.Q. (2008). Identification of *Drosophila* type II neuroblast lineages containing transit amplifying ganglion mother cells. Developmental Neurobiology *68*, 1185-1195.

Bossing, T., Udolph, G., Doe, C.Q., and Technau, G.M. (1996). The embryonic central nervous system lineages of *Drosophila melanogaster*. I. Neuroblast lineages derived from the ventral half of the neuroectoderm. Dev Biol *179*, 41-64.

Boulay, J.L., Stiefel, U., Taylor, E., Dolder, B., Merlo, A., and Hirth, F. (2009). Loss of heterozygosity of TRIM3 in malignant gliomas. BMC Cancer *9*, 71-71.

Bowman, S.K., Rolland, V., Betschinger, J., Kinsey, K.A., Emery, G., and Knoblich, J.A. (2008). The tumor suppressors Brat and Numb regulate transit-amplifying neuroblast lineages in *Drosophila*. Developmental Cell *14*, 535-546.

Bozorgi, A., Khazaei, M., and Khazaei, M.R. (2015). New findings on breast cancer stem cells: A review. Journal of Breast Cancer *18*, 303-312.

Bradshaw, A., Wickremsekera, A., Tan, S., Peng, L., Davis, P., and Itinteang, T. (2016). Cancer stem cell hierarchy in glioblastoma multiforme. Frontiers in Surgery *3*.

Brand, A.H., and Livesey, F.J. (2011). Neural stem cell biology in vertebrates and invertebrates: more alike than different? Neuron *70*, 719-729.

Broadus, J., Fuerstenberg, S., and Doe, C.Q. (1998). Staufen-dependent localization of *prospero* mRNA contributes to neuroblast daughter-cell fate. Nature *391*, 792-795.

Brody, T., and Odenwald, W.F. (2000). Programmed transformations in neuroblast gene expression during *Drosophila* CNS lineage development. Developmental Biology *226*, 34-44.

Caldwell, M.C., and Datta, S. (1998). Expression of Cyclin E or DP/E2F rescues the G1 arrest of trol mutant neuroblasts in the *Drosophila* larval central nervous system. Mechanisms of Development *79*, 121-130.

Capaccione, K.M., and Pine, S.R. (2013). The Notch signaling pathway as a mediator of tumor survival. Carcinogenesis *34*, 1420-1430.

Carney, T.D., Miller, M.R., Robinson, K.J., Bayraktar, O.A., Osterhout, J.A., and Doe, C.Q. (2012). Functional genomics identifies neural stem cell sub-type expression profiles and genes regulating neuroblast homeostasis. Developmental Biology *361*, 137-146.

Carney, T.D., Struck, A.J., and Doe, C.Q. (2013). *midlife crisis* encodes a conserved zinc-finger protein required to maintain neuronal differentiation in *Drosophila*. Development *140*, 4155-4164.

Cattenoz, P.B., and Giangrande, A. (2013). Lineage specification in the fly nervous system and evolutionary implications. Cell Cycle (Georgetown, Tex) *12*, 2753-2759.

Caussinus, E., and Gonzalez, C. (2005). Induction of tumor growth by altered stem-cell asymmetric division in *Drosophila melanogaster*. Nature Genetics *37*, 1125-1129.

Cenci, C., and Gould, A.P. (2005). *Drosophila* Grainyhead specifies late programmes of neural proliferation by regulating the mitotic activity and Hox-dependent apoptosis of neuroblasts. Development (Cambridge, England) *132*, 3835-3845.

Chandel, N.S. (2014). Mitochondria as signaling organelles. BMC biology *12*, 34-34.

Chell, J.M., and Brand, A.H. (2010). Nutrition-responsive glia control exit of neural stem cells from quiescence. Cell *143*, 1161-1173.

Cheng, L.Y., Bailey, A.P., Leevers, S.J., Ragan, T.J., Driscoll, P.C., and Gould, A.P. (2011). Anaplastic lymphoma kinase spares organ growth during nutrient restriction in *Drosophila*. Cell *146*, 435-447.

Chia, W., Somers, W.G., and Wang, H. (2008). *Drosophila* neuroblast asymmetric divisions: cell cycle regulators, asymmetric protein localization, and tumorigenesis. The Journal of Cell Biology *180*, 267-272.

Choksi, S.P., Southall, T.D., Bossing, T., Edoff, K., de Wit, E., Fischer, B.E., van Steensel, B., Micklem, G., and Brand, A.H. (2006). Prospero acts as a binary switch between self-renewal and differentiation in *Drosophila* neural stem cells. Developmental Cell *11*, 775-789.

Cleary, M.D., and Doe, C.Q. (2006). Regulation of neuroblast competence: multiple temporal identity factors specify distinct neuronal fates within a single early competence window. Genes Dev *20*, 429-434.

Codony-Servat, J., Verlicchi, A., and Rosell, R. (2016). Cancer stem cells in small cell lung cancer. Translational Lung Cancer Research *5*, 16-25.

Couturier, L., Vodovar, N., and Schweisguth, F. (2012). Endocytosis by Numb breaks Notch symmetry at cytokinesis. Nature Cell Biology *14*, 131-139.

Cruz, A.L.S., Barreto, E.d.A., Fazolini, N.P.B., Viola, J.P.B., and Bozza, P.T. (2020). Lipid droplets: platforms with multiple functions in cancer hallmarks. Cell Death & Disease *11*, 105.

Cuevas, P., Carceller, F., Angulo, J., González-Corrochano, R., Cuevas-Bourdier, A., and Giménez-Gallego, G. (2011). Antiglioma effects of a new, low molecular mass, inhibitor of fibroblast growth factor. Neuroscience Letters *491*, 1-7.

Datta, S. (1995). Control of proliferation activation in quiescent neuroblasts of the *Drosophila* central nervous system. Development *121*, 1173-1182.

Deepa, P.V., Akshaya, A.S., and Solomon, F.D.P. (2009). Wonder animal model for genetic studies - *Drosophila melanogaster* - Its life cycle and breeding methods - A review Sri Ramachandra Journal of Medicine *2*, 33-38.

DeSalvo, M.K., Mayer, N., Mayer, F., and Bainton, R.J. (2011). Physiologic and anatomic characterization of the brain surface glia barrier of *Drosophila*. Glia *59*, 1322-1340.

Deshors, P., Toulas, C., Arnauduc, F., Malric, L., Siegfried, A., Nicaise, Y., Lemarié, A., Larrieu, D., Tosolini, M., Cohen-Jonathan Moyal, E*., et al.* (2019). Ionizing radiation induces endothelial transdifferentiation of glioblastoma stem-like cells through the Tie2 signaling pathway. Cell Death & Disease *10*, 816.

Dirks, P.B. (2010). Brain tumor stem cells: The cancer stem cell hypothesis writ large. Molecular Oncology *4*, 420-430.

Doe, C.Q. (2008). Neural stem cells: balancing self-renewal with differentiation. Development *135*, 1575-1587.

Doetsch, F., Caillé, I., Lim, D.A., García-Verdugo, J.M., and Alvarez-Buylla, A. (1999). Subventricular zone astrocytes are neural stem cells in the adult mammalian brain. Cell *97*, 703-716.

Dong, J., Zhao, Y., Huang, Q., Fei, X., Diao, Y., Shen, Y., Xiao, H., Zhang, T., Lan, Q., and Gu, X. (2011). Glioma stem/progenitor cells contribute to neovascularization via transdifferentiation. Stem Cell Reviews and Reports *7*, 141-152.

Ebens, A.J., Garren, H., Cheyette, B.N., and Zipursky, S.L. (1993). The *Drosophila* anachronism locus: a glycoprotein secreted by glia inhibits neuroblast proliferation. Cell *74*, 15-27.

Edwards, T.N., Nuschke, A.C., Nern, A., and Meinertzhagen, I.A. (2012). Organization and metamorphosis of glia in the *Drosophila* visual system. The Journal of Comparative Neurology *520*, 2067-2085.

Egger, B., Boone, J.Q., Stevens, N.R., Brand, A.H., and Doe, C.Q. (2007). Regulation of spindle orientation and neural stem cell fate in the *Drosophila* optic lobe. Neural Development *2*, 1.

Egger, B., Gold, K.S., and Brand, A.H. (2011). Regulating the balance between symmetric and asymmetric stem cell division in the developing brain. Fly (Austin) *5*, 237-241.

Egger, B., Leemans, R., Loop, T., Kammermeier, L., Fan, Y., Radimerski, T., Strahm, M.C., Certa, U., and Reichert, H. (2002). Gliogenesis in *Drosophila*: genome-wide analysis of downstream genes of glial cells missing in the embryonic nervous system. Development *129*, 3295-3309.

Feliciano, P. (2012). Dedifferentiation in glioma. Nature Genetics *44*, 1293-1293.

Feng, X., Zhang, B., Wang, J., Xu, X., Lin, N., and Liu, H. (2011). Adenovirus-mediated transfer of siRNA against basic fibroblast growth factor mRNA enhances the sensitivity of glioblastoma cells to chemotherapy. Medical Oncology *28*, 24-30.

Flici, H., Erkosar, B., Komonyi, O., Karatas, O.F., Laneve, P., and Giangrande, A. (2011). Gcm/Glide-dependent conversion into glia depends on neural stem cell age, but not on division, triggering a chromatin signature that is conserved in vertebrate glia. Development *138*, 4167-4178.

Foo, L.C., Song, S., and Cohen, S.M. (2017). miR-31 mutants reveal continuous glial homeostasis in the adult *Drosophila* brain. The EMBO Journal *36*, 1215-1226.

Fortini, M.E. (2009). Notch signaling: the core pathway and its posttranslational regulation. Developmental Cell *16*, 633-647.

Freeman, M.R., and Doe, C.Q. (2001). Asymmetric Prospero localization is required to generate mixed neuronal/glial lineages in the *Drosophila* CNS. Development *128*, 4103-4112.

Friedmann-Morvinski, D., Bushong, E.A., Ke, E., Soda, Y., Marumoto, T., Singer, O., Ellisman, M.H., and Verma, I.M. (2012). Dedifferentiation of neurons and astrocytes by oncogenes can induce gliomas in mice. Science *338*, 1080-1084.

Frise, E., Knoblich, J.A., Younger-Shepherd, S., Jan, L.Y., and Jan, Y.N. (1996). The Drosophila Numb protein inhibits signaling of the Notch receptor during cell-cell interaction in sensory organ lineage. Proc Natl Acad Sci U S A *93*, 11925-11932.

Froldi, F., and Cheng, L.Y. (2016). Understanding how differentiation is maintained: lessons from the *Drosophila* brain. Cellular And Molecular Life Sciences: CMLS *73*, 1641-1644.

Froldi, F., Szuperák, M., and Cheng, L.Y. (2015a). Neural stem cell derived tumourigenesis. AIMS Genetics *2*, 13-24.

Froldi, F., Szuperak, M., Weng, C.F., Shi, W., Papenfuss, A.T., and Cheng, L.Y. (2015b). The transcription factor Nerfin-1 prevents reversion of neurons into neural stem cells. Genes Development *29*, 129-143.

Gaiano, N., and Fishell, G. (2002). The role of notch in promoting glial and neural stem cell fates. The Annual Review of Neuroscience *25*, 471-490.

Galli, R., Binda, E., Orfanelli, U., Cipelletti, B., Gritti, A., De Vitis, S., Fiocco, R., Foroni, C., Dimeco, F., and Vescovi, A. (2004). Isolation and characterization of tumorigenic, stem-like neural precursors from human glioblastoma. Cancer Research *64*, 7011.

Garnier, D., Renoult, O., Alves-Guerra, M.-C., Paris, F., and Pecqueur, C. (2019). Glioblastoma stem-like cells, metabolic strategy to kill a challenging target. Frontiers in Oncology *9*, 118-118.

Geng, F., Cheng, X., Wu, X., Yoo, J.Y., Cheng, C., Guo, J.Y., Mo, X., Ru, P., Hurwitz, B., Kim, S.H.*, et al.* (2016). Inhibition of SOAT1 suppresses Glioblastoma growth via blocking SREBP-1-mediated lipogenesis. Clinical cancer research : an official journal of the American Association for Cancer Research *22*, 5337-5348.

Geng, F., and Guo, D. (2017). Lipid droplets, potential biomarker and metabolic target in glioblastoma. Internal medicine review (Washington, DC : Online) *3*, 10.18103/imr.v18103i18105.18443.

Ghabrial, A., Luschnig, S., Metzstein, M.M., and Krasnow, M.A. (2003). Branching morphogenesis of the *Drosophila* tracheal system. Annual Review of Cell and Developmental Biology *19*, 623-647.

Gimple, R.C., Bhargava, S., Dixit, D., and Rich, J.N. (2019). Glioblastoma stem cells: lessons from the tumor hierarchy in a lethal cancer. Genes Development *33*, 591-609.

Gómez-López, S., Lerner, R.G., and Petritsch, C. (2014). Asymmetric cell division of stem and progenitor cells during homeostasis and cancer. Cellular and Molecular Life Sciences *71*, 575-597.

Goto, Y., De Silva, M.G., Toscani, A., Prabhakar, B.S., Notkins, A.L., and Lan, M.S. (1992). A novel human insulinoma-associated cDNA, IA-1, encodes a protein with "zinc-finger" DNA-binding motifs. Journal of Biological Chemistry *267*, 15252-15257.

Goudarzi, K.M., Espinoza, J.A., Guo, M., Bartek, J., Nistér, M., Lindström, M.S., and Hägerstrand, D. (2018). Reduced expression of *PROX1* transitions glioblastoma cells into a mesenchymal gene expression subtype. Cancer Research *78*, 5901.

Grosskortenhaus, R., Pearson, B.J., Marusich, A., and Doe, C.Q. (2005). Regulation of temporal identity transitions in *Drosophila* neuroblasts. Developmental Cell *8*, 193-202.

Grosskortenhaus, R., Robinson, K.J., and Doe, C.Q. (2006). Pdm and Castor specify late-born motor neuron identity in the NB7-1 lineage. Genes Development *20*, 2618-2627.

Hakes, A.E., and Brand, A.H. (2019). Neural stem cell dynamics: the development of brain tumours. Current Opinion in Cell Biology *60*, 131-138.

Hakes, A.E., and Brand, A.H. (2020). Tailless/TLX reverts intermediate neural progenitors to stem cells driving tumourigenesis via repression of asense/ASCL1. Elife *9*, e53377.

Halder, G., and Mills, G.B. (2011). *Drosophila* in cancer research: to boldly go where no one has gone before. Oncogene *30*, 4063-4066.

Hales, K.G., Korey, C.A., Larracuente, A.M., and Roberts, D.M. (2015). Genetics on the fly: A primer on the *Drosophila* model system. Genetics *201*, 815-842.

Hardavella, G., George, R., and Sethi, T. (2016). Lung cancer stem cells—characteristics, phenotype. Translational Lung Cancer Research *5*, 272-279.

Harding, K., and White, K. (2018). Drosophila as a mdel for Developmental Biology: Stem cell-fate decisions in the developing nervous system. J Dev Biol *6*, 25.

Hartenstein, V. (2011). Morphological diversity and development of glia in *Drosophila*. Glia *59*, 1237-1252.

Hartenstein, V., Nassif, C., and Lekven, A. (1998). Embryonic development of the *Drosophila* brain. II. Pattern of glial cells. The Journal of Comparative Neurology *402*, 32-47.

Hétié, P., de Cuevas, M., and Matunis, E. (2014). Conversion of quiescent niche cells to somatic stem cells causes ectopic niche formation in the *Drosophila* testis. Cell Reports *7*, 715-721.

Hirata, J., Nakagoshi, H., Nabeshima, Y., and Matsuzaki, F. (1995). Asymmetric segregation of the homeodomain protein Prospero during *Drosophila* development. Nature *377*, 627-630.

Hofbauer, A., and Campos-Ortega, J.A. (1990). Proliferation pattern and early differentiation of the optic lobes in *Drosophila melanogaster*. Wilhelm Roux's archives of developmental biology *198*, 264-274.

Hojo, M., Ohtsuka, T., Hashimoto, N., Gradwohl, G., Guillemot, F., and Kageyama, R. (2000). Glial cell fate specification modulated by the bHLH gene Hes5 in mouse retina. Development *127*, 2515.

Holland, E.C. (2000). Glioblastoma multiforme: the terminator. Proc Natl Acad Sci U S A *97*, 6242-6244.

Homem, C.C., and Knoblich, J.A. (2012). *Drosophila* neuroblasts: a model for stem cell biology. Development *139*, 4297-4310.

Homem, C.C., Reichardt, I., Berger, C., Lendl, T., and Knoblich, J.A. (2013). Long-term live cell imaging and automated 4D analysis of *Drosophila* neuroblast lineages. PLoS One *8*, e79588.

Homem, C.C.F., Repic, M., and Knoblich, J.A. (2015). Proliferation control in neural stem and progenitor cells. Nature Reviews Neurosciece *16*, 647-659.

Hosoya, T., Takizawa, K., Nitta, K., and Hotta, Y. (1995). *glial cells missing*: a binary switch between neuronal and glial determination in *Drosophila*. Cell *82*, 1025-1036.

Hovinga, K.E., Shimizu, F., Wang, R., Panagiotakos, G., Van Der Heijden, M., Moayedpardazi, H., Correia, A.S., Soulet, D., Major, T., Menon, J.*, et al.* (2010). Inhibition of notch signaling in glioblastoma targets cancer stem cells via an endothelial cell intermediate. Stem Cells *28*, 1019-1029.

Ikeshima-Kataoka, H., Skeath, J.B., Nabeshima, Y., Doe, C.Q., and Matsuzaki, F. (1997). Miranda directs Prospero to a daughter cell during *Drosophila* asymmetric divisions. Nature *390*, 625-629.

Irizarry, J., and Stathopoulos, A. (2015). FGF signaling supports *Drosophila* fertility by regulating development of ovarian muscle tissues. Developmental Biology *404*, 1-13.

Isshiki, T., Pearson, B., Holbrook, S., and Doe, C.Q. (2001). *Drosophila* neuroblasts sequentially express transcription factors which specify the temporal identity of their neuronal progeny. Cell *106*, 511-521.

Ito, K., and Hotta, Y. (1992). Proliferation pattern of postembryonic neuroblasts in the brain of *Drosophila melanogaster*. Developmental Biology *149*, 134-148.

Iwasaki, Y.H., T.; Takebayashi, H.; Ogawa, Y.; Hotta, Y.; Ikenaka, K. (2003). The potential to induce glial differentiation is conserved between *Drosophila* and mammalian glial cells missing genes. Development *130*, 6027-6035.

Izergina, N., Balmer, J., Bello, B., and Reichert, H. (2009). Postembryonic development of transit amplifying neuroblast lineages in the *Drosophila* brain. Neural Development *4*.

Januschke, J., and Gonzalez, C. (2008). *Drosophila* asymmetric division, polarity and cancer. Oncogene *27*, 6994-7002.

Jarman, A.P., Grau, Y., Jan, L.Y., and Jan, Y.N. (1993). *atonal* is a proneural gene that directs chordotonal organ formation in the *Drosophila* peripheral nervous system. Cell *73*, 1307-1321.

Jennings, B.H. (2011). Drosophila – a versatile model in biology and medicine. Materials Today *14*, 190-195.

Ji, J., Ding, K., Luo, T., Xu, R., Zhang, X., Huang, B., Chen, A., Zhang, D., Miletic, H., Bjerkvig, R.*, et al.* (2020). PMEPA1 isoform a drives progression of glioblastoma by promoting protein degradation of the Hippo pathway kinase LATS1. Oncogene *39*, 1125-1139.

Johannessen, T.C., Wang, J., Skaftnesmo, K.O., Sakariassen, P., Enger, P., Petersen, K., Øyan, A.M., Kalland, K.H., Bjerkvig, R., and Tysnes, B.B. (2009). Highly infiltrative brain tumours show reduced chemosensitivity associated with a stem cell-like phenotype. Neuropathology and Applied Neurobiology *35*, 380-393.

Johnson, J.E. (2003). Numb and Numblike control cell number during vertebrate neurogenesis. Trends in Neurosciences *26*, 395-396.

Jones, B.W. (2005). Transcriptional control of glial cell development in *Drosophila*. Developmental Biology *278*, 265-273.

Jones, B.W., Fetter, R.D., Tear, G., and Goodman, C.S. (1995). *glial cells missing*: a genetic switch that controls glial versus neuronal fate. Cell *82*, 1013-1023.

Joy, T., Hirono, K., and Doe, C.Q. (2015). The RanGEF Bj1 promotes Prospero nuclear export and neuroblast self-renewal. Developmental neurobiology *75*, 485-493.

Kageyama, R., Ohtsuka, T., Shimojo, H., and Imayoshi, I. (2008). Dynamic Notch signaling in neural progenitor cells and a revised view of lateral inhibition. Nature Neuroscience *11*, 1247-1251.

Kaltezioti, V., Kouroupi, G., Oikonomaki, M., Mantouvalou, E., Stergiopoulos, A., Charonis, A., Rohrer, H., Matsas, R., and Politis, P.K. (2010). Prox1 regulates the notch1-mediated inhibition of neurogenesis. PLoS Biology *8*, e1000565.

Kambadur, R., Koizumi, K., Stivers, C., Nagle, J., Poole, S.J., and Odenwald, W.F. (1998). Regulation of POU genes by castor and hunchback establishes layered compartments in the *Drosophila* CNS. Genes Dev *12*, 246-260.

Kammermeier, L., Leemans, R., Hirth, F., Flister, S., Wenger, U., Walldorf, U., Gehring, W.J., and Reichert, H. (2001). Differential expression and function of the *Drosophila Pax6* genes *eyeless* and *twin of eyeless* in embryonic central nervous system development. Mechanisms of Development *103*, 71-78.

Kanai, M.I., Okabe, M., and Hiromi, Y. (2005). *seven-up* controls switching of transcription factors that specify temporal identities of *Drosophila* neuroblasts. Developmental Cell *8*, 203-213.

Kelsom, C., and Lu, W. (2012). Uncovering the link between malfunctions in *Drosophila* neuroblast asymmetric cell division and tumorigenesis. Cell & Bioscience *2*, 38-38.

Kerr, K., S., Fuentes-Medel, Y., Brewer, C., Barria, R., Ashley, J., Abruzzi, K.C., Sheehan, A., Tasdemir-Yilmaz, O.E., Freeman, M.R., and Budnik, V. (2014). Glial wingless/Wnt regulates glutamate receptor clustering and synaptic physiology at the *Drosophila* neuromuscular junction. J Neurosci *34*, 2910-2920.

Khalek, F.J.A., Gallicano, G.I., and Mishra, L. (2010). Colon cancer stem cells. Gastrointestinal Cancer Research : GCR, S16-S23.

Kidd, S., Lieber, T., and Young, M.W. (1998). Ligand-induced cleavage and regulation of nuclear entry of Notch in *Drosophila melanogaster* embryos. Genes Dev *12*, 3728-3740.

Kim, J., Jones, B.W., Zock, C., Chen, Z., Wang, H., Goodman, C.S., and Anderson, D.J. (1998). Isolation and characterization of mammalian homologs of the *Drosophila* gene Glial cells missing. Proceedings of the National Academy of Sciences *95*, 12364.

Kis, V., Barti, B., Lippai, M., and Sass, M. (2015). Specialized cortex glial cells accumulate lipid droplets in *Drosophila melanogaster*. PLoS One *10*, e0131250.

Knoblich, J.A., Jan, L.Y., and Jan, Y.N. (1995). Asymmetric segregation of Numb and Prospero during cell division. Nature *377*, 624-627.

Knoblich, J.A., Jan, L.Y., and Jan, Y.N. (1997). The N terminus of the *Drosophila* Numb protein directs membrane association and actin-dependent asymmetric localization. Proceedings of the National Academy of Sciences *94*, 13005-13010.

Kobayashi, N.C.C.a., and de Noronha, S.M.R. (2014). Cancer stem cells: a new approach to tumor development.

Kong, D.S. (2012). Cancer stem cells in brain tumors and their lineage hierarchy. International Journal of Stem Cells *5*, 12-15.

Kraut, R., and Campos-Ortega, J.A. (1996). *inscuteable*, a neural precursor gene of *Drosophila*, encodes a candidate for a cytoskeleton adaptor protein. Dev Biol *174*, 65-81.

Kraut, R., Chia, W., Jan, L.Y., Jan, Y.N., and Knoblich, J.A. (1996). Role of *inscuteable* in orienting asymmetric cell divisions in *Drosophila*. Nature *383*, 50-55.

Kuzin, A., Brody, T., Moore, A.W., and Odenwald, W.F. (2005). Nerfin-1 is required for early axon guidance decisions in the developing *Drosophila* CNS. Developmental Biology *277*, 347-365.

Lacin, H., and Truman, J.W. (2016). Lineage mapping identifies molecular and architectural similarities between the larval and adult *Drosophila* central nervous system. Elife *5*, e13399.

Lai, S.L., and Doe, C.Q. (2014). Transient nuclear Prospero induces neural progenitor quiescence. Elife *3*, e03363.

Lanet, E., and Maurange, C. (2014). Building a brain under nutritional restriction: insights on sparing and plasticity from Drosophila studies. Frontiers in Physiology *5*, 117.

Lapidot, T., Sirard, C., Vormoor, J., Murdoch, B., Hoang, T., Caceres-Cortes, J., Minden, M., Paterson, B., Caligiuri, M.A., and Dick, J.E. (1994). A cell initiating human acute myeloid leukaemia after transplantation into SCID mice. Nature *367*, 645-648.

Lasky, J.L., Choe, M., and Nakano, I. (2009). Cancer stem cells in pediatric brain tumors. Current Stem Cell Research & Therapy *4*, 298-305.

Lathia, J.D., Hitomi, M., Gallagher, J., Gadani, S.P., Adkins, J., Vasanji, A., Liu, L., Eyler, C.E., Heddleston, J.M., Wu, Q.*, et al.* (2011). Distribution of CD133 reveals glioma stem cells self-renew through symmetric and asymmetric cell divisions. Cell Death & Disease *2*, e200.

Lathia, J.D., Mack, S.C., Mulkearns-Hubert, E.E., Valentim, C.L.L., and Rich, J.N. (2015). Cancer stem cells in glioblastoma. Genes Dev *29*, 1203-1217.

Lee, C.Y., Andersen, R.O., Cabernard, C., Manning, L., Tran, K.D., Lanskey, M.J., Bashirullah, A., and Doe, C.Q. (2006a). *Drosophila* Aurora-A kinase inhibits neuroblast self-renewal by regulating aPKC/Numb cortical polarity and spindle orientation. Genes Development *20*, 3464-3474.

Lee, C.Y., Wilkinson, B.D., Siegrist, S.E., Wharton, R.P., and Doe, C.Q. (2006b). Brat is a Miranda cargo protein that promotes neuronal differentiation and inhibits neuroblast self-renewal. Developmental Cell *10*, 441-449.

Lee, G., Auffinger, B., Guo, D., Hasan, T., Deheeger, M., Tobias, A.L., Kim, J.Y., Atashi, F., Zhang, L., Lesniak, M.S.*, et al.* (2016). Dedifferentiation of Glioma cells to glioma stem-like cells by therapeutic stress-induced HIF signaling in the recurrent GBM model. Mol Cancer Ther *15*, 3064-3076.

Lee, J.H., Lee, J.E., Kahng, J.Y., Kim, S.H., Park, J.S., Yoon, S.J., Um, J.-Y., Kim, W.K., Lee, J.-K., Park, J.*, et al.* (2018). Human glioblastoma arises from subventricular zone cells with low-level driver mutations. Nature *560*, 243-247.

Lee, K.M., Mathies, L.D., and Grotewiel, M. (2019). Alcohol sedation in adult *Drosophila* is regulated by Cysteine proteinase-1 in cortex glia. Communications Biology *2*, 252.

Lee, T. (2017). Wiring the *Drosophila* brain with individually tailored neural lineages. Current Biology *27*, R77-R82.

Lee, T., Lee, A., and Luo, L. (1999). Development of the *Drosophila* mushroom bodies: sequential generation of three distinct types of neurons from a neuroblast. Development *126*, 4065.

Lee, T., and Luo, L. (1999). Mosaic analysis with a repressible cell marker for studies of gene function in neuronal morphogenesis. Neuron *22*, 451-461.

Lee, T., and Luo, L. (2001). Mosaic analysis with a repressible cell marker (MARCM) for *Drosophila* neural development. Trends in Neurosciences *24*, 251-254.

Li, L., and Vaessin, H. (2000). Pan-neural Prospero terminates cell proliferation during *Drosophila* neurogenesis. Genes Development *14*, 147-151.

Li, X., Chen, Z., and Desplan, C. (2013a). Temporal patterning of neural progenitors in *Drosophila*. Current Topics in Developmental Biology *105*, 69-96.

Li, X., Erclik, T., Bertet, C., Chen, Z., Voutev, R., Venkatesh, S., Morante, J., Celik, A., and Desplan, C. (2013b). Temporal patterning of *Drosophila* medulla neuroblasts controls neural fates. Nature *498*, 456-462.

Lim, D.A., Cha, S., Mayo, M.C., Chen, M.-H., Keles, E., VandenBerg, S., and Berger, M.S. (2007). Relationship of glioblastoma multiforme to neural stem cell regions predicts invasive and multifocal tumor phenotype. Neuro Oncol *9*, 424-429.

Lindberg, N., Kastemar, M., Olofsson, T., Smits, A., and Uhrbom, L. (2009). Oligodendrocyte progenitor cells can act as cell of origin for experimental glioma. Oncogene *28*, 2266-2275.

Liu, H.K., Wang, Y., Belz, T., Bock, D., Takacs, A., Radlwimmer, B., Barbus, S., Reifenberger, G., Lichter, P., and Schütz, G. (2010). The nuclear receptor tailless induces long-term neural stem cell expansion and brain tumor initiation. Genes Dev *24*, 683-695.

Loedige, I., Stotz, M., Qamar, S., Kramer, K., Hennig, J., Schubert, T., Löffler, P., Längst, G., Merkl, R., Urlaub, H.*, et al.* (2014). The NHL domain of BRAT is an RNA-binding domain that directly contacts the *hunchback* mRNA for regulation. Genes Dev *28*, 749-764.

Loilome, W., Joshi, A.D., ap Rhys, C.M., Piccirillo, S., Vescovi, A.L., Gallia, G.L., and Riggins, G.J. (2009). Glioblastoma cell growth is suppressed by disruption of Fibroblast Growth Factor pathway signaling. Journal of Neurooncology *94*, 359-366.

Luo, Z., Mu, L., Zheng, Y., Shen, W., Li, J., Xu, L., Zhong, B., Liu, Y., and Zhou, Y. (2019). NUMB enhances Notch signaling by repressing ubiquitination of NOTCH1 intracellular domain. Journal of Molecular Cell Biology *12*, 345-358.

Maher, E.A., Furnari, F.B., Bachoo, R.M., Rowitch, D.H., Louis, D.N., Cavenee, W.K., and DePinho, R.A. (2001). Malignant glioma: genetics and biology of a grave matter. Genes Development *15*, 1311-1333.

Mani, S.A., Guo, W., Liao, M.J., Eaton, E.N., Ayyanan, A., Zhou, A.Y., Brooks, M., Reinhard, F., Zhang, C.C., Shipitsin, M.*, et al.* (2008). The epithelial-mesenchymal transition generates cells with properties of stem cells. Cell *133*, 704-715.

Mao, H., Lv, Z., and Ho, M.S. (2012). Gcm proteins function in the developing nervous system. Developmental Biology *370*, 63-70.

Marumoto, T., Tashiro, A., Friedmann-Morvinski, D., Scadeng, M., Soda, Y., Gage, F.H., and Verma, I.M. (2009). Development of a novel mouse glioma model using lentiviral vectors. Nature Medicine *15*, 110-116.

Matsuzaki, F., Ohshiro, T., Ikeshima-Kataoka, H., and Izumi, H. (1998). Miranda localizes Staufen and Prospero asymmetrically in mitotic neuroblasts and epithelial cells in early *Drosophila* embryogenesis. Development *125*, 4089-4098.

Maurange, C., Cheng, L., and Gould, A.P. (2008). Temporal transcription factors and their targets schedule the end of neural proliferation in *Drosophila*. Cell *133*, 891-902.

Mazaud, D., Kottler, B., Gonçalves-Pimentel, C., Proelss, S., Tüchler, N., Deneubourg, C., Yuasa, Y., Diebold, C., Jungbluth, H., Lai, E.C.*, et al.* (2019). Transcriptional regulation of the Glutamate/GABA/Glutamine Cycle in adult glia controls motor activity and seizures in *Drosophila*. The Journal of Neuroscience *39*, 5269.

McDermott, S.P., and Wicha, M.S. (2010). Targeting breast cancer stem cells. Molecular Oncology *4*, 404-419.

Melom, J.E., and Littleton, J.T. (2013). Mutation of a NCKX eliminates glial microdomain calcium oscillations and enhances seizure susceptibility. Journal of Neuroscience *33*, 1169-1178.

Mettler, U., Vogler, G., and Urban, J. (2006). Timing of identity: spatiotemporal regulation of hunchback in neuroblast lineages of *Drosophila* by Seven-up and Prospero. Development *133*, 429-437.

Minocha, S., Boll, W., and Noll, M. (2017). Crucial roles of Pox neuro in the developing ellipsoid body and antennal lobes of the *Drosophila* brain. PLoS One *12*, e0176002.

Mirzoyan, Z., Sollazzo, M., Allocca, M., Valenza, A.M., Grifoni, D., and Bellosta, P. (2019). *Drosophila melanogaster*: A model organism to study cancer. Front Genet *10*, 51-51.

Miyata, T., Yoshimatsu, T., So, T., Oyama, T., Uramoto, H., Osaki, T., Nakanishi, R., Tanaka, F., Nagaya, H., and Gotoh, A. (2015). Cancer stem cell markers in lung cancer. Personalized Medicine Universe *4*, 40-45.

Morante, J., Vallejo, D.M., Desplan, C., and Dominguez, M. (2013). Conserved miR-8/miR-200 defines a glial niche that controls neuroepithelial expansion and neuroblast transition. Developmental Cell *27*, 174-187.

Morrison, S.J., Perez, S.E., Qiao, Z., Verdi, J.M., Hicks, C., Weinmaster, G., and Anderson, D.J. (2000). Transient Notch activation initiates an irreversible switch from neurogenesis to gliogenesis by neural crest stem cells. Cell *101*, 499-510.

Mukherjee, S., Tucker-Burden, C., Zhang, C., Moberg, K., Read, R., Hadjipanayis, C., and Brat, D.J. (2016). *Drosophila* Brat and human ortholog TRIM3 maintain stem cell equilibrium and suppress brain tumorigenesis by attenuating Notch nuclear transport. Cancer research *76*, 2443-2452.

Narbonne-Reveau, K., Lanet, E., Dillard, C., Foppolo, S., Chen, C.H., Parrinello, H., Rialle, S., Sokol, N.S., and Maurange, C. (2016). Neural stem cell-encoded temporal patterning delineates an early window of malignant susceptibility in *Drosophila*. Elife *5*, e13463.

Neumüller, R.A., and Knoblich, J.A. (2009). Dividing cellular asymmetry: asymmetric cell division and its implications for stem cells and cancer. Genes Dev *23*, 2675-2699.

Northcott, P.A., Robinson, G.W., Kratz, C.P., Mabbott, D.J., Pomeroy, S.L., Clifford, S.C., Rutkowski, S., Ellison, D.W., Malkin, D., Taylor, M.D*., et al.* (2019). Medulloblastoma. Nature Reviews Disease Primers *5*, 11.

Novotny, T., Eiselt, R., and Urban, J. (2002). Hunchback is required for the specification of the early sublineage of neuroblast 7-3 in the *Drosophila* central nervous system. Development *129*, 1027-1036.

Omoto, J.J., Lovick, J.K., and Hartenstein, V. (2016). Origins of glial cell populations in the insect nervous system. Current Opinion in Insect Science *18*, 96-104.

Omoto, J.J., Yogi, P., and Hartenstein, V. (2015). Origin and development of neuropil glia of the *Drosophila* larval and adult brain: Two distinct glial populations derived from separate progenitors. Developmental Biology *404*, 2-20.

Ou, J., He, Y., Xiao, X., Yu, T.M., Chen, C., Gao, Z., and Ho, M.S. (2014). Glial cells in neuronal development: recent advances and insights from *Drosophila melanogaster*. Neuroscience Bulletin *30*, 584-594.

Oxenkrug, G.F. (2010). The extended life span of *Drosophila melanogaster* eye-color (white and vermilion) mutants with impaired formation of kynurenine. Journal of Neural Transmission (Vienna) *117*, 23-26.

Packer, R.J., and Vezina, G. (2008). Management of and prognosis with medulloblastoma: therapy at a crossroads. Archieves of Neurology *65*, 1419-1424.

Park, H.J., Kim, J.K., Jeon, H.M., Oh, S.Y., Kim, S.H., Nam, D.H., and Kim, H. (2010). The neural stem cell fate determinant TLX promotes tumorigenesis and genesis of cells resembling glioma stem cells. Molecules and Cells *30*, 403-408.

Parks, A.L., Stout, J.R., Shepard, S.B., Klueg, K.M., Dos Santos, A.A., Parody, T.R., Vaskova, M., and Muskavitch, M.A.T. (2006). Structure-function analysis of *delta* trafficking, receptor binding and signaling in *Drosophila*. Genetics *174*, 1947-1961.

Pece, S., Serresi, M., Santolini, E., Capra, M., Hulleman, E., Galimberti, V., Zurrida, S., Maisonneuve, P., Viale, G., and Di Fiore, P.P. (2004). Loss of negative regulation by Numb over Notch is relevant to human breast carcinogenesis. The Journal of Cell Biology *167*, 215-221.

Pereanu, W., Shy, D., and Hartenstein, V. (2005). Morphogenesis and proliferation of the larval brain glia in *Drosophila*. Developmental Biology *283*, 191-203.

Peterson, C., Carney, G.E., Taylor, B.J., and White, K. (2002). *reaper* is required for neuroblast apoptosis during *Drosophila* development. Development *129*, 1467-1476.

Piazzi, G., Bazzoli, F., and Ricciardiello, L. (2012). Epigenetic silencing of Notch signaling in gastrointestinal cancers. Cell cycle (Georgetown, Tex) *11*, 4323-4327.

Pierfelice, T., Alberi, L., and Gaiano, N. (2011). Notch in the vertebrate nervous system: an old dog with new tricks. Neuron *69*, 840-855.

Pinto-Teixeira, F., Konstantinides, N., and Desplan, C. (2016). Programmed cell death acts at different stages of *Drosophila* neurodevelopment to shape the central nervous system. FEBS Lett *590*, 2435-2453.

Poon, C.L.C., Mitchell, K.A., Kondo, S., Cheng, L.Y., and Harvey, K.F. (2016). The Hippo pathway regulates neuroblasts and brain size in *Drosophila melanogaster*. Current Biology *26*, 1034-1042.

Popkova, A., Bernardoni, R., Diebold, C., Van de Bor, V., Schuettengruber, B., González, I., Busturia, A., Cavalli, G., and Giangrande, A. (2012). Polycomb controls gliogenesis by regulating the transient expression of the Gcm/Glide fate determinant. PLoS Genetics *8*, e1003159.

Prehoda, K.E. (2009). Polarization of Drosophila neuroblasts during asymmetric division. Cold Spring Harbor Perspectives in Biology *1*, a001388.

Prokop, A., Bray, S., Harrison, E., and Technau, G.M. (1998). Homeotic regulation of segment-specific differences in neuroblast numbers and proliferation in the *Drosophila* central nervous system. Mechanisms of Development *74*, 99-110.

Prokop, A., and Technau, G.M. (1991). The origin of postembryonic neuroblasts in the ventral nerve cord of *Drosophila melanogaster*. Development *111*, 79-88.

Quiñones-Hinojosa, A., Sanai, N., Soriano-Navarro, M., Gonzalez-Perez, O., Mirzadeh, Z., Gil-Perotin, S., Romero-Rodriguez, R., Berger, M.S., Garcia-Verdugo, J.M., and Alvarez-Buylla, A. (2006). Cellular composition and cytoarchitecture of the adult human subventricular zone: a niche of neural stem cells. Journal of Comparative Neurology *494*, 415-434.

Ramat, A., Hannaford, M., and Januschke, J. (2017). Maintenance of Miranda localization in *Drosophila* neuroblasts involves interaction with the Cognate mRNA. Current Biology *27*, 2101-2111.e2105.

Read, R.D. (2011). *Drosophila melanogaster* as a model system for human brain cancers. Glia *59*, 1364-1376.

Read, T.-A., Fogarty, M.P., Markant, S.L., McLendon, R.E., Wei, Z., Ellison, D.W., Febbo, P.G., and Wechsler-Reya, R.J. (2009). Identification of CD15 as a marker for tumor-propagating cells in a mouse model of Medulloblastoma. Cancer Cell *15*, 135-147.

Reddy, B.V., and Irvine, K.D. (2011). Regulation of *Drosophila* glial cell proliferation by Merlin-Hippo signaling. Development *138*, 5201-5212.

Reichardt, I., Bonnay, F., Steinmann, V., Loedige, I., Burkard, T.R., Meister, G., and Knoblich, J.A. (2018). The tumor suppressor Brat controls neuronal stem cell lineages by inhibiting Deadpan and Zelda. EMBO Rep *19*, 102-117.

Reifegerste, R., Schreiber, J., Gülland, S., Lüdemann, A., and Wegner, M. (1999). mGCMa is a murine transcription factor that overrides cell fate decisions in *Drosophila*. Mechanisms of Development *82*, 141-150.

Ren, Q., Awasaki, T., Wang, Y.-C., Huang, Y.-F., and Lee, T. (2018). Lineage-guided Notch-dependent gliogenesis by *Drosophila* multi-potent progenitors. Development (Cambridge, England) *145*, dev160127.

Ren, Q., Yang, C.-P., Liu, Z., Sugino, K., Mok, K., He, Y., Ito, M., Nern, A., Otsuna, H., and Lee, T. (2017). Stem cell-intrinsic, Seven-up-triggered temporal factor gradients diversify intermediate neural progenitors. Current Biology *27*, 1303-1313.

Ricci-Vitiani, L., Pallini, R., Biffoni, M., Todaro, M., Invernici, G., Cenci, T., Maira, G., Parati, E.A., Stassi, G., Larocca, L.M., *et al.* (2010). Tumour vascularization via endothelial differentiation of glioblastoma stem-like cells. Nature *468*, 824-828.

Rothenbusch-Fender, S., Fritzen, K., Bischoff, M.C., Buttgereit, D., Oenel, S.F., and Renkawitz-Pohl, R. (2017). Myotube migration to cover and shape the testis of *Drosophila* depends on Heartless, Cadherin/Catenin, and myosin II. Biology Open *6*, 1876-1888.

Rudrapatna, V.A., Cagan, R.L., and Das, T.K. (2012). *Drosophila* cancer models. Dev Dyn *241*, 107-118.

Saini, N., and Reichert, H. (2012). Neural stem cells in *Drosophila*: Molecular genetic mechanisms underlying normal neural proliferation and abnormal brain tumor formation. Stem Cells International, 1-10.

Sakurai, K., and Osumi, N. (2008). The neurogenesis-controlling factor, Pax6, inhibits proliferation and promotes maturation in murine astrocytes. J Neurosci *28*, 4604-4612.

San-Juán, B.P., and Baonza, A. (2011). The bHLH factor deadpan is a direct target of Notch signaling and regulates neuroblast self-renewal in *Drosophila*. Developmental Biology *352*, 70-82.

Sanai, N., Alvarez-Buylla, A., and Berger, M.S. (2005). Neural stem cells and the origin of gliomas. N Engl J Med *353*, 811-822.

Sanai, N., Tramontin, A.D., Quiñones-Hinojosa, A., Barbaro, N.M., Gupta, N., Kunwar, S., Lawton, M.T., McDermott, M.W., Parsa, A.T., Manuel-García Verdugo, J., *et al.* (2004). Unique astrocyte ribbon in adult human brain contains neural stem cells but lacks chain migration. Nature *427*, 740-744.

Satow, T., Bae, S.K., Inoue, T., Inoue, C., Miyoshi, G., Tomita, K., Bessho, Y., Hashimoto, N., and Kageyama, R. (2001). The basic helix-loop-helix gene hesr2 promotes gliogenesis in mouse retina. J Neurosci *21*, 1265-1273.

Schober, M., Schaefer, M., and Knoblich, J.A. (1999). Bazooka recruits inscuteable to orient asymmetric cell divisions in *Drosophila* neuroblasts. Nature *402*, 548–551.

Schreiber, J., Enderich, J., and Wegner, M. (1998). Structural requirements for DNA binding of GCM proteins. Nucleic acids research *26*, 2337-2343.

Schweisguth, F. (2004). Regulation of notch signaling activity. Current Biology *14*, R129-138.

Scully, S., Francescone, R., Faibish, M., Bentley, B., Taylor, S.L., Oh, D., Schapiro, R., Moral, L., Yan, W., and Shao, R. (2012). Transdifferentiation of glioblastoma stem-like cells into mural cells drives vasculogenic mimicry in glioblastomas. J Neurosci *32*, 12950-12960.

Shaw, R.E., Kottler, B., Ludlow, Z.N., Buhl, E., Kim, D., Morais da Silva, S., Miedzik, A., Coum, A., Hodge, J.J., Hirth, F., *et al.* (2018). *In vivo* expansion of functionally integrated

GABAergic interneurons by targeted increase in neural progenitors. The EMBO journal *37*, e98163.

Shen, C.P., Jan, L.Y., and Jan, Y.N. (1997). Miranda is required for the asymmetric localization of Prospero during mitosis in *Drosophila*. Cell *90*, 449-458.

Shimokawa, M., Ohta, Y., Nishikori, S., Matano, M., Takano, A., Fujii, M., Date, S., Sugimoto, S., Kanai, T., and Sato, T. (2017). Visualization and targeting of LGR5+ human colon cancer stem cells. Nature *545*, 187-192.

Siegrist, S.E., Haque, N.S., Chen, C.H., Hay, B.A., and Hariharan, I.K. (2010). Inactivation of both *foxo* and *reaper* promotes long-term adult neurogenesis in *Drosophila*. Current Biology, 643.

Singh, S.K., Clarke, I.D., Terasaki, M., Bonn, V.E., Hawkins, C., Squire, J., and Dirks, P.B. (2003). Identification of a cancer stem cell in human brain tumors. Cancer Research *63*, 5821.

Skeath, J.B., and Thor, S. (2003). Genetic control of *Drosophila* nerve cord development. Current Opinion in Neurobiology *13*, 8-15.

Smith, C.A., Lau, K.M., Rahmani, Z., Dho, S.E., Brothers, G., She, Y.M., Berry, D.M., Bonneil, E., Thibault, P., Schweisguth, F.*, et al.* (2007). aPKC-mediated phosphorylation regulates asymmetric membrane localization of the cell fate determinant Numb. The EMBO Journal *26*, 468-480.

Somasundaram, K., Reddy, S.P., Vinnakota, K., Britto, R., Subbarayan, M., Nambiar, S., Hebbar, A., Samuel, C., Shetty, M., Sreepathi, H.K.*, et al.* (2005). Upregulation of ASCL1 and inhibition of Notch signaling pathway characterize progressive astrocytoma. Oncogene *24*, 7073-7083.

Song, Y., and Lu, B. (2011). Regulation of cell growth by Notch signaling and its differential requirement in normal vs. tumor-forming stem cells in *Drosophila*. Genes Development *25*, 2644-2658.

Sonoda, J., and Wharton, R.P. (2001). *Drosophila* brain tumor is a translational repressor. Genes and Development *15*, 762–773.

Sousa-Nunes, R., Cheng, L.Y., and Gould, A.P. (2010). Regulating neural proliferation in the *Drosophila* CNS. Current Opinion in Neurobiology *20*, 50-57.

Sousa-Nunes, R., Yee, L.L., and Gould, A.P. (2011). Fat cells reactivate quiescent neuroblasts via TOR and glial insulin relays in *Drosophila*. Nature *471*, 508-512.

Southall, T.D., Davidson, C.M., Miller, C., Carr, A., and Brand, A.H. (2014). Dedifferentiation of neurons precedes tumor formation in *lola* mutants. Developmental Cell *28*, 685-696.

Stivers, C., Brody, T., Kuzin, A., and Odenwald, W.F. (2000). Nerfin-1 and -2, novel *Drosophila* Zn-finger transcription factor genes expressed in the developing nervous system. Mechanisms of Development *97*, 205-210.

Stork, T., Bernardos, R., and Freeman, M.R. (2012). Analysis of glial cell development and function in *Drosophila*. Cold Spring Harb Protoc *2012*, 1-17.

Stork, T., Engelen, D., Krudewig, A., Silies, M., Bainton, R.J., and Klämbt, C. (2008). Organization and function of the blood-brain barrier in *Drosophila*. J Neurosci *28*, 587-597.

Stork, T., Sheehan, A., Tasdemir-Yilmaz, O.E., and Freeman, M.R. (2014). Neuron-glia interactions through the Heartless FGF receptor signaling pathway mediate morphogenesis of *Drosophila* astrocytes. Neuron *83*, 388-403.

Suzuki, T., Kaido, M., Takayama, R., and Sato, M. (2013). A temporal mechanism that produces neuronal diversity in the *Drosophila* visual center. Developmental Biology *380*, 12-24.

Suzuki, T., Takayama, R., and Sato, M. (2016). eyeless/Pax6 controls the production of glial cells in the visual center of *Drosophila* melanogaster. Developmental Biology *409*, 343-353.

Syed, M.H., Mark, B., and Doe, C.Q. (2017). Steroid hormone induction of temporal gene expression in *Drosophila* brain neuroblasts generates neuronal and glial diversity. Elife *6*.

Taïb, B., Aboussalah, A.M., Moniruzzaman, M., Chen, S., Haughey, N.J., Kim, S.F., and Ahima, R.S. (2019). Lipid accumulation and oxidation in glioblastoma multiforme. Scientific Reports *9*, 19593-19593.

Taylor, O.G., Brzozowski, J.S., and Skelding, K.A. (2019). Glioblastoma multiforme: An overview of emerging therapeutic targets. Frontiers in Oncology *9*, 963.

Templeton, A.K., Miyamoto, S., Babu, A., Munshi, A., and Ramesh, R. (2014). Cancer stem cells: progress and challenges in lung cancer. Stem Cell Investig *1*, 9.

Toyoda, K., Tanaka, K., Nakagawa, S., Thuy, D.H., Ujifuku, K., Kamada, K., Hayashi, K., Matsuo, T., Nagata, I., and Niwa, M. (2013). Initial contact of glioblastoma cells with existing normal brain endothelial cells strengthen the barrier function via fibroblast growth factor 2 secretion: a new *in vitro* blood-brain barrier model. Cellular and Molecular Neurobiology *33*, 489-501.

Truman, J., and Bate, M. (1988). Spatial and temporal patterns of neurogenesis in the central nervous system of *Drosophila* melanogaster. Developmental Biology *125*, 145-157.

Tsuji, T., Hasegawa, E., and Isshiki, T. (2008). Neuroblast entry into quiescence is regulated intrinsically by the combined action of spatial Hox proteins and temporal identity factors. Development *135*, 3859-3869.

Udolph, G., Rath, P., and Chia, W. (2001). A requirement for Notch in the genesis of a subset of glial cells in the *Drosophila* embryonic central nervous system which arise through asymmetric divisions. Development *128*, 1457.

Uhrbom, L., Dai, C., Celestino, J.C., Rosenblum, M.K., Fuller, G.N., and Holland, E.C. (2002). Ink4a-Arf loss cooperates with KRas activation in astrocytes and neural progenitors to generate glioblastomas of various morphologies depending on activated Akt. Cancer Research *62*, 5551-5558.

Umesono, Y., Hiromi, Y., and Hotta, Y. (2002). Context-dependent utilization of Notch activity in *Drosophila* glial determination. Development *129*, 2391-2399.

Unhavaithaya, Y., and Orr-Weaver, T.L. (2012). Polyploidization of glia in neural development links tissue growth to blood-brain barrier integrity. Genes Development *26*, 31-36.

Vaiopoulos, A.G., Kostakis, I.D., Koutsilieris, M., and Papavassiliou, A.G. (2012). Colorectal cancer stem cells. Stem Cells *30*, 363-371.

van den Ameele, J., and Brand, A.H. (2019). Neural stem cell temporal patterning and brain tumour growth rely on oxidative phosphorylation. Elife *8*.

Velasco-Velázquez, M.A., Popov, V.M., Lisanti, M.P., and Pestell, R.G. (2011). The role of breast cancer stem cells in metastasis and therapeutic implications. The American Journal of Pathology *179*, 2-11.

Viktorin, G., Riebli, N., Popkova, A., Giangrande, A., and Reichert, H. (2011). Multipotent neural stem cells generate glial cells of the central complex through transit amplifying intermediate progenitors in *Drosophila* brain development. Developmental Biology *356*, 553-565.

Viktorin, G., Riebli, N., and Reichert, H. (2013). A multipotent transit-amplifying neuroblast lineage in the central brain gives rise to optic lobe glial cells in *Drosophila*. Developmental Biology *379*, 182-194.

Vincent, S., Vonesch, J.L., and Giangrande, A. (1996). Glide directs glial fate commitment and cell fate switch between neurones and glia. Development *122*, 131.

Vinson, K.E., George, D.C., Fender, A.W., Bertrand, F.E., and Sigounas, G. (2016). The Notch pathway in colorectal cancer. International Journal of Cancer *138*, 1835-1842.

Vissers, J.H.A., Froldi, F., Schröder, J., Papenfuss, A.T., Cheng, L.Y., and Harvey, K.F. (2018). The Scalloped and Nerfin-1 transcription factors cooperate to maintain neuronal cell fate. Cell Reports *25*, 1561-1576.e1567.

Visvader, J., and Lindeman, G. (2008). Cancer stem cells in solid tumours: accumulating evidence and unresolved questions. Nature Reviews Cancer *8*, 755-768.

Volkenhoff, A., Weiler, A., Letzel, M., Stehling, M., Klämbt, C., and Schirmeier, S. (2015). Glial glycolysis is essential for neuronal survival in *Drosophila*. Cell Metabolism *22*, 437-447.

Walsh, K.T., and Doe, C.Q. (2017). *Drosophila* embryonic type II neuroblasts: origin, temporal patterning, and contribution to the adult central complex. Development (Cambridge, England) *144*, 4552-4562.

Wang, H., Somers, G.W., Bashirullah, A., Heberlein, U., Yu, F., and Chia, W. (2006). Aurora-A acts as a tumor suppressor and regulates self-renewal of *Drosophila* neuroblasts. Genes Development *20*, 3453-3463.

Wang, R., Chadalavada, K., Wilshire, J., Kowalik, U., Hovinga, K.E., Geber, A., Fligelman, B., Leversha, M., Brennan, C., and Tabar, V. (2010). Glioblastoma stem-like cells give rise to tumour endothelium. Nature *468*, 829-833.

Ward, R.J., Lee, L., Graham, K., Satkunendran, T., Yoshikawa, K., Ling, E., Harper, L., Austin, R., Nieuwenhuis, E., Clarke, I.D*., et al.* (2009). Multipotent CD15+ cancer stem cells in patched-1-deficient mouse medulloblastoma. Cancer Res *69*, 4682-4690.

White, K., and Kankel, D.R. (1978). Patterns of cell division and cell movement in the formation of the imaginal nervous system in *Drosophila melanogaster*. Developmental Biology *65*, 296-321.

Wirtz-Peitz, F., Nishimura, T., and Knoblich, J.A. (2008). Linking cell cycle to asymmetric division: Aurora-A phosphorylates the Par complex to regulate Numb localization. Cell *135*, 161-173.

Witte, H.T., Jeibmann, A., Klämbt, C., and Paulus, W. (2009). Modeling glioma growth and invasion in *Drosophila melanogaster*. Neoplasia *11*, 882-888.

Wodarz, A., Ramrath, A., Grimm, A., and Knust, E. (2000). *Drosophila* atypical protein kinase C associates with Bazooka and controls polarity of epithelia and neuroblasts. The Journal of Cell Biology *150*, 1361–1374,.

Wodarz, A., Ramrath, A., Kuchinke, U., and Knust, E. (1999). Bazooka provides an apical cue for Inscuteable localization in *Drosophila* neuroblasts. Nature *402*, 544-547.

Wu, D., Wu, L., An, H., Bao, H., Guo, P., Zhang, B., Zheng, H., Zhang, F., Ge, W., Cai, Y.*, et al.* (2019). RanGAP-mediated nucleocytoplasmic transport of Prospero regulates neural stem cell lifespan in *Drosophila* larval central brain. Aging Cell *18*, e12854-e12854.

Wu, P.S., Egger, B., and Brand, A.H. (2008). Asymmetric stem cell division: lessons from *Drosophila*. Seminars in Cell and Developmental Biology *19*, 283-293.

Yasugi, T., and Nishimura, T. (2016). Temporal regulation of the generation of neuronal diversity in *Drosophila*. Development, Growth and Differentiation *58*, 73-87.

Yasugi, T., Umetsu, D., Murakami, S., Sato, M., and Tabata, T. (2008). *Drosophila* optic lobe neuroblasts triggered by a wave of proneural gene expression that is negatively regulated by JAK/STAT. Development *135*, 1471-1480.

Yu, H.-H., Awasaki, T., Schroeder, M.D., Long, F., Yang, J.S., He, Y., Ding, P., Kao, J.-C., Wu, G.Y.-Y., Peng, H.*, et al.* (2013). Clonal development and organization of the adult *Drosophila* central brain. Current Biology *23*, 633-643.

Yuasa, Y., Okabe, M., Yoshikawa, S., Tabuchi, K., Xiong, W.C., Hiromi, Y., and Okano, H. (2003). *Drosophila* homeodomain protein REPO controls glial differentiation by cooperating with ETS and BTB transcription factors. Development *130*, 2419-2428.

Zhang, H., Geng, D., Gao, J., Qi, Y., Shi, Y., Wang, Y., Jiang, Y., Zhang, Y., Fu, J., Dong, Y.*, et al.* (2016). Expression and significance of Hippo/YAP signaling in glioma progression. Tumor Biology *37*, 15665-15676.

Zhang, M., Li, Z., Zhang, X., and Chang, Y. (2014). Cancer stem cells as a potential therapeutic target in breast cancer. Stem Cell Investigation *1*.

Zhong, W., Jiang, M.M., Schonemann, M.D., Meneses, J.J., Pedersen, R.A., Jan, L.Y., and Jan, Y.N. (2000). Mouse numb is an essential gene involved in cortical neurogenesis. Proceedings of the National Academy of Sciences *97*, 6844-6849.

Zhu, Y., Guignard, F., Zhao, D., Liu, L., Burns, D.K., Mason, R.P., Messing, A., and Parada, L.F. (2005). Early inactivation of p53 tumor suppressor gene cooperating with NF1 loss induces malignant astrocytoma. Cancer Cell *8*, 119-130.

Zhu, Y., and Parada, L.F. (2002). The molecular and genetic basis of neurological tumours. Nature Reviews Cancer *2*, 616-626.

Zilian, O., Saner, C., Hagedorn, L., Lee, H.Y., Säuberli, E., Suter, U., Sommer, L., and Aguet, M. (2001). Multiple roles of mouse Numb in tuning developmental cell fates. Current Biology *11*, 494-501.

Zong, H., Verhaak, R.G.W., and Canoll, P. (2012). The cellular origin for malignant glioma and prospects for clinical advancements. Expert Rev Mol Diagn *12*, 383-394.

Zou, Y., Niu, W., Qin, S., Downes, M., Burns, D.K., and Zhang, C.L. (2012). The nuclear receptor TLX is required for gliomagenesis within the adult neurogenic niche. Molecular and Cellular Biology *32*, 4811-4820.